Centre Européen de Recherche et de Formation Avancée en Calcul Scientifique
European Center for Research and Advanced Training in Scientific Computing

# CERFACS
# Scientific Activity Report
# Jan. 2019 – Dec. 2020

**CERFACS**
**42, Avenue Gaspard Coriolis, 31057 Toulouse Cedex 1, FRANCE.**
**Tel. : 33 (0) 561 19 31 31 – Fax : 33 (0) 561 19 30 30**
secretar@cerfacs.fr – http://www.cerfacs.fr

# Contents

# Foreword

Welcome to the 2019-2020 CERFACS Scientific Activity Report.

CERFACS is a mutualized center of research, development, transfer and training regarding simulation and high performance computing for the benefit of its industrial and public shareholders on a set of major themes.

The mission of CERFACS was defined in the status of the company during the creation of the Civil Society in 1996. The purpose of CERFACS is as follows:

- To develop scientific and technical research to improve methods of advanced computing, including a better consideration of the physical processes involved, and the development of efficient algorithms for new computers architectures;
- To allow access, either on their own or in shared mode, to computers with new architectures which could provide a significant performance gain;
- To transfer the scientific knowledge and the technical methods for application in major industrial sectors and areas;
- To train highly qualified scientists and engineers and provide advanced training
- And, generally, all civil transactions related directly or indirectly to this object and which do not change the civilian character of the company.

These general targets remain the same and CERFACS must adjust its strategy to meet three key factors of success:

- To master and develop differentiating skills and innovation
- To give priority to the mutualized needs of shareholders
- To be a key actor of national and European networks

This report reflects Cerfacs Research activity over the last two years.
During this period, we developped the Strategic Research Plan 2018-2022, based on a core of generic activities "Strategic Axes", which provides both methods, tools and building blocks. A very fruitful interaction between science and application will be encouraged through Application Axes, developed with strong relationships with our shareholders.

CERFACS handles the following 5 themes in its core as Strategic Axes:

- Linear algebra
- Excascale
- Numerical methods for PDE

- Coupling
- Data Driven Modelling ( Data Assimilation, Uncertainty Quantification, Data Science )

6 Application Axes perfuse and sustain the Strategic Axes:

- Climate variability and predictability: from ocean to continental impacts
- Full Gas Turbine simulation
- Methane-Lox engine simulation
- Full Aircraft simulation
- Modelling for environment and safety
- Physics of oil reservoirs (including history matching).

The CERFACS research teams are multidisciplinary with physicists, numerical analysts, algorithm and data scientists, computer engineers,....
There were 3 research teams in CERFACS until mid-2018:

- Parallel Algorithms and Scientific Software Operational Performance (ALGO-COOP): Applied mathematics, Development of advanced numerical algorithms to be used on massively parallel computing platforms, Technology watch & support for leadership class frontier simulations and Research codes industrialization & management of complex simulation workflows.
- Computational Fluid Dynamics (CFD): Aerodynamics, Combustion and Turbomachines
- Climate Modelling and Global Change (GLOBC): Climate, Data Assimilation & Couplers, Modelling and simulation of aircraft emissions & atmospheric chemistry data assimilation.

In addition to the research teams, a transverse team named CSG is devoted to Computer Support for the research teams.

This activity report is written in independent parts so that readers interested mainly in a particular field will easily find both a detailed description of the work that has been achieved, and a complete list of references, including papers in the reviewed literature and internal reports (which can be made available upon request). I sincerely hope that through the detailed reports of the teams you will find interest to continue our collaboration or to initiate new ones.

Enjoy your reading.

Dr Catherine LAMBERT - CERFACS Director

# CERFACS Structure

As a “Société Civile” CERFACS is governed by two bodies.
Firstly, the “Conseil de Gérance”, composed of 7 managers nominated by the 7 shareholders (see table i), follows quite closely the CERFACS activities and the financial aspects. It meets four times per year. Secondly, the Board of Governors is composed of the 7 representatives of CERFACS shareholders and of 3 invited personalities, including the Chairman of the Scientific Council. It meets twice a year.

CERFACS Scientific Council met 2 times during this period 2019-2020 under the chairmanship of Dr Jean-François Minster.

| | |
|---|---|
| CENTRE NATIONAL D’ETUDES SPATIALES (CNES) | 21.3% |
| METEO-FRANCE | 21.3% |
| AIRBUS | 13 % |
| ELECTRICITE DE FRANCE (EDF) | 13% |
| SAFRAN | 13% |
| OFFICE NATIONAL D’ETUDES ET DE RECHERCHES AEROSPATIALES (ONERA) | 9% |
| TOTAL | 9% |

Table i: CERFACS Shareholders with the % of participation

The general organization of CERFACS is depicted in the following CERFACS chart.

**CERFACS chart as of Dec. 31, 2020**

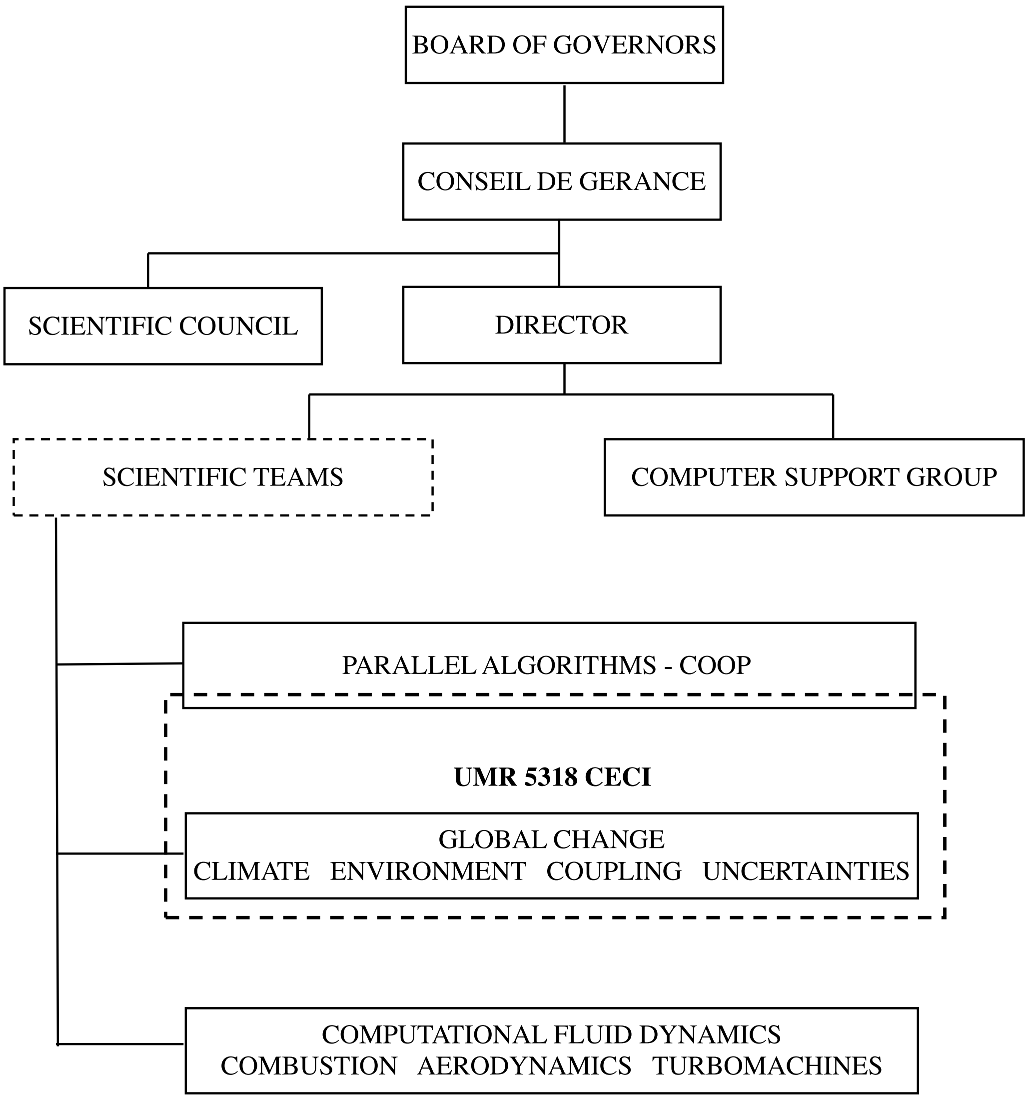

# CERFACS Staff

The staff of the scientific teams and of the computing support group, consisting of, on December 31, 2019, a total of 142 scientists and technical staff is shown in Tables ii and iii.

| POSITION | ALGO-COOP | CFD | CSG | GLOBC |
|---|---|---|---|---|
| Team Leader | 0,2 | 0,3 | 1,0 | 0,2 |
| Senior | 6,5 | 8,8 | | 7,6 |
| Research Engineer | 2,4 | 6,5 | 3,0 | 12,4 |
| Post Doc | 5,6 | 8,6 | | 1,4 |
| Ph.D Student | 6,3 | 37,3 | | 9,0 |
| Studies Engineer | 2,8 | 7,2 | | 1,5 |
| Trainee-Teacher | 2,2 | 4,0 | | 1,1 |
| Consultant | 0,6 | 0,5 | | 1,4 |
| Technician | | | 2,0 | |

Table ii: 2019 Full time equivalent teams distribution.

| POSITION | ALGO-COOP | CFD | CSG | GLOBC |
|---|---|---|---|---|
| Team Leader | 0,2 | 0,3 | 1,0 | 0,2 |
| Senior | 5,6 | 8,0 | | 7,8 |
| Research Engineer | 2,7 | 4,9 | 3,0 | 10,7 |
| Post Doc | 4,3 | 10,2 | | 1,3 |
| Ph.D Student | 9,2 | 38,4 | | 11,5 |
| Studies Engineer | 3,6 | 5,2 | | |
| Trainee-Teacher | 1,5 | 7,4 | 0,1 | 0,8 |
| Consultant | 0,4 | 0,5 | | 1,2 |
| Technician | 0,3 | | 2,0 | |

Table iii: 2020 Full time equivalent teams distribution.

# CERFACS Wide-Interest Seminars

**Pierre Kestener** (CEA Saclay) *Multi-architecture implementation of Spectral Difference Methods (SDM) for compressible flows using performance portable programing tools (c++ kokkos).* (2019, February 15th)

**William Exbrayat** (OMP) *Comment faire efficacement de la bibliographie et de la bibliométrie quand (on n'est pas doué et) qu'on n'a pas le temps ?* (2019, May 21st)

**Valentjin Pauwels** (University of Monash, Melbourne) *Modelling activities to support flood and drought management in Australia.* (2019, May 21st)

**Dorian Micou** (CNES) *From coal combustion to red blood cell modelling: the HPC as a tool in solving complex problems.* (2019, June 28th)

**Roland Séférian** (Météo-France, Toulouse): *Rapport Spécial du GIEC sur 1,5°C de réchauffement planétaire: une rupture avec les précédents rapport du GIEC ?* (2019, December 5th)

**Bertrand Carissimo** (CEREA) *Récents développements pour la modélisation CFD de l'environnement atmosphérique à l'échelle locale.* (2019, December 10th)

# 1

# Parallel Algorithms and Scientific Computing (ALGO-COOP)

# Introduction

The Parallel Algorithms Team (ALGO) was merged in January 2020 with the Scientific Software Operational Performance Team (COOP) team, so that this section already reports on the combined activities in the new ALGO-COOP team. The combined expertise of the two teams will create synergies in some fields, such as in exascale computing, software engineering, and data driven computing. This requires that structural and scientific differences be better bridged. Parts of the former COOP team are oriented towards providing support for other teams, i.e. towards optimizing legacy programs and porting scientific software to new architectures. These activities are important for CERFACS and its shareholders, but their potential to develop new research directions has not been fully exploited in the past. These topics are oriented towards computer science, and therefore include fields such as software engineering, computer architecture, compilers and programming languages, adaptive mesh generation, parallel load balancing, as well as the rapidly growing fields of machine learning and artificial intelligence.

At its core, the ALGO-COOP team conducts research on advanced numerical algorithms and innovative methods for the solution of problems in Computational Science and Engineering (CSE) that employ advanced parallel computing platforms. Researchers in ALGO-COOP study the design, the analysis, and the implementation of algorithms for problems that are out of reach of current standard numerical methods. Such limitations can be due to the computational cost when extremely fine resolutions are required, or innovative new methods may be needed for special nonlinear problems, or when the stochastic nature of the data must be considered. Recent research activities also include aspects of software engineering, program tuning and porting for exascale, and novel artificial intelligence techniques.

ALGO-COOP research is performed in collaboration with the shareholders of CERFACS, with FAU, or with other external partners. In particular, the linear algebra and mathematical research activities are often done in collaboration with IRIT in the context of the joint CERFACS-IRIT Common Laboratory or with INRIA plus other collaborators. This international network is well-documented in coauthorships of our publications. Two ALGO-COOP senior scientists are associate researchers in the chair of S. Gratton within the Toulouse AI institute ANITI. This research is focused on the use of deep learning techniques for inverse problems in data assimilation and forward problems in fast surrogate solvers. Our research on Lattice Boltzmann methods relies on the availability of waLBerla, a highly scalable and efficient Lattice-Boltzmann framework developed at FAU in Erlangen. Similarly, some of the research on multigrid methods and iterative solvers is also conducted in collaboration with U. Ruede's group at FAU Erlangen-Nürnberg. Two PhD students are expected to graduate in 2021 at French universities and at FAU Erlangen-Nuremberg in cotutelle-agreements. One graduate of FAU will defend his PhD in the CFD team at CERFACS, another one is expected to start his PhD in 2021 (delayed from 2020 due to Corona). Two senior scientists of ALGO-COOP have guest researcher status at FAU and have taught courses there. This and frequent mutual visits help us to exploit the synergies between FAU Erlangen-Nuremberg and CERFACS. Unfortunately, in most of 2020 travel was restricted due to the pandemic situation and thus the collaboration had to resort to using telecommunication.

Mathematical research in ALGO-COOP builds on more than three decades of successful work on parallel numerical methods and we are constantly expanding its scope into new areas. Continued progress in computer technology to an ever higher degree of parallelism creates the need for new algorithms and revising known algorithms to achieve improved scalability. Many new supercomputer architectures use hardware accelerators, such as GPUs. Therefore existing successful software must be adapted to these architectures and novel programming paradigms must be developed for the better use of such architectures in the future. Another significant trend is towards a better use of data in scientific computing tasks. For example, in weather, ocean and climate simulations this leads to research on advanced data assimilation algorithms. In this area, ALGO-COOP has a long-standing collaboration with ECMWF, particularly in the areas of algorithmic development for 4D-Var and in ocean data assimilation through the development of the NEMOVAR platform. Additionally, the abundance of data can be tackled with new methods from machine learning and artificial intelligence. This, in particular, creates many new challenges and opportunities, For example, deep learning techniques have undergone a most rapid development and this is also reflected in current ALGO-COOP research activities. Additionally, quantum computing becomes another new research direction.

In many application fields, classical forward simulations are now used as building blocks for more complex and challenging computational goals. These include optimization problems, inverse problems, model reduction techniques, and data driven computing. In the past few years, the ALGO-COOP has successfully developed new research directions in these fields. This includes research in the context of optimization and data assimilation and the systematic quantification of uncertainties. Such methods are expected to become even more important in the future as the basis of decision support systems in fields of scientific or societal relevance. Naturally these research topics are interconnected, since e.g. large-scale inverse problems (as they arise in big data applications) or the solution of nonlinear systems eventually all require approximate solutions of linearized systems. These developments at ALGO-COOP rely on the strong research expertise in mathematical modelling, numerical analysis, partial differential equations, Lattice Boltzmann methods, scientific computing, and computational science. For the research in ALGO-COOP it is often essential to identify the abstract mathematical structure of a given problem and to exploit it in the design of innovative algorithms.

Generally, an important role of the ALGO-COOP team within CERFACS is to bridge from the fundamental mathematical aspects to research for real-life applications. To this end, novel parallel algorithms and methods are proposed, designed, and analysed in terms of their accuracy and their computational cost. This includes the study of convergence properties and the accuracy achieved, and especially also the efficiency and scalability of the methods on advanced parallel computer architectures. However, pragmatic solutions must also take programmer productivity and development cost into account, and this is especially true in an industrial environment. We point to an interesting study presented in Section 7.1 of this report.

The solution of sparse linear systems is considered by tackling both sparse direct methods as well as projection based iterative methods. These methods can also be combined to derive hybrid algebraic methods, with a special emphasis on multiscale and multigrid methods. In addition to linear algebra and functional analysis, these activities rest upon the strong expertise in scientific software development and on an up-to-date knowledge of the current parallel computing platforms. Here the expertise of ALGO-COOP in the use of modern tools and techniques is often essential to realize efficient solutions in practice.

Optimization methods occur in several applications at CERFACS. ALGO-COOP works in both differentiable optimization and derivative-free optimization and is deeply involved in the design and analysis of algorithms for data assimilation. Algorithms related to differentiable optimization or derivative-free optimization are considered together with filtering techniques. All these algorithms must be adapted and improved before tackling potential applications in seismic, oceanography, atmospheric chemistry or meteorology. ALGO-COOP has developed specific expertise in the field of correlation error modelling based on the iterative solution of an implicitly formulated diffusion equation.

Finally the ALGO-COOP takes an active part in the training programs at CERFACS and also regularly organizes seminars and workshops in numerical linear algebra, high performance computing, mesh generation, Lattice-Boltzmann methods, scientific computing, exascale computing, artificial intelligence, and data assimilation.

# Numerical Linear Algebra

## 2.1 Application of an iterative Golub-Kahan algorithm to structural mechanics problems with multi-point constraints

Kinematic relationships between degrees of freedom, also named multi-point constraints, are frequently used in structural mechanics. In [ALG41], the Craig variant of the Golub-Kahan bidiagonalization algorithm is used as an iterative method to solve the arising linear system with a saddle point structure. The condition number of the preconditioned operator is shown to be close to unity and independent of the mesh size. This property is proved theoretically and illustrated on a sequence of test problems of increasing complexity, including concrete structures reinforced with pretension cables and the coupled finite element model of a reactor containment building. The Golub-Kahan algorithm converges in only a small number of steps for all considered test problems and discretization sizes. Furthermore, it is robust in practical cases that are otherwise considered to be difficult for iterative solvers.

## 2.2 Parallel solution of saddle point systems with nested iterative solvers based on the Golub-Kahan bidiagonalization

The Golub-Kahan bidiagonalization is widely used in the singular value decomposition of rectangular matrices and has been generalized to an iterative solver for symmetric indefinite linear systems with a two-by-two block structure. In [ALG42], we present a scalability study of this generalized solver as implemented in a recent release of the parallel numerical library PETSc (Portable, Extensible Toolkit for Scientific Computation). We present an improved solver performance for the two-dimensional (2D) Stokes equations as compared to previous work. Furthermore, we investigate the performance of different parallel inner solvers in the outer Golub-Kahan iteration for a three-dimensional Stokes problem. The study includes parallel sparse direct solvers and multigrid methods. When increasing the number of cores for a fixed total problem size, the solver exhibits good speedups of up to 50% on 1024 cores. For the tests in which the total problem size grows while the workload in each core stays constant, the parallel performance of the solver scales almost linearly with the increase in the number of cores. In particular, the computation time increases by only about 15% when the number of cores increases from 80 to 1024 for a 2D test case.

## 2.3 Parallel adaptive FETI-DP using lightweight asynchronous dynamic load balancing

A parallel FETI-DP domain decomposition method using an adaptive coarse space is presented in [ALG38]. The implementation builds on a recently introduced adaptive FETI-DP approach for elliptic problems in three dimensions and uses small, local eigenvalue problems for faces and, additionally, for a small number of edges. The condition number of the preconditioned operator then satisfies a bound that is independent of coefficient heterogeneities in the problem. The computational cost of the local eigenvalue problems is not negligible, and also a significant load imbalance can be introduced. As a remedy, certain eigenvalue problems are discarded by a theory-guided heuristic strategy, based on the diagonal entries of the stiffness matrices. Additionally, a lightweight pairwise dynamic load balancing strategy is implemented for the eigenvalue problems. The load balancing is supervised by an orchestrating rank using asynchronous point-to-point communication. The resulting method shows good weak and strong scalability up to thousands of cores while fast convergence is obtained even for heterogeneous problems.

## 2.4 An h-multigrid method for Hybrid High-Order discretizations

In [ALG48], we consider a second order elliptic PDE discretized by the Hybrid High Order (HHO) method, for which globally coupled unknowns are located on faces. To efficiently solve the resulting linear system, we propose a geometric multigrid algorithm that keeps the degrees of freedom on the faces at every level. The core of the algorithm resides in the design of the prolongation operator that passes information from coarse to fine faces through the reconstruction of an intermediate polynomial of higher degree on the cells. Higher orders are naturally handled by keeping the same polynomial degree at every level. The proposed algorithm requires a hierarchy of nested meshes where the faces are also successively coarsened. Numerical tests on homogeneous and heterogeneous diffusion problems in square and cubic domains show fast convergence, scalability in the mesh size and polynomial order, and robustness with respect to heterogeneity of the diffusion coefficient.

# Data assimilation

Covariance modelling and the representation of model error in 4D data assimilation algorithms were two focus areas for research in the 2019–2020 period. Firstly, we describe a specific development in background-error covariance modelling, which was to develop computationally efficient methods for estimating the diagonal of a diffusion-based covariance matrix. The diagonal is required in order to normalize the covariance matrix to obtain a correlation matrix for the data assimilation algorithm. Secondly, we outline a related method based on a diffusion operator, which has been developed for modelling observation-error correlations when observations are spatially distributed in an unstructured manner. Finally, we describe methods for representing model error within the context of both weak-constraint 4D-Var and a weak-constraint generalization of the Iterative Ensemble Kalman Smoother (IEnKS) algorithm [1].

## 3.1 Background-error covariance modelling

Developing effective ways to model and cycle the background-error covariance matrix is an active area of research in data assimilation. An important aspect of this problem when using a filter to model the background-error correlations is the computation of normalization factors to ensure that the diagonal elements of the modelled correlation matrix are all equal to one. Updating the parameters of a flow-dependent correlation model on each assimilation cycle requires updating the normalization factors, which is costly using traditional methods such as randomization. In [ALG60] we discuss the normalization problem within the context of a diffusion filter-based covariance model used for background-error modelling in the NEMOVAR variational data assimilation system. We evaluated various methods for estimating normalization factors when the diffusion tensor of the correlation model is derived from an ensemble of ocean states. Our results show that estimates produced using inexpensive methods derived from analytical considerations of the diffusion equation can have significant errors, especially near boundaries. Estimates obtained using randomization with a small sample size ($\sim$100) are more accurate in a globally averaged sense but are noisy and can have unacceptably large errors locally. Next, we focused on the specific problem of accounting for flow-dependent correlation parameters in the vertical component of the diffusion operator only, which is important for improving the assimilation of surface observations such as SST. Remarkably accurate estimates are obtained by approximating the normalization matrix as a separable product of two normalization matrices: one computed using randomization with the horizontal diffusion operator only and the other computed using randomization with the vertical diffusion operator only (see Figure 3.1). If the parameters of the horizontal component of the diffusion operator are static then only the normalization factors of the flow-dependent vertical component need to be recomputed at each cycle. This result is of significant practical interest since the vertical diffusion operator employs an inexpensive direct solver and thus can be applied on each cycle with a large random sample to obtain a good approximation of the normalization matrix.

## 3.2 Modelling spatially correlated observation errors

A method for representing spatially correlated observation errors in variational data assimilation has been developed by [ALG67, ALG36]. The method is based on the numerical solution of a diffusion equation,

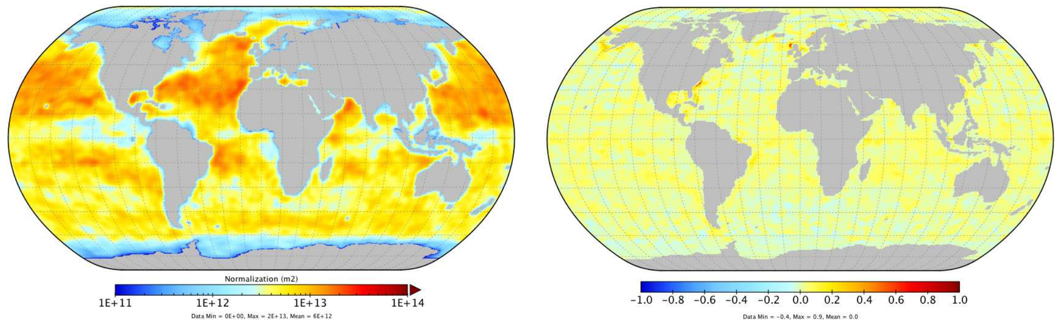


Figure 3.1: *Left panel.* The reference normalization factors ($\mathrm{m}^2$) for temperature at 5 metres depth (the surface level) for the implicit diffusion operator where the diffusion tensor has been estimated from a climatological ensemble. The normalization factors have been computed using the randomization method with a sample size of $10^4$. The colour palette uses a $\log_{10}$ scale. *Right panel.* The relative error in the normalization factors when using normalization factors approximated as a product of factors estimated separately for the horizontal and vertical diffusion components using randomization with a sample size of $10^4$. This approximation has significant practical benefits by reducing the cost of normalization when using flow-dependent vertical correlation length scales. Source: [ALG60].

a technique commonly used for representing spatially correlated background errors. The discretization of the pseudo-time derivative of the diffusion equation is done implicitly using a backward Euler scheme. The solution of the resulting elliptic equation can be interpreted as a correlation operator whose kernel is a correlation function from the Matérn family. In order to account for the possibly heterogeneous distribution of observations, a spatial discretization technique based on the finite element method (FEM) has been chosen where the observation locations are used to define the nodes of an unstructured mesh on which the diffusion equation is solved. By construction, the method leads to a convenient operator for the inverse of the observation-error correlation matrix, which is an important requirement when applying it with standard minimization algorithms in variational data assimilation. Previous studies have shown that spatially correlated observation errors can also be accounted for by assimilating the observations together with their directional derivatives up to arbitrary order. In the continuous framework, we showed that the two approaches are formally equivalent for certain parameter specifications. The FEM provides an appropriate framework for evaluating the derivatives numerically, especially when the observations are heterogeneously distributed. Numerical experiments were performed using a realistic data distribution from the Spinning Enhanced Visible and InfraRed Imager (SEVIRI). Correlations obtained with the FEM-discretized diffusion operator were compared with those obtained using the analytical Matérn correlation model. The method has been shown to produce an accurate representation of the target Matérn function in regions where the data are densely distributed. The presence of large gaps in the data distribution degrades the quality of the mesh and leads to numerical errors in the representation of the Matérn function. Strategies to improve the accuracy of the method in the presence of such gaps are discussed in [ALG67, ALG36].

## 3.3 Exploring the potential and limitations of weak-constraint 4D-Var

The standard formulation of 4D-Var assumes random zero mean errors for all sources of information used in the analysis. This assumption is usually not well verified in real-world applications. The performance of a weak-constraint 4D-Var formulation (the so-called ‘forcing’ formulation) is studied in [ALG45] in a simplified experimental setting using *additive model errors* of different length-scales and observing systems of different coverage and accuracy. A set of twin experiments is carried out and results show that weak-constraint 4D-Var can accurately estimate the actual model errors and the initial state only when background and model errors have different spatial scales and when the observations are unbiased and spatially homogeneous. We also present preliminary results from a different weak-constraint 4D-Var formulation (the so-called 'state' formulation) which could in principle overcome some of these limitations, but at the cost of a substantial increase of computational and memory requirements. These findings help identify the potential but also the intrinsic limitations of the weak-constraint 4D-Var approach. They also help to clarify the experimental results seen in the operational ECMWF analysis system where the analysis and first-guess temperature bias is reduced by up to 50% in the stratosphere.

## 3.4 IEnKS in the presence of additive model error

Ensemble variational methods are being increasingly used in the field of geophysical data assimilation. Their efficiency comes from the combined use of ensembles, which provide statistics estimates, and a variational analysis, which handles nonlinear operators through iterative optimization techniques. Taking model error into account in 4D ensemble variational algorithms is challenging because the state trajectory over the data assimilation window (DAW) is no longer determined by its sole initial condition. In particular, the control variable dimension scales with the DAW length, which yields a high numerical complexity. This is unfortunate since accuracy improvement is expected with longer DAWs. In [ALG35] we discussed how to algorithmically construct and numerically test an iterative ensemble Kalman smoother with additive model error (IEnKS-Q) which is thought to be the natural weak-constraint generalization of the IEnKS. The number of model evaluations per cycle of the IEnKS-Q is also examined. Solutions based on perturbation decomposition are proposed to dissociate those numerically costly evaluations from the control variable dimension.

**References**

[1] M. Bocquet and P. Sakov, (2014), An iterative ensemble Kalman smoother, *Quarterly Journal of the Royal Meteorological Society*, **140**, 1521–1535.

# Uncertainty Quantification

## 4.1 Multilevel Monte Carlo Covariance Estimation for the Computation of Sobol' Indices

Crude and quasi Monte Carlo (MC) sampling techniques are common tools dedicated to estimating statistics (expectation, variance, covariance) of a random quantity of interest. We focus on the uncertainty quantification framework where the quantity of interest is the output of a numerical simulator fed with uncertain input parameters. Then, sampling the output involves running the simulator for different samples of the inputs, which may be computationally time-consuming. To reduce the cost of sampling, a first approach consists in replacing the numerical simulator by a surrogate model that is cheaper to evaluate, thus making it possible to generate more samples of the output and therefore leading to a lower sampling error. However, this approach adds to the sampling error an unavoidable model error. Another approach, which does not introduce any model error, is the so-called multilevel MC (MLMC) method. Given a sequence of levels corresponding to numerical simulators with increasing accuracy and computational cost, MLMC combines samples obtained at different levels to construct an estimator at a reduced cost compared to standard MC sampling. In [ALG52, ALG13], we extended theorems of MLMC theory to covariance estimation, and we proposed a novel version of the multilevel algorithm, driven by a target cost. These results were then used in a sensitivity analysis context in order to derive a multilevel estimation of Sobol' indices, whose building blocks can be written as covariance terms in a pick-and-freeze formulation. These contributions were successfully tested on an initial value problem with random parameters.

## 4.2 Iterative solver strategies for the sampling of discretized stochastic elliptic PDEs

In the general context of the iterative solution, by means of a Krylov method, of a sequence of symmetric positive definite (SPD) linear systems arising from the sampling of a discretized stochastic elliptic PDE, one strategy consists in recycling part of the spectral information from one linear system to the next. This is typically achieved by constructing a deflation subspace based on approximations of the Ritz pairs associated with the previous solve, which are constructed at limited cost during the iterations of the Krylov method. These deflation techniques can be very efficient when one has to solve several times the same system with different right-hand-sides. However, in the case of a stochastic coefficient field (e.g. diffusivity), the matrix of the linear system changes with each sample. Some similarity (or correlation) between successive samples must then be introduced, which can be achieved using Markov Chain Monte Carlo (MCMC) or MC/MCMC hybrid sampling. Deflation can then accelerate the convergence of the iterative solution of successive linear systems when combined with a non-scalable preconditioner (e.g. block-Jacobi). However, it does not substantially improve the convergence when a scalable preconditioner is used (e.g. an algebraic multigrid) [ALG19]. Future work will focus on preconditioning strategies based on fixed preconditioners corresponding to a partitioning of the stochastic space of the uncertain coefficient field.

# Numerical methods for partial differential equations

## 5.1 Sparsified discrete wave problem involving a radiation condition on a prolate spheroidal surface

In [ALG20], we develop and analyse a high-order outgoing radiation boundary condition for solving three-dimensional scattering problems by elongated obstacles. This Dirichlet-to-Neumann condition is constructed using the classical method of separation of variables that allows one to define the scattered field in a truncated domain. It reads as an infinite series that is truncated for numerical purposes. The radiation condition is implemented in a finite element framework represented by a large dense matrix. Fortunately, the dense matrix can be decomposed into a full block matrix that involves the degrees of freedom on the exterior boundary and a sparse finite element matrix. The inversion of the full block is avoided by using a Sherman–Morrison algorithm that reduces the memory usage drastically. Despite being of high order, this method has only a low memory cost.

## 5.2 A painless automatic hp-adaptive strategy for elliptic problems

In [ALG30], we introduce a novel hp-adaptive strategy. The main goal is to minimize the complexity and implementational efforts hence increasing the robustness of the algorithm while keeping close to optimal numerical results. We employ a multi-level hierarchical data structure imposing Dirichlet nodes to manage the so-called hanging nodes. The hp-adaptive strategy is based on performing quasi-optimal unrefinements. Taking advantage of the hierarchical structure of the basis functions both in terms of the element size h and the polynomial order of approximation p, we mark those with the lowest contributions to the energy of the solution and remove them. This straightforward unrefinement strategy does not need a fine grid or complex data structures, making the algorithm flexible to many practical situations and existing implementations. On the other hand, we also identify some limitations of the proposed strategy, namely: (a) data structures only support isotropic h-refinements (although p-anisotropic refinements are enabled), (b) we assume certain quasi-orthogonality properties of the basis functions in the energy norm, and (c) in this work, we restrict ourselves to symmetric and positive definite problems. We illustrate these and other advantages and limitations of the proposed hp-adaptive strategy with several one-, two- and three-dimensional Poisson examples.

## 5.3 Energy-minimizing, symmetric finite differences for anisotropic meshes and energy functional extrapolation

Self-adjoint differential operators often arise from variational calculus on energy functionals. In this case, a direct discretization of the energy functional induces a discretization of the differential operator. Following this approach, the discrete equations are naturally symmetric if the energy functional was self-adjoint, a property that may be lost when using standard difference formulas on nonuniform meshes or when the differential operator has varying coefficients. Low order finite difference or finite element systems can be derived using this approach in a systematic way and on logically structured meshes they become compact difference formulas. Extrapolation formulas used on the discrete energy can then lead to higher order approximations of the differential operator. A rigorous analysis is presented in [ALG43] for extrapolation used in combination with nonstandard integration rules for finite elements. Extrapolation can likewise be applied on matrix-free finite difference stencils. In our applications, both schemes show up to quartic order of convergence.

# Data Science and Artificial Intelligence

## 6.1 Overview of Data Science and its relevance to Cerfacs

Data Science (DS) activites at Cerfacs started coordinating in 2018 around the HELIOS work group. This has enabled us to mature the strategy of our approach to the field of DS in computational physics. DS is an umbrella term regrouping many recent advances, as well as older well established approaches, in data management, statistics and statistical learning. We decompose this into 3 fields:

1. **Big Data** refers to an ensemble of technologies that enable fast access to very large, distributed, heterogeneous data. The rise of these technologies has been concurrent with the accumulation of unprecedented amounts of data, mostly by web-based tech companies.
2. **"Classical" Machine Learning (ML)** is a field of computational statistics backed by at least 50 years of research and development. Many ML tools have a high degree of maturity today, as they have been available for several years or even decades. However, the use of these techniques in the face of vast amounts of data, readily available thanks to Big Data technologies, is a relatively recent evolution, and this is the branch of computational statistics often referred to as "Data Science".
3. **Artificial Intelligence** is a loaded term, first introduced in the '50s, with a meaning that has evolved to the point of switching to opposite side of the domain [2]. Today, it is often used to refer to the most cutting edge research in machine learning, associated mostly with the field of Deep Learning (DL), where deep Artificial Neural Networks are trained for specific tasks [3].

Big Data has some specific relevance at Cerfacs in the Earth Sciences, where single very large simulations are run and subsequently exploited for analysis by a wide array of users. Specific progress on this topic is described in the Climate and Environment part of this report. Otherwise, Big Data technologies relate to High Performance Data Analytics (HPDA) infrastructures, and are not fully relevant to HPC clusters such as those used by or at Cerfacs.
ML is an important field full of evolutions that can potentially be of use to Cerfacs' interests, but statistical learning is already an integral part of many studies at Cerfacs today. Data Assimilation (DA) and Uncertainty Quantification (UQ), treated elsewhere in this report, both rely heavily on mathematics sharing a large common basis with machine learning approaches. Identifying the relationships between DA, UQ and ML is mostly a problem of translating terms between disjoint communities. This work will progress as many DA and UQ studies build bridges between the communities, but this type of cultural change takes time. As such, no extreme cases of the strong potential of ML to transform traditional workflows have been identified, we choose to continue to investigate the topic of ML, but it will not be the focus point of our data science strategy.
Deep Learning has enabled spectacular breakthroughs in fields of computer perception, such as computer vision and natural language processing in the past decade [4]. What's more, these groundbreaking changes were largely unforeseen by experts in the field [2]. This has prompted much speculation about other fields that could undergo similar breakthroughs thanks to these techniques, including physical modelling. But the analogy between computer perception on the one hand, and fields governed by physical laws and their equations on the other, is not easy to make. The computational physics community is still actively searching for ways in which DL can impact and improve traditional computational workflows, and Cerfacs is at the forefront of this exploration.

## 6.2 Artificial Intelligence

AI is an extremely active field, with dozens of thousands of papers contributed each year. The practices of this immense body of work have not yet transferred to the computational physics community, and there is no clear picture of all the possible applications yet. At Cerfacs, a tentative classification of current activities is proposed as follows, from most mature to still mostly prospective:

| Most mature |
|---|
| 1. AI & Data Wrangling |
| 2. AI & CFD |
| 3. AI & Hardware |
| 4. AI & Robustness |
| 5. AI & Interpretation |
| Least mature |

For this activity report, we will focus only on point 2., where most activity has been focused in the past two years. It should be noted however that a technical report [ALG62] has been written on a topic of point 1., and a publication should follow shortly. The subject is the use of deep neural networks to identify key elements of the operating conditions of an engine, using only sparse sensor data.

## 6.3 AI & CFD

The field of CFD has not yet massively leveraged the tools of AI. One reason for this is that the tools of CFD are already quite mature, and involve complex solvers with many steps of computation. Determining where AI can be useful in this loop is a major challenge. There are a number of options however (Fig. 6.1).

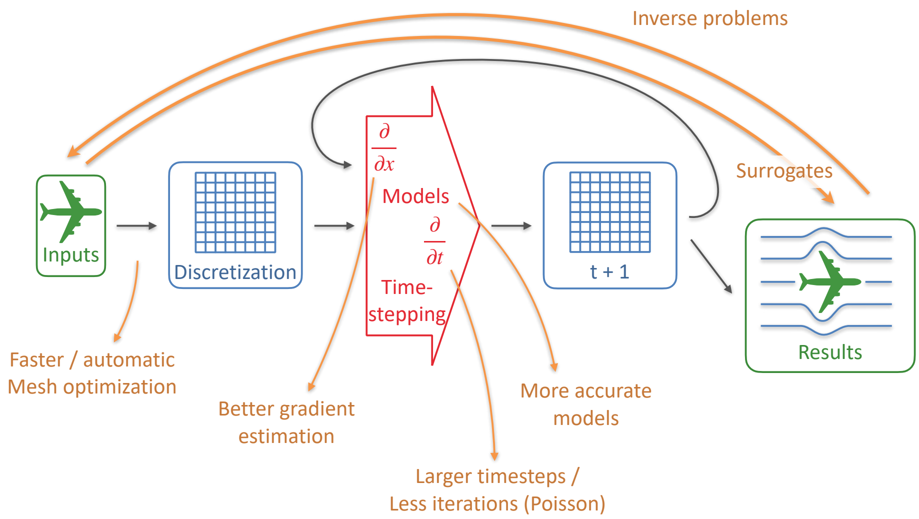


Figure 6.1: The CFD process (from Inputs to Results) involves many steps, usually with iterative solvers. At each step, AI can be leveraged.

The work at Cerfacs explores several of these options, with the following results in the past two years:

- Direct surrogate of the entire chain, as was applied in our work on a hydraulic Saint-Venant solver surrogate [ALG9]. There, we showed how data-driven techniques, taken both from the field of traditional machine learning and deep learning, compared against the Telemac-Mascaret hydraulic solver. Interestingly, when using real-world data for training, data-driven techniques slightly outperformed the solver.

- More accurate models inside the resolution loop, as performed on the issue of subgrid-scale turbulent-flame interactions [ALG47]. In this work, the flame-turbulence interaction at the subgrid-scale level, where the turbulence and the flame are not solved for, is modelled using a standard thickened flame approach. In it, the flame is artificially thickened, so as to be resolved by the mesh. All unresolved interactions are modelled using an efficiency function, which increases the fuel consumption speed based on the additional flame surface that cannot be represented at the chosen resolution. This efficiency was accurately modelled in an *a priori* study by a convolutional neural network (CNN).

However, the full spectrum of interactions between CFD and AI is under investigation at CERFACS, and publications are being prepared in ongoing work on this topic. We are optimistic that this relatively new activity will have much to show in two years time, for the next activity report.

**References**

[2] D. Cardon, J.-P. Cointet, and A. Mazières, (2018), La revanche des neurones, *Réseaux*, 173–220.

[3] I. Goodfellow, Y. Bengio, A. Courville, and Y. Bengio, (2016), *Deep learning*, vol. 1, MIT press Cambridge.

[4] Y. LeCun, Y. Bengio, and G. Hinton, (2015), Deep learning, *nature*, **521**, 436–444.

# Software Engineering for Computational Science

The COOP-CSE subteam supports research with expertise in tools and best computational practices. This is increasingly important for producing high quality and high performance scientific software. One part of the work is the technology survey in a rapidly evolving field to take advantage of new approaches at the right time. In 2020, the team created an open technical blog for easy access to the COOP-CSE work. This format is more cost-effective than presentations or technical reports, since it has a larger impact over time. For the present scientific report, we have chosen from this blog two topics highlighting our research and support activities.

## 7.1 Fortran versus Python

Quite generally, a polarizing debate rages summarized by the question

> Why are more and more time-critical scientific computations formerly performed in Fortran now written in Python, a slower language?

The terms are vague, encouraging unproductive controversies. In COOP-CSE we try to bring the debate to a scientific level with the goal to use the right tool for the right purpose. Python has the reputation of being significantly slower than compiled languages such as Fortran, C, C++, or Rust. A google search “why is python slow” yields heaps of pages on the topic. Python is an *interpreted* language. This implies a significant overhead slowing down massive computations. In this sense, plain Python is much slower than Fortran.

However Python is often used as a *gluing layer*, relying on compiled optimized packages that it strings together to perform the computation. One of the most widespread packages in scientific computing is NumPy. Here, numerical data is manipulated not in plain Python. Behind the scenes all the heavy lifting is done by compiled routines in C/C++ or Fortran. This can decrease the overhead of the interpreted approach by 2 to 3 orders of magnitude, bringing it into the ballpark of compiled approaches. Realistic performance evaluations for scientific computing should therefore be based on this type of approach. In computational practice, Python gains popularity, while Fortran is less and less used, making it also increasingly difficult to find experienced Fortran programmers.

HPC creates specific challenges. In particular, current HPC software relies on a range of approaches, including traditional monolithic compiled codes (mostly in Fortran and C++), code generation approaches (such as domain specific languages, DSLs), and hybrid interpreted/compiled approaches. The latter category includes successful approaches, such as PyFR or FEniCS. We here follow a mixed strategy:

- keeping our Fortran/C++/C flagship codes afloat.
- trying several of these new approaches (*e.g.* Python or DSL based) on practical applications.

We highlight here the different approaches with the experience of rewriting a ten year old software tool originally written in Fortran in Python. The task of the tool is the projection of millions of points to a 3D object represented of by millions of polygons. The compiled legacy code is highly specific and well-validated, but it is quite complex and has therefore become increasingly difficult to maintain. The new

Python version, in contrast, is based on using the data structures of NumPy and pre-existing, optimized functions from e.g. the SciPy package. In particular, efficient KDTree data structures are availabe and are used in the Python version. This simplifies the implementation tremendously and makes the resulting code much easier to maintain. For performance tests, a case with 1 billion cells, 10 million multi-perforated boundary nodes, and 18 thousand perforations was chosen. While the old Fortran version executes this task in 6 hours and 30 minutes, the KDTree-based Python version needs only 4 minutes, leading to a speedup of almost a 100 times faster for an equally accurate result.

An analysis shows that the computational bottleneck of the problem is searching for points in a 3D point cloud. The Fortran version uses a hand coded search in a Fortran array, each individual search costing $O(n)$ operations. The KDTree is a data structure specifically designed to reduce the complexity of such searches to $O(\log(n))$. Clearly, for large $n$, any language-induced execution overhead will be superseded by the reduced complexity of the better algorithm. So, Fortran would likely have been significantly faster if the same algorithm were implemented. However, a tailored implementation of KDTrees in Fortran is beyond what could be realistically achieved in the legacy code.

Summarizing, using a higher level language allows more experimentation with the software. For the initial Fortran version there was no strong incentive to change the implementation fundamentally. Considering the complexity of the code and developer time available, the possible return of investment was too uncertain. Only in the agile Python version has the realization of more advanced computer science technology became a practical option. This balance of programmer productivity versus program efficiency is a recurring theme in software engineering, but may still be undervalued in some of the more conservative scientific computing communities. In traditional scientific computing, there is a tendency to overestimate the importance of low level code efficiency. However, the execution speed of instructions is irrelevant if an inadequate algorithm is used that performs redundant instructions. This is of course obvious, but nevertheless often an obstacle in scientific computing, when a community may not have a systematic computer science training in algorithms and data structures.

## 7.2 Agent Based Modelling and CFD for Covid-19: the Muxu project

This project is motivated by the COVID-19 pandemic. Studies show that aerosols play an important role in the spread of infections, i.e. droplets emitted by people can stay in the air for a long time. In order to reduce the risk, measures can be devised to constrain the mobility of people. The Muxu project is a feasibility study of how aerosol spread can be simulated by coupling agent based modelling (ABM) with fluid dynamics (CFD) software. ABM programs can typically simulate the evacuation of buildings. During evacuation, all agents aim at the exit. They will therefore initially follow different trajectories which will at some point merge and then follow the same path. In our context, we do not model an evacuation scenario, but the circulation of agents in a building. We will use this to study the effect of rules that can be designed to reduce contact between agents.

CROMOSIM is an open-source software for agent based modelling coded in Python. We choose it as basis of the simulations and implement a number of modifications and extensions to turn it into a software to simulate the effect of social distancing measures. In particular, we add the notion of temporary walls and we impose a maximum flow rate of agents at a checkpoint. Additionally we add a “one-way” constraint. Based on this, CROMOSIM can output the positions, speeds, and gradients of agents going from a point A to a point B, thus representing the movement of a crowd of agents in a building. Here we model the CERFACS building with all its offices, patios, and hallways in CROMOSIM.

For the simulation, we need the initialization of agents, definition of groups, and the simulation domain. Other parameters can be chosen to define the movement of the agents, such as the number of agents in a group, departure location, velocity distribution (normal or uniform), coordinates of the initial location, arrival location, and a number of parameters defining agent interaction.

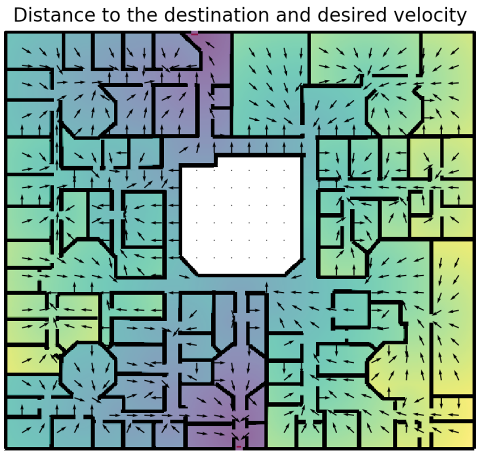


Figure 7.1: Map of CERFACS building with gradient based forces defining the direction to the exit.

The dynamics of the aerosols is simulated with simple CFD software. Here we chose Barbatruc, a CFD package dedicated to training. We realise the coupling by modelling so that each agent is continuously emitting an airborne marker, i.e. aerosols, and that every agent sets the air flow in motion through its drag. The fluid motion will transport the aerosols according to flow created by the agents or the ventilation and air conditioning system (not included in the current results). During the simulation, each agent is exposed to the aerosols exhaled by the other agents. By adding instantaneous expositions during the computation, we obtain *the cross exposition* for each agent in the form of matrix.

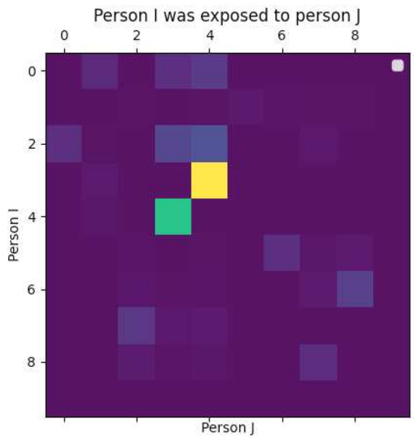


Figure 7.2: The cross exposition matrix for each agent simulated (single simulation)

If we sum the exposition in a row of the matrix, we obtain a quantification of “how much a specific agent was exposed?”. Summing the column, we find “how much a specific agent has exposed others?”. From such a computation, we can identify “super-exposers” and “super-exposed” agents. In other words, this analysis identifies the agents who created the highest risks. By comparing configurations, we can further evaluate which modifications and rules can help to reduce the exposition.
In a particular example, the mean equivalent exposition could be reduced from 0.868 to 0.272. This would mean that the risk is reduced by 70% when specific rules are enforced on the movement of the agents.

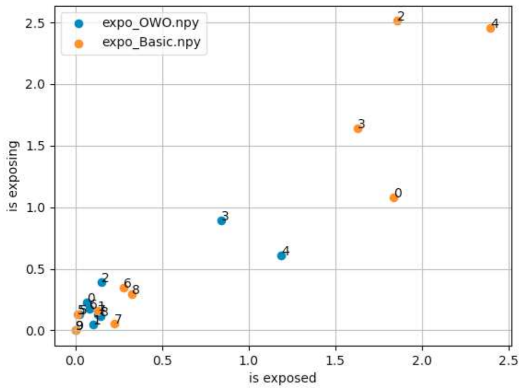


Figure 7.3: Cross exposition scatter plot for the base scenario (orange) and the one-way scenario (blue), Each dot is the exposition received/induced by each agent.

We must note here that the prototype has not been further validated since it serves only as a feasibility study. As such it provides insight into what is possible, but for realistic simulations various extensions and improvements of the model are needed. However, we have already developed techniques that induce fluid motion and model aerosol transport by coupling CFD software to an agent based simulation. Furthermore, practical tools for post-processing of the simulation data have been created.
We expect that a full scale realization of such simulation software could be helpful for private and public enterprises that must implement measures for reducing the risk of infections. Note that the Muxu project initially did not have specific funding. It started as a toy project in summer 2020 driven by current developments. The code volume is remarkably short: only 80 lines (CFD), 46 lines (postprocessing), and 500 lines (agent based modelling).
At the end of 2020, Muxu eventually became a part of the EU Center of Excellence "Excellerat", as example of a "Keystone Application": a light, small scale simulation environment able to attract and let potentials customer try out a simulation workflow without going to the HPC world. Once the test is done, the customer knows what insights he can gain, and ask to a laboratory like CERFACS a higher precision simulation on a fully fledged HPC environment.
Many thanks to B. Maury (ENS Ulm & Univ. Paris-Saclay) and S. Faure (CNRS) for providing the agent-based modelling tool to the community.

# High performance computing

## 8.1 Overview of exascale computing and its relevance to Cerfacs

High performance computing (HPC) has always been an important core activity of CERFACS. HPC activities are strategically distributed among all groups but in coordination with the computer support group (CSG).

HPC activities within the ALGO-COOP team fall strategically into the following three themes:

1. Legacy code optimisation toward exascale
2. Exploring Quantum computing applications to HPC
3. Technology watch on emerging hardware architectures and programming models

## 8.2 Towards exascale computing

Exascale challenges to high performance computing are addressed within the ALGO-COOP team in three broad domains that are summarised below.

### 8.2.1 Hardware or topology awareness computing

This is a key area where we focus on partitioning, optimal load-balancing and problem placement by exploiting the network and hardware hierarchy. This problem is critical for exascale computing where communication and load-imbalance add significantly to the energy cost. We have developed TreePart[ALG12], an open-source hardware-aware partitioning and load-balanced library to address the problem of massive-scale unstructured mesh partitioning and load-balancing. TreePart exploits the hardware hierarchy to avoid communication cost by optimally placing partitions to the given hardware at runtime. Both static and dynamic load-balancing can be achieved using a standalone program or a library API interface akin to ParMetis. It provides shared and distributed communication pathways which fully exploit the topology to choose the most optimal one at runtime using MPI-3 shared memory paradigm. TreePart was successfully coupled to the AVBP solver and excellent speedup was achieved. Large unstructured meshes in excess of 1.4B elements were partitioned online using TreePart, which previously could not be realised in AVBP.

### 8.2.2 Hybrid computing using GPUs

A second challenge in exascale computing is porting or supporting hardware architectures based on accelerators, namely GPUs. Overall 3 out of the top 4 exascale architecture designs are GPU or accelerator based, making hybrid architectures the main-stream solution for the Exascale era. Keeping this in mind, the AVBP solver is being ported to GPUs using directive-based parallelisation using OpenACC. This work is conducted in collaboration with IDRIS, HPE and IBM. A first release of AVBP (v7.7 septembre 2020) has

been published supporting simple academic gaseous cases on GPUs with an acceleration of the order of 2 (full CPU node versus full GPU node). Further optimisation and porting activities are under way.
Addtionally, graph colouring (distance-2 and partial-distance-2) algorithms were implemented in TreePart to remove data-race in threaded applications. A lock-free OpenMP+MPI version of AVBP solver was also implemented as part of the H2020 EPEEC project using this colouring interface allowing for hybrid execution.

### 8.2.3 Parallel unstructured mesh adaption

The third area is the development of a parallel mesh adaptation framework. Mesh generation at the exascale level can no longer be a manual process and requires specialised automated tools. The basic idea here is to begin the simulation using a coarse mesh and use adaptation to distribute or add degrees-of-freedom in order to meet a required error estimate in some desired quantity of interest. We exploited the hardware-aware load-balancing infrastructure of TreePart and built a generic adaptation framework that piggybacks any serial mesh adaptation tool on top to realise a massively-parallel online mesh adaptation tool: TreeAdapt. Presently we have demonstrated the framework by coupling it with the MMG3D serial adaptation tool scaling up to 1.4B meshes on 4K MPI ranks. In this case, the mesh adaptation framework allowed for a 5000 times speedup compared to the existing sequential meshing tool. Currently we are coupling the TreeAdapt infrastructure to the AVBP solver to enable runtime mesh adaptation in the near future.

## 8.3 Quantum Computing

Quantum computing has attracted tremendous interest recently due to the availability of quantum emulators and the public access to real quantum hardware. Ensuing a technology watch project in this area, A. Suau a Phd student at CERFACS started his thesis work on numerical methods using quantum computing at the end of 2019. During the year his research activity focused on the application and development of Variational Quantum Linear Solver (VQLS). VQLS is a variational algorithm used to solve linear system of equations on a quantum computer. In fact most scientific problems can be reformulated into solving a linear system of equations. Therefore it is of particular interest due to the widespread use of linear solvers in scientific computing. The goal of this research was to explore one of the possible paths for solving Partial Differential Equation (PDE): can we use the VQLS algorithm along with some well-known classical discretisation techniques to solve efficiently a PDE? This is still a work in progress and we anticipate a publication in Q2 2021. Another area A. Suau is currently working on is the quantum compilation process. This topic is of considerable interest to software library developers and hardware designers. Improvements to the quantum compilation is most significant because it can potentially improve the overall performance of a quantum circuit. The outcomes of our research in quantum computing have materialised into three journal articles [ALG33, ALG59, ALG53].

## 8.4 Technology Watch

Our current technology watch is carried out in close collaboration with the CSG. Presently we are exploring alternative processor architectures to Intel x86, namely the AMD and ARM processors. Access to these systems was possible through the bilateral collaborations with Cellule de Veille technologique de GENCI and CERFACS. The main highlight in 2020 has been the porting and optimisation of the AVBP code to the AMD Epyc 2 platform. This allows CERFACS to exploit the IRENE AMD HPC system from PRACE/GENCI at TGCC. We achieved excellent performance up to 132k cores. Similar results were obtained on the AMD HPC cluster at Méteo France and HLRS.

Our initial experiences with porting to ARM processors shows a clear potential but further research is warranted to understand and fully exploit these new processor architecture. This will be made possible with access to the new A64FX system at TGCC from the cellule de veille technologique in early 2021.
Lastly our main technology watch activity in 2020 revolved around GP-GPU based accelerator architectures (focused on NVIDIA V100 cards). We are extending the technology watch by testing the newer A100 architecture as well as AMD accelerators in 2021.

# Publications

## 9.1 Books

[ALG1] F. Chatelin, (2019), *Experimental Architecture: designing the unknown*, Routledge.

## 9.2 Conferences Proceedings

[ALG2] S. Bauer, H.-p. Bunge, D. Drzisga, S. Ghelichkhan, M. Huber, N. Kohl, M. Mohr, U. Rüde, D. Thoennes, and B. Wohlmuth, (2020), TerraNeo—Mantle Convection Beyond a Trillion Degrees of Freedom, In *Software for Exascale Computing - SPPEXA 2016-2019*, vol. 136 of LNCSE, Lecture Notes in Computational Science and Engineering 136, Springer, 569–610.

[ALG3] M. Bauer, B. Nestler, U. Rüde, J. Hötzer, D. Ernst, J. Hammer, M. Seiz, H. Hierl, J. Hönig, H. Köstler, and et al., (2019), Code generation for massively parallel phase-field simulations, *Proceedings of the International Conference for High Performance Computing, Networking, Storage and Analysis on - SC '19*.

[ALG4] I. Duff, P. Leleux, D. Ruiz, and S. Torun, (2020), Improving the scalability of the ABCD Solver with a combination of new load balancing and communication minimization techniques, In *Parallel Computing: Technology Trends*, F. et al. (Eds.), ed., vol. 36, Prague, Czech Republic, The International Conference on Parallel Computing ParCo 2019, IOS Press Ebooks, 277 – 286.

[ALG5] A. Dumitrasc, P. Leleux, and U. Rüde, (2019), Block partitioning of sparse rectangular matrices, *PAMM*, **19**, e201900287.

[ALG6] A. Gazaix, F. Gallard, V. Ambert, D. Guénot, M. Hamadi, S. Grihon, P. Sarouille, T. Druot, J. Brézillon, V. Gachelin, J. Plakoo, N. Desfachelles, N. Bartoli, T. Lefebvre, S. Gûrol, B. Pauwels, C. Vanaret, and R. Lafage, (2019), Industrial Application of an Advanced Bi-level MDO Formulation to Aircraft Engine Pylon Optimization, In *AIAA 2019-3109*, Dallas, Texas, AIAA Aviation 2019 Forum.

[ALG7] M. Huber, N. Kohl, P. Leleux, U. Rüde, D. Thönnes, and B. Wohlmuth, (2020), Massively Parallel Multigrid with Direct Coarse Grid Solversv, In *NIC Symposium 2020*, A. T. Marcus Müller, Kurt Binder, ed., vol. 50 of NIC Series, Jûlich, Germany, John von Neumann Institute for Computing (NIC), 335–344.

[ALG8] C. Kruse, M. Sosonkina, M. Arioli, N. Tardieu, and U. Rüde, (2020), Parallel Performance of an Iterative Solver Based on the Golub-Kahan Bidiagonalization, In *Parallel Processing and Applied Mathematics*, R. W. D. D. Karczewski, ed., vol. 12043, Bialystok, Poland, PPAM 2019 - 13th INTERNATIONAL CONFERENCE ON PARALLEL PROCESSING AND APPLIED MATHEMATICS, Springer, 104–116.

[ALG9] C. J. Lapeyre, N. Cazard, P. T. Roy, S. Ricci, and F. Zaoui, (2020), Reconstruction of hydraulic data by machine learning, In *Advances in Hydroinformatics*, Springer, 701–715.

[ALG10] C. Lapeyre, A. Misdariis, N. Cazard, V. Xing, D. Veynante, and T. Poinsot, (2019), A convolutional neural network-based efficiency function for sub-grid flame-turbulence interaction in LES, In *17th International Conference on Numerical Combustion*, Aachen (Germany).

[ALG11] L. Le Gorrec, S. Mouysset, I. Duff, P. Knight, and D. Ruiz, (2019), Uncovering hidden block structure for clustering, Würzburg, Germany, ECMLPKDD.

[ALG12] P. Mohanamuraly and G. Staffelbach, (2020), Hardware Locality-Aware Partitioning and Dynamic Load-Balancing of Unstructured Meshes for Large-Scale Scientific Applications, In *PASC '20: Platform for Advanced Scientific Computing Conference Geneva Switzerland June, 2020*, vol. 7, PASC '20: Platform for Advanced Scientific Computing Conference Geneva Switzerland June, 2020, Association for Computing Machinery - New York - United States, 1–10.

[ALG13] P. Mycek and M. De Lozzo, (2019), Multilevel Monte Carlo estimation of Sobol' indices for sensitivity analysis, In *Uncertainty Quantification & Optimization Conference (UQOP)*, Sorbonne University , Paris, France, UQOP 2019.

[ALG14] U. Rüde, (2020), Massively Parallel Lattice Boltzmann Methods for Suspensions with Geometrically Resolved Particles, In *Séminaire sur LA MECANIQUE DES FLUIDES NUMERIQUE 2020*, Paris, Parallel LBM for suspensions.

[ALG15] U. Rüde, (2020), Matrix-free multigrid for extreme scale computing, The Pennsylvania State University, USA, Penn State Computational and Applied Mathematics Colloquium.

[ALG16] U. Rüde, (2020), Solvers for Extreme Scale Computing, In *Mathematisches Kolloquium Uni Bayreuth*.

[ALG17] U. Rüde, (2020), waLBerla - Towards extreme scale multiphysics simulations, In *Excalibur SLE Exascale Computing for System-Level Engineering*.

[ALG18] T. Sengupta, S. Sengupta, and P. Sundaram, (2020), Dynamical System Theory of Flow Instability Using the Impulse and the Frequency Response Approaches, In *Mathematical Modeling and Computational Tools*, P. in Mathematics & Statistics, ed., vol. 320, Singapore, International Conference on Applied and Computational Mathematics ICACM 2018, Springer, Singapore, 151–169.

[ALG19] N. Venkovic, P. Mycek, L. Giraud, and O. Le Maître, (2019), Recycling Krylov subspace strategies to solve stochastic elliptic equations, In *Uncertainty Quantification & Optimization Conference (UQOP)*, UQOP 2019.

## 9.3 Journal Publications

[ALG20] H. Barucq, F. M'Barek, C. Kruse, and S. Tordeux, (2019), Sparsified discrete wave problem involving a radiation condition on a prolate spheroidal surface, *IMA Journal of Numerical Analysis*.

[ALG21] M. Bauer, S. Eibl, C. Godenschwager, N. Kohl, M. Kuron, C. Rettinger, F. Schornbaum, C. Schwarzmeier, D. Thönnes, H. Köstler, and U. Rüde, (2020), waLBerla: A block-structured high-performance framework for multiphysics simulations, *Computers and Mathematics with Applications*.

[ALG22] S. Bauer, M. Huber, S. Ghelichkhan, M. Mohr, U. Rüde, and B. Wohlmuth, (2019), Large-scale simulation of mantle convection based on a new matrix-free approach, *Journal of Computational Science*, **31**, 60–76.

[ALG23] M. Bauer, H. Kostler, and U. Rüde, (2020), lbmpy: A flexible code generation toolkit for highly efficient lattice Boltzmann simulations.

[ALG24] M. Bauer, H. Kostler, and U. Rüde, (2020), lbmpy: Automatic code generation for efficient parallel lattice Boltzmann methods, *Journal of Computational Science*.

[ALG25] M. Bauer, G. Silva, and U. Rüde, (2020), Truncation errors of the D3Q19 lattice model for the lattice Boltzmann method, *Journal of Computational Physics*, **405**.

[ALG26] P. Boudier, A. Fillion, S. Gratton, and S. Gürol, (2020), DAN – An optimal Data Assimilation framework based on machine learning Recurrent Networks.

[ALG27] A. Buttari, M. Huber, P. Leleux, T. Mary, U. Rüde, and B. Wohlmuth, (2020), Block Low Rank Single Precision Coarse Grid Solvers for Extreme Scale Multigrid Methods.

[ALG28] S. Cayrols, I. Duff, and F. Lopez, (2020), Parallelization of the solve phase in a task-based Cholesky solver using a sequential task flow model, *International Journal of High Performance Computing Applications*, **34**, 340–356.

[ALG29] S. Cayrols, I. Duff, and F. Lopez, (2020), Parallelization of the solve phase in a task-based Cholesky solver using a sequential task flow model, *International Journal of High Performance Computing Applications*, **34**, 340–356.

[ALG30] V. Darrigrand, D. Pardo, T. Chaumont-Frelet, I. Gomez Revuelto, and L. Garcia Castillo, (2020), A painless automatic hp-adaptive strategy for elliptic problems, *Finite Elements in Analysis and Design*, **178**.

[ALG31] T. Davis, I. Duff, and S. Nakov, (2020), Design and Implementation of a Parallel markowitz Threshold Algorithm, *SIAM Journal on Matrix Analysis and Applications*, **41**, 573–590.

[ALG32] I. Duff, J. Hogg, and F. Lopez, (2020), A New Sparse Symmetric Indefinite Solver Using A Posteriori Threshold Pivoting, *SIAM Journal on Scientific Computing*, **42**, C23–C42.

[ALG33] S. Dutta, A. Suau, S. Dutta, S. Roy, B. Behera, and P. Panigrahi, (2020), Quantum circuit design methodology for multiple linear regression, *IET Quantum Communication*, **1**, 55 – 61.

[ALG34] S. Eibl and U. Rüde, (2019), A systematic comparison of runtime load balancing algorithms for massively parallel rigid particle dynamics, *Computer Physics Communications*, **244**, 76–85.

[ALG35] A. Fillion, M. Bocquet, S. Gratton, S. Gürol, and P. Sakov, (2020), An Iterative Ensemble Kalman Smoother in Presence of Additive Model Error, *SIAM/ASA Journal on Uncertainty Quantification*, **8**, 198–228.

[ALG36] O. Guillet, A. Weaver, X. Vasseur, Y. Michel, S. Gratton, and S. Gürol, (2019), Modelling spatially correlated observation errors in variational data assimilation using a diffusion operator on an unstructured mesh, *Quarterly Journal of the Royal Meteorological Society*, **145**, 1947–1967.

[ALG37] M. Huber, U. Rüde, and B. Wohlmuth, (2019), Adaptive control in roll-forward recovery for extreme scale multigrid, *International Journal of High Performance Computing Applications*, **33**, 817–837.

[ALG38] A. Klawonn, M. Kühn, and O. Rheinbach, (2019), Parallel adaptive FETI-DP using lightweight asynchronous dynamic load balancing, *International Journal for Numerical Methods in Engineering*, **121**, 621–643.

[ALG39] N. Kohl and U. Rüde, (2020), Textbook efficiency: massively parallel matrix-free multigrid for the Stokes system.

[ALG40] N. Kohl, J. Hötzer, F. Schornbaum, M. Bauer, C. Godenschwager, H. Köstler, B. Nestler, and U. Rüde, (2019), A scalable and extensible checkpointing scheme for massively parallel simulations, *International Journal of High Performance Computing Applications*, **33**, 571–589.

[ALG41] C. Kruse, V. Darrigrand, N. Tardieu, M. Arioli, and U. Rüde, (2020), Application of an iterative Golub-Kahan algorithm to structural mechanics problems with multi-point constraints, *Advanced Modeling and Simulation in Engineering Sciences*, **7**, 1–20.

[ALG42] C. Kruse, M. Sosonkina, M. Arioli, N. Tardieu, and U. Rüde, (2020), Parallel solution of saddle point systems with nested iterative solvers based on the Golub-Kahan Bidiagonalization, *Concurrency and computation-Practice and Experience*.

[ALG43] M. Kühn, C. Kruse, and U. Rüde, (2020), Energy-minimizing, symmetric finite differences for anisotropic meshes and energy functional extrapolation.

[ALG44] M. Kühn, C. Kruse, and U. Rüde, (2020), Implicitly extrapolated geometric multigrid on disk-like domains for the gyrokinetic Poisson equation from fusion plasma applications.

[ALG45] P. Laloyaux, M. Bonavita, M. Chrust, and S. Gürol, (2020), Exploring the potential and limitations of of weak constraint 4D Var, *Quarterly Journal of the Royal Meteorological Society*, **146**, 4067–4082.

[ALG46] C. Lapeyre, A. Misdariis, N. Cazard, D. Veynante, and T. Poinsot, (2019), Training convolutional neural networks to estimate turbulent sub-grid scale reaction rates, *Combustion and Flame*, **203**, 255–264.

[ALG47] C. J. Lapeyre, A. Misdariis, N. Cazard, D. Veynante, and T. Poinsot, (2019), Training convolutional neural networks to estimate turbulent sub-grid scale reaction rates, *Combustion and Flame*, **203**, 255–264.

[ALG48] P. Matalon, P. Mycek, U. Rüde, D. Di Pietro, F. Hülsemann, and D. Ruiz, (2020), An h-Multigrid method for Hybrid High-Order discretizations.

[ALG49] F. Mercier, Y. Michel, T. Montmerle, P. Jolivet, and S. Gürol, (2019), Speeding up the ensemble data assimilation system of the limited-area model of Météo-France using a block Krylov algorithm, *Quarterly Journal of the Royal Meteorological Society*, **145**, 910–929.

[ALG50] P. Mohanamuraly and J. Müller, (2020), An Adjoint assisted Multilevel Multifidelity Method for Uncertainty Quantification And Its Application To Turbomachinery Manufacturing Variability, *International Journal for Numerical Methods in Engineering*.

[ALG51] A. Moore, M. Martin, S. Akella, H. Arango, M. Balmaseda, L. Bertino, S. Ciavatta, B. Cornuelle, J. Cummings, S. Frolov, P. Lermusiaux, P. Oddo, P. Oke, A. Storto, A. Teruzzi, A. Vidard, and A. Weaver, (2019), Synthesis of Ocean Observations Using Data Assimilation for Operational, Real-Time and Reanalysis Systems: A More Complete Picture of the State of the Ocean, *Frontiers in Marine Science*, **6**, 90.

[ALG52] P. Mycek and M. De Lozzo, (2019), Multilevel Monte Carlo Covariance Estimation for the Computation of Sobol' Indices, *SIAM/ASA Journal on Uncertainty Quantification*, **7**, 1323–1348.

[ALG53] S. NIU, A. Suau, G. Staffelbach, and A. Todri-Sanial, (2020), A Hardware-Aware Heuristic for the Qubit Mapping Problem in the NISQ Era, *IEEE Transactions on Quantum Engineering*.

[ALG54] C. Rettinger and U. Rüde, (2019), Dynamic Load Balancing Techniques for Particulate Flow Simulations, *Computation*, **7**, 9.

[ALG55] C. Rettinger and U. Rüde, (2020), An efficient four-way coupled lattice Boltzmann-discrete element method for fully resolved simulations of particle-laden flows, *Journal of Computational Physics*.

[ALG56] U. Rüde, (2019), Mehrgittermethode: Grundlage der computergestützten Wissenschaften, *Informatik Spektrum*, **42**, 138–143.

[ALG57] I. Rybak, C. Schwarzmeier, E. Eggenweiler, and U. Rüde, (2020), Validation and calibration of coupled porous-medium and free-flow problems using pore-scale resolved models, *Computational Geosciences*.

[ALG58] S. Sengupta, T. Sengupta, J. Puttam, and S. Vajjala, (2020), Global spectral analysis for convection-diffusion-reaction equation in one and two-dimensions: Effects of numerical anti-diffusion and dispersion, *Journal of Computational Physics*, **408**.

[ALG59] A. Suau, G. Staffelbach, and H. Calandra, (2020), Practical Quantum Computing: solving the wave equation using a quantum approach. Accepted in ACM TQC, waiting for publication.

[ALG60] A. Weaver, M. Chrust, B. Ménétrier, and A. Piacentini, (2020), An evaluation of methods for normalizing diffusion-based covariance operators in variational data assimilation, *Quarterly Journal of the Royal Meteorological Society*.

## 9.4 Technical Reports

[ALG61] S. Cayrols, I. Duff, and F. Lopez, (2020), Parallelization of the solve phase in a task-based Cholesky solver using a sequential task flow model, working note, RAL-TR-2018-008.

[ALG62] A. Cellier, (2020), Detection and Identification of Instability and Blow-off/Flashback Precursors in Aeronautical Engines using Deep Learning techniques, working note, Cerfacs.

[ALG63] I. Khalfaoui-Hassani, P. Leleux, and D. Ruiz, (2020), Internship report: The Column Block Cimmino Method, technical report, CERFACS, 42 avenue Gaspard Coriolis, 31057 Toulouse Cedex 1.

[ALG64] A. Patil, (2019), Development of Deep Learning Methods for Inflow Turbulence Generation, working note, Cerfacs.

[ALG65] N. Venkovic, P. Mycek, L. Giraud, and O. Le Maître, (2020), Comparative study of harmonic and Rayleigh-Ritz procedures with applications to deflated conjugate gradients, technical report, CERFACS, 42 Avenue G. Coriolis, 31057 Toulouse Cedex 1, France.

## 9.5 Thesis

[ALG66] A. Fillion, (2019), *Ensemble variational methods and variational optimization for the geosciences*, phd thesis, Ecole Doctorale SIE - Université Paris Est.

[ALG67] O. Guillet, (2019), *Modelling spatially correlated observation errors in varational data assimilation on unstructured meshes. Modelling spatially correlated observation errors in varational data assimilation on unstructured meshes*, phd thesis, Université de Toulouse - Ecole Doctorale : SDU2E.

[ALG68] J. Latre, (2019), *Hypercomplex algebras for Computation*, phd thesis, Université de Toulouse - Ecole Doctorale : MITT.

# 2

# Climate and Environment

# Introduction

## 1.1 Climate Modeling

Five research axes constitute the “Climate Modeling” chapter, leading to a high rate of publications.

The “Decadal variability and predictability” axis strongly contributes to the “Decadal Climate Prediction Project” (DCPP) of the “Coupled Model Intercomparison Project (Phase 6)” (CMIP6) in the framework of the “World Climate Research Program” (WCRP). European projects such as PRIMAVERA and collaborations with Cerfacs partners, such a CNRM or EDF, have enabled the contribution of several PhD thesis and numerous publications in high level international journals. Improvements of skillful decadal predictions have been performed with a focus in societal relevant variables such as living marine resources. In collaboration with CNRM, strong efforts have led to a new prediction system at seasonal and decadal scales.

This axis is strongly connected with the “Attribution of regional climate changes”, with a focus, during this report period, on winter rainfall trends and sea ice decline in the Northern hemisphere. Various methods such as “dynamical adjustment”, idealized simulation or partial-coupling experiments are used to untangle the respective roles of the natural climate variability and both anthropogenic and natural external forcing. Significant results have been published such asymmetric responses of the Northern hemisphere or the strengthening of teleconnections due to warming.

High performance computing is at the heart of the “Climate change and impacts” axis, with resolution pushed to its limits for both global (GCMs) and regional (RCMs) climate models. A series of comparison between the projections produced by both type of models has provided fruitful insight in their sensitivity to parameters such as solar radiation of aerosols. It has been shown, among other effects, that higher resolutions leads to an intensification of extremes events such as precipitations. The impact of climate changes on aviation enters in this axis for the present report period and will become an important axis in the future, shared with the CFD team.

Methods involved in the above axes, such as the dynamical adjustment approach and sensitivity to model resolutions, have been used the “Sea ice variability” axis. Beyond the amplified pole warming induced by a likely strong sea ice decline in the next decades, other significant climate impacts have been identified, such as shifts of the subpolar jet or modification of the ocean variability. The comparison of the seasonal prediction between a perfect and an operational model opens doors for improvements of Arctic sea ice predictions.

Following the increase in computer power, the increase the model resolution is also feeding progress for the “Air-sea interaction” axis. In the continuation of highly visible previous studies, further identification of climate model biases has been made through the ocean and atmosphere coupling of mesoscale structures. Incorrect surface winds and heat fluxes lead to biased oceanic upwelling while oceanic mesoscale structures misrepresentation influence large scale atmospheric circulation over Europe.

## 1.2 Environmental Systems

The ”Environmental Systems” chapter gathers various research and development activities mixing high-fidelity numerical simulations and methodologies such as data assimilation, uncertainty quantification or high performance computing, with applications such as air quality, atmospheric chemistry, wildland fire, hydrodynamics and oceanography.

Satellites assimilation gained an important role in the forecast and reanalysis of the atmospheric composition. We made significant progress in the direct assimilation of satellite radiances from infrared and UV sounders. In this report we summarize results with respect to ozone analyses using Metop instruments (IASI and GOME-2).

Large-eddy simulations using several micro-scale models have been used to simulate the atmospheric dispersion of pollutants in various configurations: benchmarking of several models compared to a reference field-scale experiment, urban canopy strongly influenced by inflow conditions, or dispersion of chemical species in a fictive airport. Numerical and methodological developments such as immersed boundary method or surrogate models have been achieved for these applications.

Several data-driven modeling methods have been designed and applied to wildland fire behavior modeling to design reanalysis of fire events validated against controlled burn experiments: assimilation of front data with metrics used in image-processing, combination of state and parameter estimations, uncertainty quantification to analyze model dependency, sensitivity analysis to reduce the control space, use of surrogate models or fire and atmosphere models coupling.

Flood forecasting research activities benefit from studies in sensitivity analysis to identify and classify major sources of uncertainties that are then reduced with ensemble data assimilation, making the most of in-situ and remote sensing observations. Major efforts were invested in preliminary studies for SWOT mission that will be launched in 2022 and in the development of ensemble uncertainty quantification (including surrogate modeling) and data assimilation algorithms for 1D and 2D hydrodynamics models. Multi-physics modeling and machine learning strategies were also investigated in order to increase forecast lead time for operational purposes.

Progress has been made in global ocean data assimilation through developments in the representation of background-error covariances using an Ensemble of Data Assimilations (EDA). In this report we describe a specific aspect of this work, which is to develop computationally efficient methods to account for flow-dependent vertical correlations. This work has important implications for improving the assimilation of surface observations such as SST.

In the final section, we describe some broader developments in data assimilation methodology. This work addresses the modelling of spatially correlated observation error in variational data assimilation, and the representation of model error in weakly constrained versions of 4D-Var and the IEnKS.

## 1.3 Coupling, HPC and Data for Climate

The “Coupling, HPC and Data for Climate” chapter gathers coupler developments, coupling methods implementation for various application and advanced expertise on scientific computing.

The development of two couplers, OpenPALM and OASIS3-MCT, have been pursued with complementary purposes and mutual enrichment. A strong collaboration with ONERA has led to the integration of the CWIPI library in the OpenPALM coupler. Cerfacs has also participated to the development of the CWIPI, which provides high order interpolations and fully parallel communications for mesh-based coupling. OpenPALM has been used in a large variety of applications ranging from groundwater modeling to multi-physics and multi-components CFD applications. In strong interaction with the Earth modeling community, the OASIS3-MCT coupler development team has be reinforced thanks to various projects at national and European levels. Significant improvements of the software have been achieved, from the reduction of interpolation computer time with better conservation properties to software layers to address wider communities.

In addition to these tool developments, innovations in the choice and implementation of coupling methods have been provided for various applications. The use of Schwarz iterations in the ocean atmosphere coupling has proved to improve the diurnal cycle for coupling steps as high as a half day. This same algorithm has also been implemented for the coupling of 1D and 2D river hydrodynamics modeling, in the context of floodplains dynamics. A tight collaboration with EDF on this topic has played a significative role in this works and widened the range of potential applications. Significant computer time reductions have been achieved for CFD applications through the coupling of solver with different time steps. The validity of such Local Time Stepping (LTS) have been assessed with test cases such as the convection of a vortex through domains of different grid sizes.

Cerfacs expertise on the use of supercomputer are motived by the needs of the various applications detailed above. With the increase of the resolution of the climate models, new optimizations are necessary to reduce the computing time. Significant improvements have been obtained by separating components, such as the sea-ice and ocean models, and coupling them with the OASIS coupler. The huge amount of data produced through ensemble climate simulation, involves specific skills for data processing. The reduction from PetaBytes to TerraBytes scales of these data, to be published on public portal, requires the development of robust data management workflow. In addition to the production of the large and valuable results of climate simulation, Cerfacs strongly contributes the development of data infrastructures at the European and international level. Among other significant contributions, optimized software packages to compute climate indices have been integrated in these data infrastructures and contribute to the international outreach of Cerfacs.

# Climate Modeling

## 2.1 Introduction

Research activities are presented through five axes: Decadal variability and predictability, Attribution of regional climate changes, Climate change and Impacts, Predicting sea ice variability and changes and their impact on the climate system, Air-sea interaction and climate model biases. They cover a wide range of spatial and temporal scales, from short extreme events to century long changes, and from small-scale interaction involving ocean eddies to planetary scales. They also focus on various geographical domains, from the tropics to polar regions and almost always involve coupling between different components of the Earth climate system.

## 2.2 Decadal variability and predictability

The importance for many societal applications of improved information about near-term (from one year to a decade in advance) climate evolution at regional scale has prompted a sustained research effort in the field of decadal climate variability, predictability and prediction [4]. Cerfacs has played a leading role in the definition of the CMIP6 DCPP-C sensitivity ensemble experiments designed to specifically investigate the ocean-land and ocean inter-basin teleconnections associated with the Pacific Decadal variability (PDV) and the Atlantic Multidecadal Variability (AMV) [3]. The protocol consists in restoring the North Atlantic Sea Surface Temperature (SST) to observed anomalies representative of the two AMV or PDV phases. During the past 2 years, Cerfacs has analyzed the outcome of those experiments in a multi-model framework focusing on North Atlantic stormtracks in winter [CE111] and European heatwaves in summer [CE104]. In addition to CMIP6, in order to evaluate the sensitivity of the AMV magnitude, large ensembles of simulations have been carried out by multiplying targeted SST anomalies by 2 and 3. The AMV atmospheric teleconnection over Europe have been analyzed during the PhD of S. Qasmi and it is shown that while pattern-scaling is a valid hypothesis to evaluate the summer AMV-forced response in terms of temperature and precipitation over Europe, it is clearly not the case in winter [CE103]. Sensitivity of the AMV-induced teleconnection to models resolution has been assessed within PRIMAVERA. Twin experiments have been conducted with CNRM-CM6.1-HR and compared to standard resolution simulations. Evidence is provided that increasing the horizontal resolution does not significantly change the overall response of the model, except in the deep tropics with enhanced displacement of the InterTropical Convergence Zone in response to SST anomalies in the tropical Atlantic (Hodson et al. submitted). In parallel, studies have been continued to better understand the physical origins of the modes of variability at decadal timescale, with a special focus on the low-frequency relationship between the Pacific and the Atlantic basins [CE67] and the role of anthropogenic aerosols and Atlantic Meridional Overturning Circulation (AMOC) to set the cold phase of the AMV observed in the 1960-1990s [CE95].
As part of the Cerfacs-EDF PREVINTEP project aiming at better evaluating and understanding the range of climate future outcomes at near term over Europe, we have produced a set of large ensembles (30 members) for the four CMIP6 representative ssp scenarios over the 2015-2040 period. This allows to discriminate the uncertainties associated with the forcing (dependence of scenario) from the one due to internal climate variability (dependence on members). Preliminary analyses show that temperature continues to rise over Europe by about 1 degree on average compared to the 1995-2014 historical period, with scenario sensitivity

in the order of 0.1-0.3 degrees depending on regions and seasons. The weight of internal variability versus forced response remains high in winter, without clear emergence for temperature and precipitation as opposed to summertime, especially along the European Mediterranean Coast. We applied the so-called storyline framework to partition the full range of internal variability into four classes depending on drivers known to affect the climate over Europe. We show that reduced warming in the future is associated with stronger decline of the Atin response to anthropogenic forcing combined with persistent negative phases of the North Atlantic Oscillation (Line et al. 2020 in prep). This work has been carried out as part of A. Line PhD, which started in Nov. 2019.
While skillful predictions of societal relevant variables like temperature and rainfall over land remain limited to few areas at decadal time scale, recent improvements in global dynamical climate prediction systems have lead to enhanced predictability of variables that are relevant for living marine resources, with strong implications for fisheries for instance. In this context, Cerfacs is involved in the H2020-TRIATLAS project running over 2019-2022, which aims at providing seamless seasonal-to-decadal predictions and scenario simulations over the entire Atlantic ocean using state-of-the-art Earth system models (ESMs), with a special focus on relevant climate, marine ecosystems and fisheries variables as inputs for End-to-End marine ecosystem models (MEMs). During the last two years period, considerable effort has been made in collaboration with CNRM/GMGEC to develop a new seasonal-to-decadal (s2d) prediction system based on the CNRM-ESM2.1 Earth system model model. Through targeted sensitivity experiments, we have explored several ways to initialise the different components of the models with the ultimate goal to minimise the initial shock and drift in the climate predictions. For that, several initialisation tests have been performed to build the optimal s2d prediction platform. We plan to start the production of the seasonal and decadal predictions at the beginning of 2021. The decadal predictions performed within the TRIATLAS project are compliant with the so-called DCPP-A protocol and will feed the CMIP6 decadal forecast database as the contribution of the CNRM-CERFACS modelling group.
Work has been pursued to better understand the pronounced multidecadal variations in river flows observed in France since the late 19th century [2]. Hydrometeorological reconstructions on the Seine basin beginning in the middle of the 19th century have been produced based on a statistical downscaling method developed at Cerfacs, which combines atmospheric reanalysis and in-situ observations to produce meteorological forcings as input for hydrological models [CE64]. Results suggest that most of the observed variability at decadal timescale for the Seine river basin is attributable to internal climate variability and not anthropogenic factors.

## 2.3 Attribution of regional climate changes

Regional-scale attribution is defined as the process of evaluating the relative contributions of multiple causal factors (or drivers) to a continental or regional climate change. Note that this definition slightly differs from the usual definition of attribution used in the detection and attribution community. In particular, the preliminary detection step is not required to perform attribution since causal factors may also include drivers of internal variability, such as the Atlantic and Pacific multidecadal variability (AMV and PDV) among many others, in addition to external natural and anthropogenic forcing. During the 2019-2020 period, the focus has been on Northern hemisphere winter precipitation trends at mid-to-high latitudes and contribution of the AMV to the recent Arctic sea ice decline.

Detecting and attributing a human influence on observed rainfall trends is a major challenge due to the presence of large amplitude internal variability on all time scales and by limited temporal and spatial observational data coverage. Attribution of precipitation changes is also limited by model errors regarding the representation of key processes of the hydrological cycle. Previous studies have attempted to detect anthropogenic signals in the observed record by using zonal mean precipitation averaged over large latitude bands rather than full two-dimensional continental or regional fields. We have applied a “dynamical adjustment” methodology [6] to observed monthly precipitation data sets to estimate an anthropogenic influence on long-term (1920–2015) precipitation trends over North America and Eurasia during winter (November–March) [CE81]. The dynamical adjustment approach aims to remove mean atmospheric circulation influences from precipitation interannual variability and trends, thereby revealing the thermodynamically-induced component as a residual. The geographical pattern and amplitude of this observed thermodynamic residual precipitation trend are in good agreement with anthropogenically forced trends obtained from ensembles of historical climate model simulations. Such consistency helps to reconcile observations and models and provides compelling evidence for a human influence on century-scale precipitation trends over North America and Eurasia during the cold season. While there is strong evidence of a key role of anthropogenic forcing on Arctic sea ice decline, the possible role of internal variability has not been robustly quantified. Based on partial-coupling experiments with three climate models, we have shown that the atmospheric teleconnections resulting from a phase shift to positive AMV can lead to a decadal ice thinning trend in the Arctic Ocean on the order of 8–16 percent of the reconstructed long-term trend, and a decadal trend (decline) in September Arctic sea ice area of up to 21 percent of the observed long-term trend [CE68]. However, in order to claim a key influence from internal variability in Arctic sea ice decline, it remains to quantify whether the recent AMV time evolution is mainly due to internal variability or if it has been largely influenced by external forcing [CE95].

Another potential difficulty in attribution studies is the possible interaction between the response to external forcing and internal variability. This question can be tackled from two opposite but complementary viewpoints. The first one is to ask whether the forced response can depend on the phase of low-frequency climate modes such as the PDV and AMV. The second is to ask whether the forced response can modify some aspects of internal variability (spatial patterns, frequency spectrum, teleconnections, ...). Regarding the first viewpoint, we have used a set of idealized simulations to study the sensitivity of the response to greenhouse gas (GHG) and aerosol forcings to the phase of the AMV in the initial oceanic conditions [CE85]. We have shown that the Northern hemisphere response to forcing is asymmetric, with western Eurasia warming 20–30 percent more, and North America and the extratropical North Pacific warming 20–30 percent less, in positive AMV than in negative AMV phase. This asymmetry can be explained by the atmospheric response to differences in the initial sea ice concentration in the Atlantic Arctic sector, and by a large-scale atmospheric teleconnection pattern originating in the tropical Indo-Pacific.
With regard to the second viewpoint, we have used a set of sensitivity experiments based on partial coupling simulations to study changes in El Nino Southern Oscillation (ENSO) remote influence in a much warmer climate (end of 21st century following GHG scenario RCP8.5) compared to a pre-industrial period [CE71]. A substantial sensitivity to the mean state is found over the North Atlantic due to a strengthening of the ENSO–North Atlantic Oscillation (NAO) teleconnection in a warmer world. A stronger and eastward-extended mean upper-level jet over the North Pacific and an eastward-shifted ENSO teleconnection over the North Pacific contribute to a better inflow of synoptic storms coming from the Pacific into the Atlantic. This downstream penetration into the North Atlantic basin favors more systematically the NAO circulation pattern. This influence is more active for cold phases of ENSO, enhancing the occurrence of NAO positive phase.

## 2.4 Climate change and Impacts

Never before have so many large ensembles of climate projections, with a great variety of configurations (global climate models, high resolution global climate models, Earth System Model, regional climate models, convective permitting regional climate models etc.) been available. This is clearly an opportunity but also a major challenge. There is indeed still a long way to go to transform this data deluge into the accurate climate information needed by society to deal with climate change and its impacts. These issues have been a focus of our work over the past two years.

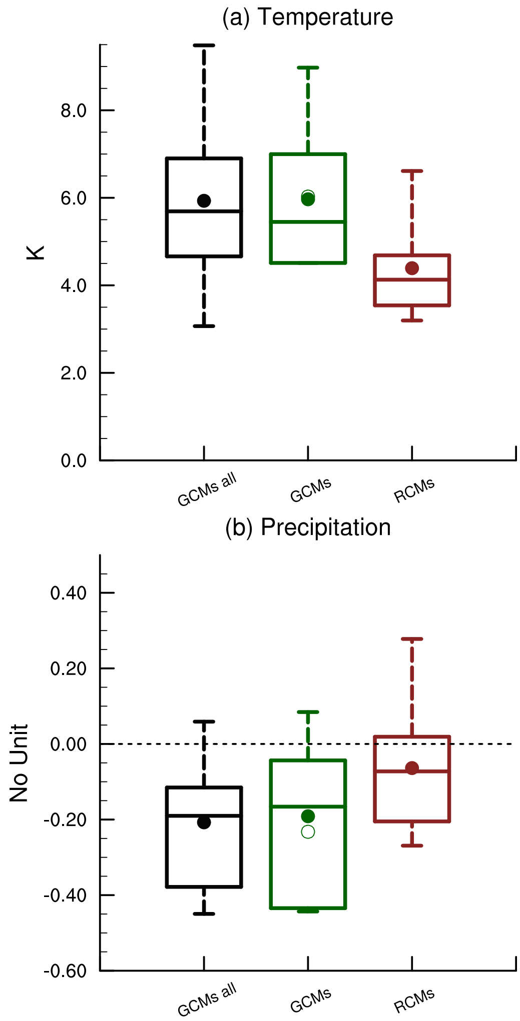


Figure 2.1: Intermodel distribution of (a) changes in summer temperature (K) and (b) relative changes in summer precipitation (no unit), averaged over western and central Europe, in the complete ensemble of CMIP5 models ("GCMs all"), in the CMIP5 models used to drive the 12 km EURO-CORDEX RCMs ("GCMs") and in the RCMs ("RCMs"). The differences between 2070-2099 and 1970-1999 are calculated. See the description of the boxplots in Section 2. Circles: ensemble means. For the forcing GCMs, the empty circle shows the unweighted ensemble mean. The filled circle show the weighted ensemble mean, according to the number of RCMs forced by each GCM.

Regional climate models (RCMs) are commonly used as an intermediary step between global climate projections and impact studies. Surprisingly, the crucial questions of whether RCMs results are consistent with those of global climate models (GCMs) at large scales, and if not, whether more confidence should be placed in RCMs or GCMs, have received very little attention to date. We have shown that current RCMs from EURO-CORDEX project in average much less severe climate changes in summer over central and western Europe than their forcing GCMs or the full ensemble of GCMs from the Coupled Model Intercomparison Project phase 5 (CMIP5), with a smaller warming (up to 2°C smaller for the RCP8.5 scenario) and a smaller decrease in precipitation [CE62] (Figure 2.1). These differences are related to a much smaller increase in solar radiation at surface and a much smaller decrease in evapotranspiration in RCMs. We have shown that the fact that most RCMs do not use time-varying aerosols contrary to GCMs plays a major role in the differences in solar radiation changes. We also have discussed some potential mechanisms regarding the differences in evapotranspiration changes. It is likely that the physiological effect of CO2, which is simulated by a majority of GCMs but by none of the RCMs play a important role.

Given the increase in computing resources, it is now possible to run GCMs at resolutions close to the ones commonly used in RCMs, i.e. satisfactory for impact studies. Within the H2020 PRIMAVERA project and in relation with the High Resolution Model Intercomparison Project of CMIP6, we have investigated the impact of atmospheric resolution on the present-day representation of precipitation extremes worldwide [CE59]. We have compared the results of pairs of global atmospheric simulations at lower and higher resolutions, forced by observed sea surface temperatures (SST). Different observed datasets have been used to take into account the large observational uncertainties that exist in that context. The model resolution clearly impacts precipitation extremes, with generally intensification at higher resolutions, although it is very model- and region-dependent. This intensification at higher resolutions does not necessarily lead to more realistic precipitation extremes, pointing to the crucial role of other aspects of models (e.g. physics parameterizations). Within the PRIMAVERA project, we have participated in other studies on the impact of resolution, e.g. on tropical cyclones [CE86];[CE124], Atlantic meridional overturning circulation [CE109], atmospheric blockings [CE117], water and energy budgets [CE123].

Exploring climate projection uncertainties with ensembles of opportunity such as CMIP or CORDEX has some limits. These ensembles are neither specifically designed to understand the source of uncertainties in climate projections nor to explore the full range of uncertainties. Perturbed physics ensembles are very useful in that context. During the last two years, the core of the RISCCI Make Our Planet Great Again project has been the establishment of a CNRM ensemble platform to explore parametric uncertainty in the Météo-France climate model. Two initial ensemble experiments have been completed, iterating on parameter sampling strategies and experimental configurations to explore both climatological performance and greenhouse gas response uncertainty. In parallel with these efforts, the project has conducted a number of simple climate modeling studies to address fundamental questions of how climate sensitivity metrics relate to future climate projection uncertainty and long term projection risk [CE115]; [CE116].

Confronting models to observations, in particular regarding past climate trends, and understanding the causes of differences should they exist is also necessary. Past studies have concluded that climate models tended to underestimate the large long-term temperature trend that have been observed in summer over Western Europe, with no clear explanation. We have investigated whether it is still true in the new generation of climate models [CE63]. As an ensemble, climate models from the H2020 PRIMAVERA project warm less over western Europe and warm more over eastern Europe than observed on the 1951–2014 period, but it is difficult to conclude this is directly due to systematic errors given the large potential impact of internal variability. These differences in temperature trends are explained to an important extent by an anti-correlation of sea level pressure trends over the North Atlantic / Europe domain between models and observations. The observed trend tends to warm (cool) western (eastern) Europe but the simulated trends generally have the opposite effect, both in new generation and past generation climate models. The differences between observed and simulated sea level pressure trends are likely the result of systematic model errors, which might also impact future climate projections. Neither a higher resolution nor the realistic representation of the evolution of sea surface temperature and sea ice leads to a better simulation of sea level pressure trends.

The last two years have also seen the emergence of the study of the impacts of climate changes on aviation in the Climate and Environment team, in collaboration with the CFD team. As part of the Impact of Climate Change on Aviation (ICCA) project, a six-months internship was carried out in 2019. The work consisted of the analysis of the evolution of extreme hot temperatures, at a global scale, and their impact on aircraft take-off performance, in terms of weight restricted days, over a list of vulnerable airports worldwide. A PhD thesis started in November 2019 as a continuation of this work. The aim of the thesis is to assess the impact of the increase in the magnitude and in the frequency of extreme heat events in future climate, in the Euro-Mediterranean region, on the performance of aircraft's engines during take-off. The impact on take-off distance of uncertainties in atmospheric variables evolution under climate change scenarios and of uncertainties in engine aircraft behavior was investigated during two internships. Preliminary results quantified the increase of the take-off distance as the increase in temperature significantly reduces the engine thrust [CE161].

## 2.5 Predicting sea ice variability and changes and their impact on the climate system

Arctic sea ice has been declining at a rate larger than 10% per decade since the beginning of satellite measurements (Stroeve et al. 2012) and the latest climate projections suggest that ice-free conditions during the summer are likely to occur before the year 2050 (SIMIP, 2020). To better understand the influence of these long-term changes in Arctic sea ice on midlatitude weather and climate, several studies have been dedicated to the analysis of atmospheric linkages driven by sea ice decline [CE98];[CE168]. As shown in the PhD thesis of S. Chripko using dedicated sensitivity experiments performed with the CNRM-CM6 model in the framework of the H2020 PRIMAVERA and APPLICATE projects, a strong decline of Arctic sea ice leads to a warming of most of the Northern Hemisphere that is largely amplified near the pole. We showed that this Arctic amplification is associated with a narrowing of the subtropical jet stream in late fall/early winter and a weakening of the polar vortex. We showed that despite the large-scale warming induced by Arctic sea ice reduction in most regions over the Northern Hemisphere, cold anomalies could be found in particular over Central Asia in winter (Figure 2.2). Using the dynamical adjustment approach described in [6], we decomposed the atmospheric response into a dynamical component that reflects circulation changes and a residual component that include the contribution of several processes like the advection of anomalous oceanic air masses by the climatological flow and local thermodynamical effects due to changes in surface land conditions (snow cover or soil moisture). Applying this decomposition regionally, we showed that the wintertime Asian cooling to the simulated Arctic sea ice reduction in CNRM-CM6 can be mainly explained by dynamical changes in the atmospheric circulation rather than thermodynamical changes (Figure 2.3). We also showed that the magnitude of this sea-ice induced cooling remains small compared to the large internal variability. Further, using comparable experiments that only differ in the horizontal resolution of the atmospheric and oceanic model components, we showed that the atmospheric response to Arctic sea ice decline is not sensitive to resolution changes from 130km to 50km in the atmosphere, suggesting similar mechanisms driving the response at the two resolutions tested in these experiments.

To better understand the influence of a more realistic Arctic sea ice reduction as expected for a projected 2°C global warming and assess the models robustness, we have been strongly involved in the design, production and joint analyses of coordinated experiments for the CMIP6 Polar Amplification Model Intercomparison Project (PAMIP) [CE120]. The analysis of these experiments indicate that the reduction of Arctic sea ice can impact the midlatitude westerlies with a response that projects onto the negative phase of the Arctic Oscillation and a southward shift of the subpolar jet. The response is about 10% stronger at the core of the jet for the multimodel mean when coupling with the ocean is allowed. We have also done multidecadal coupled experiments to investigate the impact of Arctic sea ice reduction on the oceanic circulation and in particular on the AMOC.

Over the past two years, we have pursued work to identify the mechanisms contributing to the predictability of Arctic sea ice on seasonal time scales. Using a perfect model approach that provides an estimate of the intrinsic predictability and highlights the prediction errors due to imperfect initial conditions on one hand, and to model biases on the other hand, we completed the first direct comparison of perfect model and operational seasonal prediction skill for regional Arctic sea ice extent with a common prediction system. In

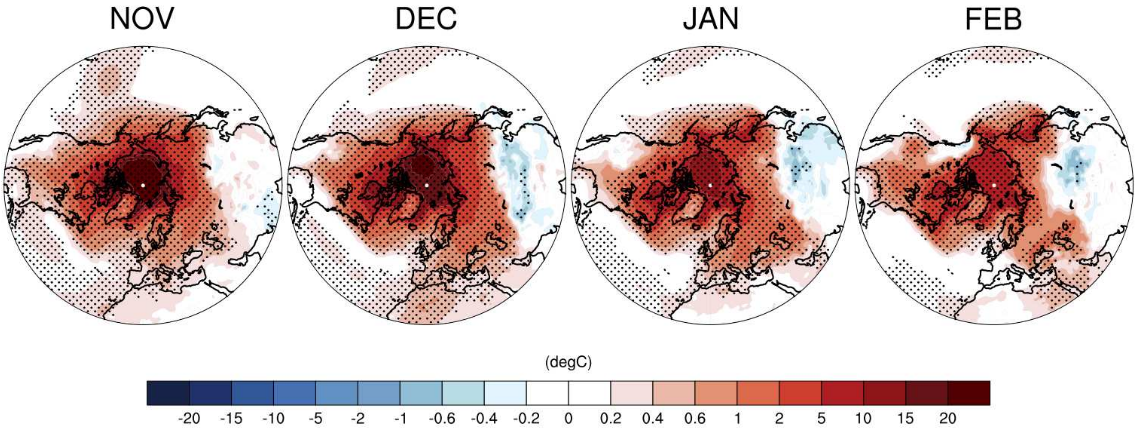


Figure 2.2: 2m air temperature response to Arctic sea decline during the cold season (November to February) in the CNRM-CM6 model. The response is defined as the difference between a control simulation and a perturbed one in which sea ice melts due to an imposed large albedo reduction. 200 members are used for each experiment and the response shown here is the ensemble mean. Dots indicate the grid points that are statistically significant at the 95% confidence level using a two-sided Student's t-test and applying the False Discovery Rate [8].

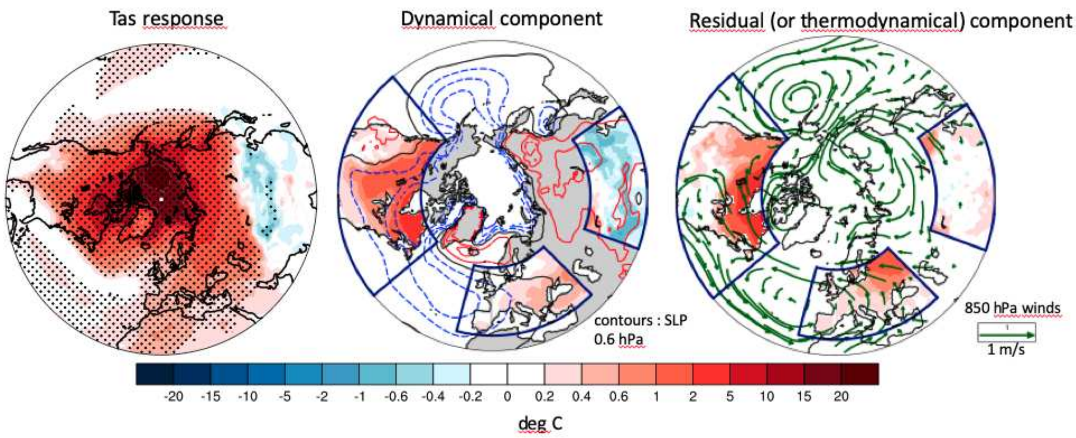


Figure 2.3: Decomposition of the CNRM-CM6 wintertime (December) 2m air temperature response to Arctic sea decline into a dynamical and a residual component. The response is defined as in figure 2.2. To help interpreting the results, the SLP response is superimposed in contours to the dynamical response, and the 850hPa winds are superimposed to the thermodynamical response.

nearly all Arctic regions, we found a substantial skill gap between perfect model and operational predictions of regional sea ice extent, suggesting a high potential for future improvements of regional Arctic sea ice extent predictions, in particular during winter [CE65]. We also showed the importance of sustained observations in the ocean to seasonal predictions of winter sea ice in the Barents Sea [CE66].

## 2.6 Air-sea interactions and climate model biases

We have a long-time history and recognized expertise on coupling between the ocean and atmosphere and how this coupling can explain biases in climate models. From coupled experiments in which model components are initialised from observations, we investigated the coupled mechanisms leading to the emergence of systematic model biases in climate models in the Tropical Atlantic region. We showed that model errors mostly originate from the atmospheric component and then propagate into the ocean subsurface at longer timescales, leading eventually to a biased mean state of the Tropical Atlantic basin. In particular, deficiencies in simulating correct surface winds and heat fluxes inhibit the influence of ocean dynamics on upper-ocean variability and lead to unrealistic thermodynamic control of the ocean state through overly dominant mixed layer processes. This results have been published in Goubanova et al. 2019 [CE79] and Voldoire et al. 2019 [CE126]. Within the H2020-TRIATLAS project (South and Tropical Atlantic climate-based marine ecosystem prediction for sustainable management), we have also evaluated the ability of CMIP6 climate models to reproduce the main characteristics of the two upwelling systems in the Tropical Atlantic region. These systems are the CANUS the BUS for respectively Canary and Benguela upwelling systems. By using upwelling indices based on SSTs and wind stress and following the approach in Sylla et al. 2019 [1], we show that CMIP6 models capture most of the upwelling properties in despite of their coarse resolution. We have also analysed the added-value of increasing model resolution in the representation of the CANUS by using the numerical experiments performed within the H2020 PRIMAVERA. Results show an improvement, but the impact of model resolution is weak. A paper of these results is in preparation (Sylla et al. in prep).

In these last two years we have also continued research devoted to the influence of mesoscale SST structures on the atmosphere over the Gulf Stream region as initiated by the PhD thesis of Marie Piazza (Piazza 2014) and now continued with the PhD thesis of Victor Rousseau (October 2017 - November 2020) within the H2020-PRIMAVERA project ([CE170]). Two mechanisms have been proposed to explain the MABL (Marine Atmospheric Boundary Layer) response to mesoscale SSTs: the Vertical Mixing Mechanism (VMM) and the Pressure Adjustment Mechanism (PAM). The relative role of these two mechanisms is still under debate. We have analysed the VMM and PAM in different configurations (low resolution, high resolution) of the ARPEGE6 atmospheric model forced by observed SSTs. The ERA5 atmospheric reanalysis was also used as reference. In our approach, we have studied the VMM and PAM under different atmospheric conditions obtained from a classification method based on the deciles of the statistical distribution of winter turbulent heat fluxes over the Gulf Stream. Lowest deciles (d1) are associated with weak air-sea interactions and anticyclonic atmospheric circulation over the Gulf Stream, whereas highest deciles (d10) are related to strong air-sea interactions and a cyclonic circulation. We found that the occurrence of anticyclonic and cyclonic perturbations associated with different anomalous wind regimes can locally modulate the near surface wind divergence field (Figure 2.4). We showed in particular that the cyclonic events (d10) explain most of the time-mean convergence over the Gulf Stream. We also showed that atmospheric patterns can modulate the VMM and PAM and their respective roles in shaping the wind convergence field. Our results highlight the influence of the atmospheric circulation and associated anomalous winds on the response of the MABL to mesoscale SSTs. These results were included in an article which is currently in revision (Rousseau et al. in rev).

In order to better disentangle the role of the SST mesoscale structures on the large scale atmospheric circulation in the North Atlantic-European sector, sensitivity experiments based on the same high resolution version of ARPEGEV6 have been performed and analysed. In the control experiment, the atmospheric model was forced by the SSTs from the very high resolution GLORYS12 dataset. A smooth experiment (SMTH) was then defined in which the SSTs in the frontal region over the Gulf Stream were spatially filtered to remove mesoscale features and weaken the SST gradient. We found significant changes in the surface temperature and precipitation over Europe when the Gulf Stream SST was smoothed. This could partially be explained by downstream changes in the large scale atmospheric circulation in the North Atlantic. Further investigation is under progress to interpret the temperature and precipitation responses found in Europe.

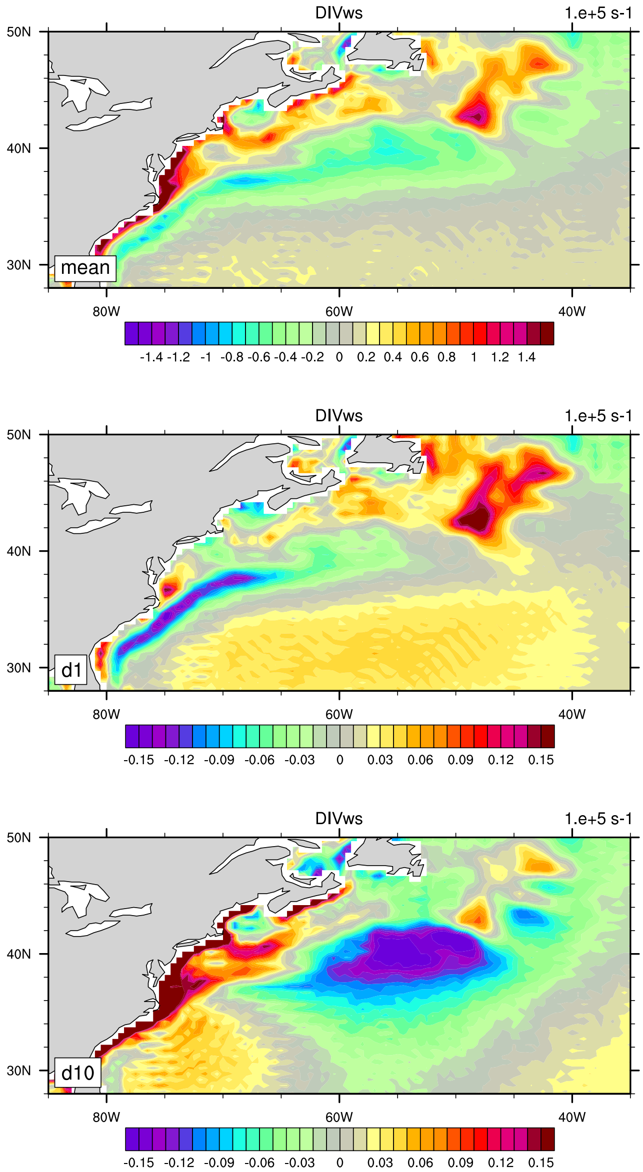


Figure 2.4: Near surface wind divergence in winter (DJF) computed from an atmospheric forced simulation performed with the high resolution version of ARPEGEV6 model. (Top) Time-mean divergence computed for the whole period (1950-2014); (middle) Divergence obtained by compositing anticyclonic events (d1) ; (bottom) Divergence obtained by compositing cyclonic events (d10). Positive values indicate divergence, negative values indicate convergence. Units are in 1.e+5 s-1.

From similar sensitivity experiment but performed in a coupled model framework, Small et al. (2019) went further and highlighted that changes in absolute SSTs can also have a larger impact on baroclinicity and North Atlantic storm-track than changes in SST gradients. They stressed the difficulty of detecting climate

impacts of oceanic mesoscale eddies in coupled models, given the dominant influence of model SST biases that remain large even when resolution is increased.
The impact of model resolution on the representation of air-sea coupling over the Gulf Stream region have also been studied in the multi-model ensemble produced within the H2020-PRIMAVERA project (Bellucci et al. in revision). Lead-lag correlation and covariance patterns between sea surface temperature (SST) and turbulent heat flux were diagnosed to identify the leading regimes of air-sea interactions. Based on these statistical metrics it was found that coupled models based on “laminar”(eddy-parameterised) and eddy-permitting oceans are able to discriminate between an ocean-driven regime, dominating the region controlled by the Gulf Stream dynamics,and an atmosphere-driven regime, typical of the open ocean regions. They showed however that the increase of model resolution leads to a better representation of SST and latent heat cross-covariance patterns, and that the major improvements could be largely attributed to a refinement of the oceanic model component.

## References

[1] S. A., J. Mignot, and X. Capet, (2019), Weakening of the Senegalo–Mauritanian upwelling system under climate change, *Climate Dynamics*, **53**, 4447–4473.

[2] J. Boé and F. Habets, (2014), Multi-decadal river flow variations in France, *Hydrology and Earth System Sciences*, **18**, 691–708.

[3] G. J. Boer, D. M. Smith, C. Cassou, F. Doblas-Reyes, G. Danabasoglu, B. Kirtman, Y. Kushnir, M. Kimoto, G. A. Meehl, R. Msadek, W. A. Mueller, K. E. Taylor, F. Zwiers, M. Rixen, Y. Ruprich-Robert, and R. Eade, (2016), The Decadal Climate Prediction Project (DCPP) contribution to CMIP6, *Geoscientific Model Development*, **9**, 3751–3777.

[4] C. Cassou, Y. Kushnir, E. Hawkins, A. Pirani, F. Kucharski, I.-S. Kang, and N. Caltabiano, (01 Mar. 2018), Decadal Climate Variability and Predictability: Challenges and Opportunities, *Bulletin of the American Meteorological Society*, **99**, 479 – 490.

[5] S. Community, (2020), Arctic Sea Ice in CMIP6, *Geophysical Research Letters*, **47**, e2019GL086749.

[6] C. Deser, L. Terray, and A. Phillips, (2016), Forced and Internal Components of Winter Air Temperature Trends over North America during the past 50 Years: Mechanisms and Implications, *Journal of Climate*, **29**, 2237–2258.

[7] J. Stroeve, M. C. Serreze, M. M. Holland, J. E. Kay, J. Malanik, and A. P. Barrett, (2012), The Arctic’s rapidly shrinking sea ice cover: a research synthesis., *Climatic Change*, **1105-1027**, 100.

[8] D. Wilks, (2016), The stippling shows statistically significant grid points”: How research results are routinely overstated and overinterpreted, and what to do about it., *Bulletin of the American Meteorological Society*, **97**, 2263–2273.

# Environmental Systems

## 3.1 Introduction

Research dedicated to Environmental Systems at CECI is shared over the following topics: atmospheric chemistry data assimilation, atmospheric pollutant dispersion simulation and metamodeling, wildland fire modeling and data assimilation, sensitivity analysis and uncertainty reduction for flood forecasting, global-scale ocean data assimilation and generic data assimilation algorithms for large scale problems, with a particular focus on data assimilation and high-fidelity numerical simulations. This research is multidisciplinary and addresses a wide variety of objectives (environment surveillance, early warning system, monitoring, reanalysis, scenarios, forecasting), spatio-temporal scales (from micro- and meso-scales to regional and global scales), simulation tools and algorithms (data assimilation, uncertainty quantification, machine learning, code coupling, high performance computing).

These research activities, mostly carried out with in the GLOBC team in synergy with the CECI research strategy, rely on collaborations with other research axis from the Climate and Environment topic (Climate Modeling and Coupling, HPC and Data for Climate) as well as on collaborations with ALGO, CFD and CSG teams at CERFACS.

## 3.2 Atmospheric chemistry data assimilation

CERFACS activities on atmospheric composition continue regularly since 2003 and are based on a strong collaboration with Météo-France and external funding from Europe (Copernicus and H2020 programs), CNES (Tosca program) and Occitanie region. The research on data assimilation aims at improving the accuracy of chemical forecasts and reanalysis with the aid of satellite and ground measurements. During the 2019-2020 period, the main efforts were dedicated to the assimilation of satellite radiances for ozone analyses:

**(1) Observation error covariance for IASI assimilation.** The direct assimilation of IR radiances for $O_3$ analyses provides superior results with respect to the assimilation of the corresponding Level 2 retrievals, when the setup of the observation operator and the specification of their errors are kept identical [CE73]. However, the appearance of stratospheric biases is observed with both techniques (L1 and L2 assimilation). A possible culprit for analysis degradation is the mi-specification of the background or observation error covariances (**R**) in the assimilation. The assimilation system allows a diagnostic of the observation error covariance that has already proven effective in meteorological applications. This so called Desroziers diagnostics permit to infer information on the full error covariances (diagonal and off-diagonal terms) with a negligible numerical cost. We employed this technique to re-evaluate the error covariance matrix for IASI ozone channels and analysed the impact of using such matrix for the assimilation. Results showed that strong error correlations are present in the ozone window, due to redundant information content and radiative transfer errors. When these correlations are taken in account stratospheric biases are significantly reduced and the minimization algorithm converges faster [9].

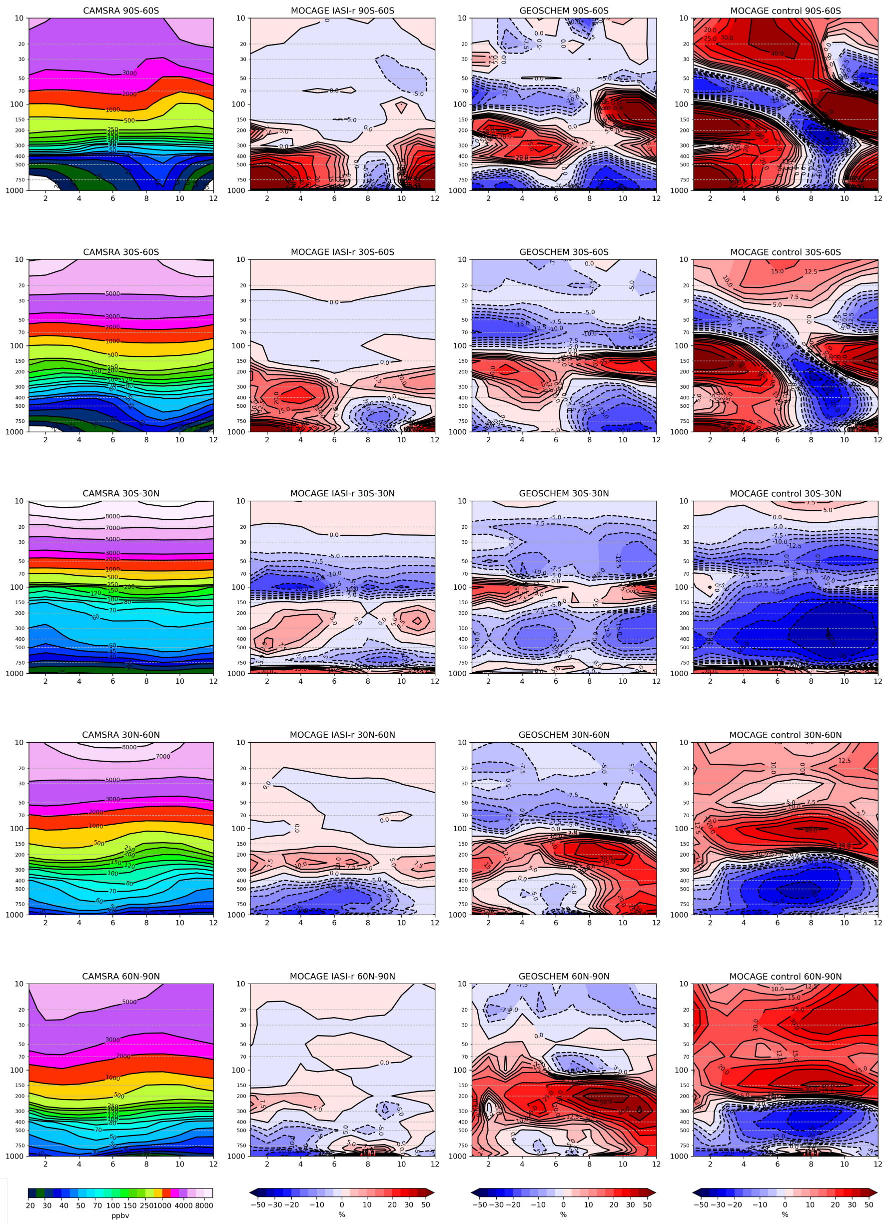


Figure 3.1: Ozone zonal averages in 2010 as a function of month (x-axis) and altitude (y-axis in hPa) for five latitude bands separately (90°S-60°S, 60°S-30°S, 30°S-30°N, 30°N-60°N, 60°N-90°N from top to bottom). CAMSRA $O_3$ (ECMWF chemical reanalysis) is plotted on the first column. The relative differences between the new CERFACS reanalysis (second column), the GEOS-CCM chemistry-climate free simulation (third column), the MOCAGE control simulation (fourth column) and CAMSRA $O_3$ are given in percent of the CAMSRA $O_3$.

**(2) Global ozone reanalysis.** A new version of the IASI global $O_3$ reanalysis has been computed for 2010, based on all methodological improvements achieved so far [CE73, 9]. The new reanalysis has been compared to the previous version of the CERFACS reanalysis [18], which showed neutral to negative gains in the extra-tropics due to biases in the original IASI Level 2 retrievals. The new reanalysis provides significant improvements in the mid-latitudes. It also compares well to state-of-the-art reanalyses such as the ECMWF chemical reanalysis (CAMSRA), which is based on a more complex chemical mechanism and assimilation of greater number of satellite measurements (Figure 3.1). The results of this study have been submitted to the Geoscientific Model Developments journal. In parallel, a revision of the IASI $O_3$ Level 2 retrieval algorithm that was inspired by our results, showed also improved skills in the extra-tropic [CE60]. The progress made so far on infrared radiances assimilation for ozone assimilation will permit an implementation in the Météo France operational systems in the near-future.

**(3) Assimilation of UV radiances.** Within the Copernicus CAMS-42 project we developed and tested the direct assimilation of UV spectra from the GOME-2 instrument. GOME-2 and IASI are both onboard the Meteosat platforms MetOp, which started operations in 2006 and are meant to provide uninterrupted series of measurements for the next two to three decades. UV sounders are complementary to IR ones since they are mostly sensitive to the stratospheric ozone content, whereas IR information content peaks in the upper troposphere and lower stratosphere. Being able to assimilate both type of measurements to constrain the ozone column is an important challenge in the perspective of generating climate reanalyses. During the last year of the project we finalized the implementation of the radiative transfer code developed by the German Aerospace Agency (DLR) in MOCAGE. The assimilation of UV spectra from GOME-2 (270-330 nm) has been evaluated and compared to the assimilation of L2 retrievals provided by the Netherlands Meteorological Institute (KNMI). The two approaches produce similar total ozone columns but different vertical distributions. In particular, the direct assimilation of GOME-2 spectra reduced ozone biases in the tropopause region [CE138]. Given the high numerical cost of radiative transfer in the UV and the necessity of employing multiple outer loops to correctly handle the radiative transfer non-linearities [CE139], additional research might be needed to envisage an operational application.

## 3.3 Atmospheric pollutant dispersion simulation and metamodeling

Accurately predicting the unsteady short-to-medium range plume dynamics and dispersion induced by point-source emissions remains a challenge for safety prevention and emergency risk assessment linked to air quality and health impact issues. Large-eddy simulations have been identified at CERFACS since 2016 as a promising tool to tackle this micro-scale challenge due to the complex, transient flow patterns induced by the presence of obstacles (buildings and mountains for instance) in a urban district or an industrial site. We addressed this problem through several projects, among whom the 2017-2019 MOSIQAA-CORAC project aiming at designing accurate air quality simulations on airport site in collaboration with ONERA and INERIS; and the 2018-2020 RTRA-STAE PPM project in collaboration with CNRM, ONERA and CEREA. Additional PhD projects by B. Nony (in collaboration with LIMSI, funded by CERFACS) and E. Lumet (in collaboration with LAAS, funded by Université de Toulouse/Région Occitanie) have recently started on this topic. This part was partly supported by GENCI HPC computational resources.

**(1) Immersed boundary method to simulate micro-scale surface/atmosphere interactions.** An immersed boundary method (IBM) was implemented in the MesoNH atmospheric model [14] to explicitly represent complex surface topography. The MesoNH-IBM model was validated using the MUST field-scale experiment [CE58]. It was then used to simulate at airport scale emission dispersion induced by daily aviation activity [CE151], and at urban scale the 2001 AZF industrial accident in Toulouse [CE57]. Turbulence synthetic generation was found to be an important aspect in the large-eddy simulation design to have realistic inflow boundary conditions. Large-eddy simulations were used to analyze in which meteorological situation air quality significantly degrades locally and to characterize exposition to a given pollutant concentration threshold.

**(2) Benchmark case of micro-scale large eddy simulations.** We carried out an extensive comparison of large-eddy simulations in the framework of the MUST experiment in near-neutral boundary layer conditions, including MesoNH-IBM, YALES2 and AVBP. The first objective was to investigate the capability of LES to capture the unsteady short-to-medium-range plume dynamics and dispersion within the urban canopy [CE44]. The second objective was to analyze the sensitivity of the LES results to different physical and numerical choices (model equations, computational grids, numerical schemes, physical assumptions) to quantify multi-model variability (Figure 3.2). The large-eddy simulation results were found in very good agreement with the experimental measurements, especially for tracer concentrations above 1 ppm. The different solutions provided by AVBP, MesoNH-IBM and YALES2 did not feature significant discrepancies highlighting their consistency. In particular, AVBP and YALES2 captured a deviation of the plume centerline that was observed during the MUST trial. This deviation modified the structure of the lateral and vertical pollutant dispersion within the idealized canopy, which is important to predict the location of tracer concentration peak values. We thereby obtained an estimate of the multi-model variability in the tracer concentration LES predictions [22, CE162]. In the frame of this benchmark, additional developments were also performed in AVBP to implement an artificial compressibility approach (pressure gradient scaling [20]), applicable both to environmental flows and reactive flows. This makes the fully-compressible, explicit approach used in AVBP competitive with incompressible solvers in terms of computational cost for low-Mach flows typically found for atmospheric dispersion, fires and many other CFD applications (e.g. aeronautical engines combustion chamber).

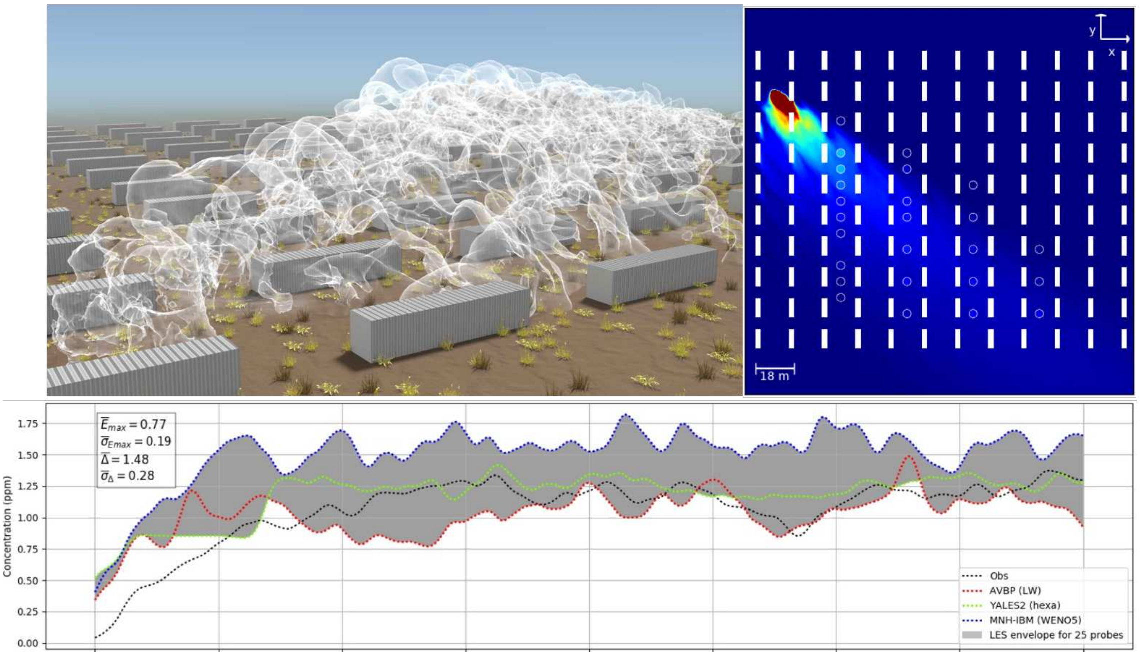


Figure 3.2: Large-eddy simulation of a MUST trial over an idealized urban environment. Top left panel: Instantaneous view of the simulated plume. Top right panel: Time-averaged simulated tracer concentration at 1.6 m high (observations are given by the symbol colors). Bottom panel: Time series of the best large-eddy simulation configurations, in blue for MesoNH-IBM, in green for YALES2 and in red for AVBP obtained for 25 sensors throughout the canopy. Source: [22, CE162].

**(3) Sensitivity of micro-scale large-eddy simulations to parametric uncertainties.** Large-eddy simulation predictions of atmospheric pollutant dispersion are highly dependent on the inflow boundary conditions that are influenced by meso-scale meteorological conditions and by the source characteristics (position, emission rate). These conditions may be subject to uncertainties when simulating a dispersion event. They can be classified as parametric uncertainties subject to space and time variability. It is thus of great interest to study how these input parameters affect the pollutant concentration within the urban canopy. Since large-eddy simulations are computationally expensive, we have access to a limited number of simulations to carry out this uncertainty quantification step. To overcome this issue, we investigated the use of an emulator to replace the large-eddy simulation model [CE42]. The key idea was to use a limited number of LES to form a training data set over which statistical models could learn the large-eddy simulation response (in terms of flow field mean and fluctuations, and tracer concentration field mean and fluctuations) to changes in the input parameters. The performance of several emulators was compared (multi-linear regression, gaussian process, random forest, etc.) for a simplified test case (two-dimensional flow over a wall-mounted obstacles) to i) determine the most suitable emulating strategy to emulate time-transient atmospheric flows, and ii) evaluate its robustness with respect to the training size. Preliminary results provided a proof-of-concept. This work was part of B. Nony' PhD thesis. Future work includes extending the emulating strategy to 3-D full-scale dispersion cases and to combine the statistical model with a reduced-order modeling strategy to increase the ensemble size and gain in accuracy in the emulating process. Future work also includes integrating the emulator within a data assimilation algorithm to reduce parameteric uncertainties in large-eddy simulations as part of E. Lumet's PhD thesis.

## 3.4 Wildland fire behavior modeling and data assimilation

Simulating landscape-scale wildland fire behavior remains a scientific challenge due to the complexity of the physical processes and to the cascade of uncertainties, from biomass fuel (type, properties, moisture content of dead and living fuels) to micro-scale meteorology (local near-surface wind conditions induced by terrain topography and large-scale atmospheric conditions at synoptic and meso-scales). To improve wildland fire models and quantify related uncertainties, there is a need to develop a framework, a virtual fire laboratory, aggregating all sources of available information, from observations (spaceborne, airborne or UAV remote sensing platforms) and from numerical models.

**(1) Front data assimilation for joint state/parameter estimation.** One research axis pursued at CERFACS (in collaboration with the University of Maryland, INRIA and LIMSI) is to design a robust data assimilation framework able to produce reanalyses of wildland fires. The key idea is to reconstruct the time history of a given wildland fire event to provide insights into the dominating processes enhancing fire spread and intensity. While the application of classical data assimilation techniques to wildland fires clearly benefits from past developments made for numerical weather and environmental predictions, it is important to recognize that there are yet a number of application-specific technical barriers that need to be overcome. We addressed two of them in recent works detailed in the following. This work was part of C. Zhang's PhD thesis (University of Maryland, 2018) [26, CE131, CE132] funded by NSF (NSF-1331615, WIFIRE, 2014-2018) in complement to SMAI, CNRS INSU/LEFE and LabEx AMIES funding. This collaboration with the University of Maryland will be pursued through new projects (among whom NSF-1854952, WUI-MAPR, 2019-2022).

- **Design of fire front data assimilation.** Wildland fire spread is represented as a front-tracking problem, where the fire front may present irregularities due to wind-terrain interactions and have complex topology due to fire spotting. To overcome some limitations of standard data assimilation algorithms, we developed in collaboration with INRIA and LIMSI [21], an object-oriented data assimilation strategy that is derived from image segmentation theory and that is able to deal with position errors as well as amplitude errors through a new innovation term based on a Chan-Vese-type front shape similarity measure. The object-oriented data assimilation algorithm applied to wildland fire was developed within VerdandInMatlab for a proof-of-concept study for both lagrangian and eulerian front-tracking solvers [CE131]. The merits of the methodological developments were shown on field-scale controlled burns (RxCADRE experiment) [CE131, CE132]. Some further developments are foreseen to better represent shape-based error statistics in adequacy with front shape similarity measure.

- **Added value of state-parameter estimation.** We demonstrated the merits of combining state estimation and parameter estimation approaches to reduce fire model bias and improve forecast performance [CE132]. Parameter estimation is important due to the presence of large bias in the input parameters such as the near-surface wind (which can be influenced by the fire) and the biomass fuel parameters (for instance, the dead fuel moisture content that is subject to short-term temporal variability linked to atmospheric conditions – relative humidity, temperature, etc.). Sensitivity analysis can be useful to identify the main sources of influence among the input parameters to the fire model [21, 11].

**(2) Fire behavior observational datasets for model validation.** Data assimilation offers a mathematical framework to take advantage of infrared remote sensing [17, CE55] from which fire front positions can be extracted using machine learning approaches, in order to reduce uncertainties in fire model predictions. We developed a strategy based on convolutional neural networks to label such fire front positions and thus to build high-resolution (metric scale and second-time scale) fire behavior observational datasets [CE36, CE37]. This would be valuable for future model validation and this is in line with current efforts in the fire research community [15, 19]. This work will be pursued as part of the MSCA-3DFIRELAB (2020-2022) project; a new collaboration with CERTEC will be enhanced by this project.

**(3) Fire/atmosphere interaction simulations at micro-scale.** Another research axis (in collaboration with CNRM and the University of Corsica) is to design a fire/atmosphere coupled modeling system to represent in an interactive way, the impacts of the fire on the atmosphere and their feedbacks on the fire behavior. Such a model can represent the different types of fire regimes (wind-driven and plume-dominated fires) and thereby provide insights into the strong interactions between a wildland fire and the atmosphere, which can ultimately lead to extreme fire behaviors. For this purpose, we designed a new atmosphere/fire model based on MesoNH and a fire spread model called Blaze. Blaze includes i) a fire spread component using a level-set front-tracking solver and a rate-of-spread parameterization, and ii) a flux component based on a latent and sensible heat flux parameterization. This replaces the previous system MesoNH/FOREFIRE [13], which has shown some scalability limitations. The new coupled system MesoNH/Blaze was validated against canonical test cases and the FireFlux controlled grassland experiment (Figure 3.3). The new subgrid fireline reconstruction method implemented in Blaze has shown its ability to run coarse fire simulations and save computational time compared to the litterature.Variability in the inflow turbulence was shown to have a significant impact on the fire behavior and thereby demonstrated the need to adopt a stochastic viewpoint when simulating wildland fire behavior. This work is part of A. Costes' PhD thesis (ongoing, in collaboration with CNRM) [CE16] funded by ANR (ANR-16-CE04-0006, FIRECASTER, 2017-2021) in complement to CNES/TOSCA. Future work includes adapting the data assimilation algorithm to the coupled system, to have a more realistic representation of the turbulent wind spatial and temporal variability, and thereby improve prior information. In the longer term, future work includes studying pyroconvection processes that are important in extreme fire behavior as well as designing emulating strategies [CE42] on MesoNH-Blaze to evaluate the sensitivity of fire emissions to the fire propagation at the land surface.

## 3.5 Sensitivity analysis and uncertainty reduction for flood forecasting

Predicting free surface river flow characteristics with numerical models requires the description of the catchment and/or the river, water input to the system such as rainfall or hydrologic and/or maritime

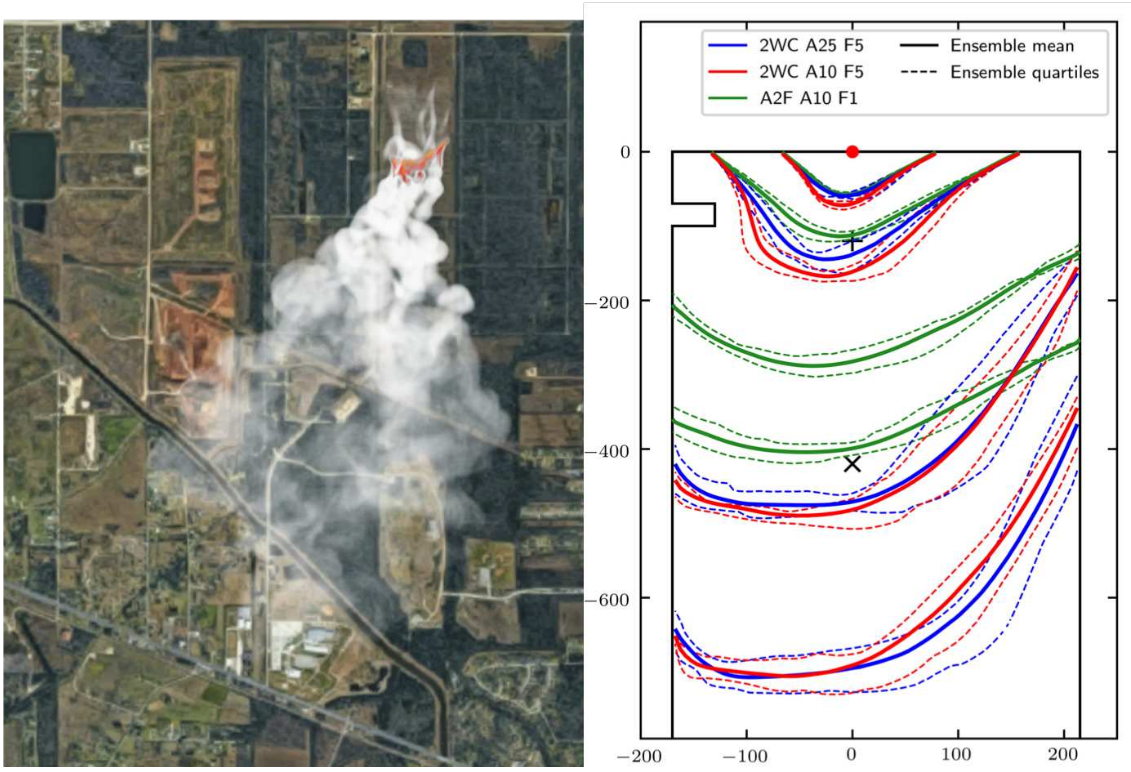


Figure 3.3: Coupled atmosphere/fire simulations for the FireFlux controlled burn. Left panel: Instantaneous view of the simulated fire (warm colors represent the fire front at the land surface, grey colors represent the smoke plume). Right panel: Ensembles of fire front positions at the land surface (solid lines represent mean values, dashed lines represent quartiles): green colors represent non-coupled simulations; blue and red colors represent two-way coupled simulations at two atmospheric horizontal resolutions (25 and 10 m). Source: [CE16].

inflow (boundary conditions) as well physical parameters for hydrology and hydraulics such as friction coefficients. The limited knowledge in this data translate into uncertainties in water elevation and discharge estimation. Quantifying and reducing these uncertainties is a pre-requisite for short to medium lead-time flood forecasting. Building from previous works in data assimilation for real-time flood forecasting [CE54], the challenge of going beyond deterministic simulation in order to quantify and reduce uncertainties is tackled. In an ensemble framework, the question of identifying, quantifying and reducing predominant sources of uncertainties is addressed. In order to do so, while meeting with operational constraints and lowering the computational cost, a surrogate model is used in place of the direct solver. Decision support systems in charge of flood forecasting need numerical solutions to represent multi-physics mechanisms and need to make the most of various types of observations. The focus is thus made on the one hand, on the improvement of modeling capabilities, including surrogate modeling and multi-physics modeling and, on the other hand, on the assimilation of remote sensing data. This work is achieved using the Telemac software (opentelemac.org); it should be noted that python Application Programming Interface classes dedicated to data driven integration of the solvers were developed at CERFACS and integrated in the SVN source code repository for Telemac. This research activity is supported by CERFACS shareholders (EDF, CNES, Météo-France), with complementary funding from national (TOSCA, Région Occitanie) and European (H2020) programs as well as from governmental and operational agencies

(CEREMA, SCHAPI), in collaboration with various institutes among which LHSV, INRAE and ARTELIA.

**(1) Generation and assimilation of SWOT-like continental water elevation data with ensemble data assimilation.** For several years, CERFACS has actively taken part to preparatory studies for the SWOT mission for large scale hydrology [CE72], [CE83] and small scale hydrodynamics. In hydrodynamics, the merits of assimilating global and high-resolution water level from SWOT complementary to in situ data were highlighted over the Garonne catchment (Figure 3.4a-), considering scenarios of spatial and temporal coverage as well as observation errors with synthetical observations [CE24]. It is shown in Figure 3.4c- and Figure 3.4d- that the mean deviation and RMSE of the analysed water height, calculated with respect to the ”true” simulation are largely reduced by the addition of SWOT type data, at a frequency of 1 or 3 days (curves denoted by ”1d” or ”3d”), and significantly improves the results of assimilation of low density in-situ data (curves denoted by ”is”). These experiments have been carried out using the Ensemble Kalman Filter algorithm from the SMURF python library developed at CERFACS ([CE26], [16], OpenSource code available at https://gitlab.com/cerfacs/Smurf). The python package ToolBoxSWOT (https://gitlab.com/cerfacs/toolboxswot, [CE137]) is now available to generate synthetical data from 1D models (Figure 3.4b-) and further work is on going for 2D model outputs. This work was achieved with funding support from CNES (TOSCA and SWOT-aval).

**(2) Sensitivity of water elevation and discharge to friction and hydrologic/maritim boudary conditions.** Non intrusive stochastic uncertainty quantification and sensitivity analysis methods are applied to identify which uncertain inputs such as friction and hydrologic/maritime boundary conditions, have predominant influence on water level and discharge, especially for high flow conditions [12] [23]. High tide coefficients combined with high meteorological surge levels and high discharges over the Garonne and Dordogne rivers in the Gironde estuary may lead to high water levels and floods with important economic and social impacts. A global sensitivity analysis was performed with Telemac-2D in the context of V. Laborie’s PhD in collaboration with LHSV and CEREMA [CE169]. The generation of the ensemble involves sampling scalar and functional aleatory variables such as time-varying hydrological and maritime forcing. The temporal perturbation of time-dependent upstream hydrological and downstream maritime forcing is assumed to be represented by a Gaussian process derived from observed chronicles [CE90]. Results showed that the maritime boundary condition and the estuarine friction coefficients are the main sources of uncertainties, thus defining the control vector for a data assimilation algorithm. Uncertainty quantification and sensitivity analysis in the presence of large-dimension input and output spaces requires dimension reduction strategies and computational cost limitation. The dynamics of the flood-plain is nonlinear; it may even be discontinuous with respect to the uncertainty sources. Building on previous expertise in surrogate modeling for Telemac2D in stationnary flow [CE19], [CE18], [CE17], and in order to overcome these difficulties, a mixture of experts relying of machine learning algorithms was combined with dimension reduction strategies as well as with polynomial chaos and Gaussian surrogate modeling strategies [CE20] in the context of S. El Garroussi’s PhD.

**(3) Extension of forecast lead time in hydrodynamics.** Forecast lead time for flooding can be extended when taking into account inputs of atmospheric (rain) and hydrologic (inflow) observed or forecasted data in the modeling strategy. This objective is investigated under two perspectives:

- The cascade of uncertainties for chained hydrologic-hydraulics modeling is accounted for with ensemble post-processing and data assimilation in the framework of A.-L. Tiberi’s PhD in collaboration with LHSV and CEREMA. Predominant parameters for discharge estiamtion are identified with a sensitivity study carried out for two hydrological models (GRP-lumped and MORDOR-semi distributed) over the Odet catchment [25]. Sobol sensitivity indices timeseries show a similar response for both models: the major uncertainty in discharge forecasts is controlled by precipitation, its corrective factor and routing scheme parameters. With respect to this ranking,

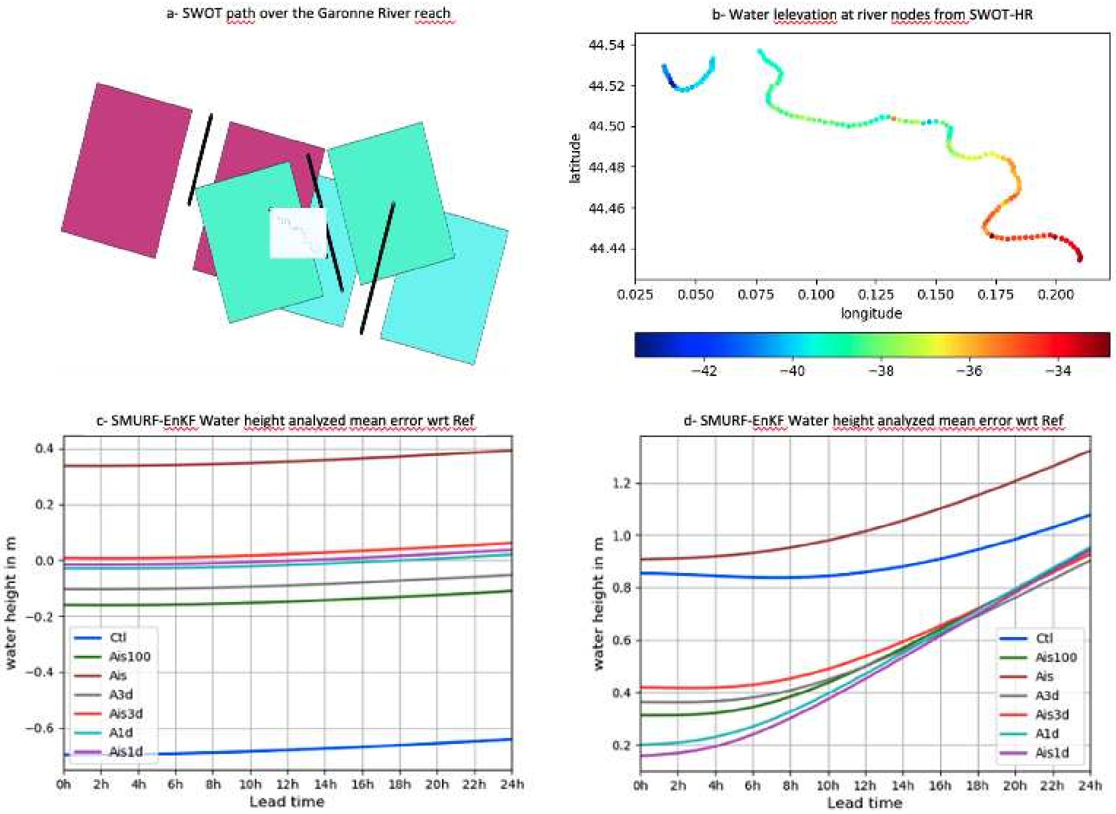


Figure 3.4: a- SWOT paths over the Tonneins-La Réole reach. b- SWOT-like data generated with SWOT-HR from Mascaret 1D hyrodynamics simulation at river nodes (200m). Mean deviation (c-) and RMSE (d-) of the analysed water height, calculated with respect to the "true" simulation for SWOT data assimilation at 1-day (1d) and 3-day (3d) frequency complementary to in-situ (is) data. The control simulation (no assimilation) is plotted in blue. Source: [CE25]

Hydrological Ensemble Forecats was implemented [24] and ensemble forecast was statistically calibrated with Quantile Random Forest. A sensitivity study was then carried out over the Odet hydraulic model with hydrological inflows prescribed by hydrological MORDOR forecasts; it was shown that the simulated water level is mainly controlled by river and flood plain friction coefficients [CE49]. Hydrologic-hydraulic chained ensemble with both statistical calibration and data assimilation is currently being investigated in the A.-L. Tiberi PhD.

- The merits of Machine Learning technics such as Gradient Boosting and Convolutional Neuronal Network have been demonstrated to forecast discharge from in-situ observations from upstream stations [CE22]. This comes as an alternative to imperfect and data dependent hydrologic-hydraulic numerical modeling and has been investigated for extended lead-time flood forecasting in Toulouse in the context of collaboration with operational SPC in Toulouse [CE156]. It was shown that learning algorithms manage to deal with non-linearities inherent to the dynamics of the watershed due to complex phenomena such as underground flows and groundwater-river exchanges or anthropogenic withdrawals. The possibility of further extending the lead-time is currently under investigation in the famework of Théo Defontaine's PhD, taking into account radar and in-situ rainfall data. This raises issues regarding feature engineering as well as regarding robustness and extrapolation capabilities of the method for events of larger amplitude then those provided in the learning data base.

## 3.6 Global-scale ocean data assimilation

During the 2019–2020 period, the global ocean data assimilation activity has been supported by a Copernicus Climate Change Service (C3S) contract aimed at improving ocean data assimilation methods at ECMWF for the initialization of seasonal forecasts and for reanalysis. A major component of that work is the development of an Ensemble of Data Assimilations (EDA) for the NEMOVAR system which is co-developed by CERFACS, ECMWF, INRIA and the UK Met Office. We have contributed to the EDA through developments to the background-error covariance matrix to account for uncertainty information provided by the ensemble.

Developing effective ways to model and cycle the background-error covariance matrix is an active area of research in data assimilation. An important aspect of this problem when using a filter to model the background-error correlations is the computation of normalization factors to ensure that the diagonal elements of the modelled correlation matrix are all equal to one. Updating the parameters of a flow-dependent correlation model on each assimilation cycle requires updating the normalization factors, which is costly using traditional methods such as randomization. In [ALG60] we discuss the normalization problem within the context of a diffusion filter-based covariance model used for background-error modelling in the NEMOVAR variational data assimilation system. We evaluated various methods for estimating normalization factors when the diffusion tensor of the correlation model is derived from an ensemble of ocean states. Our results show that estimates produced using inexpensive methods derived from analytical considerations of the diffusion equation can have significant errors, especially near boundaries. Estimates obtained using randomization with a small sample size ($\sim$100) are more accurate in a globally averaged sense but are noisy and can have unacceptably large errors locally. Next, we focused on the specific problem of accounting for flow-dependent correlation parameters in the vertical component of the diffusion operator only, which is important for improving the assimilation of surface observations such as SST. Remarkably accurate estimates are obtained by approximating the normalization matrix as a separable product of two normalization matrices: one computed using randomization with the horizontal diffusion operator only and the other computed using randomization with the vertical diffusion operator only (see Figure 3.5). If the parameters of the horizontal component of the diffusion operator are static then only the normalization factors of the flow-dependent vertical component need to be recomputed on each cycle. This result is of significant practical interest since the vertical diffusion operator employs an inexpensive direct solver and thus can be applied on each cycle with a large random sample to obtain a good approximation of the normalization matrix.

## 3.7 Generic developments in data assimilation methodology

Covariance modelling and model error representation in 4D data assimilation algorithms are two areas where we have developed techniques that are largely generic in the sense that they are relevant to a wide-range of data assimilation applications. This is the case for the covariance modelling techniques described by [ALG60] and outlined in Section 3.6. There, the emphasis was on background-error covariance modelling, using a technique based on a diffusion operator. Here, we outline a related method that has been developed for modelling observation-error covariances such as those present in satellite observations. For the representation of model error, we considered the problem within the context of weak-constraint

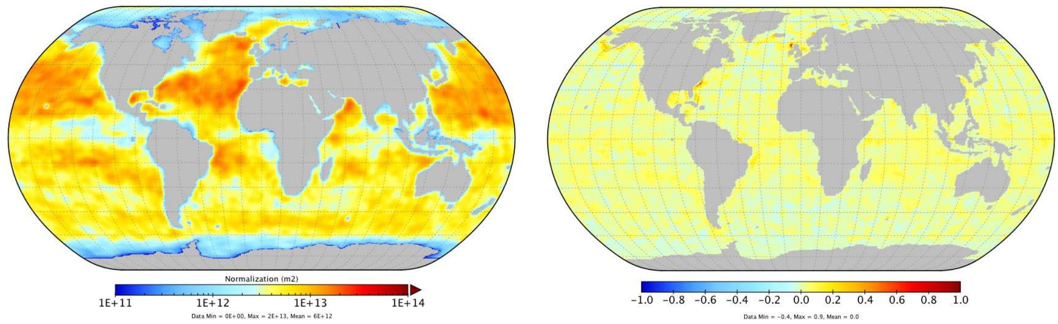


Figure 3.5: *Left panel*. The reference normalization factors ($\mathrm{m}^2$) for temperature at 5 metres depth (the surface level) for the implicit diffusion operator where the diffusion tensor has been estimated from a climatological ensemble. The normalization factors have been computed using the randomization method with a sample size of $10^4$. The colour palette uses a $\log_{10}$ scale. *Right panel*. The relative error in the normalization factors when using normalization factors approximated as a product of factors estimated separately for the horizontal and vertical diffusion components using randomization with a sample size of $10^4$. This approximation has significant practical benefits by reducing the cost of normalization when using flow-dependent vertical correlation length scales. Source: [ALG60].

4D-Var as well as a weak-constraint generalization of the Iterative Ensemble Kalman Smoother (IEnKS) algorithm [10].

### 3.7.1 Modelling spatially correlated observation errors

A method for representing spatially correlated observation errors in variational data assimilation has been developed by [ALG67, ALG36]. The method is based on the numerical solution of a diffusion equation, a technique commonly used for representing spatially correlated background errors. The discretization of the pseudo-time derivative of the diffusion equation is done implicitly using a backward Euler scheme. The solution of the resulting elliptic equation can be interpreted as a correlation operator whose kernel is a correlation function from the Matérn family. In order to account for the possibly heterogeneous distribution of observations, a spatial discretization technique based on the finite element method (FEM) has been chosen where the observation locations are used to define the nodes of an unstructured mesh on which the diffusion equation is solved. By construction, the method leads to a convenient operator for the inverse of the observation-error correlation matrix, which is an important requirement when applying it with standard minimization algorithms in variational data assimilation. Previous studies have shown that spatially correlated observation errors can also be accounted for by assimilating the observations together with their directional derivatives up to arbitrary order. In the continuous framework, we showed that the two approaches are formally equivalent for certain parameter specifications. The FEM provides an appropriate framework for evaluating the derivatives numerically, especially when the observations are heterogeneously distributed. Numerical experiments were performed using a realistic data distribution from the Spinning Enhanced Visible and InfraRed Imager (SEVIRI). Correlations obtained with the FEM-discretized diffusion operator were compared with those obtained using the analytical Matérn correlation model. The method has been shown to produce an accurate representation of the target Matérn function in regions where the data are densely distributed. The presence of large gaps in the data distribution degrades the quality of the mesh and leads to numerical errors in the representation of the Matérn function. Strategies to improve the accuracy of the method in the presence of such gaps are discussed in [ALG67, ALG36].

### 3.7.2 Exploring the potential and limitations of weak-constraint 4D-Var

The standard formulation of 4D-Var assumes random zero mean errors for all sources of information used in the analysis. This assumption is usually not well verified in real-world applications. The performance of a weak-constraint 4D-Var formulation (the so-called 'forcing' formulation) is studied in [ALG45] in a simplified experimental setting using *additive model errors* of different length-scales and observing systems of different coverage and accuracy. A set of twin experiments is carried out and results show that weak-constraint 4D-Var can accurately estimate the actual model errors and the initial state only when background and model errors have different spatial scales and when the observations are unbiased and spatially homogeneous. We also present preliminary results from a different weak-constraint 4D-Var formulation (the so-called 'state' formulation) which could in principle overcome some of these limitations, but at the cost of a substantial increase of computational and memory requirements. These findings help identify the potential but also the intrinsic limitations of the weak-constraint 4D-Var approach. They also help to clarify the experimental results seen in the operational ECMWF analysis system where the analysis and first-guess temperature bias is reduced by up to 50% in the stratosphere.

### 3.7.3 IEnKS in presence of additive model error

Ensemble variational methods are being increasingly used in the field of geophysical data assimilation. Their efficiency comes from the combined use of ensembles, which provide statistics estimates, and a variational analysis, which handles nonlinear operators through iterative optimization techniques. Taking model error into account in 4D ensemble variational algorithms is challenging because the state trajectory over the data assimilation window (DAW) is no longer determined by its sole initial condition. In particular, the control variable dimension scales with the DAW length, which yields a high numerical complexity. This is unfortunate since accuracy improvement is expected with longer DAWs. In [ALG35] we discussed how to algorithmically construct and numerically test an iterative ensemble Kalman smoother with additive model error (IEnKS-Q) which is thought to be the natural weak-constraint generalization of the IEnKS. The number of model evaluations per cycle of the IEnKS-Q is also examined. Solutions based on perturbation decomposition are proposed to dissociate those numerically costly evaluations from the control variable dimension.

**References**

[9] M. E. Aabaribaoune, E. Emili, and V. Guidard, (2020), Estimation of the error covariance matrix for IASI radiances and its impact on ozone analyses, *Atmospheric Measurement Techniques Discussions*, **2020**, 1–26.

[10] M. Bocquet and P. Sakov, (2014), An iterative ensemble Kalman smoother, *Quarterly Journal of the Royal Meteorological Society*, **140**, 1521–1535.

[11] A. Costes, M. C. Rochoux, C. Lac, and V. Masson, (2020), Exploring the effect of inflow turbulence in coupled atmosphere-fire simulations using innovative subgrid fire front reconstruction. (In review for publication in Fire Safety Journal).

[12] N. Elmocayd, S. Ricci, N. Goutal, M. Rochoux, S. Boyaval, C. Goeury, D. Lucor, and O. Thual, (2018), Polynomial Surrogates for Open-Channel Flows in Random Steady State, *Environmental Modeling and Assessment*, **23**, 309–331.

[13] J.-B. Filippi, X. Pialat, and C. B. Clements, (2013), Assessment of ForeFire/Meso-NH for wildland fire/atmosphere coupled simulation of the FireFlux experiment, *Proceedings of the Combustion Institute*, **34**, 2633–2640.

[14] C. Lac, J.-P. Chaboureau, V. Masson, J.-P. Pinty, P. Tulet, J. Escobar, M. Leriche, C. Barthe, B. Aouizerats, C. Augros, P. Aumond, F. Auguste, P. Bechtold, S. Berthet, S. Bielli, F. Bosseur, O. Caumont, J.-M. Cohard, J. Colin, F. Couvreux, J. Cuxart, G. Delautier, T. Dauhut, V. Ducrocq, J.-B. Filippi, D. Gazen, O. Geoffroy, F. Gheusi, R. Honnert, J.-P. Lafore, C. Lebeaupin Brossier, Q. Libois, T. Lunet, C. Mari, T. Maric, P. Mascart, M. Mogé, G. Molinié, O. Nuissier, F. Pantillon, P. Peyrillé, J. Pergaud, E. Perraud, J. Pianezze, J.-L. Redelsperger, D. Ricard, E. Richard, S. Riette, Q. Rodier, R. Schoetter, L. Seyfried, J. Stein, K. Suhre, M. Taufour, O. Thouron, S. Turner, A. Verrelle, B. Vié, F. Visentin, V. Vionnet, and P. Wautelet, (2018), Overview of the Meso-NH model version 5.4 and its applications, *Geoscientific Model Development*, **11**, 1929–1969.

[15] Y. Liu, A. Kochanski, K. R. Baker, W. Mell, R. Linn, R. Paugam, J. Mandel, A. Fournier, M. A. Jenkins, S. Goodrick, G. Achtemeier, F. Zhao, R. Ottmar, N. H. F. French, N. Larkin, T. Brown, A. Hudak, M. Dickinson, B. Potter, C. Clements, S. Urbanski, S. Prichard, A. Watts, and D. McNamara, (2019), Fire behaviour and smoke modelling: model improvement and measurement needs for next-generation smoke research and forecasting systems, *International Journal of Wildland Fire*, **28**, 570–588.

[16] I. Mirouze and S. Ricci, (2020), Smurf: System for Modelling with Uncertainty Reduction, and Forecasting, *Journal of Open Research Software*. (under revision).

[17] R. Paugam, M. Wooster, and G. Roberts, (2013), Use of handheld thermal imager data for airborne mapping of fire radiative power and energy and flame front rate of spread, *IEEE Transactions on Geoscience and Remote Sensing*, **51**, 3385–3399.

[18] H. Peiro, E. Emili, D. Cariolle, B. Barret, and E. Le Flochmoën, (2018), Multi-year assimilation of IASI and MLS ozone retrievals: variability of tropospheric ozone over the tropics in response to ENSO, *Atmospheric Chemistry and Physics*, **18**, 6939–6958.

[19] S. Prichard, N. S. Larkin, R. Ottmar, N. H. French, K. Baker, T. Brown, C. Clements, M. Dickinson, A. Hudak, A. Kochanski, R. Linn, Y. Liu, B. Potter, W. Mell, D. Tanzer, S. Urbanski, and A. Watts, (2019), The Fire and Smoke Model Evaluation Experiment – A plan for integrated, large fire–atmosphere field campaigns, *Atmosphere*, **10**.

[20] J. Ramshaw, P. O'Rourke, and L. Stein, (1985), Pressure gradient scaling method for fluid flow with nearly uniform pressure, *Journal of Computational Physics*, **58**, 361–376.

[21] M. Rochoux, A. Collin, C. Zhang, A. Trouvé, D. Lucor, and P. Moireau, (2018), Front shape similarity measure for shape-oriented sensitivity analysis and data assimilation for Eikonal equation, *ESAIM: Proceedings and Surveys*, **63**, 215–236.

[22] M. C. Rochoux, L. Thouron, G. Rea, F. Auguste, T. Jaravel, and O. Vermorel, (2020), Large-eddy simulations of micro-scale meteorology and pollutant dispersion: Multi-model variability for the MUST experiment. (In review for publication in Boundary-Layer Meteorology).

[23] P. Roy, N. Elmocayd, S. Ricci, J.-C. Jouhaud, N. Goutal, M. De Lozzo, and M. Rochoux, (2018), Comparison of Polynomial Chaos and Gaussian Process surrogates for uncertainty quantification and correlation estimation of spatially distributed open-channel steady flows, *Stochastic Environmental Research and Risk Assessment*, **32**, 1723–1741.

[24] A.-L. Tiberi, N. Goutal, S. Ricci, P. Sergent, M. Taillardat, F. Bouttier, and C. Monteil, (2020), Strategies for hydrologic ensemble generation and calibratio: on the merits of using model-based predictors, *Journal of Hydrology*. (under revision).

[25] A.-L. Tiberi, N. Goutal, S. Ricci, P. Sergent, J. Viatge, C. Monteil, and F. Bouttier, (2020), Etude de sensibilité golbale comparée des modèles hydrologiques GRP et MORDOR-TS, *La Houille Blanche*. (under revision).

[26] C. Zhang, (2018), *Data-driven simulations of wildfire spread at regional scales*, PhD thesis, University of Maryland, College Park.

# Coupling, HPC and Data for Climate

## 4.1 Introduction

Research activities at CERFACS are characterized by a balance of scientific studies and development of tools and methods supporting these studies.
The development of coupling software is one recognized area of CERFACS expertise since the first release of the OASIS coupler in 1993, which specializes in coupling components of the Earth System. CERFACS expertise in code coupling is further reinforced with the development of the more generalist OpenPALM coupler, which main difference with respect to OASIS is the dynamic launching of the coupled components. Beyond developing couplers, CERFACS is also involved in different projects working on coupling methods, as is described below with the work on inconsistencies in the representation of the coupling at the ocean-atmosphere interface and on hydrological multidimensional coupling. CERFACS also participate in improving coupled model performances, by proposing new coupling algorithms and implementations, as illustrated below for an ocean biogeochemistry component.
Another central activity is to help manage the deluge of data resulting from climate runs, from production to preservation and dissemination through dedicated networks. We focus on innovating technical solutions for data access and close-to-data analysis.

## 4.2 Coupler development

### 4.2.1 OpenPALM

OpenPALM implements methods to easily integrate high performance computing applications in a flexible and evolutive way, proposing solutions to the balance between performance, software reuse and numerical accuracy. OpenPALM is composed of three complementary components: (1) the PALM library, (2) the CWIPI library and (3) the graphical interface PrePALM. As the application programming interface is available in Fortran and C/C++, OpenPALM can couple codes written in different languages. Developed mainly by CERFACS, PALM and PrePALM implement dynamic launching of the coupled components, full independence of the components from the application algorithm, parallel data exchanges with redistribution and separation of the physics from the algebraic manipulations performed by the PALM algebra toolbox. More recently, CERFACS participates in the development of ONERA's coupling library CWIPI. The library provides a fully parallel communication layer for mesh-based coupling (1D, 2D or 3D) between several parallel codes with MPI communications.
During the last 2 years, the following main developments have been integrated into the libraries:

- Integration of dynamic distributors for PALM parallel communications in collaboration with KIT (Karlsruhe Institute of Technology);
- Possibility to run an OpenPALM application without the driver when needed (mainly for multiphysics and multicomponent simulations with CWIPI library);
- Development of a save-and-reuse (in memory or on disc) strategy of mesh localisation and interpolation weights in CWIPI for periodic simulation such as in turbomachinery applications;

- Development of a preliminary version of an inline update of the localisations for moving mesh applications such as turbomachinery and fluid/structure interactions.
- Tests of the new developments on high-order interpolation in CWIPI done by ONERA and its integration in OpenPALM. The development of high-order solvers such as Discontinuous Galerkin methods Spectral differences received this last decade a growing attention in the CFD field. Such solvers imply curved elements defined by high-order polynomials and ONERA has implemented in CWIPI algorithms to perform interpolations compliant with such high-order numerical schemes. This interpolation is for the moment limited for surfaces and CERFACS has validated its strong scalability up to 8000 cores. Results show that the localisation time depends on the order of the interpolation, the higher the order the longer the localisation. The scaling of this coupling step is almost equivalent for all orders illustrating that the performances of the CWIPI library are not degraded by the high-order treatment. Concerning the time taken by the interpolation and exchange of data, the same observation is made except that at high number of cores, this time is equivalent for all interpolation orders.

Here after is the list of OpenPALM applications that were developed or maintained at CERFACS for its own use or for the needs of its partners during the last two years :

- In the context of atmospheric chemistry, the variational DA suite for the Meteo France chemistry transport model MOCAGE (DAIMON) is currently based on OpenPALM, which is used to schedule the DA tasks and monitor their execution.
- OpenPALM is used for multidimensional coupling between 1D and 2D hydraulic solvers. In this work, the coupling interface is parallel to the flow and the 2D model activated only when the river over flows in the flood plain. This work is carried out at LHSV, in collaboration with EDF, INRIA and CERFACS.
- AquiFR (http://www.metis.upmc.fr/ aqui-fr/), which aims to monitor and forecast groundwater resources in France as well as to facilitate climate change impact assessments. OpenPALM makes it possible to manage the various hydro-geological applications of the 3 models (computing codes) integrated to date (Eros, Marthe and Eau-dyssee). CERFACS provided PALM support to the laboratories in charge of the development of Aqui-FR (BRGM, Meteo-France, UPMC,...). Details of this support is given in [CE155];
- OpenPALM is intensively used in many multi-physic and multi-component studies in the Computational Fluid Dynamic team of CERFACS. Firstly, an important axis deals with aerothermal simulations for aeronautic (combustion chambers, turbine blades, ...) and automotive applications. In this context, a coupled model based on three codes (AVBP for the convection, AVTP for the conduction is solids and PRISSMA for the radiation) was developed with OpenPALM.
- TurboAVBP system that couples several instances of the AVBP code with OpenPALM is intensively used for compressor, turbine and integrated combustion chamber/turbine simulations in CFD team. Recent developments have concerned the interpolation order as detail in the CFD Team section 2.5.1 of the report.
- OpenPALM is used for deep learning around the AVBP code in the CSG/COOP team, it allows to send directly from memory to memory the unstructured AVBP meshes by interpolating them on structured meshes necessary for the deep learning code.
- An aeroacoustics application is developed with AIRBUS in the CFD team to simulate by coupling the interactions between an aircraft and its engines. The purpose of this application is to model the aircraft and engines separately between AIRBUS and SAFRAN and to perform the simulation on two different sites without having to exchange meshes, which remain confidential for both

companies. The solver is ONERA elsA code and data exchanges at the interface between the aircraft and engines are performed by OpenPALM client/server mode with TCP/IP protocol, which allows communications between heterogeneous computers. More details in the CFD Team section 2.5.2 of this report.

- The CLUE platform (urban climate, the successor of ACCLIMAT) is a little aside since it is now hosted and maintained at Meteo-France by the DSM. Nevertheless, it strongly relies on openPALM and CWIPI: the assembling of the core model components into a single platform is ensured with PALM and CWIPI library is used for high-frequency coupling between MesoNH and Surfex-offline. In the future, Meteo-France is willing to maintain this tool operational to answer study demands over metropolitan and DOM-TOM cities. The openPALM/CWIPI know-how have now been transferred to the DSM and Cerfacs remains present for backup support.

The last version of OpenPALM is currently used mainly in France in more than 150 applications. Beyond CERFACS, OpenPALM is used by all CERFACS teams and by almost all partners, including Safran, Onera, Météo-France, CNES, EDF and AIRBUS. This generates a lot of support and consulting work for applications in extremely varied fields for which CERFACS multi-disciplinary expertise is extremely valuable. One OpenPALM training session was provided each year in 2019 and 2020.

### 4.2.2 OASIS3-MCT

The OASIS coupler is an open source software developed at CERFACS to couple numerical codes modelling the different components of the Earth System. The last official version of the coupler, OASIS3-MCT_4.0, was released in June 2018. OASIS3-MCT provides fully parallel coupling including parallel matrix vector multiplication for the remapping and parallel exchanges of coupling fields, using the Model Coupling Toolkit (MCT), developed by the Argonne National Laboratory (USA), as a lower layer.

OASIS is developed in an international perspective being one of the key elements of the European ENES infrastructure, fostering the common development of models and tools for HPC climate modelling in Europe. At the national level, OASIS is one cornerstone of CLIMERI-France infrastructure for climate modelling and it is used in many research laboratories besides CERFACS (CNRM, LOCEAN, LMD, LSCE, LA, LATMOS, LEGOS, LGGE, IFREMER, ENSTA, SHOM).

Besides the permanent manpower ensured by CERFACS (0.5 FTE) and CNRS (0.5 FTE), the main sources of external funding in 2019 and 2020 came from EU projects (35 pms from IS-ENES3 and 16 pms from ESiWACE2 over the 2019-2022 period). The priority of the developments realized in these projects is established by the developers, based on perceived user needs, and is reviewed and approved by the OASIS Advisory Board. The OASIS development plan was updated in 2019 [CE165] and in 2020 [CE166] .

The user survey realised in 2019 confirmed that OASIS3-MCT is used by at least 67 modelling groups to assemble more than 80 different coupled applications over the 5 continents. These applications include global or regional configurations of ocean and atmosphere models but also sea ice, sea level, wave, ocean biogeochemistry, land, vegetation, river routing, hydrological and atmospheric chemistry models. In particular, OASIS3-MCT_4.0 sources were downloaded about 500 times since its release in July 2018 from groups all over the world. OASIS3-MCT is used in 5 of the 7 European Earth System Models participating to CMIP6.

In 2019 and 2020, CERFACS intensively used the climate models developed by the CNRM-CERFACS group, in particular to realise the numerical experiments of the following MIPs of the 6th international Coupled Model Intercomparison Project (CMIP6): HighResMIP (High Resolution Model Intercomparison Project), PAMIP (Polar Amplification Model Intercomparison Project) and DCPP-C (part C of the Decadal Climate Prediction Project) and also other experiments on the sea ice and on the Atlantic multidecadal variability in the PRIMAVERA European project. These models are the ocean/sea-ice/atmosphere/land/river-routing models CNRM-CM6-1-LR at low resolution (NEMO-Gelato at $\sim 1\circ$, ARPEGE-Surfex T127 ~150 km) and CNRM-CM6-1-HR at high resolution (NEMO-Gelato at ~0.25 $\circ$, ARPEGE-Surfex T350 ~50 km), and the Earth System version, CNRM_ESM2-1 that also includes atmospheric chemistry, aerosols as well as interactive land and ocean carbon cycles. CERFACS also assembled the "very-high resolution" version of CNRM-CM6-1, CNRM-CM6-1-VHR, based on the same components than CNRM-CM6-1-HR, except that NEMO v3.6 is used in the ORCA12 (1/12 degree) configuration; this work is still on-going. Finally, we note that OASIS3-MCT is also a building block of CNRM regional climate model coupling ALADIN_Climate V6, SURFEX v8, CTRIP, and NEMOMED12 (a regional version of NEMOv3.6).

Active user support was continuously delivered by CERFACS to the OASIS user community during these past 2 years through mail exchanges and via the forum, by maintaining the web site (https://portal.enes.org/oasis), and by organizing training sessions. One traditional in-person two-day sessions was organised at CERFACS with 3 participants in March 2019. Another session was organised for 9 persons in July 2020 and due to the current sanitary context, on-line training was preferred, in the form of a SPOC (Small Private Online Course, see https://cerfacs.fr/code_coupling_with_oasis3-mct/). This SPOC, mixing theory, videos, quizzes and hands-on, took place over one week and required about 15 hours of work from each participant.

Dedicated user support, i.e. organising the visit of an OASIS developer to a chosen institute to help setting up or optimising a coupled system, was provided in the IS-ENES3 and ESiWACE2 context. In 2019, the support was provided as planned to 3 groups (ETH Zürich, UK MetOffice, GEOMAR Kiel) with a visit of one month each. In 2020, the support has suffered some delay due to covid-19. One support was provided remotely to NERSC Bergen and the service planned to GEOMAR Kiel has been delayed beginning of 2021. We are however confident that the total level of services planned will be provided before the end of those two projects.

Finally, CERFACS was the main organizer of the 5th Workshop on Coupling Technologies for Earth System Models (CW2020, [CE167]) that was held virtually on September 21st-24th 2020. 152 leading researchers and practitioners in the field of coupling infrastructure for Earth System Models from all around the world registered, and about 80 people attended each session to discuss the latest updates on coupling technologies, coupled applications in Earth System modelling, computational performances of coupled models, links between data assimilation and coupling, and coupled model workflows.

Regarding specific developments done over 2019 and 2020, we can list the main following ones:

- In OASIS3-MCT_4.0, the SCRIP library was parallelized with OpenMP/MPI, leading to a reduction in the calculation time of the remapping weights for high-resolution grids by 2 or 3 orders of magnitude as compared to the sequential version. But the SCRIP still shows specific problems near the pole for some grids and some algorithms ([CE164], [CE140]) and this motivates the investigation of other parallel interpolation libraries of higher quality. ESMF, XIOS, ATLAS, YAC, MOAB/TempestRemap are being considered. We have been working intensively on this task in 2020, which is one of the main tasks funded in IS-ENES3.

- To be truly conservative, remapping weights have to be normalised by the "true" area of the grid cells i.e. the area of the cells as considered by the models themselves and not as calculated by the remapping library. This option discussed in the CMIP6 context is now available on the trunk version of OASIS3-MCT.

- Python bindings have been developed to allow the coupling of models coming from a much wider community. We think that these new bindings will help attract countries less advanced in HPC into code coupling. A beta version of OASIS3-MCT including those Python bindings is available and under test.

- LUCIA is the tool delivered with OASIS3-MCT to automatically evaluate the load balance of the coupled components. The analysis provided by LUCIA, which was previously only providing an integrated view over the whole simulation, has been extended so to identify the load imbalance at every coupling time step.

- The API routine oasis_get_intracomm that merges two MPI communicators from two components to form a new communicator has been extended to more than 2 components. This is needed in coupled models involving both OASIS3-MCT and XIOS when XIOS manages ensemble simulations.
- Source management has been migrated from SVN to GIT. This will be is of great benefit for OASIS3-MCT users given GIT distributed method for version control. GIT branching and merging features are also more evolved than in SVN.

In conclusion, given the latest performance improvements implemented in OASIS3-MCT_4.0 and evolutions planned for OASIS3-MCT_5.0 due December 2021, we consider that OASIS3-MCT provides and will keep on providing an efficient and easy-to-use coupling solution for many climate modelling groups for at least the next 5 years.

## 4.3 Coupling Methods

### 4.3.1 Iterative methods for ocean-atmosphere coupling

CERFACS also contributes to improved representation of air-sea interactions in coupled models, working in particular on inconsistencies linked to the discretization in space and in time. In space, physical inconsistencies result from the difference in the numerical grids used by atmospheric and oceanic models; the work on this theme involving the concept of an ”exchange grid” was reported in the previous scientific report. In time, current asynchronous coupling algorithms do not allow for a correct phasing between the ocean and the atmosphere, and hence between their diurnal cycles, potentially inducing biases in the estimation of daily maxima.

One way to have a consistent interface is to implement Schwarz iterations [31] while coupling the models. The principle of the method is to repeat each coupling period many times, with the same initial condition for each iteration, but with boundary conditions calculated by the other model for the same period (and not during the previous coupling period as in the asynchronous scheme) during the previous iteration. This is repeated until convergence of the surface variables and fluxes.

Schwarz iterations have been implemented in simulations using CNRM-CM6-1D, a single-column version of CNRM-CM6-1 [27]. The simulation performed for one point in the Indian ocean covers one day (November 13, 2011) of the Cindy Dynamo campaign [30] from which the atmospheric lateral forcings are obtained. Runs with coupling periods of 300 s (which is the timestep of the models), 3600 s, 3 hrs, 6 hrs and 12 hrs. were realized. Figure 4.1 shows the resulting diurnal cycle of the Sea Surface Temperature (SST) obtained with the different coupling periods for A) traditional asynchronous coupling and B) after convergence of Schwarz iterations.

These results show that the coupling period can have a strong impact on asynchronous simulations (Fig.4.1-A). The longer the coupling period is, the more lagged the diurnal cycle is. As shown on Fig.4.1-B, the Schwarz method is very efficient to reposition the diurnal cycle. It even succeeds in reversing the diurnal cycle obtained for the run with the coupling period of 12 hours. In the current case, 20 iterations were realized for each coupling period but it was observed that strong convergence is always obtained in less than 10 iterations and that most of the correction is achieved after two iterations only.

The Schwarz iterative method represents an efficient way of correcting the inconsistencies introduced by the asynchronous coupling and obtaining a coherent ocean-atmosphere interface. However, the cost involved is clearly very high for 3D models as applying even only two iterations would double the cost of the simulation. Work is underway to identify subsystem in the models, e.g. only the atmospheric physics and not the whole dynamics, onto which the iterations could be applied, thereby reducing the cost of the

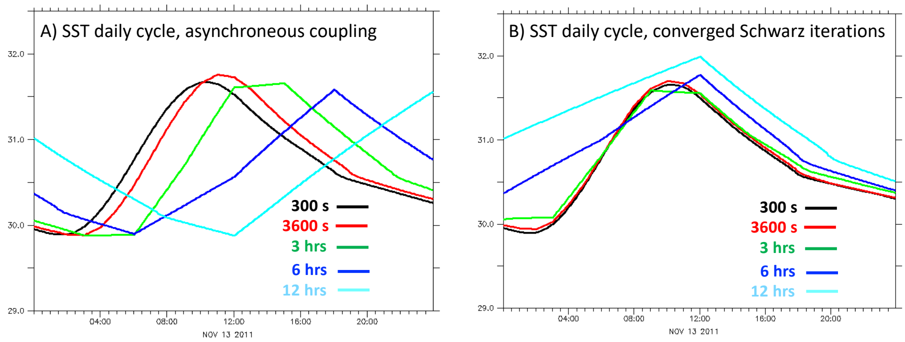


Figure 4.1: Diurnal cycle for a one-day simulation realized with CNRM-CM-1D with different coupling periods of 300 s, 3600 s, 3 hrs, 6 hrs and 12 hrs: A) traditional asynchronous coupling, B) after convergence of Schwarz iterations.

method. Schwarz iterations can also be considered as a method to provide a clean reference coupled solution that can be used to evaluate the biases of other coupling methods.

### 4.3.2 Methods for hydrological multidimensional coupling

Multi-dimensional coupling strategies were investigated in the context of river hydrodynamics to reduce the cost and input data description burden of full 2D models. The flow is represented with a 1D model when mono-dimensional, making the most of past expertise and calibration, and with a 2D local model in confluence and floodplains for high flow. This research axis was investigated in collaboration with EDF-LNHE, LHSV, ARTELIA, SCHAPI and INRIA. CERFACS, is part of the TELEMAC-MASCARET Consortium. [28] present the 1-D/2-D longitudinal coupling between MASCARET and TELEMAC on the Adour river. With this strategy, the 1-D and 2-D models are coupled at their longitudinal boundaries with an iterative Schwarz algorithm applied at each interface (Fig. 4.2-left). It was shown that the coupling algorithm converges with at most five Schwarz iterations; the water level and velocity continuity is guaranteed at the model interfaces and the 1-D/2-D coupled model is approximately eight times faster than a full 2-D model. An alternative solution for floodplains dynamics is lateral coupling. The river bed is represented by a unique 1D model overflowing into the floodplains through local 2D models inheriting their boundary condition from the 1D (Fig. 4.2-right). The flux at the interface is computed with a Riemann solver.
The longitudinal coupling strategy was implemented making use of TELEMAC-MASCARET APIs (Application Programming Interface) as well as complementary classes dedicated to data driven integration of the solvers, to be as non-intrusive as possible in the numerical solvers. Python language was used with Mpi4Py for easier portability within any workflow platform. These developments were integrated in the

SVN source code repository for Telemac (opentelemac.org). This work was presented in the Workshop Session of the Telemac User Conference 2019 [CE159]. The choice of the coupling parameters such as coupling time step, checkpoint along time, criteria for convergence of the iterative Schwarz algorithm should be further studied for use in operational applications and real-time flood forecasting as this remains case-dependent.

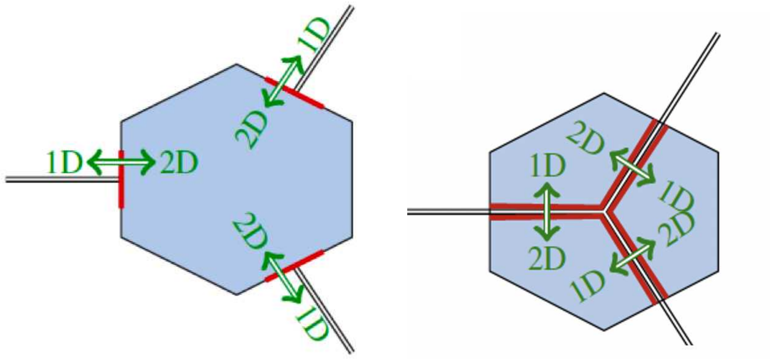


Figure 4.2: MASCARET-TELEMAC2D coupling strategies. (left) 1D-2D longitudinal coupling, (right) 1D-2D lateral coupling

### 4.3.3 Coupling Method for Local Time Stepping in Computational Fluid Dynamics simulations

Local Time Stepping (LTS) techniques bring a potential solution to mitigate the CPU cost induced by the stability constraints of explicit time-advancement methods in Computational Fluid Dynamics (CFD) solvers. With LTS strategies, the initial domain is divided in multiple sub-domains, each one with its own stability constraint. By doing so, the limit of maximum allowable time steps is relaxed for each sub-domain, bringing significant cost reduction compared to the initial simulation. Knowing the distribution of mesh cells in each domain as well as their respective time step, the theoretical acceleration can be computed. Such an approach necessitates careful numerical analysis of a given numerical scheme / LTS method aggregate, if applied to a Large-Eddy Simulation (LES) solver.

The LTS method is implemented in the AVBP solver developed by CERFACS. The exchange of conservative variables at the interface between the different domains is performed by the CWIPI library developed by ONERA. Both the theoretical CPU cost reduction and scheme properties have been validated on cases with increasing complexities such as the 2D convection of an isentropic vortex (Fig. 4.3) and turbomachinery applications. To validate the spatial convergence of LTS on the 2D vortex case, the pressure fields of the reference and the LTS coupled cases at $t = T = 2L_x/U_0$ are compared to the analytical solution at the same time. Associated quadratic errors are plotted as a function of the cell size $\Delta x$ of the central domain, *i.e.* the coarser mesh (Fig. 4.4). For different values of $n_{ratio}$ defining the ratio between the time-steps of the two domains, results are very satisfying (Fig. 4.4). The spatial orders of each numerical scheme are correctly recovered.

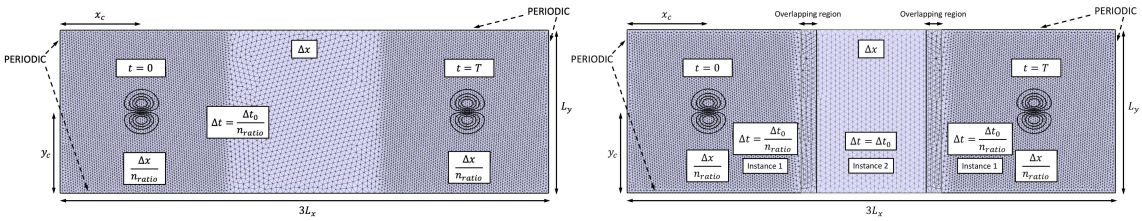


(a) Reference case, single grid, no interface.

(b) LTS case, two instances.

Figure 4.3: Example of computational domain for the convected vortex test case.

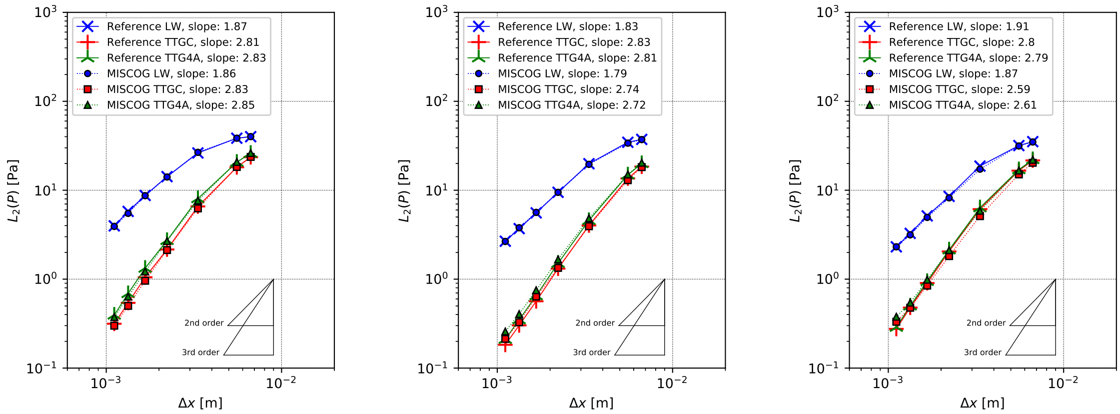


(a) $n_{ratio} = 1$.

(b) $n_{ratio} = 2$.

(c) $n_{ratio} = 4$.

Figure 4.4: Quadratic error on the pressure at time $t = T$ for the reference and the LTS coupled cases, for numerical schemes available in AVBP LW (2nd order in time and space), TTGC (3rd order in time and space) and TTG4A (4th order in time and 3 in space) and for different ratio of time steps $n_{ratio}$.

## 4.4 High Performance computing and data management for climate modelling

### 4.4.1 Coupled model components performance

Representation of always more phenomena, at always smaller scales in space and time requires to optimally make the most of the available computing power. In this trend, the inclusion of ocean biogeochemistry (BGC), for carbon cycle modelling in ESMs [CE118], is particularly demanding. As put in evidence in [CE141], the chemical species reactions and advection can multiply the NEMO ocean model cost by a factor of more than 3. On our most powerful supercomputers, this forbids to switch on this BGC module, called TOP-PISCES at global spatial resolution higher than 1 degree. A finer representation of the ocean circulation would increase ESMs reliability, but the same dependency to resolution is not as clear for BGC processes. This leads to the idea of a coupled system that includes ocean and BGC submodels with different spatial resolution.

As a first step, we followed the strategy already proposed for NEMO ocean and sea ice components [32]: the surface module, which includes the sea ice, is separated from the ocean. Communication of surface quantities between the two new executables is ensured by the OASIS coupler (see section 4.2). This implementation, recently updated in NEMO 4.0 [CE146], shows interesting computing performance. The separation of the two submodels in two executables allows to perform their computations concurrently, increasing what we call the macro-task parallelism. The separated codes are more modular (they can be developed and upgraded separately) and an optimum number of resources can be allocated for each of them, which usually improve the performance of the whole coupled system (assuming that a good load balancing between components can be achieved). Finally, the modularity of this configuration will facilitate the last step of the solution we are proposing here for the biogeochemistry: a multi-grid coupled system.

To compose the new coupled model, we started from the offline version of the biogeochemistry (BGC) model, TOP-PISCES, and defined its OASIS interface for coupling with the stand alone NEMO ocean/sea-ice configuration, to be able to exchange 3D quantities at model time step frequency. This configuration produces the same results than the standard online ocean/sea-ice/BGC single executable, even if bit to bit result cannot be reproduced. We find no significant bias to the concurrent (instead of sequential) execution of ocean and BGC calculations. In that concurrently coupled configuration, performance can be enhanced (25% of the maximum speed), but an estimation of the extra cost induced by the exchange between the two components of several 3D variables at each model time step is relatively big (around 20%) and limits any further performance gain [CE150]. The coarsening of the BGC component (reduction of the horizontal resolution, [29]) is now the next goal toward a breakthrough performance gain. This OASIS based coupled system can pave the way for a modular and perennial implementation of this coarsening.

### 4.4.2 Data production and management for CMIP6

This activity conducted at Cerfacs during the past 2 years is in the straight continuity of the CNRM-CERFACS modelling group contribution to the 6th phase of the international Coupled Model Intercomparison Project (CMIP6). This international exercise, on which the IPCC report is based, is a long-term project Cerfacs is engaged in since mid-2016. While the first years were mainly devoted to model development and tuning, runtime environment development, and realization of the HighResMIP numerical experiments, the last two years were rather focused on data management and data sharing through the PRIMAVERA data server (CEDA/Jasmin) and data publication on the ESGF distributed data Network, so that the data produced becomes available to the whole climate community. These tasks required to get expertise on community tools like the ESGF publisher and to develop a data management tool suite so as to ensure data handling over their whole life cycle (Fig. 4.5). In addition, CNRM-CM6 model runs continued over this period for DCPP-C and PAMIP, the two other MIPs the Cerfacs is responsible for on behalf of the CNRM-CERFACS group.

We are clearly in massive data management context (30 times CERFACS production for CMIP5 if considering the final useful data) that requires careful attention, important human resources and a robust data management workflow. Over the 2016-2020 period, 70 million core-hours were consumed by Cerfacs on the Meteo-France Bull-X computer (25 million over 2019-2020) and about 1.5 PB used on Hendrix (the HPC storage) for a final useful data volume of about 650 TB. This represents about 1500 simulations and 9000 simulated years (including PRIMAVERA additional simulations that are variants of DCPP-C or sensitivity experiments). Up to now, about one third in volume ( 200 TB) is published on ESGF (accessible on any ESGF data portal, e.g. https://esgf-node.ipsl.upmc.fr/search/cmip6-ipsl/), which represents 100 000 datasets; reported in percent of simulated years it reaches 80% which means that most of the frequently used data is available on ESGF (apart PAMIP which publication will start end of 2020). The remaining data are mainly high frequency and less requested by scientific users but will be published as well.

Like in previous report, we want to mention that this activity was only made possible thanks to an intense cooperation with IPSL and CNRM engineers and scientists involved in CMIP6. Cerfacs also benefited from CMIP6 dedicated computational resources and storage allocated yearly since 2016 by Meteo-France.

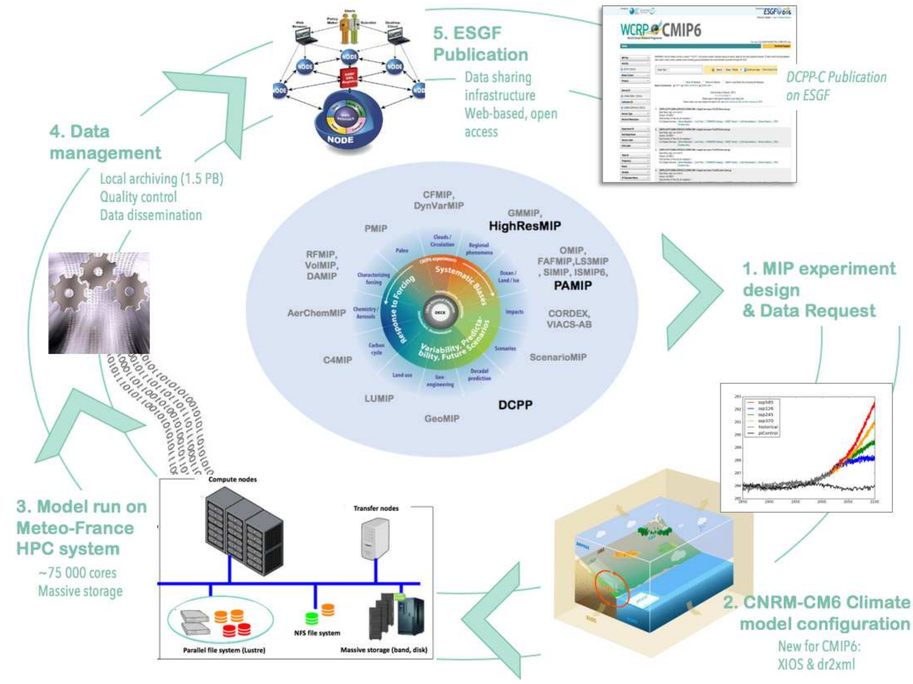


Figure 4.5: CMIP6 data life cycle: sequence of steps from the design of CMIP6 experiments to the data publication on the ESGF nodes.

### 4.4.3 European and International Data infrastructures

The development of the scientific data infrastructure for researchers at the European and international levels is very important to support our activities and the dissemination of our results. We have been involved in many related European projects and initiatives, and we have now gained a very good reputation and visibility. Consequently, we are solicited to participate in several consortium leading project proposals on this thematic, funded by H2020 and CEF (Connecting Europe Facility) research frameworks, as well as being invited to events and to give invited presentations on the subject.

During the last years, European funded projects that sustained those activities were CEF PHIDIAS and H2020 IS-ENES3 and DARE. One project proposal is in preparation to continue developing this activity (Green Deal). In addition, CERFACS has been approved as a new member of the EUDAT CDI. The IS-ENES3 project also sustains those activities, especially on the user interface (IS-ENES CDI C4I: climate4impact.eu), the processing back-ends as well as the interfaces to other infrastructures and e-infrastructures. Those projects also favor CERFACS active engagement in the ESGF Compute Working Team (CWT) supporting CMIP model simulations as well as IPCC reports.

Major results are:

- Further developments and significant optimization of the python-based open-source climate indices workflow back-end created and developed by CERFACS: ICCLIM (https://icclim.readthedocs.io). This python package has seen a rapid increase of interest internationally, associated with active interests from many groups. The climate indices are those identified as the most used and useful by the international community: currently, the 49 climate indices as defined by European Climate Assessment & Dataset based on air temperature and precipitation variables are included (http://www.ecad.eu/). Significant achievements: used for CMIP6 official products/indices calculation, and chosen as the main processing package for Ouranos/CRIM Canadian climate research infrastructure;

- Our commitment in the EUDAT CDI is sustaining the installation of the EUDAT B2SHARE service locally at CERFACS, operated by CSG. This service can be used to distribute climate simulations and datasets that we provide to other partners in our projects, as well as hosting datasets linked to published articles;
- Development of data processing workflow platforms interfacing the IS-ENES climate4impact.eu (IS-ENES3, DARE and EUDAT CDI);
- Developing collaboration with shareholders IT (Météo-France DSI and CNRM, CNES, EDF) and close collaborators (Mercator-Ocean) on data analytics and on-demand data processing in the context of European and International e-Infrastructures. CERFACS is actively involved in this context through international initiatives and projects. Regular meetings will be organized to strengthen the collaboration on this thematic.

## References

[27] A. Y. Abdel-Lathif, R. Roehrig, I. Beau, and H. Douville, (2018), Single-column modeling of convection during the CINDY2011/DYNAMO field campaign with the CNRM climate model version 6., *J. Adv. Mod. Earth Systems*, **10**, 578–602.

[28] S. Barthélémy, S. Ricci, T. Morel, N. Goutal, E. Le Pape, and F. Zaoui, (2018), On operational flood forecasting system involving 1D/2D coupled hydraulic model and data assimilation, *Journal of Hydrology*, **562**, 623–634.

[29] S. Berthet, R. Séférian, C. Bricaud, M. Chevallier, A. Voldoire, and C. Ethé, (2019), Evaluation of an online grid-coarsening algorithm in a global eddy-admitting ocean biogeochemical model, *Journal of Advances in Modeling Earth Systems*, **11**, 1759–1783.

[30] P. E. Ciesielski, H. Yu, R. H. Johnson, K. Yoneyama, M. Katsumata, and C. N. e. a. Long, (2014), Quality-controlled upper-air sounding dataset for DYNAMO/CINDY/AMIE: Development and corrections, *Journal of Atmospheric and Oceanic Technology*, **31**, 741–764.

[31] F. Lemarié, E. Blayo, and L. Debreu, (2015), Analysis of Ocean-atmosphere Coupling Algorithms: Consistency and Stability, *Procedia Computer Sci.*, **51**, 2066–2075.

[32] E. Maisonnave and S. Masson, (2015), Ocean/sea-ice macro task parallelism in NEMO, technical report, CECI, Université de Toulouse, CNRS, CERFACS, Toulouse, France.

# Publications

## 5.1 Books

[CE1] N. Gallois, N. Flipo, J. Schuite, A. Rivière, P. Viennot, F. Baratelli, B. Labarthe, R. Bonnet, and J. Boé, (2019), *Rapports de synthèse de fin de phase VII du programme PIREN Seine*, vol. 4 of Mesures hydrogéophysiques et biogéochimiques haute-fréquence et time lapse des interfaces nappe-rivière : évolution des ressources en eau, PIREN Seine.

[CE2] J. Johnston, R. Paugam, E. Whitman, A. Cantin, and T. Schiks, (2019), *Encyclopedia of Wildfires and Wildland-Urban Interface (WUI)*, Fires. Springer, Cham.

[CE3] E. Whitman, J. Johnston, T. Schiks, R. Paugam, and A. Cantin, (2019), *Encyclopedia of Wildfires and Wildland-Urban Interface (WUI)*, Fires. Springer, Cham.

## 5.2 Conferences Proceedings

[CE4] M. Atkinson, R. Filgueira Vicente, I. Klampanos, A. Koukourikos, A. Krause, F. Magnoni, C. Pagé, A. Rietbrock, and A. Spinuso, (2019), Comprehensible Control for Researchers and Developers Facing Data Challenges, In *15th International Conference on eScience (eScience 2019), San Diego, CA, USA, 24-27 September*.

[CE5] J. Boé, R. Bonnet, G. Dayon, F. Habets, and E. Martin, (2019), Projection des changements hydro-climatiques au cours du 21ème siècle: de l´échelle mondiale au bassin de la Seine, In *Colloque les 30 ans du PIREN-SEINE, 11-13 décembre, Paris*.

[CE6] J. Boé, S. Sommot, L. Corre, and P. Nabat, (2019), Discrepancies in summer climate change over Europe as projected by global and regional models: role of aerosols, In *6th Med-CORDEX workshop, 25-29 novembre, Toulouse*.

[CE7] J. Boé, (2019), Tendances passées de température en été sur l´Europe de l´Ouest : des progrès dans CMIP6 ?, In *Atelier CMIP6, 27-28 mai, Bordeaux*.

[CE8] M. Bushuk, R. Msadek, M. Winton, and G. Vecchi, (2019), Seasonal predictions of Arctic sea ice, In *Workshop on Sea Ice in the Earth System. Brest, 4-6 June , France,*.

[CE9] A. Cazenave, F. Birol, M. Passaro, Y. Gouzenes, P. Rogel, J. Legeais, and J. Benveniste, (2019), Present-day Sea Level Changes in the World Coastal Zones, In *AGU Fall Meeting American Geophysical Union, San Francisco, USA, 9-13 décembre*.

[CE10] S. Chripko, R. Msadek, E. Sanchez-Gomez, and L. Terray, (2019), Northern Hemisphere atmospheric response to Arctic summer sea ice loss in CNRM-CM6, In *APPLICATE General Assembly 2019, Reading, 28 January-1 February, United Kingdom*.

[CE11] S. Chripko, R. Msadek, E. Sanchez-Gomez, and L. Terray, (2019), Northern Hemisphere atmospheric response to Arctic summer sea ice loss in the CNRM-CM6 climate model : mechanisms and impacts, In *EGU General Assembly, Vienna, Austria, 7-12 April*.

[CE12] S. Chripko, R. Msadek, E. Sanchez-Gomez, L. Terray, M.-P. Moine, and L. Bessières, (2019), Atmospheric Response to Arctic Sea Ice Loss in Low and High Resolution Coupled Experiments, In *Fall Meeting AGU, San Francisco, USA, 9-13 décembre*.

[CE13] S. Chripko, R. Msadek, E. Sanchez-Gomez, L. Terray, M.-P. Moine, and L. Bessières, (2019), Atmospheric response to Arctic sea ice reduction in the CNRM-CM6 model, In *2019 IUGG meeting, Montreal, July 8-18, Canada*.

[CE14] S. Chripko, R. Msadek, E. Sanchez-Gomez, L. Terray, M.-P. Moine, and L. Bessières, (2019), Northern Hemisphere atmospheric response to Arctic summer sea ice loss in the CNRM-CM6 climate model, In *Exeter University, 3 May, United Kingdom.*

[CE15] S. Chripko, R. Msadek, E. Sanchez-Gomez, L. Terray, M.-P. Moine, and L. Bessières, (2019), Northern Hemisphere autumn and winter atmospheric response to Arctic summer sea ice loss in the CNRM-CM6 climate model, In *Workshop on Sea Ice in the Earth System. Brest, 4-6 June, France*.

[CE16] A. Costes, C. Lac, V. Masson, and M. Rochoux, (2019), Compressible version of the Meso-NH model and application to coupled fire-atmosphere simulations, In *Journées Utilisateurs Meso-NH, OMP Toulouse, 7-8 October*.

[CE17] S. El Garroussi, M. De Lozzo, S. Ricci, D. Lucor, N. Goutal, C. Goeury, and S. Boyaval, (2019), Uncertainty quantification in a two-dimensional river hydraulic model, In *UNCECOMP 2019, Crete, Greece, 24-26 June*.

[CE18] S. El Garroussi, S. Ricci, M. De Lozzo, N. Goutal, and D. Lucor, (2019), Mixture of polynomial chaos expansions for uncertainty propagation, In *Telemac User Conférence, Toulouse, France, 15-17 Oct.*

[CE19] S. El Garroussi, S. Ricci, M. De Lozzo, P. Roy, I. Mirouze, N. Goutal, S. Boyaval, D. Lucor, and V. Laborie, (2019), Contribution and on-going research on sensitivity analysis and surrogate models at CERFACS with an application in 2D hydrodynamics, In *OpenTURNS Journee Utilisateurs, June, 7th 2019*.

[CE20] S. El Garroussi, S. Ricci, M. De Lozzo, N. Goutal, and D. Lucor, (2020), Assessing uncertainties in flood forecasts using a mixture of generalized polynomial chaos expansions, In *TELEMAC User Conference, Toulouse, 14-15 Octobre*.

[CE21] A. Klampanos, A. Gemûnd, M. Atkinson, A. Koukourikos, R. Filgueira, A. Krause, A. Spinuso, A. Charalambidis, F. Magnoni, E. Casarotti, C. Pagé, M. Lindner, A. Ikonomopoulos, and V. Karkaletsis, (2019), DARE: A Reflective Platform Designed to Enable Agile Data-Driven Research on the Cloud. Bridging from Concepts to Data and Computation for eScience, In *Workshop (BC2DC´19), 15th International Conference on eScience (eScience 2019), San Diego, CA, USA, 24-27 September*.

[CE22] C. Lapeyre, N. Cazard, P. Roy, S. Ricci, and F. Zaoui, (2019), Prediction and reconstruction of hydraulic state with machine learning, In *SimHydro 2019, 12-14 June, Sophia-Antipolis, France.*

[CE23] E. Maisonnave, (2019), What opportunities and constraints will the future evolution of HPC systems provide for sea ice modelling ?, In *Conférence IS-ENES, 23-25 Sept 2019*, Laugarvatn, Islande.

[CE24] I. Mirouze, S. Ricci, and N. Goutal, (2019), The impact of observation densification in an ensemble Kalman Filter., In *Telemac User Conférence, Toulouse, France, 15-17 Oct.*

[CE25] I. Mirouze, S. Ricci, N. Goutal, L. Martin, and D. Desroche, (2019), Generation and assimilation of synthetical SWOT data with an Ensemble Kalman filter for 1D and 2D hydrodynamics models, In *ST SWOT, Bordeaux June 2019*.

[CE26] I. Mirouze, S. Ricci, P. Roy, M. De Lozzo, and N. Goutal, (2019), Diagnosing data assimilation with sensitivity analysis, In *14th International EnKF workshop, 3-5 June 2019, Vossenvagen, Norway*.

[CE27] R. Msadek and C. Cassou, (2019), Internal oceanic multidecadal variability: an important modulator of Arctic climate response to CO2 forcing, In *2019 IUGG meeting, Montreal, July 8-18, Canada*.

[CE28] R. Msadek, S. Chripko, E. Sanchez-Gomez, and L. Terray, (2019), Atmospheric response to Arctic sea ice decline in global climate model experiments : sensitivity to the sea ice pattern and experimental set up, 24 avril, Université de Exeter.

[CE29] R. Msadek, S. Chripko, E. Sanchez-Gomez, and L. Terray, (2019), Influence of Background Mean State on the Atmospheric Response to Arctic Sea Ice Decline, In *AGU Fall Meeting, San Francisco, USA, 9-13 December*.

[CE30] R. Msadek, S. Chripko, E. Sanchez-Gomez, L. Terray, and M.-P. Moine, (2019), Atmospheric response to Arctic sea ice decline in the CNRM model: initial results from PAMIP experiments, In *PAMIP workshop, Dartington Hall, 25-27 June, United Kingdom,*.

[CE31] R. Msadek, Y. Kushnir, and M. of the CLIVAR Decadal Climate Variability Panel, (2019), Decadal Climate Variability and Predictability : Relevance for the Climate Dynamics Panel, In *CLIVAR CDP meeting, Mykonos, Greece, 30 September - 4 October*.

[CE32] C. Pagé, M. Plieger, W. Som de Cerff, E. Vreede, N. Drost, I. Klampanos, M. Atkinson, and X. Pivan, (2019), Climate Data Access: Re-thinking our Data Analysis Workflows, In *Gateways 2019 - San Diego, CA, USA, 23-25 September*.

[CE33] C. Pagé, W. Som de Cerff, M. Plieger, A. Spinuso, and X. Pivan, (2019), Ease Access to Climate Simulations for Researchers: IS-ENES climate4impact. Bridging from Concepts to Data and Computation for eScience Workshop (BC2DC´19), In *15th International Conference on eScience (eScience 2019), San Diego, CA, USA, 24-27 September*.

[CE34] C. Pagé, W. Som de Cerff, M. Plieger, A. Spinuso, and X. Pivan, (2019), Enabling Transparent Access to Heterogeneous Architectures for IS-ENES climate4impact using the DARE Platform, In *15th International Conference on eScience (eScience 2019), San Diego, CA, USA, 24-27 September*.

[CE35] C. Pagé, W. Som de Cerff, M. Plieger, A. Spinuso, E. Vreede, and N. Drost, (2019), Climate Data Analysis: Enhancing Usage of Research Data with Climate4impact, EUDAT and DARE., In *AGU Fall Meeting, San Francisco, USA, 9-13 December*.

[CE36] R. Paugam, M. Rochoux, N. Cazard, C. Lapeyre, W. Mell, J. Johnston, and M. Wooster, (2019), Computing high resolution fire behavior metrics from prescribed burn using handheld airborne thermal camera observations, In *6th International Fire Behavior and Fuels Conference, Marseille, 29 April-3 May, France*.

[CE37] R. Paugam, M. Rochoux, N. Cazard, C. Lapeyre, W. Mell, and M. Wooster, (2019), Image segmentation – Fire front extraction for rate of spread estimation, In *European Geophysical Union (EGU), Vienna, 15-19 April, Austria,*.

[CE38] R. Paugam, M. Rochoux, N. Cazard, C. Lapeyre, W. Mell, and M. Wooster, (2019), Image segmentation – Fire front extraction for rate of spread estimation, In *Journée thématique Intelligence Artificielle et Océan-Atmosphère-Climat (LEFE), 6 February, Rennes, France*.

[CE39] M. Plieger, W. Som de Cerff, A. Spinuso, E. Vreede, C. Pagé, and N. Drost, (2019), Enhance usage of research data and support researchers with climate analysis, In *Geophysical Research abstracts, Vol. 21, EGU2019-11077*, April, Austria, EGU General Assembly.

[CE40] S. Ricci, V. Lemiale, I. Mirouze, N. Thio, and P. Roy, (2019), Sensitivity analysis for flood evacuation model, In *SAMO conference, Barcelona, 28-30 octobre*.

[CE41] S. Ricci, (2019), Uncertainty quantification and reduction with data assimilation, In *Application in hydrodynamics, University of Melbourne, August 9th*.

[CE42] M. Rochoux, A. Costes, R. Paugam, G. Rea, L. Thouron, A. Trucchia, C. Zhang, T. Jaravel, C. Lac, V. Masson, A. Trouvé, O. Vermorel, and D. Lucor, (2019), Emulating environmental modeling systems in presence of uncertainties: overview and challenges, In *Workshop on Frontiers of Uncertainty Quantification in Fluid Dynamics, Pisa,11-13 September, Italy*.

[CE43] M. Rochoux, A. Costes, R. Paugam, C. Zhang, A. Trouvé, A. Collin, and P. Moireau, (2019), Data assimilation for wildland fire behavior, In *Drone Garden Workshop organized by GIS Micro-drones, Toulouse (France), 6-7 June*.

[CE44] M. Rochoux, T. Jaravel, O. Vermorel, F. Auguste, B. Nony, G. Rea, and L. Thouron, (2019), High-resolution simulation and uncertainty analysis for air pollutant dispersion at site scale, In *Journées Utilisateurs Meso-NH, OMP Toulouse, 7-8 October*.

[CE45] M. Rochoux, C. Zhang, N. Frebourg, A. Collin, P. Moireau, D. Lucor, and A. Trouvé, (2019), Front data assimilation and sensitivity analysis for data-driven wildland fire spread simulations, In *6th International Fire Behavior and Fuels Conference, Marseille, 29 April-3 May, France*.

[CE46] V. Rousseau, E. Sanchez-Gomez, and R. Msadek, (2019), Physical processes involved in small scale air-sea interactions in the Gulf Stream region, In *2019 IUGG meeting, Montreal, July 8-18, Canada*.

[CE47] V. Rousseau, E. Sanchez-Gomez, R. Msadek, M.-P. Moine, and L. Coquart, (2019), Assessing the role of extreme events in shaping air-sea interactions in the Gulf Stream Region, In *AGU Fall Meeting, San Francisco, USA, 9-13 December*.

[CE48] E. Sanchez-Gomez, A. Voldoire, and R. Séférian, (2019), Evaluation des modèles CNRM-CM6-1 et CNRM-ESM2 dans l´Atlantique Tropical, In *Bordeaux CMIP6 workshop – 27-28 May*.

[CE49] A.-L. Tiberi, S. Ricci, N. Goutal, P. Sergent, and C. Monteil, (2019), Sensitivity Analysis of the Mascaret model on the Odet River, In *Telemac User Conférence, Toulouse, France, 15-17 Oct.*

[CE50] F. Tocquer, P. Simon, L. Corre, M. Kerdoncuff, S. Somot, R. Vautard, and C. Pagé, (2019), A reduced regional climate projection ensemble for the French national climate service : DRIAS, In *9th EURO-CORDEX General Assembly, Hamburg, Germany, 28-30 January*.

[CE51] S. Valcke, L. Coquart, A. Craig, G. Jonville, E. Maisonnave, and A. Piacentini, (2019), Latest developments of the OASIS3-MCT coupler for improved performance, In *Coupled Problems 2019, 03-06 June 2019, Barcelona (Sitges), Spain*.

[CE52] S. Valcke, (2020), OASIS3-MCT, latest news, In *IS-ENES3 1 st General Assembly, 25-27 th March 2020, Toulouse, France*.

## 5.3 HDR

[CE53] J. Boé, (2019), *Du début de la période industrielle á la fin du 21ème siècle: 250 ans de variations climatiques et hydrologiques sur la France.*, hdr, CNRS-CERFACS, Université de Toulouse.

[CE54] S. Ricci, (2019), *Quantification et réduction des incertitudes par assimilation de données en géosciences – Application á l´hydraulique á surface libre.*, hdr, CECI, Université de Toulouse, CNRS, CERFACS.

## 5.4 Journal Publications

[CE55] N. Andela, D. Morton, L. Giglio, R. Paugam, Y. Chen, S. Hantson, G. Van Der Werf, and J. Randerson, (2019), The Global Fire Atlas of individual fire size, duration, speed and direction, *Earth System Science Data*, **11**, 529–552.

[CE56] V. Arora, A. Katavouta, R. Williams, C. Jones, V. Brovkin, P. Friedlingstein, J. Schwinger, L. Bopp, O. Boucher, P. Cadule, M. Chamberlain, J. Christian, C. Delire, R. Fisher, H. Tomohiro, T. Ilyina, E. Joetzjer, M. Kawamiya, C. Koven, J. Krasting, R. Law, D. Lawrence, A. Lenton, K. Lindsay, J. Pongratz, T. Raddatz, R. Séférian, K. Tachiiri, J. Tjiputra, A. Wiltshire, T. Wu, and T. Ziehn, (2020), Carbon–concentration and carbon–climate feedbacks in CMIP6 models and their comparison to CMIP5 models, *Biogeosciences*, **17**, 4173–4222.

[CE57] F. Auguste, C. Lac, V. Masson, and D. Cariolle, (2020), Large-eddy simulations with an immersed boundary method: pollutant dispersion over urban terrain, *Atmosphere*, **11**, 113–135.

[CE58] F. Auguste, G. Rea, R. Paoli, C. Lac, V. Masson, and D. Cariolle, (2019), Implementation of an immersed boundary method in the Meso-NH v5.2 model: applications to an idealized urban environment, *Geoscientific Model Development*, **12**, 2607–2633.

[CE59] M. Bador, J. Boé, L. Terray, L. Alexander, A. Baker, A. Bellucci, R. Haarsma, T. Koenigk, M.-P. Moine, K. Lohmann, D. Putrasahan, C. Roberts, M. Roberts, E. Scoccimarro, R. Schiemann, J. Seddon, R. Senan, S. Valcke, and B. Vannière, (2020), Impact of higher spatial atmospheric resolution on precipitation extremes over land in global climate models, *Journal of Geophysical Research*, **125**, e2019JD032184.

[CE60] B. Barret, E. Emili, and E. Le Flochmoën, (2020), A tropopause-related climatological a priori profile for IASI-SOFRID ozone retrievals: improvements and validation, *Atmospheric Measurement Techniques*, **13**, 5237–5257.

[CE61] E. Blockley, M. Vancoppenolle, E. Hunke, C. Bitz, D. Feltham, J.-F. Lemieux, M. Losch, E. Maisonnave, D. Notz, P. Rampal, S. Tietsche, B. Tremblay, A. Turner, F. Massonnet, E. Olason, A. Roberts, Y. Aksenov, T. Fichefet, G. Garric, D. Iovino, G. Madec, C. Rousset, D. Salas y Melia, and D. Schroeder, (2020), The Future of Sea Ice Modeling : Where Do We Go from Here?, **101**, E1304–E1311.

[CE62] J. Boé, S. Somot, L. Corre, and P. Nabat, (2020), Large discrepancies in summer climate change over Europe as projected by global and regional climate models: causes and consequences, *Climate Dynamics*, **54**, 2981–3002.

[CE63] J. Boé, L. Terray, M.-P. Moine, S. Valcke, A. Bellucci, S. Drijfhout, R. Haarsma, K. Lohmann, D. Putrasahan, C. Roberts, M. Roberts, E. Scoccimarro, R. Senan, and K. Wyser, (2020), Past long-term summer warming over western Europe in new generation climate models: role of large-scale atmospheric circulation, *Environmental Research Letters*, **15**, 084038.

[CE64] R. Bonnet, J. Boé, and F. Habets, (2020), Influence of multidecadal variability on high and low flows:the case of the Seine basin, *Hydrology and Earth System Sciences*, **24**, 1611–1631.

[CE65] M. Bushuk, R. Msadek, M. Winton, G. Vecchi, X. Yang, A. Rosati, and R. Gudgel, (2019), Regional Arctic sea–ice prediction: potential versus operational seasonal forecast skill, *Climate Dynamics*, **52**, 2721–2743.

[CE66] M. Bushuk, X. Yang, M. Winton, R. Msadek, M. Harrison, A. Rosati, and R. Gudgel, (2019), The Value of Sustained Ocean Observations for Sea Ice Predictions in the Barents Sea, *Journal of Climate*, **32**, 7017–7035.

[CE67] W. Cai, L. Wu, M. Lengaigne, T. Li, S. McGregor, J. Kug, J. Yu, M. Stuecker, A. Santoso, X. Li, Y. Ham, Y. Chikamoto, B. Ng, M. MacPhaden, F. Jia, N. Keenlyside, X. Lin, J. Luo, M. Martin-Rey, Y. Ruprich-Robert, G. Wang, S. Xie, Y. Yang, S. Kang, B. Gan, G.-I. Kim, C. Kim, S. Kim, J. Kim, and P. Chang, (2019), Pantropical climate interactions, *Science*, **363**, eaav4236.

[CE68] F. Castruccio, Y. Ruprich-Robert, S. Yeager, G. Danabasoglu, R. Msadek, and T. Delworth, (2019), Modulation of Arctic Sea Ice Loss by Atmospheric Teleconnections from Atlantic Multidecadal Variability, *Journal of Climate*, **32**, 1419–1441.

[CE69] M. Descheemaecker, M. Plu, V. Marécal, M. Claeyman, F. Olivier, Y. Aoun, P. Blanc, L. Wald, J. Guth, B. Sic, J. Vidot, A. Piacentini, and B. Josse, (2019), Monitoring aerosols over Europe: an assessment of the potential benefit of assimilating the VIS04 measurements from the future MTG/FCI geostationary imager, *Atmospheric Measurement Techniques*, **12**, 1251–1275.

[CE70] A. Dosio, A. Turner, A. Tamoffo, M. Sylla, C. Lennard, R. Jones, L. Terray, G. Nikulin, and B. Hewitson, (2020), A tale of two futures: contrasting scenarios of future precipitation for West Africa from an ensemble of regional climate models, *Environmental Research Letters*, **15**, 064007.

[CE71] M. Drouard and C. Cassou, (2019), A Modeling- and Process-Oriented Study to Investigate the Projected Change of ENSO-Forced Wintertime Teleconnectivity in a Warmer World, *Journal of Climate*, **32**.

[CE72] C. Emery, S. Biancamaria, A. Boone, S. Ricci, M. Rochoux, V. Pedinotti, and C. David, (2020), Assimilation of wide-swath altimetry water elevation anomalies to correct large-scale river routing model parameters, *Hydrology and Earth System Sciences*, **24**, 2207–2233.

[CE73] E. Emili, B. Barret, E. Le Flochmoën, and D. Cariolle, (2019), Comparison between the assimilation of IASI Level 2 ozone retrievals and Level 1 radiances in a chemical transport model, *Atmospheric Measurement Techniques*, **12**, 3963–3984.

[CE74] V. Eyring, P. Cox, G. Flato, P. Gleckler, G. Abramowitz, P. Caldwell, W. Collins, B. Gier, A. Hall, F. Hoffman, G. Hurt, A. Jahn, C. Jones, S. Klein, J. Krasting, L. Kwiatkowski, R. Lorentz, E. Maloney, G. Meehl, A. Pendergrass, R. Pincus, A. Ruane, J. Russel, B. Sanderson, B. Santer, S. Sherwood, I. Simpson, R. Stouffer, and M. Williamson, (2019), Taking climate model evaluation to the next level, *Nature Climate Change*, **9**, 102–110.

[CE75] R. Fisher and C. Koven, (2020), Perspectives on the future of land surface models and the challenges of representing complex terrestrial systems, *Journal of Advances in Modeling Earth Systems*, **12**, e2018MS001453.

[CE76] R. Fisher, W. Wieder, B. Sanderson, C. Koven, K. Oleson, C. Xu, J. Fisher, M. Shi, A. Walker, and D. Lawrence, (2019), Parametric controls on vegetation responses to biogeochemical forcing in the CLM5, *Journal of Advances in Modeling Earth Systems*, **11**, 2879–2895.

[CE77] G. Foltz, P. Brandt, I. Richter, B. Rodríguez-Fonseca, F. Hernandez, M. Dengler, R. Rodrigues, J. Schmidt, L. Yu, N. Lefevre, L. Cotrim Da Cunha, M. McPhaden, M. Araujo, J. Karstensen, J. Hahn, M. Martin-Rey, C. Patricola, P. Poli, R. Hummels, R. Perez, V. Hatje, J.-F. Lûbbecke, I. Polo, R. Lumpkin, B. Bourles, F. Asuquo, P. Lehodey, A. Conchon, P. Chang, P. Dandin, C. Schmid, A. Sutton, H. Giordani, Y. Xue, S. Illig, T. Losada, S. Grodsky, F. Gasparin, T. Lee, E. Mohino, P. Nobre, R. Wanninkhof, N. Keenlyside, V. Garcon, E. Sanchez-Gomez, H. Nnamchi, M. Drévillon, A. Storto, E. Remy, A. Lazar, S. Speich, M. Goes, T. Dorrington, W. Johns, J. Moum, C. Robinson, C. Perruche, R. de Souza, A. Gaye, J. Lopez-Parages, P. Monerie, P. Castellanos, N. Benson, M. Hounkonnou, J. Trotte Duha, R. Laxenaire, and N. Reul, (2019), The tropical atlantic observing system, *Frontiers in Marine Science*, **6**.

[CE78] M. Goret, V. Masson, R. Schoetter, and M.-P. Moine, (2019), Inclusion of CO2 flux modelling in an urban canopy layer model and an evaluation over an old European city centre, *Atmospheric Environment: X*, **3**, 100042.

[CE79] K. Goubanova, E. Sanchez-Gomez, C. Frauen, and A. Voldoire, (2019), Respective roles of remote and local wind stress forcings in the development of warm SST errors in the South-Eastern Tropical Atlantic in a coupled high-resolution model, *Climate Dynamics*, **52**, 1359–1382.

[CE80] M. Gourault, S. Petton, Y. Thomas, L. Pecquerie, G. Marques, C. Cassou, E. Fleury, Y.-M. Paulet, and S. Pouvreau, (2019), Modeling reproductive traits of an invasive bivalve species under contrasting climate scenarios from 1960 to 2100, *Journal of Sea Research*, **143**, 128–139.

[CE81] R. Guo, C. Deser, L. Terray, and F. Lehner, (2019), Human influence on winter precipitation trends (1921–2015) over North America and Eurasia revealed by dynamical adjustment, *Geophysical Research Letters*, **46**, 3426–3434.

[CE82] J. Gutiérrez, D. Maraun, M. Widmann, R. Huth, E. Hertig, R. Benestad, O. Roessler, J. Wibig, R. Wilcke, S. Kotlarski, D. San Martin, S. Herrera, J. Bedia, A. Casanueva, R. Manzanas, M. Iturbide, M. Vrac, M. Dubrovsky, J. Ribalaygua, J. Portoles, O. Räty, J. Räisänen, B. Hingray, D. Raynaud, M. Casado, P. Ramos, T. Zerenner, M. Turco, T. Bosshard, P. Stepanek, J. Bartholy, R. Pongracz, D. Keller, A. Fischer, R. Cardoso, P. Soares, B. Czernecki, and C. Pagé, (2019), An intercomparison of a large ensemble of statistical downscaling methods over Europe: Results from the VALUE perfect predictor cross-validation experiment, *International Journal of Climatology*, **39**, 3750–3785.

[CE83] V. Häfliger, E. Martin, A. Boone, S. Ricci, and S. Biancamaria, (2019), Assimilation of Synthetic SWOT River Depths in a Regional Hydrometeorological Model, *Water*, **11**, 2–24.

[CE84] J. Holm, R. Knox, R. Fisher, C. Koven, A. Nogueira Lima, and W. Riley, (2020), The Central Amazon biomass sink under current and future atmospheric CO2: Predictions from big-leaf and demographic vegetation models, *Journal of Geophysical Research-Biogeosciences*, **125**, e2019JG005500.

[CE85] S. Hyatt, C. Fletcher, C. Cassou, Y. Ruprich-Robert, and L. Terray, (2020), The dependence of the northern extratropical climate response to external forcing on the phase of Atlantic Multidecadal Variability, *Climate Dynamics*, **55**, 487–502.

[CE86] G. Jiaxiang, M. Shoshiro, M. Roberts, R. Haarsma, D. Putrasahan, C. Roberts, E. Scoccimarro, L. Terray, B. Vannière, and P. Vidale, (2020), Influence of model resolution on bomb cyclones revealed by HighResMIP-PRIMAVERA simulations, *Environmental Research Letters*, **15**, 084001.

[CE87] S. Kotlarski, P. Szabo, S. Herrera, O. Räty, K. Keuler, P. Soares, R. Cardoso, T. Bosshard, C. Pagé, F. Boberg, J. Gutiérrez, F. Isotta, A. Jaczewski, F. Kreienkamp, M. Liniger, C. Lussana, and K. Pianko-Kluczynska, (2019), Observational uncertainty and regional climate model evaluation: A pan-European perspective, *International Journal of Climatology*, **39**, 3730–3749.

[CE88] C. Koven, R. Knox, R. Fisher, J. Chambers, B. Christoffersen, S. Davies, M. Detto, M. Dietze, B. Faybishenko, J. Holm, M. Huang, M. Kovenock, L. Kueppers, G. Lemieux, E. Massoud, N. McDowell, H. Muller-Landau, J. Needham, R. Norby, T. Powell, A. Rogers, S. Serbin, J. Shuman, A. Swann, C. Varadharajan, A. Walker, S. Wright, and C. Xu, (2020), Benchmarking and parameter sensitivity of physiological and vegetation dynamics using the Functionally Assembled Terrestrial Ecosystem Simulator (FATES) at Barro Colorado Island, Panama, *Biogeosciences*, **17**, 3017–3044.

[CE89] L. Krishnamurthy, A. Munoz, G. Vecchi, R. Msadek, A. Wittenberg, B. Stern, R. Gudgel, and F. Zeng, (2019), Assessment of summer rainfall forecast skill in the Intra-Americas in GFDL high and low-resolution models, *Climate Dynamics*, **52**, 1965–1982.

[CE90] V. Laborie, S. Ricci, M. De Lozzo, N. Goutal, Y. Audoin, and P. Sergent, (2020), Quantifying forcing uncertainties in the hydrodynamics of the Gironde estuary, *Computational Geosciences*, **24**, 181–202.

[CE91] D. Lawrence, R. Fisher, C. Koven, K. Oleson, S. Swenson, G. Bonan, N. Collier, B. Ghimire, L. van Kampenhout, D. Kennedy, E. Kluzek, P. Lawrence, F. Li, H. Li, D. Lombardozzi, W. Riley, W. Sacks, M. Shi, M. Vertenstein, W. Wieder, C. Xu, A. Ali, A. Badger, G. Bisht, M. van der Broeke, M. Brunke, S. Burns, J. Buzan, M. Clark, A. Craig, K. Dahlin, B. Drewniak, J. Fisher, M. Flanner, A. Fox, P. Gentine, F. Hoffman, G. Keppel-Aleks, R. Knox, S. Kumar, J. Lenaerts, L. Ruby Leung, W. Lipscomb, Y. Lu, A. Pandey, J. Pelletier, J. Randerson, D. Ricciuto, B. Sanderson, A. Slater, Z. Subin, J. Tang, R. Thomas, M. Val Martin, and X. Zeng, (2019), The Community Land Model version 5: Description of new features, benchmarking, and impact of forcing uncertainty, *Journal of Advances in Modeling Earth Systems*, **11**, 4245–4287.

[CE92] P. Le Moigne, F. Besson, E. Martin, J. Boé, A. Boone, B. Decharme, P. Etchevers, S. Faroux, F. Habets, M. Lafaysse, D. Leroux, and F. Rousset-Regimbeau, (2020), The latest improvements with SURFEX v8.0 of the Safran–Isba–Modcou hydrometeorological model for France, *Geoscientific Model Development*, **13**, 3925–3946.

[CE93] M. Martin-Rey, I. Polo, B. Rodriguez de Fonseca, A. Lazar, and T. Losada, (2019), Ocean dynamics shapes the structure and timing of Atlantic Equatorial Modes, *Journal of Geophysical Research Oceans*, **124**, 7529–7544.

[CE94] E. Massoud, C. Xu, R. Fisher, R. Knox, A. Walker, S. Serbin, B. Christoffersen, J. Holm, L. Kueppers, D. Ricciuto, L. Wei, D. Johnson, J. Chambers, C. Koven, N. McDowell, and J. Vrugt, (2019), Identification of key parameters controlling demographically structured vegetation dynamics in a land surface model: CLM4.5(FATES), *Geoscientific Model Development*, **12**, 4133–4164.

[CE95] M. Menary, J. Robson, R. Allan, B. Booth, C. Cassou, G. Gastineau, J. Gregory, D. Hodson, C. Jones, J. Mignot, M. Ringer, R. Sutton, L. Wilcox, and R. Zhang, (2020), Aerosol-Forced AMOC Changes in CMIP6 Historical Simulations, *Geophysical Research Letters*, **47**.

[CE96] F. Molteni, C. Roberts, R. Senan, S. Keeley, A. Bellucci, S. Corti, R. Franco, R. Haarsma, X. Levine, D. Putrasahan, M. Roberts, and L. Terray, (2020), Boreal-winter teleconnections with tropical Indo-Pacific rainfall in HighResMIP historical simulations from the PRIMAVERA project, *Climate Dynamics*, **55**, 1843–1873.

[CE97] P. Monerie, E. Sanchez-Gomez, M. Gaetani, E. Mohino, and B. Dong, (2020), Future evolution of the Sahel precipitation zonal contrast in CESM1, *Climate Dynamics*, **55**, :2801–2821.

[CE98] A. Monnerie, T. Oudar, and E. Sanchez-Gomez, (2019), Respective impacts of Arctic sea ice decline and increasing greenhouse gases concentration on Sahel precipitation, *Climate Dynamics*, **52**, 5947–5964.

[CE99] R. Msadek, G. Garric, S. Fleury, F. Garnier, L. Batté, and M. Bushuk, (2020), Prévoir les variations saisonnières de la glace de mer arctique et leurs impacts sur le climat, *La Météorologie*, 24–33.

[CE100] P. Nabat, S. Somot, C. Cassou, M. Mallet, M. Michou, D. Bouniol, B. Decharme, T. Druge, R. Roehrig, and D. Saint-Martin, (2020), Modulation of radiative aerosols effects by atmospheric circulation over the Euro-Mediterranean region, **20**, 8315–8349.

[CE101] J. Needham, J. Chambers, R. Fisher, R. Knok, and C. Koven, (2020), Forest responses to simulated elevated CO2 under alternate hypotheses of size- and age-dependent mortality, *Global Change Biology*, **26**, 5734– 5753.

[CE102] O. Pannekoucke and R. Fablet, (2020), PDE-NetGen 1.0: from symbolic partial differential equation (PDE) representations of physical processes to trainable neural network representations, *Geoscientific Model Development*, **13**, 3373–3382.

[CE103] S. Qasmi, C. Cassou, and J. Boé, (2020), Teleconnection processes linking the intensity of the Atlantic Multidecadal Variability to the climate impacts over Europe in boreal winter., *Journal of Climate*, **33**, 2681–2700.

[CE104] S. Qasmi, E. Sanchez-Gomez, Y. Ruprich-Robert, J. Boé, and C. Cassou, (09 Nov. 2020), Modulation of the occurrence of heatwaves over the Euro-Mediterranean region by the intensity of the Atlantic Multidecadal Variability, *Journal of Climate*, 1 – 50.

[CE105] S. Quesada-Ruiz, J.-L. Attié, W. Lahoz, R. Abida, P. Ricaud, L. El Amraoui, R. Zbinden, A. Piacentini, M. Joly, H. Eskes, A. Segers, L. Curier, J. de Haan, J. Kujanpää, A. Plechelmus Oude Nijhuis, J. Tamminen, R. Timmermans, and P. Veefkind, (2020), Benefit of ozone observations from Sentinel-5P and future Sentinel-4 missions on tropospheric composition, *Atmospheric Measurement Techniques*, **13**, 131–152.

[CE106] H. Rahaman, U. Srinavisu, S. Panickal, J. Durgadoo, S. Griffies, M. Ravichandran, A. Bozec, A. Cherchi, A. Voldoire, D. Sidorenko, E. Chassignet, G. Danabasoglu, H. Tsujino, K. Getzlaff, M. Ilicak, M. Bentsen, M. Long, P. Fogli, S. Danilov, S. Marsland, S. Valcke, S. Yeager, and Q. Wang, (2020), An assessment of the Indian Ocean mean state and seasonal cycle in a suite of interannual CORE-II simulations, *Ocean Modelling*, **145**, 101503.

[CE107] M. Roberts, A. Bellucci, B. Vannière, J. Camp, C. Roberts, D. Putrashan, J. Mecking, K. Hodges, L. Terray, L. Caron, P. Vidale, R. Haarsma, R. Senan, J. Seddon, M.-P. Moine, C. Kodama, Y. Yamada, C. Zarzycki, P. Ullrich, R. Mizuta, D. Fu, G. Danabasoglu, L. Wu, N. Rosenbloom, Q. Zhang, E. Scoccimarro, F. Chauvin, S. Valcke, and H. Wang, (2020), Projected Future Changes in Tropical Cyclones using the CMIP6 HighResMIP Multi-model Ensemble, *Geophysical Research Letters*, **47**, e2020GL088662.

[CE108] M. Roberts, J. Camp, J. Seddon, P. Vidale, K. Hodges, B. Vannière, J. Mecking, R. Haarsma, A. Bellucci, E. Scoccimarro, L. Caron, F. Chauvin, L. Terray, S. Valcke, M.-P. Moine, D. Putrasahan, C. Roberts, R. Senan, C. Zarzycki, and P. Ullrich, (2020), Impact of Model Resolution on Tropical Cyclone Simulation Using the HighResMIP–PRIMAVERA Multimodel Ensemble, *Journal of Climate*, **33**, 2557–2583.

[CE109] M. Roberts, L. Jackson, C. Roberts, V. Meccia, D. Docquier, T. Koenigk, P. Ortega, P. Moreno Chamarro, A. Bellucci, A. Coward, S. Drijfhout, E. Exarchou, O. Gutjahr, H. Hewitt, D. Iovino, K. Lohmann, D. Putrasahan, R. Schiemann, J. Seddon, L. Terray, X. Xu, Q. Zhang, P. Chang, S. Yeager, F. Castruccio, S. Zhang, and L. Wu, (2020), Sensitivity of the Atlantic Meridional OverturningCirculation to Model Resolution in CMIP6HighResMIP Simulations and Implicationsfor Future Changes, *Journal of Advances in Modeling Earth Systems*, **12**.

[CE110] O. Rössler, A. Fischer, H. Huebener, D. Maraun, R. Benestad, P. Christodoulides, P. Soares, R. Cardoso, C. Pagé, H. Kanamaru, and F. Kreienkampj, (2019), Challenges to link climate change data provision and user needs: Perspective from the COST-action VALUE, *International Journal of Climatology*, **39**, 3704–3716.

[CE111] P. Ruggieri, A. Bellucci, D. Nicoli, P. Athanasiadis, S. Gualdi, C. Cassou, F. Castruccio, G. Danabasoglu, P. Davini, N. Dunstone, R. Eade, G. Gastineau, B. Harvey, L. Hermanson, S. Qasmi, Y. Ruprich-Robert, E. Sanchez-Gomez, D. Smith, S. Wild, and M. Zampieri, (08 Oct. 2020), Atlantic Multidecadal Variability and North Atlantic Jet: a multi-model view from the Decadal Climate Prediction Project, *Journal of Climate*, 1 – 47.

[CE112] B. Sanderson and R. Fisher, (2020), A fiery wake-up call for climate science, *Nature Climate Change*, 175–177.

[CE113] B. Sanderson and B. O'Neill, (2020), Assessing the costs of historical inaction on climate change, **10**, 1–12.

[CE114] B. Sanderson, C. Wobus, D. Mills, C. Zarakas, A. Crimmins, M. Sarofim, and C. Weaver, (2019), Informing Future Risks of Record-Level Rainfall in the United States, *Geophysical Research Letters*, **46**, 3963–3972.

[CE115] B. Sanderson, (2020), Relating climate sensitivity indices to projection uncertainty, *Earth System Dynamics*, **11**, 721–735.

[CE116] B. Sanderson, (2020), The role of prior assumptions in carbon budget calculations, *Earth System Dynamics*, **11**, 563–577.

[CE117] R. Schiemann, P. Athanasiadis, D. Barriopedro, F. Doblas-Reyes, K. Lohmann, M. Roberts, D. Sein, C. Roberts, L. Terray, and P. Vidale, (2020), Northern Hemisphere blocking simulation in current climate models: evaluating progress from the Climate Model Intercomparison Project Phase 5 to 6 and sensitivity to resolution, *Weather and Climate Dynamics*, **1**, 277–292.

[CE118] R. Séférian, P. Nabat, M. Michou, D. Saint-Martin, A. Voldoire, J. Colin, B. Decharme, C. Delire, S. Berthet, M. Chevallier, S. Sénési, L. Franchistéguy, J. Vial, M. Mallet, E. Joetzjer, O. Geoffroy, J.-F. Guérémy, M.-P. Moine, R. Msadek, A. Ribes, M. Rocher, R. Roehrig, D. Salas y Melia, E. Sanchez-Gomez, L. Terray, S. Valcke, R. Waldman, O. Aumont, L. Bopp, J. Deshayes, C. Ethe, and G. Madec, (2019), Evaluation of CNRM Earth System Model, CNRM-ESM2-1:Role of Earth System Processes in Present-Dayand Future Climate, *Journal of Advances in Modeling Earth Systems*, **11**, 4182–4227.

[CE119] R. Small, R. Msadek, Y.-O. Kwon, J. Booth, and C. Zarzycki, (2019), Atmosphere surface storm track response to resolved ocean mesoscale in two sets of global climate model experiments, *Climate Dynamics*, **52**, 2067–2089.

[CE120] D. Smith, J. Screen, C. Deser, J. Cohen, J. Fyfe, J. Garcia-Serrano, T. Jung, V. Kattsov, D. Matei, R. Msadek, Y. Peings, M. Sigmond, J. Ukita, J.-H. Yoon, and X. Zhang, (2019), The Polar Amplification Model Intercomparison Project (PAMIP) contribution to CMIP6: investigating the causes and consequences of polar amplification, *Geoscientific Model Development*, **12**, 1139–1164.

[CE121] A. Trucchia, V. Egorova, G. Pagnini, and M. Rochoux, (2019), On the merits of sparse surrogates for global sensitivity analysis of multi-scale nonlinear problems: application to turbulence and fire-spotting model in wildland fire simulators, *Communications in Nonlinear Science and Numerical Simulation*, **73**, 120–145.

[CE122] A. Trucchia, M. Mattei, V. Luongo, L. Frunzo, and M. Rochoux, (2019), Surrogate-based uncertainty and sensitivity analysis for bacterial invasion in multi-species biofilm modeling, *Communications in Nonlinear Science and Numerical Simulation*, **73**, 403–424.

[CE123] B. Vannière, M.-E. Demory, P. Vidale, R. Schiemann, M. Roberts, C. Roberts, M. Matsueda, L. Terray, T. Koenigk, and R. Senan, (2019), Multi-model evaluation of the sensitivity of the global energy budget and hydrological cycle to resolution, *Climate Dynamics*, **52**, 6817–6846.

[CE124] B. Vannière, M. Roberts, P. Vidale, K. Hodges, M.-E. Demory, L. Caron, E. Scoccimarro, L. Terray, and R. Senan, (2020), The Moisture Budget of Tropical Cyclones in HighResMIP Models: Large-Scale Environmental Balance and Sensitivity to Horizontal Resolution, *Journal of Climate*, **33**, 8457–8473.

[CE125] J.-P. Vergnes, N. Roux, F. Habets, P. Ackerer, N. Amraoui, F. Besson, Y. Caballero, Q. Courtois, J.-R. de Dreuzy, P. Etchevers, N. Gallois, D. Leroux, L. Longuevergne, P. Le Moigne, T. Morel, S. Munier, F. Regimbeau, D. Thiéry, and P. Viennot, (2020), The AquiFR hydrometeorological modelling platform as a tool for improving groundwater resource monitoring over France: evaluation over a 60-year period, **24**, 633–654.

[CE126] A. Voldoire, E. Exarchou, E. Sanchez-Gomez, T. Demissie, A. Deppenmeier, C. Frauen, K. Goubanova, W. Hazeleger, N. Keenlyside, S. Koseki, C. Prodhomme, J. Shonk, T. Toniazzo, and A. Traoré, (2019), Role of wind stress in driving SST biases in the Tropical Atlantic, *Climate Dynamics*, **53**, 3481–3504.

[CE127] A. Voldoire, D. Saint-Martin, S. Sénési, B. Decharme, A. Alias, M. Chevallier, J. Colin, J.-F. Guérémy, M. Michou, M.-P. Moine, P. Nabat, R. Roehrig, D. Salas y Melia, R. Séférian, S. Valcke, I. Beau, S. Belamari, S. Berthet, C. Cassou, J. Cattiaux, J. Deshayes, H. Douville, C. Ethe, L. Franchistéguy, O. Geoffroy, C. Lévy, G. Madec, Y. Meurdesoif, R. Msadek, A. Ribes, E. Sanchez-Gomez, L. Terray, and R. Waldman, (2019), Evaluation of CMIP6 DECK experiments with CNRM-CM6-1, *Journal of Advances in Modeling Earth Systems*, **11**, 2177–2213.

[CE128] M. Widmann, J. Bedia, J. Gutiérrez, T. Bosshard, E. Hertig, D. Maraun, M. Casado, P. Ramos, R. Cardoso, P. Soares, J. Ribalaygua, C. Pagé, A. Fisher, S. Herrera, and R. Huth, (2019), Validation of spatial variability in downscaling results from the VALUE perfect predictor experiment, *International Journal of Climatology*, **39**, 3819–3845.

[CE129] W. Wieder, D. Lawrence, R. Fisher, G. Bonan, S. Cheng, C. Goodale, A. Grandy, C. Koven, D. Lombardozzi, K. Oleson, and R. Thomas, (2019), Beyond static benchmarking: Using experimental manipulations to evaluate land model assumptions, **33**, 1289–1309.

[CE130] C. Xu, N. McDowell, R. Fisher, L. Wei, S. Sevanto, B. Christoffersen, E. Weng, and R. Middleton, (2019), Increasing impacts of extreme droughts on vegetation productivity under climate change, *Nature Climate Change*, **9**, 948–953.

[CE131] C. Zhang, A. Collin, P. Moireau, A. Trouvé, and M. Rochoux, (2019), Front shape similarity measure for data-driven simulations of wild land fire spread based on state estimation : Application to the RxCADRE field-scale experiment, *Proceedings of the Combustion Institute*, **37**, 4201–4209.

[CE132] C. Zhang, A. Collin, P. Moireau, A. Trouvé, and M. Rochoux, (2019), State-parameter estimation approach for data-driven wildland fire spread modeling: application to the 2012 RxCADRE S5 field-scale experiment, *Fire Safety Journal*, **105**, 286–299.

## 5.5 Technical Reports

[CE133] E. Casarotti, F. Magnoni, C. Pagé, R. Filgueira, and I. Klampanos, (2019), Training and Consulting Report I. DARE WP8 D8.4 Deliverable Report, technical report, CECI, Université de Toulouse, CNRS, CERFACS, Toulouse, France - TR-CMGC-19-217.

[CE134] R. Casta and T. Morel, (2019), Test de la fonctionnalité ordre élevé du coupleur de codes CWIPI et Intégration dans OpenPALM, technical report, CECI, Université de Toulouse, CNRS, CERFACS, Toulouse, France - TR-CMGC-19-95.

[CE135] L. Coquart and S. Valcke, (2019), ESMF v7.1.0r remapping between two structured grids and between two unstructured grids and one structured grid, technical report, CECI, Université de Toulouse, CNRS, CERFACS, Toulouse, France, TR-CMGC-19-43.

[CE136] A. Craig, (2019), GSSPOS and BSSPOS options for the global conservation in OASIS3-MCT, technical report, CECI, Université de Toulouse, CNRS, CERFACS, Toulouse, France - TR-CMGC-19-128.

[CE137] C. Emery, S. Ricci, and A. Piacentini, (2020), ToolBox SWOT User's Guide, technical report, CECI, Université de Toulouse, CNRS, CERFACS, Toulouse, France - TR-CMGC-20-142.

[CE138] E. Emili and P. Valks, (2019), CAMS42D42.3.5.1: Assessment of costs and benefits of UV radiance assimilation for ozone analyses, technical report, CECI, Université de Toulouse, CNRS, CERFACS, Toulouse, France - TR-CMGC-19-249.

[CE139] E. Emili, G. Jonville, A. Piacentini, P. Valks, O. Tuinder, and D. Efremenko, (2019), CAMS42D42.3.4.1: Implementation of tangent linear and adjoint modules for UV radiance assimilation, technical report, CECI, Université de Toulouse, CNRS, CERFACS, Toulouse, France - TR-CMGC-19-248.

[CE140] G. Jonville and S. Valcke, (2019), Analysis of SCRIP conservative remapping in OASIS3-MCT - Part B, technical report, CECI, Université de Toulouse, CNRS, CERFACS, Toulouse, France - TR-CMGC-19-155.

[CE141] E. Maisonnave and S. Masson, (2019), NEMO 4.0 performance: how to identify and reduce unnecessary communications, technical report, CECI, Université de Toulouse, CNRS, CERFACS, Toulouse, France - TR-CMGC-19-19.

[CE142] E. Maisonnave and A. Piacentini, (2019), Performance evaluation of the hybrid interactive placement with HIPPO of SCRIP interpolation tasks, working note, CECI, Université de Toulouse, CNRS, CERFACS, Toulouse, France - WN-CMGC-19-94.

[CE143] E. Maisonnave and A. Voldoire, (2019), Exchange grid and multi-ice categories coupling : comparison of two flux computation strategies, working note, CECI, Université de Toulouse, CNRS, CERFACS, Toulouse, France - WN-CMGC-19-93.

[CE144] E. Maisonnave, L. Coquart, and A. Piacentini, (2020), A better diagnostic of the load imbalance in OASIS based coupled systems, technical report, CECI, Université de Toulouse, CNRS, CERFACS, Toulouse, France - TR-CMGC-20-176.

[CE145] E. Maisonnave, C. Lévy, and S. Masson, (2019), Implementation and computing performances of NEMO ORCA-KM configuration, technical report, CECI, Université de Toulouse, CNRS, CERFACS, Toulouse, France - TR-CMGC-19-18.

[CE146] E. Maisonnave, (2019), OASIS Dedicated Support, 4th annual summary, technical report, CECI, Université de Toulouse, CNRS, CERFACS, Toulouse, France - TR-CMGC-19-149.

[CE147] E. Maisonnave, (2019), OASIS Gaussian interpolation with locally relative source-target distances, technical report, CECI, Université de Toulouse, CNRS, CERFACS, Toulouse, France - TR-CMGC-19-83.

[CE148] E. Maisonnave, (2019), persona v2.0, how to graphically patch a mask variable, working note, CECI, Université de Toulouse, CNRS, CERFACS, Toulouse, France - WN-CMGC-19-107.

[CE149] E. Maisonnave, (2020), Locally conservative OASIS interpolation using target grid nearest neighbours, technical report, CECI, Université de Toulouse, CNRS, CERFACS, Toulouse, France - TR-CMGC-20-166.

[CE150] E. Maisonnave, (2020), Ocean/Biogeochemistry macro-task parallelism in NEMO, working note, CECI, Université de Toulouse, CNRS, CERFACS, Toulouse, France - WN-CMGC-19-107, Working note.

[CE151] A. Marque, M. Rochoux, and D. Cariolle, (2019), Modélisation et simulation de la qualité aéroportuaire - Projet MOSIQAA – Livrable du lot 3., technical report, CECI, Université de Toulouse, CNRS, CERFACS, Toulouse, France - TR-CMGC-19-175.

[CE152] R. McDermott, N. Brynder, and J. Heintz, (2019), Large outdoor fire modeling (LOFM) workshop, technical report, NIST Special Publication 1245, October 2019, doi: 10.6028/NIST.SP.1245.

[CE153] T. Morel, (2019), Coupleur OpenPALM version 4.3.0, Manuel utilisateur et de formation, technical report, CECI, Université de Toulouse, CNRS, CERFACS, Toulouse, France - TR-CMGC-19-69.

[CE154] T. Morel, (2019), OpenPALM coupler version 4.3.0, User guide and training manual, technical report, CECI, Université de Toulouse, CNRS, CERFACS, Toulouse, France - TR-CMGC-19-70.

[CE155] T. Morel, (2019), Support OpenPALM 2018-2019 au projet AquiFR, technical report, CECI, Université de Toulouse, CNRS, CERFACS, Toulouse, France - TR-CMGC-19-124.

[CE156] B. Nony, (2020), Prédiction et reconstruction de données hydrauliques par apprentissage machine, technical report, CECI, Université de Toulouse, CNRS, CERFACS, Toulouse, France - TR-CMGC-19-TR-CMGC-20-145.

[CE157] C. Pagé, (2019), Pilot Tools and Services, Execution and Evaluation Report I. DARE WP7 D7.1 Deliverable Report., technical report, CECI, Université de Toulouse, CNRS, CERFACS, Toulouse, France - TR-CMGC-19-215.

[CE158] A. Piacentini and E. Maisonnave, (2020), Interactive visualisation of OASIS coupled models load imbalance, technical report, CECI, Université de Toulouse, CNRS, CERFACS, Toulouse, France - TR-CMGC-20-177.

[CE159] A. Piacentini, M.-P. Daou, S. Ricci, and N. Goutal, (2020), Mascaret-Telemac2D Longitudinal coupling - User Guide, technical report, CECI, Université de Toulouse, CNRS, CERFACS, Toulouse, France - TR-CMGC-20-146.

[CE160] A. Piacentini, (2020), Evaluation of Atlas 0.21 interpolation capability, technical report, CECI, Université de Toulouse, CNRS, CERFACS, Toulouse, France - TR-CMGC-20-105.

[CE161] L. Prado Arellano, S. Ricci, and N. Gourdain, (2020), Impact of global warming on air transportation: Sensitivity analysis study on Takeoff distance computation, technical report, Université de Toulouse, CNRS, CERFACS, Toulouse, France - TR-CMGC-20-116.

[CE162] L. Thouron, M. Rochoux, T. Jaravel, and O. Vermorel, (2020), Large-eddy simulations of the MUST trial 2681829 using AVBP, Meso-NH and YALES2, technical report, Université de Toulouse, CNRS, CERFACS, Toulouse, France - TR-CMGC-20-14.

[CE163] X. Tsilibaris, E. Galifianaki, and C. Pagé, (2019), Dissemination and Outreach Report I. DARE WP8 D8.2 Deliverable Report, technical report, CECI, Université de Toulouse, CNRS, CERFACS, Toulouse, France - TR-CMGC-19-216.

[CE164] S. Valcke and A. Piacentini, (2019), Analysis of SCRIP conservative remapping in OASIS3-MCT - Part A, technical report, CECI, Université de Toulouse, CNRS, CERFACS, Toulouse, France - TR-CMGC-19-129.

[CE165] S. Valcke, A. Craig, and L. Coquart, (2019), OASIS3-MCT development plan, November 2017, With annotation March 2019, technical report, CECI, Université de Toulouse, CNRS, CERFACS, Toulouse, France - TR-CMGC-19-64.

[CE166] S. Valcke, A. Craig, and L. Coquart, (2020), OASIS3-MCT development plan, technical report.

[CE167] S. Valcke, (2020), Coupling workshop report, technical report.

## 5.6 Thesis

[CE168] S. Chripko, (2020), *Rôle du déclin de la glace de mer en Arctique sur le climat des moyennes latitudes: téléconnexions atmosphériques*, phd thesis, Université Toulouse.

[CE169] V. Laborie, (2020), *Quantification d´incertitudes et assimilation de données pour la modélisation hydrodynamique bidimensionnelle : application au modèle de prévision des hautes eaux de l'estuaire de la Gironde*, phd thesis, Université Paris Est.

[CE170] V. Rousseau, (2020), *Etude des interactions océan-atmosphère sur le Gulf Stream: apport de la haute résolution sur la représentation des mécanismes physiques et des impacts climatiques*, phd thesis, Université Toulouse.

# 3

# Computational Fluid Dynamics

# Introduction

The CFD team is the largest team at CERFACS and it keeps growing with almost 80 members at the end of 2020. The team's activity is split in three main parts:

- Numerical methods for partial differential equations (PDEs usually the Navier Stokes equations for reacting flows) as found in all flow problems. Coupling has also become a daily task in this field.
- Physical models needed to describe chemistry, turbulence and other mechanisms which are not explicitely contained in the Navier Stokes equations
- Applications which continue to feed new research topics to the team

The development of physical models and their application to real problems remain a key activity for the team. However the numerical research activity has also increased, moving from classical finite volume solvers to new methods: Lattice Boltzmann techniques and High-order techniques. The following sections describe results obtained by the CFD team since 2019. A few important points are mentioned here:

**Academic excellence**
With an average of 14 permanent researchers present in the team over this period, the number of papers published per year and permanent researcher remains of the order of 2. This is a reasonable average when it is compared to the 60 contracts which are active at all times in the team and managed by the same 14 researchers. During the same period 2019-2020, 16 PhD were presented by CFD team members.

**New numerical paradigms for CFD**
Multiple groups worldwide explore new numerical methods to solvde the Navier Stokes equations and CERFACS does too: Lattice Boltzmann formulations as well High order spectral techniques are intensely studied through multiple PhDs and collaborations with external laboratories such as M2P2 in Marseille or ONERA. A specificity of CERFACS, however, is to avoid as much as possible theoretical controversies about the compared values of methods and to adopt a pragmatic approach: compare all codes on reference cases in a very simple framework: accuracy versus cost. This was done for CFD codes for turbomachinery 4 years ago in collaboration with SAFRAN and the overall result was that the AVBP solver was the best compromise in this (accuracy vs cost) diagram. This explains why AVBP has become today the reference code for LES of turbomachinery in the SAFRAN group.
This situation may change very rapidly and the introduction of new techniques such as Lattice Boltzmann approaches requires CERFACS to continuously question its choices and make sure that the team works on the most efficient approaches. In 2020 for example, ProLB (LBM code of M2P2), Walberla (LBM code of Erlangen, see Algo/Coop team presentation) and AVBP were compared to data obtained at EM2C (CentraleSupelec) for a non reacting flow in an aerospace-type swirler where very detailed measurements were available. For 8 months, three PhD students and seniors have worked on exactly the same case to compare the codes with precision. Results will be submitted for publication at the end of 2020. Interestingly one of the first (and maybe expected) conclusion will be that, for these high-fidelity solvers, the mesh (all codes used different meshes because of their specificities) may actually play the first role in the (accuracy vs cost) diagram.

**The Center of Excellence in Combustion: COEC**
CERFACS continues to work successfully at the intersection of physics and HPC. A good example is the Center of Excellence in Combustion (CoE-C) project (cordis.europa.eu/project/id/952181) selected by the EU in March 2020. COEC brings together 11 partners among the European leaders in numerical simulation of combustion. The objective is to develop high-performance software accessible to the industrial sector for the design of innovative combustion technologies. The project is divided into 4 main activities: computing efficiency, modeling, data processing and future technologies. CERFACS is responsible for WP7 dedicated to the realization of digital and technical demonstrators for various applications.

**The simulation of hydrogen flames and the ERC advanced grant SCIROCCO**
After the ERC (European Research Council) advanced grant INTECOCIS in the field of thermoacoustics (intecocis.inp-toulouse.fr), CERFACS and IMFT have won a second ERC advanced grant: SCIROCCO (cerfacs.fr/scirocco) has started in November 2019 for five years. It will focus on hydrogen combustion, a topic which has grown tremendously in 2020. The interest in hydrogen combustion to store energy and to decarbonize our society has sparkled a strong motivation in developing simulation methods for hydrogen flames and CERFACS is leading this activity while IMFT develops a strong experimental program. The number of researchers studying specifically hydrogen combustion at CERFACS and IMFT will be larger than 25 at the end of 2020 and the applications are numerous: from cryogenic hydrogen to replace kerosene in helicopters and aircraft to gaseous hydrogen for BBQ or house heaters.

**The simulation of explosions, fires and the LEFEX project**
CERFACS has identified safety as a key topic for a long time. This includes simulations of explosions and of fires. The simulation of explosions in buildings has been a success story of the CFD team where the combustion tools coming from aerospace research were applied to explosions in buildings containing a combustible mixture of air and gas. This project was supported by TOTAL, leading to an INCITE project in 2013 and 2014 and renewed projects in the field of safety. In 2018, CERFACS partners have expressed interest in developing an upscaled version of the AVBP code for explosions, both in the subsonic (deflagration) and supersonic (detonation) regimes. The objective was to develop truly predictive simulation methods for explosions in a field where heuristic methods and low quality CFD software are still used too often to analyse the safety of industrial installations. In 2019, CERFACS started this cooperative project on explosions called LEFEX with GRTgaz, AIR LIQUIDE and TOTAL. This is an exciting field of research where the very large size of the domains to compute stretches our HPC capacities requiring new methodologies: CERFACS has introduced adaptive mesh generation in collaboration with CORIA Rouen to track flame fronts in large domains at reduced costs, Deep Learning approaches to model subgrid flame wrinkling, reduced chemistry to diminish the CPU costs. The transition to detonation (DDT) is also addressed. The LEFEX studies have found a new application field in 2020 with hydrogen where safety will be a key issue. Discussions with multiple partners are taking place since July 2020 and should lead to new projects dedicated to H2 fires and explosions, including cases where hydrogen will be cryogenic (20 K).

**The simulation of innovative combustion chambers**
Interestingly, the tools developed for safety in the field of detonation have also found new applications in the field of aerospace where engines using rotating detonation for example, may replace present, constant pressure chambers. The gains offered by chamber concepts working at constant volume (such as CVC: constant volume combustion using valves or RDE: rotating detonation engines) are one of the only ways left to improve propulsion for aerospace applications. CERFACS is working on CVC as well as RDE. At the end of 2020, a new EU ITN project coordinated by Florence (Pr Andreini) and gathering most European experts in the field will begin to study CVC and RDE concepts. Two PhDs will start at CERFACS on these topics, extending present activities.

**LES for turbomachinery, coupling and LES and for full engines**

The challenge identified by CERFACS 10 years ago (computing a full gas turbine) has come to life in 2020 with two engine configurations computed from inlet to outlet using CERFACS LES tools in collaboration with different companies (SAFRAN HELICOPTER, SAFRAN TECH, AKIRA) which are crucial to provide all the specific tools needed to assemble such large cases. The AVBP LES solver of CERFACS was used for the combustion chambers as well as for turbomachinery and fully coupled simulations (compressor + combustion chamber or chamber + turbine) were performed thanks to GENCI and PRACE allocations. This fundamental breakthrough opens new paths for engine research and CERFACS is discussing them now with its partners: many phenomena involving coupling mechanisms between engine components have been simply ignored for a long time. They can be studied now and even if the cost of such coupled studies is high, they correspond to really 'transformative' simulations: they unveil physics which were just impossible to study otherwise.
This evolution also corresponds to a simultaneous change where stand-alone CFD methods are losing ground, compared to coupling techniques which allow multi-physics multi-component simulations. The CFD team continues to collaborate with the GlobC team and with ONERA to develop the OpenPalm/CWIPI coupling software. Coupling is not only a field of research in terms of physics: it rapidly becomes a computer science question where CERFACS has chosen to couple individual solvers rather than merge all in a single solver.

**Elearning and training**
The COVID crisis has accelerated a move which CERFACS had anticipated by developing its formation program towards online activities. Since March 2020, the CFD team formations have not stopped: they have moved towards fully online courses (cerfacs.fr/en/training-at-cerfacs/). This was a significant challenge for formations requiring hands-on periods where students must be able to run our large codes without being present onsite. A solution is used for the moment where all computations are exported outside and performed on a cloud support. This also simplifies security issues by avoiding to open intern CERFACS access to students. In terms of pedagogy, this has also lead all CERFACS teachers to remodel their courses and design them for online use.

# Numerics

## 2.1 Introduction

The CFD Team develops multiple CFD softwares where the quality of the numerical methods is critical to address all the multi-physics problems encountered in complex industrial geometries but also in academic configurations. The diversity of CFD solvers used by the Team (elsA-ONERA, AVBP, ProLB, JAGUAR) requires to use different numerical formulations: finite volumes, finite elements, Lattice Boltzmann Method and discontinuous spectral methods. This section presents some of the work done on these numerical methods. In addition to this purely numerical work, enhancing the use of high-fidelity CFD in an industrial environment requires to work on all parts of the CFD workflow. For this reason, CERFACS has developed tools to optimise the use of high-fidelity simulations (Reduced order Modeling) and to post-process the data generated by these simulations.

## 2.2 Numerical methods

This section describes the classical CFD solvers used at CERFACS (finite elements and finite volumes). First of all, research on turbulent non reflecting boundary conditions are carried out. Thus, the introduction of Riemann solver for two-phase flow simulations is studied. Finally research on temporal integration schemes to reduce CPU time for high Reynolds number flows is a permanent research activity.

### 2.2.1 Non-reflecting inlet boundary condition with waves injection

The choice of boundary conditions for compressible flows, reactive or not, is crucial to increase accuracy but also to save CPU time. In addition, the injection of three-dimensional turbulence, but also of acoustic waves is essential for many applications (in turbomachinery or aeroacoustics, for example). A novel formulation was proposed by Daviller et *al.* [CFD43] using characteristic analysis based on wave decomposition (NSCBC). As shown in Fig. 2.1, for an acoustically forced flame this new boundary condition (called NRI-NSCBC) allows to respect the target unsteady inlet velocities (for turbulence and acoustics), avoiding a drift of the mean inlet velocities and ensuring non-reflecting performances for waves reaching the inlet from the computational domain.

### 2.2.2 Riemann solver for two-phase flows

Originally introduced for large gradients in plasma applications, a HLLC Riemann solver has been implemented within AVBP, improved and assessed for liquid-gas applications through the PhD thesis of Julien Carmona.
The solver uses a 3-waves model (Fig 2.2 (left)), where $S_M = u^*,\ S_R = u + c,\ S_L = u - c.$
Assuming no pressure and velocity discontinuity through the wave $S_M$, $u^*$ can be approximated, allowing to recover velocities ${U_R}^*$ and ${U_L}^*$. Flux are finally retrieved through ${F_K}^* = F_K + S_K\left({U_K}^* - U_K\right)$. Such a scheme provides first order spatial accuracy. In order to reach a 2nd order accurate numerical scheme, a Monotonic Upstream-Centered Scheme for Conservation Law (MUSCL) reconstruction is considered, where primitive variables are interpolated at the interface. The solver has been validated on academic test

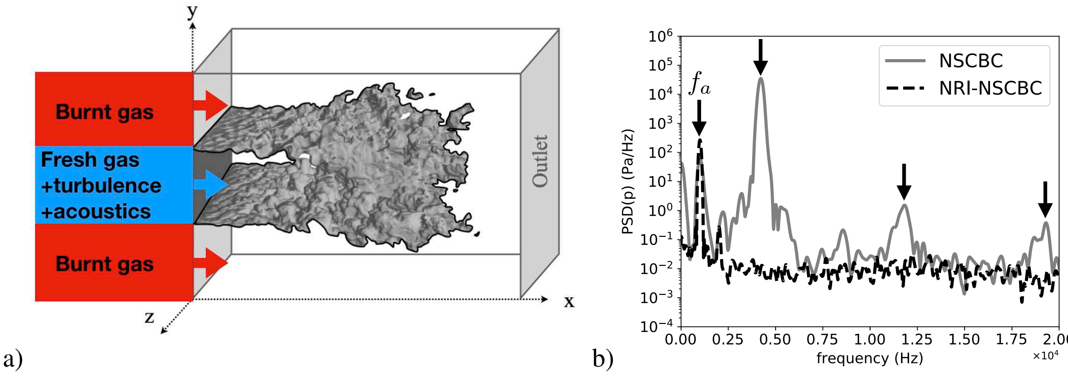


Figure 2.1: DNS of a turbulent, acoustically forced premixed flame. a) Computational domain. At the inlet, a double hyperbolic tangent profile is used to inject fresh gases in a sheet $\approx 8$ mm high, surrounded by a coflow of burnt gases. Top-bottom (along y ) and left-right (along z ) boundaries are periodic. The isosurface is a typical view of T = 1600 K. b) Pressure spectra for NSCBC (solid line) and NRI-NSCBC (dotted line) at the domain inlet. The $f_a$ arrow corresponds to the acoustic forcing at 1 kHz. The three other arrows are the first three longitudinal eigenmodes of the computational box at 4350, 12500 and 19500 Hz. The spectral resolution is 70 Hz.

cases such as shock tubes, or 2D Riemann problems. Orders of accuracy are compared in Figure 2.2 (right) together with a Finite-Volume Lax-Wendroff scheme.
The application to two-phase flows with the use of a diffuse-interface method is described in sub-section 3.4.2.

### 2.2.3 Temporal coupling scheme

RANS and LES equations have almost the same shape and their own pros and cons. In an industrial environment, it could be useful to perform LES far from the wall and RANS near the wall in order to account easily for the turbulence effects, while keeping an acceptable mesh size. Standard time integration schemes for LES and RANS equations do not follow the same constraints.
For LES, an explicit time integration is chosen today in most solvers to control spectral properties (dissipation and dispersion). For RANS equations, it is of paramount importance to reach the steady state as fast as possible, using an implicit time integration procedure. Indeed, a hybrid time integrator that allow spatial coupling of explicit and implicit time integrators was designed and named AION. Here, two standard time integration schemes (Heun explicit scheme and Crank Nicolson scheme ) are hybridized / blended using a transition function $\omega$, while keeping the standard expected properties (spectral behaviour). A spectral analysis performed on the coupled space / time schemes enabled us to check the stability of the hybrid procedure. The validation of this approach has been done on test cases of increasing complexity: from 1D shock tube to 3D Taylor Green Vortex shown on Fig. 2.3. The results with the new scheme were shown to have the same or better quality than the standard basic schemes at reduced CPU cost. This coupling procedure was then improved in two ways. The first one deals with the use of an adaptive time-step procedure. In this case, explicit cells are separated into several classes depending of their local maximum stable time step. All the cells inside the same class are time-integrated using the same time step and for two adjacent classes, time step for the smallest cells is half the one for the largest cells. This work was validated thanks to spectral space-time analysis and simulation from 1D shock tube to 2D convected isentropic vortex [CFD76] . The last improvement is the application of the proposed technique to a coupled RANS/LES computation in an industrial environment. The corner stone is the scaling of the hybrid parameter $\omega$ with

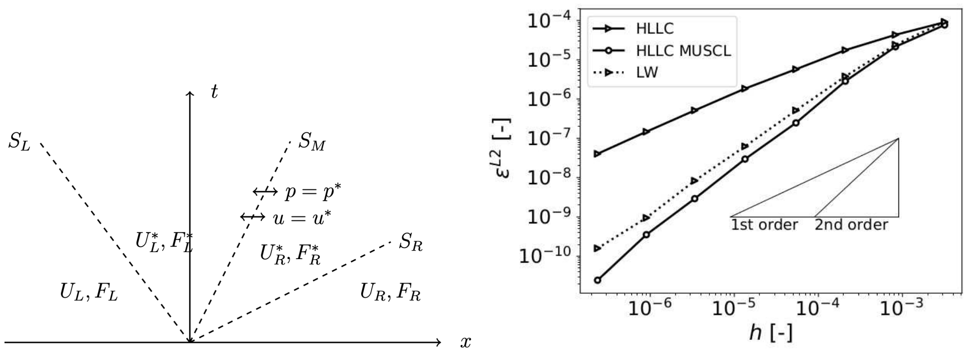


Figure 2.2: Characteristic waves for the HLLC (left). Spatial order accuracy (right).

the function that switches between RANS and LES models. The methodology was tested on a axisymmetric backward facing step [CFD75].

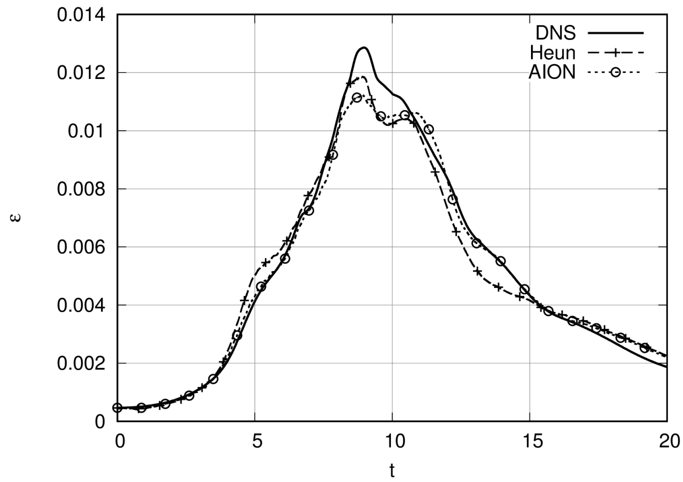


Figure 2.3: The temporal evolution of the kinetic energy dissipation rate of a 3D Taylor Green Vortex ($DOFs = 256^3$) Heun:- - × - -, AION:- - ○ - -

## 2.3 Spectral Difference Method

The next generation of CFD solvers will have to perform high-fidelity simulations (Large Eddy Simulation in most cases) in complex geometries. This requires accurate and fast simulations on unstructured grids. One promising way to acquire this feature is to use spectral discontinuous methods. Cerfacs is working on one of them called Spectral Difference (SD) in a solver named JAGUAR. This solver is being developed in close collaboration with ONERA.

### 2.3.1 hp-refinement

The present work started through the European project TILDA and continued as part of the region 3C2T project. The aim was to reduce the computational cost and memory storage of the Spectral Difference code JAGUAR without losing accuracy. This was achieved by combining mesh refinement (”$h$”) and order of accuracy (”$p$”) adaptation.
This method called hp-refinement, induces several implementation features. The p-refinement adapts the polynomial degree in each mesh element so that, as the polynomial degree varies from one element to another, the computational cost in each element differs. Thus, proper load-balancing has been added to the code JAGUAR using the ParMetis library. The h-refinement consists in refining and/or coarsening the mesh elements and requires a complex data structure. Hence, JAGUAR was linked to the p4est library that performs mesh refinement/coarsening using a tree-like data structure and offers a fast load-balanced parallel partitioning among several interesting algorithms. With the hp-refinement also comes the issue of non-conforming approximations whether due to different polynomial degrees or different interface areas of neighboring elements. The mortar element method was chosen and implemented to handle these element interfaces and to ensure that the conservation of the numerical scheme is maintained. In addition to the hp-refinement features, a sensor based on the density gradient has been implemented to facilitate choosing the distribution of the polynomial degree and level of mesh refinement.
Both h- and p-refinements show good performance to reduce the computation cost of the simulations while keeping the accuracy of the solutions. Fig. 2.4 shows normalized sensor value and corresponding polynomial distribution for an inviscid flow passing over a Gaussian bump at Mach $0.5$. Barely no loss of accuracy is found between a fully refined simulation with $p = 5$ (entropy error of $3.09 \times 10^{-7}$) and a p-adapted one (entropy error of $2.97 \times 10^{-7}$). A gain of $57.1\%$ in number of DoFs is obtained for the p-adapted simulation for a reduction of $40.2\%$ of the CPU time.

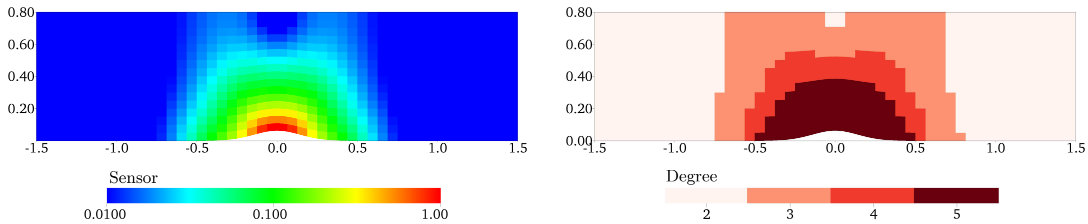


Figure 2.4: Normalized sensor value (left) and corresponding polynomial distribution (right) for the case of an inviscid flow passing over a Gaussian bump.

Fig. 2.5 shows the mesh refinement induced in the case of an isentropic vortex traveling at constant velocity through the computational domain. The h-adapted simulation conserves the accuracy of the computed solution compared to a fully refined simulation while decreasing the number of DOFs by $60\%$ and the computational time by $50\%$.
The hp-refinement has been implemented in JAGUAR in both two and three dimensions. Moreover, the h-refinement can handle high-order meshes. The development of the hp-refinement is mature to be tested on complex configurations. New sensors, however, need to be implemented to properly capture numerical and physical phenomena for these configurations.

### 2.3.2 Extension to combustion

The aim is to assess the potential of the Spectral Differences (SD) method for the simulation of turbulent combustion in aeronautical engines. The philosophy is to transfer the physical models of AVBP into JAGUAR and to make a systematic comparison of the two solvers.

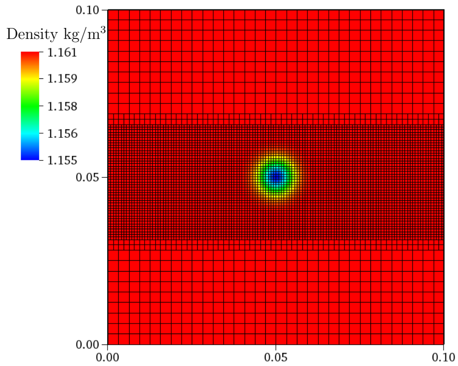


Figure 2.5: Mesh refinement for the case of the convection of an isentropic vortex.

Non-reflecting boundary conditions (NSCBC), species transport and combustion source terms were implemented in JAGUAR and validated on a one-dimensional methane-air premixed flame. The NSCBC procedure follows the one described in Fievet et al. but was extended to multispecies gas. The transport equation for species uses the Hirschfelder and Curtiss approximation where each species has a given diffusion coefficient into the rest of the mixture. The source terms in species and energy equations are computed using Arrhenius's law. The results for a one-dimensional methane-air premixed flame using the CH4/Air-2S-BFER scheme are shown in Fig. 2.6.

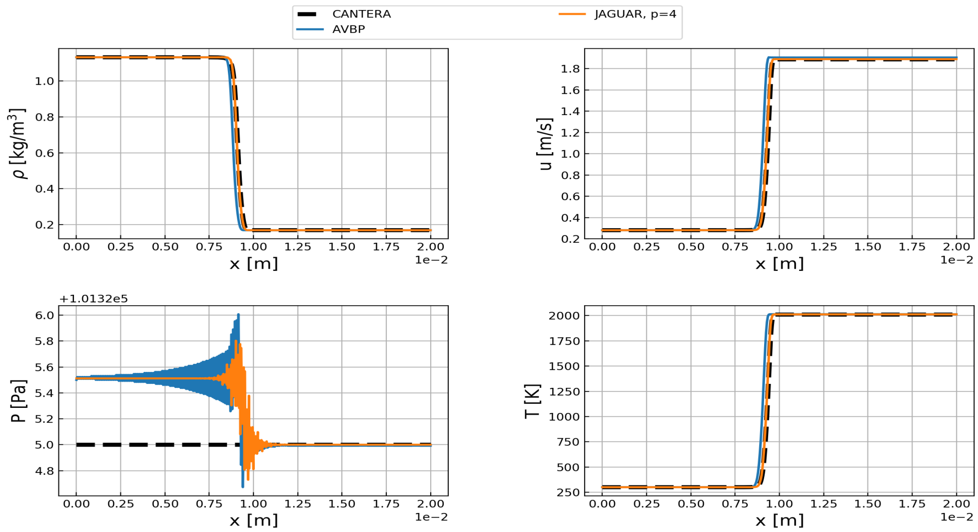


Figure 2.6: Comparison of the primitive variables at $T_f = 0.1$ s between JAGUAR with $p = 4$, AVBP using TTGC scheme and CANTERA for the 1D methane-air premixed flame at $\phi = 0.8$

Following this work, the implementation of the thickened flame (TF) model, which keeps the same flame speed by thickening the flame by a factor $\mathcal{F} > 1$ and dividing combustion source terms by this same factor, was done and validated on the same one-dimensional flame. This allows the use of coarser meshes.
One-dimensional flame simulations have also been performed using a more complicated chemistry called Analytically Reduced Chemistry (ARC). These chemical schemes are considered as intermediate mechanisms between detailed and one or two-steps mechanisms because they keep the more important

species for flame properties (flame speed, flame thickness, burnt gas temperature...) and remove the others. Consequently, these schemes tend to have between ten to fifty species to transport which is still affordable in a LES context. For instance, the ARC mechanism that we used for the one-dimensional flame with JAGUAR was composed of 15 transported species reacting through 256 reactions.
Finally, a two dimensional premixed methane-air burner was simulated using the CH4/Air-2S-BFER chemical scheme. This was done to evaluate the boundary conditions (NSCBC, walls and symmetry) in JAGUAR when combustion is simulated. The two-dimensional heat release fields are shown in Fig. 2.7 for both JAGUAR and AVBP simulations.

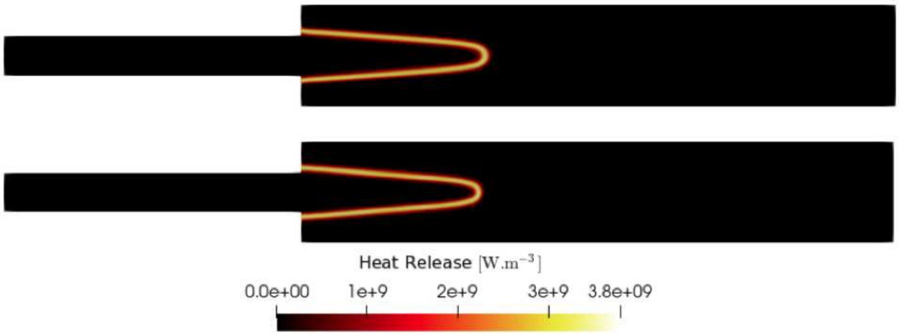


Figure 2.7: Two-dimensional heat release fields for the burner case. Top: AVBP. Bottom: JAGUAR

### 2.3.3 Implicit Time Integration

In the H2020 HIFI-TURB project (High-Fidelity LES/DNS Data for Innovative Turbulence Models), Cerfacs develops time implicit methods for high-order methods. The solver JAGUAR based on the Spectral Difference Method is very efficient on massively parallel platform (95% efficiency on 200,000 CPU cores), thus the only way to reduce the CPU cost is to work on numerical algorithms. Indeed, the time integration is based on explicit Runge-Kutta formulations which suffer from severe restrictions on CFL stability conditions. The efficiency can be very low when walls are present in high-fidelity turbulent simulations as in wall-resolved LES for industrial configurations.
To increase the time step and reduce the turn-around times of LES, without uncontrolled loss of accuracy, an implicit time integration technique has been implemented in JAGUAR. The approach relies on a matrix-free Newton Krylov technique fully integrated in the parallel framework of the solver. The associated linear system are solved by a matrix-free Flexible GMRes method. To preserve the non-building of a Jacobian matrix, the linear system is preconditioned with a matrix-free method chosen to be the GMRes method. Another preconditioning technique based on a matrix-based LU decomposition will also be devised in the near future.

### 2.3.4 Extension to multi-element

The initial release of JAGUAR was using quadrangles and hexahedron. In order to deal with complex geometries, it is necessary to extend the SD method to other standard element-shape (triangles in 2D, tetrahedral and prismatic elements in 3D). The standard SD method applied on triangles is unstable for an order of accuracy strictly greater than two [4]. The use of Raviart–Thomas (instead of Lagrange) basis functions (SDRT) allows to overcome this issue. In addition, following the state of the art, the SDRT approach was proven to be linearly stable only up to the $4^{th}$ order.
This approach was implemented and extended up to $6^{th}$ order in JAGUAR (PhD of Adèle Veilleux,

co-funded by ONERA and CERFACS) under certain conditions (suitable temporal schemes, CFL stability limits, choice of a particular set of interior flux points...). Numerical experiments were conducted to validate the SDRT implementation for triangular (shown in Fig. 2.8) and 2D hybrid grids (illustrated in Fig. 2.9).

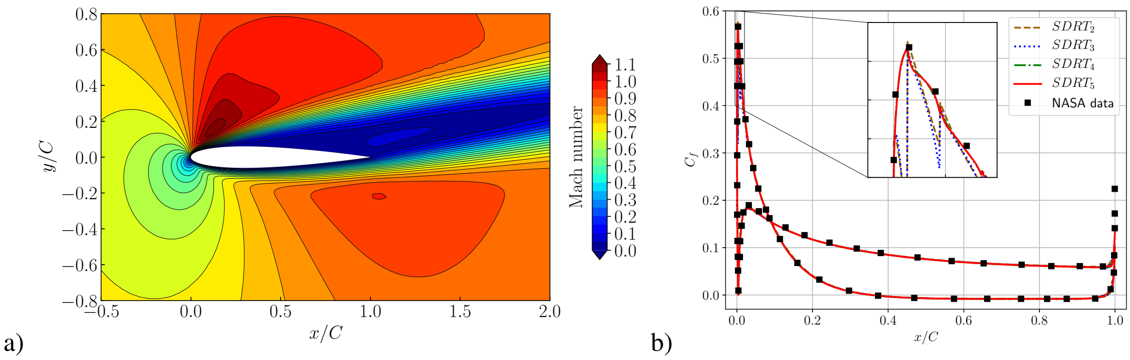


Figure 2.8: Transonic viscous flow ($M_\infty = 0.8$, $\alpha = 10^o$, $Re = 500$) over a NACA0012 airfoil using a mesh composed of quadratic triangles a) Mach number contours using SDRT$_5$ scheme ($6^{th}$ order) and b) Surface skin-friction coefficient $C_f$

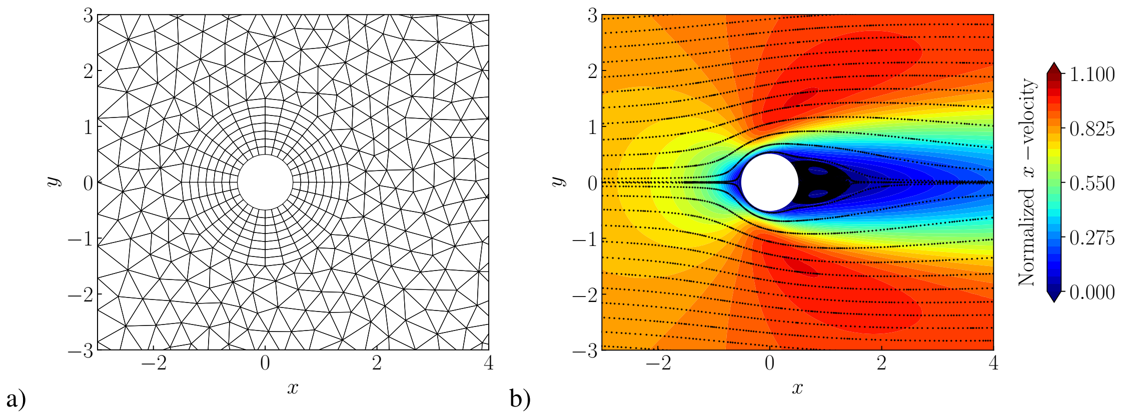


Figure 2.9: Steady laminar viscous flow at $Re = 20$ over a cylinder using a hybrid mesh composed of quadrangles and triangles a) Close view of the hybrid mesh and b) Normalized $x$-velocity contours and streamlines around the cylinder using SDRT$_4$ scheme ($5^{th}$ order)

Finally, the SDRT formulation was extended for tetrahedral elements. The linear stability is demonstrated using Fourier analysis up to $3^{rd}$ order. This formulation was implemented in JAGUAR for both inviscid and viscous flows, and validation test cases are now ongoing.

## 2.4 Lattice Boltzmann Methods

Due to its low dissipative nature, modest CPU cost and fast mesh generation, the Lattice Boltzmann Method (LBM) is an attractive alternative to standard Navier-Stokes solvers for the simulation of isothermal and weakly-compressible flows around very complex geometries. However standard LBM (isothermal and weakly-compressible) have limitations [2, 3]: the extension of the standard model to highly compressible flows presents accuracy and stability problems. Similarly, the use of mesh refinement levels results in spurious acoustic waves that spoil aeroacoustic simulations. Cerfacs is working with its partners to remove these limitations.

### 2.4.1 Compressible extension

The accuracy, the efficiency and scalability of LBM on standard lattices (D1Q3, D2Q9 and D3Q19/Q27) has been widely demonstrated for aeronautics applications involving turbulence and acoustics. Nevertheless, most existing LBM schemes relying on these lattices are restricted to isothermal and weakly compressible simulations, leading to a limitation of their range of application, particularly in the field of aeronautics. In order to perform fully compressible computations while retaining the advantages of the standard LBM, two key issues must be resolved: the compressibility defect (Galilean invariance) of standard lattices and the inability to correctly resolve the energy equation. Among the available methods, the hybrid method (HLBM) has been retained. This segregated method relies on two systems, the LBM system that solves the mass and momentum equations and a finite difference system that solves an extra energy equation. Using tailored corrective terms removing the compressibility defect, an advanced regularized collision operator, a third-order TVD scheme discretizing an entropy equation, an HLBM allowing for stable compressible simulations at subsonic and supersonic regimes has been obtained.

This HLBM have been successfully implemented in the ProLB solver relying on a D3Q19 lattice. Once adapted to the existing boundary conditions and mesh refinement algorithm, the resulting compressible HLBM allowed for stable computations of subsonic and supersonic flows including discontinuities, as illustrated on Fig. 2.10.

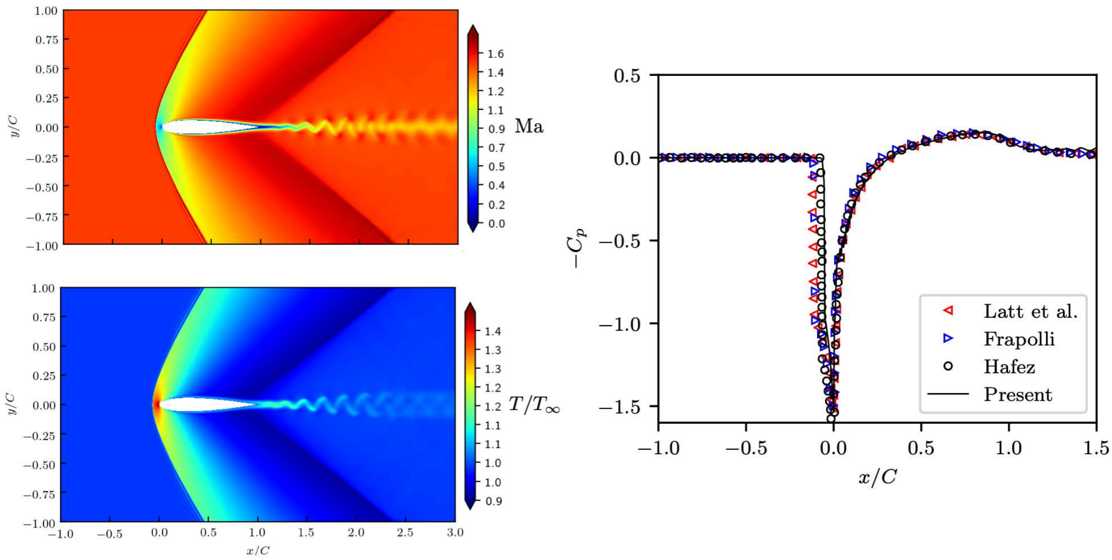


Figure 2.10: Supersonic viscous flow ($\mathrm{Ma}_\infty = 1.5$, $\mathrm{Re} = 10^4$) past a NACA0012 aerofoil computed with the D3Q19-HLBM implemented in ProLB. Several mesh refinement layers have been employed and 800 points have been considered along the chord. Instantaneous Mach number (top left) and temperature (bottom left) fields. Pressure coefficient (right) compared to reference data.

### 2.4.2 Grid refinement

In LBM simulations, the spurious noise emitted by numerical artefacts at boundary conditions or at grid refinement is of major importance. The LBM is usually discretized on a Cartesian grid: during the propagation step, probability distribution functions are missing and have to be reconstructed at the interface, when the mesh size is doubled requiring specific algorithms. Existing algorithms suffer from a lack of precision generating spurious acoustics when these interfaces are crossed by vortices. Previous theoretical work at Cerfacs [CFD33] allowed the decomposition of these spurious emissions into two distinct natures: (1) a non-hydrodynamic contribution, inherent to the LBM method and which requires to be filtered in the fluid core using an adapted collision model. This contribution does not depend on the grid coupling algorithm. (2) a spurious emission linked to the lack of precision of the grid coupling algorithm. On this last contribution, an algorithm (referred as DC) has been developed, not using grid overlap as usually done. This algorithm allows, through a specific equilibrium function, consistent to both meshes, to enhance the link between both meshes and to improve the coupling. Fig. 2.11. (b) shows the contribution on the spurious emission brought by this new algorithm on a turbulent cylinder, compared to the one we had in LaBS/ProLB so far (referred as STD). This algorithm has also been validated on the LAGOON landing gear, as shown in Fig. 2.11. (a), a 10dB reduction of the spurious noise is obtained for high frequencies and experiments are now retrieved.

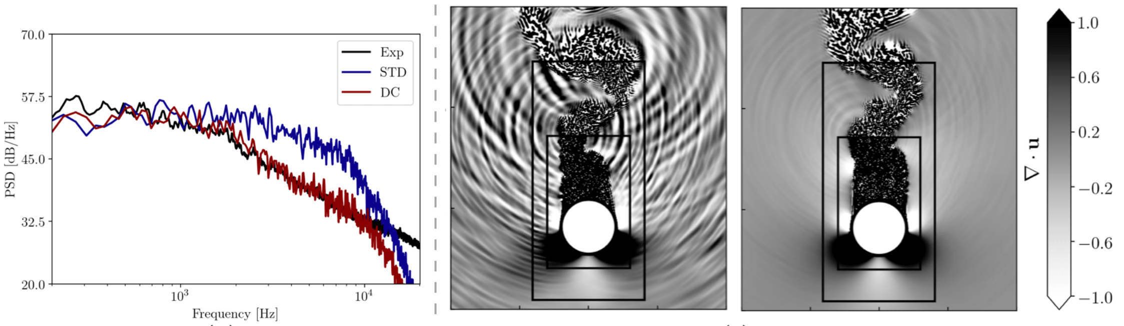


Figure 2.11: (a) PSD of pressure fluctuation on a farfield microphone of the LAGOON landing gear obtained with a FW-H solver and a permeable formulation. (b) Turbulent flow around a cylinder. Velocity divergence field. Left: STD algorithm. Right: DC algorithm.

### 2.4.3 Wall turbulence

On one hand, imposing the boundary conditions in LBM is more complicated than for Navier-Stokes based methods using body-fitted meshes, owing to the Cartesian lattice. To overcome this issue, the immersed boundary method (IBM) can be adapted to LBM, i.e. the boundary conditions are imposed inside the fluid instead of at the boundary.

On the other hand, the computational expense of fully resolving turbulent boundary layers at high Reynolds numbers with Cartesian grids is orders of magnitude larger than with classic anisotropic meshes where the mesh density can be tailored. This makes wall models a necessity, yet their implementation in conjunction with the IBM (usually referred to as “wall treatment” in this context) is significantly more complex than for Navier-Stokes based solvers. Obtaining smoothly varying surface quantities (pressure and skin friction) is particularly challenging in this context.

A thorough analysis of the near-wall behavior of a baseline wall treatment has led to the development of an improved version that implements a wall model consistently with the LBM scheme. In contrast to the baseline treatment, the improved one yields visibly smooth results, as demonstrated by the pressure coefficient $C_p$ and the skin friction coefficient $C_f$ shown in Fig.2.12 for a NACA0012 airfoil. The errors with respect to reference computational results provided by NASA with the same turbulence model (Spalart-Allmaras) are also reduced for both quantities.

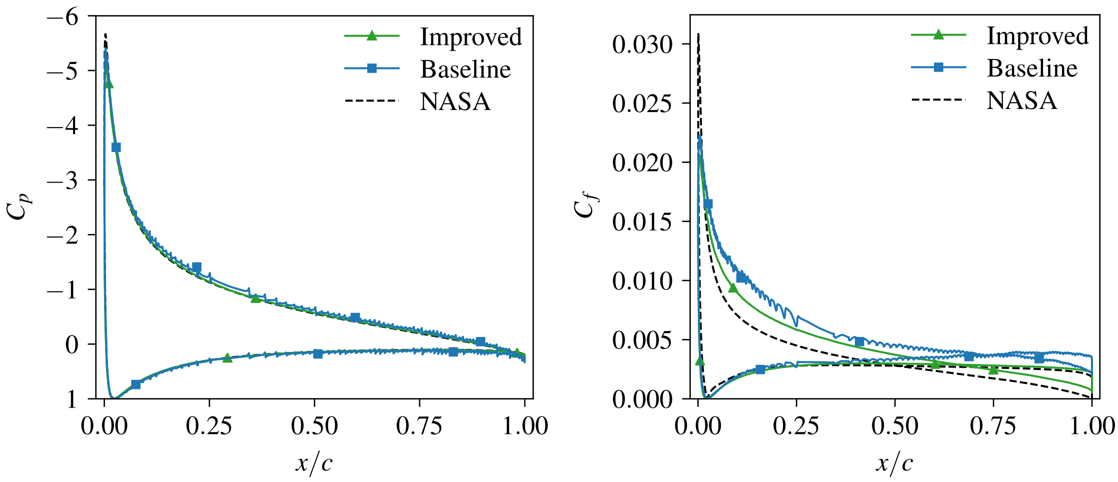


(a) Pressure coefficient

(b) Skin friction coefficient

Figure 2.12: Surface coefficients on a NACA0012 airfoil ($\mathrm{Ma} = 0.15$, $\mathrm{Re} = 6 \times 10^6$, $\alpha = 6°$, Spalart-Allmaras turbulence model) with the improved wall treatment, compared to the baseline treatment and reference computational results provided by NASA.

### 2.4.4 Stability Analysis

Standard LBM suffers from instability issues when increasing the Reynolds and/or the Mach number of the fluid flow. The von Neumann analysis (or LSA for Linear Stability Analysis) is a powerful tool to investigate the stability and accuracy of numerical schemes. CERFACS has developed a LSA library called ALIEN (Analysing the spectraL propertIes of the latticE boltzmanN method).This tool has notably allowed explaining the origin of instabilities observed with the simple BGK model. The stability analysis extended by Wissocq *et al.* [CFD100] allows to separate the hydrodynamic and non-hydrodynamic contributions of the LBM, and to analyze the content of modes in terms of the physical waves they carry. This extended model allows to highlight the dissipation errors appearing with the advanced collision models [CFD99]. In particular, regularized models which are a branch of collision operators allowing to filter non-hydrodynamic contributions, highly detrimental to the stability and accuracy of LBM simulations. These dissipation errors come from the discretization in space and time. They are also responsible of modal interactions that make the BGK model unstable. This study has allowed to make a step forward in the understanding of the dissipation and anisotropy properties of LBM schemes. In addition to the athermal LBM analysis ALIEN has been extended to the hybrid framework, and can now consider the extra energy equation solved using finite difference (FD) schemes.

### 2.4.5 Adaptive Mesh Refinement

A significant issue in modelling industrial configurations is the existence of substantial ranges in space which require huge meshes and computational time. Adaptive Mesh Refinement (AMR) methods allow to reduce these constraints by locally adjusting meshes through a physical sensor often named quantity of interest (QOI). A static approach adapted from [CFD42] has been tested on the NoiseDyn and 30P30N configurations using ProLB, to circumvent the current manual-and-inaccurate octree grid refinement and to be QOI-independent. The strategy relies on an initial coarse mesh simulation, where the time-averaged field of the QOI is computed: a smoothed iso-volume based on a lower case-dependent threshold of this sensor yields a finer resolution domain which is directly reintroduced in the octree mesher of ProLB. This process can be repeated and several QOIs can be employed. Figure 2.13 shows how the proposed approach allows to reduce the dissipation of kinetic energy $\Phi$ [CFD42] through iterative refinements on a transverse cut of the NoiseDyn swirler's injector.

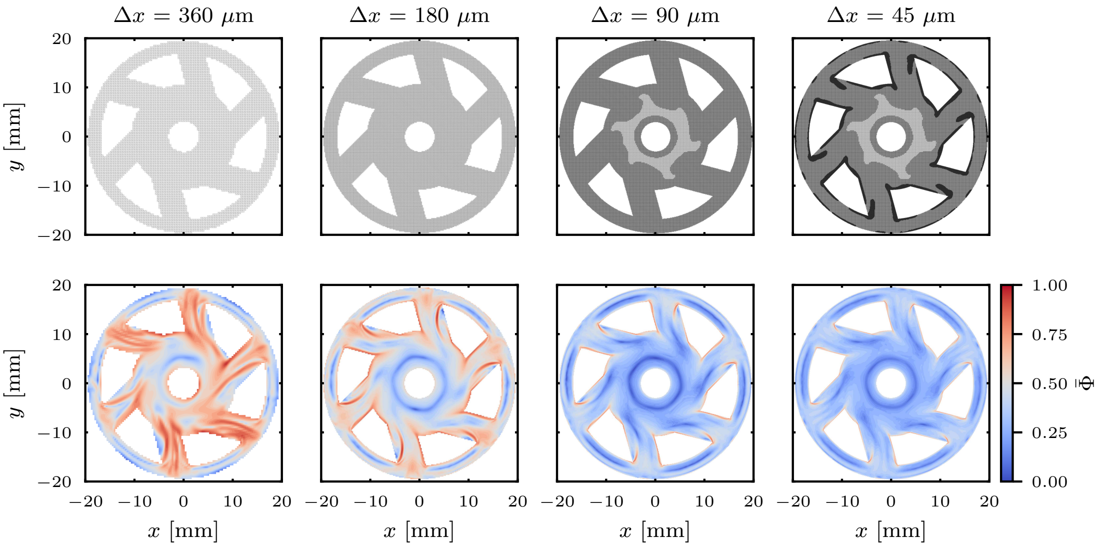


Figure 2.13: Transverse cut in the swirler stage of the NoiseDyn (Centralesupelec EM2C labo) six-vanes injector. Top: refinement grids built upon the AMR iterative strategy, Bottom: normalized fields of dissipation of kinetic energy $\bar{\Phi}$.

### 2.4.6 Multi-phase flows

Multiphase flows are characterized by the presence of at least two thermodynamic phases separated by a sharp interface (few atoms thick, considered null in most cases). The dynamic of the interface is complex to catch since the smallest structures characteristic length is similar to the eddies one. Moreover, an active field of research is the fuel atomization in engines which implies high shear stress, high density ratio (up to 100) and important Reynold numbers. Thus, a robust simulation tool is needed.

Two strategies stand out of the crowd: the tracking interface method and the diffuse interface method. The first one consists in solving a specific equation for the interface. Those methods, while being particularly consistent, need power since the smallest structures need to be computed: they are not fit to simulate industrial configuration. On another hand, diffuse interface methods consist in thickening artificially the interface, allowing a better numerical stability by paying a tribute in term of consistency. Still, these methods remain expansive, and need an efficient numerical solver. Thanks to their good parallelization capability, Lattice Boltzmann Methods could offer a satisfying compromise between accuracy and efficiency.

Our work consisted in a benchmark of the different methods proposed in the literature for diffuse interface approaches. One method in particular aroused our interest: the Gradient-Color method. This method is interesting in term of numerical efficiency, but suffers from an incomplete theoretical description that makes it impossible to interpret in term of macroscopic equations. We then proposed a theoretical analysis that showed how the recoloration step is equivalent to the Allen-Cahn equation. A link between the degree of isotropy of the equilibrium function and the spurious currents was established and a clearer and more efficient formulation of the method was proposed, allowing to solve academic cases at high density ratio (Poiseuille flow, oscillation of a static bubble, two phases cross flow).

### 2.4.7 Rheology

Cerfacs collaborates with IMFT (Pr Climent) to investigate two phase flows with high mass loading. Introducing solid particles in a fluid creates a suspension with new rheology properties. Because rigid particles resist compression, they cause an increase in energy dissipation which generally leads to an increase of viscosity of the overall suspension compared to a single phase fluid. This effect is only captured in simulations if the particles actually occupy their own volume in the simulation domain, i.e. it is not possible with point particles.

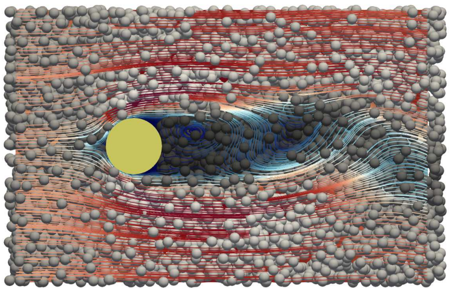

Figure 2.14: Snapshot of fluid stream lines with suspended particles

The LBM waLBerla framework of FAU Erlangen combines fluid solver and rigid body dynamics solver by mapping the particles directly into the domain. This means each cells has a flag, indicating it is either a solid or fluid cell. A no-slip boundary condition is imposed along the interface between each solid-fluid link. It is a fully coupled approach: the flow field influences the particles trajectories, while particles have an effect on the fluid and can collide with each other.
Figure 2.14 shows results for the well-known ”Kármán vortex street”, the flow around a cylindrical obstacle which becomes unsteady at a critical Reynolds number of $Re_{crit} \approx 47$.
The increase in viscosity is proportional to the volume fraction of solid particles and can be estimated by the equation proposed by Eilers [1]. Figure 2.15 shows the dampening of vortex shedding frequency for increasing solid volume fraction for the case of buoyant particles with a diameter five times smaller than the cylinder diameter. By using the effective suspension viscosity for the calculation of Reynolds number, the lines of constant Strouhal numbers become vertical lines. This shows that the suspension can be interpreted as a pure fluid at effective viscosity. The same behaviour can be observed in Figure 2.16 for the cylinder effective drag coefficient. When $Re_{eff}$ number sinks below the critical single phase Reynolds number $Re_{crit}$ the suspension drag coefficients coincide with the values of the single phase steady flow.

## 2.5 ROM coupled with machine learning

The full exploration of all cases for system design requires the computation of a very large number of expensive simulations which can easily become intractable for full CFD solvers. One of the solution to

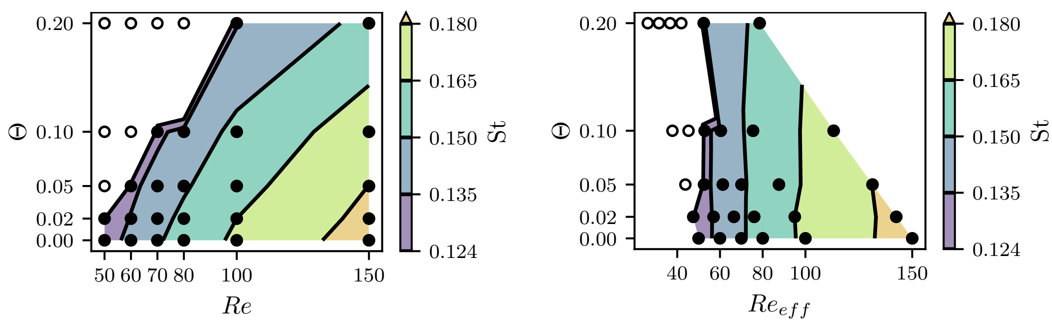


Figure 2.15: Strouhal number $St$ as measure of vortex shedding frequency over Reynolds number $Re$ and solid volume fraction $\Theta$ for the configuration of Fig. 2.14. Open symbols: no consistent vortex shedding, closed symbols: consistent vortex shedding. Left: Reynolds number based on fluid phase, right: Reynolds number based on the effective suspension viscosity.

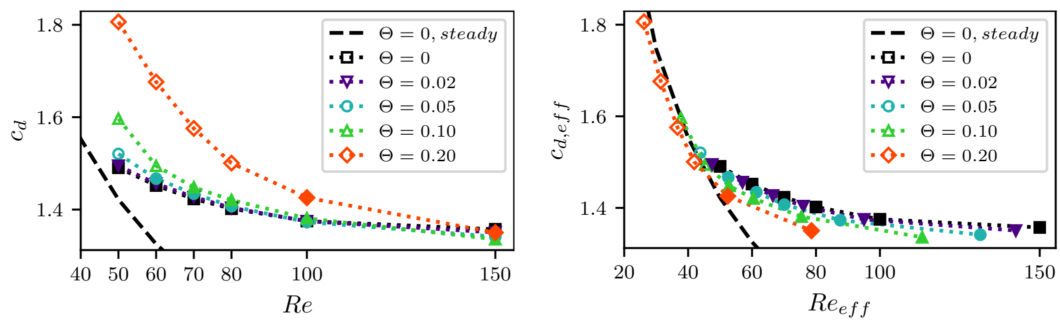


Figure 2.16: Drag coefficient $c_d$ over Reynolds number $Re$ for different solid volume fractions $\Theta$. Open symbols: no consistent vortex shedding, closed symbols: consistent vortex shedding. Left: Reynolds number based on fluid phase, right: Reynolds number based on the effective suspension viscosity. Dashed line: forced single phase steady flow.

overcome this problem is the substitution of the high fidelity simulations by a mathematical approximation much faster to be run, referred to as a surrogate model. It represents an interesting trade-off between precision and computation time. Furthermore, reducing the computational time of the exploration for high fidelity CFD can open the way to multi-physics and muldi-disciplinary simulations using surrogate models for the fluid parts.
The surrogate modeling of high-dimensional vector-valued functions is mainly performed with a reduced-order approach, called reduced-order modeling (ROM). Proper Orthogonal Decomposition (POD) is a popular method of dimension reduction used for CFD problems. It computes the basis vectors and the corresponding modal coefficients with an optimal least-square approach from a given number of high-fidelity computations, also called snapshots, at different state-parameters.
Unfortunately, the various shapes taken by the aerodynamic fields due to the multiple operation conditions pose a real challenge. In fact, problems with bifurcations can have typical characteristics, such as aerodynamic flows with varying inflow conditions leading to either subsonic or transonic regime. In these cases, the classical method computing the dominant modes in a single POD basis fails to produce accurate responses for predictions in highly nonlinear regions.
To overcome this difficulty, a classical non-intrusive POD/GPR (Gaussian Process Regression) called ”Local Decomposition Method” approach has been devised [CFD127]. It extends the classical POD/GPR

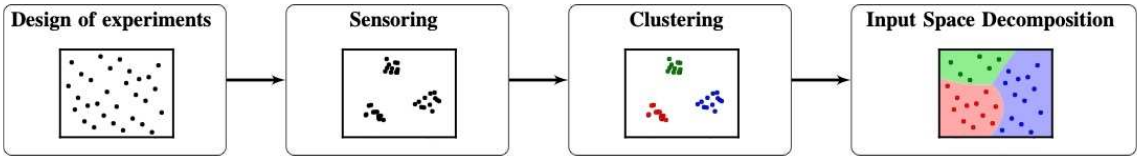


Figure 2.17: Sketch of the Local Decomposition Method

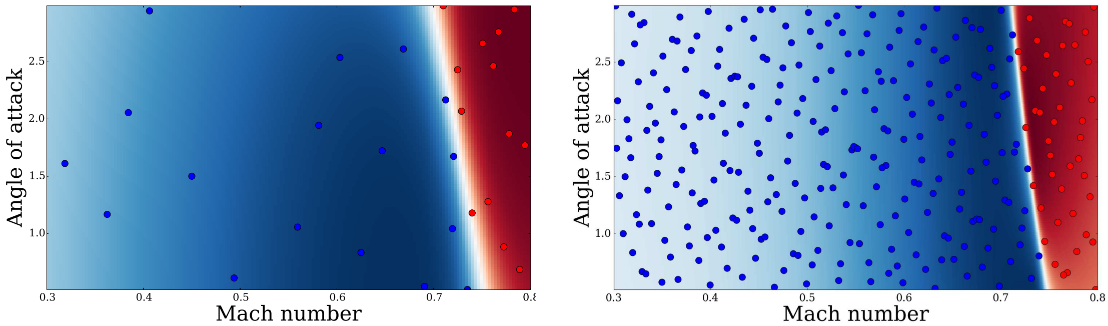


(a) Training set

(b) Test set

Figure 2.18: Input space decomposition. Each color corresponds to a cluster, the blue one is the subsonic regime and the red one is the transonic regime.

reduced-order modeling by employing a local approach, inspired by the mixture of experts and dynamic local reduced-order. Instead of a unique global POD basis, several local bases are computed using machine learning tools yielding more flexible behaviors bringing out a precise delimitation of physical regimes.

The central idea is to separate the solutions with a subsonic behavior from the transonic and high gradient solutions. First, a shock sensor computes specific features for all the snapshots. Then, the latter are clustered into different subsets thanks to the shock features. Finally, the parameter space is divided in several domains according the clustering of the snapshots.

The Fig. 2.17 sketches the process. The method includes, a feature extraction with a shock sensor, a novel resampling strategy and the application to an aerodynamics case. Active resampling is carried out by identifying the subspaces with the highest entropy. Extra snapshots are added in these specific subspaces to minimize the redundancy of the sampling, thus increasing the accuracy of the surrogate model.

The flow around a RAE2822 airfoil has been widely studied in the literature both numerically and experimentally. The interest of this test case is that inflow conditions govern the flow regime, leading to the appearance of shock waves on the suction side. The detection and the separation of these regimes represent the main challenge for the model.

The clustering phase realized by a Gaussian Mixture Model (GMM) automatically identifies the subsonic and the transonic snapshots thanks to the shock sensor. The supervised algorithm ensured by a Gaussian Process Classification (GPC) decomposes the input space parameter to determine the separation of the two physical regimes in the input parameter space (Fig. 2.18) with both training and testing sets. These two clusters can be interpreted as the subsonic and the transonic regions: the boundary is mainly influenced by the Mach number and the angle of attack. Thus, the resampling process has increased the density of samples in the transonic regime, improving the accuracy of the model where the predictions are more challenging.

## 2.6 CFD Data processing

### 2.6.1 ANTARES Python Library

Cerfacs develops a generic data-processing library called Antares since 2012. The project is managed with the web application Redmine (issue tracking, documentation, etc.), the source code with Git, and the documentation and tutorials are disseminated thanks to a website (www.cerfacs.fr/antares) and face-to-face trainings. The library helps users processing CFD data at large. It can be used all along the CFD process from the set up phase of a CFD computation (initialization) to the postprocessing of data generated during simulations. If the CFD steering process is managed by Python, ANTARES can also be used to co-process data (in situ) during massively parallel simulations and reduce the amount of generated data. This library provides a python application programming interface. The large choice of features available within the Python/NumPy framework enables to write complex data analysis procedures: CFD users can develop their own numerical tools on top of ANTARES data structures. Finally it is free for research purposes so that users have a clear view of the library contents, and can modify them if necessary. ANTARES is currently provided to many research labs and industries (cerfacs.fr/antares/partners.html). In particular, Safran Aircraft Engines, Safran Helicopter Engines and Airbus have built their own data processing software based on the ANTARES library.

### 2.6.2 CFD data coprocessing with the high-order solver JAGUAR

#### 2.6.2.1 Paraview Catalyst Library

The high-order solver JAGUAR has been interfaced with the Paraview Catalyst Library with its Fortran API to perform in-situ data coprocessing (Fig. 2.19). A demonstration on a SD7003 configuration has concluded that this approach is an efficient option to perform data coprocessing. This methodology is also directly compliant with online visualisation.

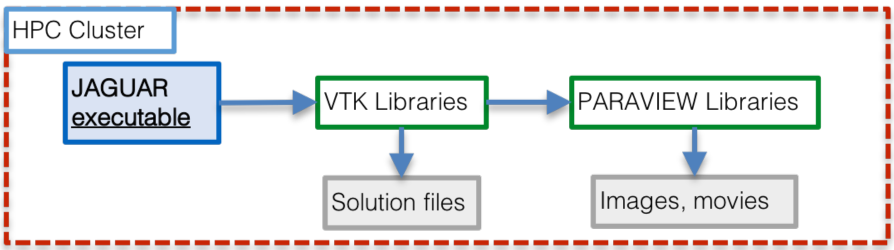


Figure 2.19: CFD coprocessing with JAGUAR and Catalyst (Fortran framework)

#### 2.6.2.2 ANTARES Library

JAGUAR has been transformed into a library callable from Python (Fig. 2.20). The memory allocation has been redesigned from Fortran to Python so that Python and Fortran share the same memory for the conservative field vector. Callback Python functions have been developed, and they can be called from Fortran code to perform data coprocessing. Finally, some specific high-order functions as the isoparametric transformation, the Gauss points distribution, the Lagrange polynomials, the Jacobian matrix and determinant computations have been implemented in Python and included in ANTARES.

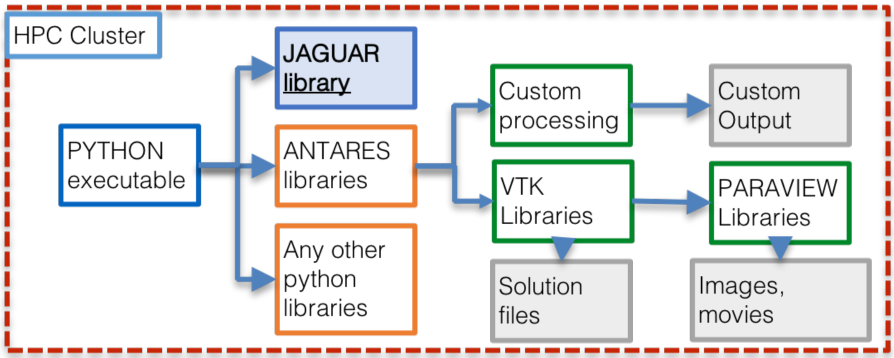


Figure 2.20: CFD coprocessing with JAGUAR and ANTARES (python framework)

### 2.6.3 Visualisation

The visualisation of CFD results on high-order elements requires specific attention. Usually, post-processing tools process data using linear relations between data vertices (slice, isosurface, graphical rendering, etc.). High-order cells, however, need further processing to extract more information from continuous polynomial fields. The VTK Lagrange cells recently introduced in Paraview were used to read JAGUAR files and reconstruct high-order data directly in Paraview. Interactive visualization with OpenGL shader was investigated. By default OpenGL interpolate linearly between vertices to create pixel colors. It is possible to modify the interpolation by anything else with the OpenGL Shading Language, like the Lagrange polynomial itself. Therefore, pixel-exact precision is reached with live computation while zooming and spanning. Physical rendering of data issued from coprocessing have been carried out with Blender.

**References**


[1] H. Eilers, (1941), Die Viskosität von Emulsionen hochviskoser Stoffe als Funktion der Konzentration, *Kolloid-Zeitschrift*, **97**, 313–321.

[2] P. Lallemand and L.-S. Luo, (2000), Theory of the lattice Boltzmann method: Dispersion, dissipation, isotropy, Galilean invariance, and stability, *Physical Review E*, **61**, 6546.

[3] D. Siebert, L. Hegele Jr, and P. Philippi, (2008), Lattice Boltzmann equation linear stability analysis: Thermal and athermal models, *Physical Review E*, **77**, 026707.

[4] K. Van den Abeele, C. Lacor, and Z.J. Wang, (2008), On the Stability and Accuracy of the Spectral Difference Method, *Journal of Scientific Computing*, **37**, 162–188.

# Modelling

## 3.1 Introduction

Modeling is the heart of numerical simulation and a key element for accurate and reliable prediction of complex systems. In the framework of Large Eddy Simulation (LES), if wall flows and wall transfers still are an important topic for all CERFACS applications, most modelling issues are related to combustion and the new low-emission burner concepts, currently under development in industry, and to the future use of alternative fuels. These evolutions require new capabilities of LES, which should correctly describe fuel effects on operability and stability.
The team also continues the recently started activity on cold plasma modeling, for electric propulsion of satellites but also to new ignition systems in aeronautical engines.

## 3.2 Near Wall Modeling

Wall flows inevitably arise in real engineering applications and their modelling remains a key in fundamentals of CFD modeling. Although near-wall flow modeling and understanding has benefited from many years of theoretical developments addressing fully turbulent, laminar or transitioning regimes, taking into account weak / favorable / unfavorable main stream pressure gradients, wall flows remain at the heart of simulations especially if LES or multi-physics applications are targeted. Indeed, the wall flow state is crucial in determining the rate of heat transfer through the solid wall of the combustor. It also determines the performance of wing profiles and turbomachinery blades, and plays a critical role in flame stabilization.

Within the recent studies dedicated to these specific issues, CERFACS has devised two frames of work and developments:

- Near wall flow dynamics,
- Heat transfer and multi-physics.

### 3.2.1 Near wall flow dynamics

Pure aerodynamics as well as heat transfer require fine predictions of boundary layers, which in LES and more broadly in CFD can be addressed in a wall-resolved or wall-modeled manner: *i.e.* with a grid resolution that respects the near wall scaling of the flow dynamics or provides the necessary quantities at a low grid resolution level (and thereof at a lower computational cost).

- For wall-resolved LES around profiles, first requirements aside the near-wall grid resolution, are to adequately represent the flow state around and prior to the blade so as to trigger the proper flow mechanisms controlling the near wall dynamics. Such requirements are not necessarily easy to master due to uncertainties in measurements or in numerics as well as implementations of boundary conditions in fully unsteady CFD solvers. One continuous topic of interest in this framework is boundary layer transition to turbulence and intermittency. A recent study by D. Dupuy (RTRA post-doctorate located at CERFACS) [CFD49] demonstrated that wall-resolved LES is able to reproduce transitioning and that intermittency is one key element that needs to be quantified to properly recover heat transfer measurements, Fig. 3.1.

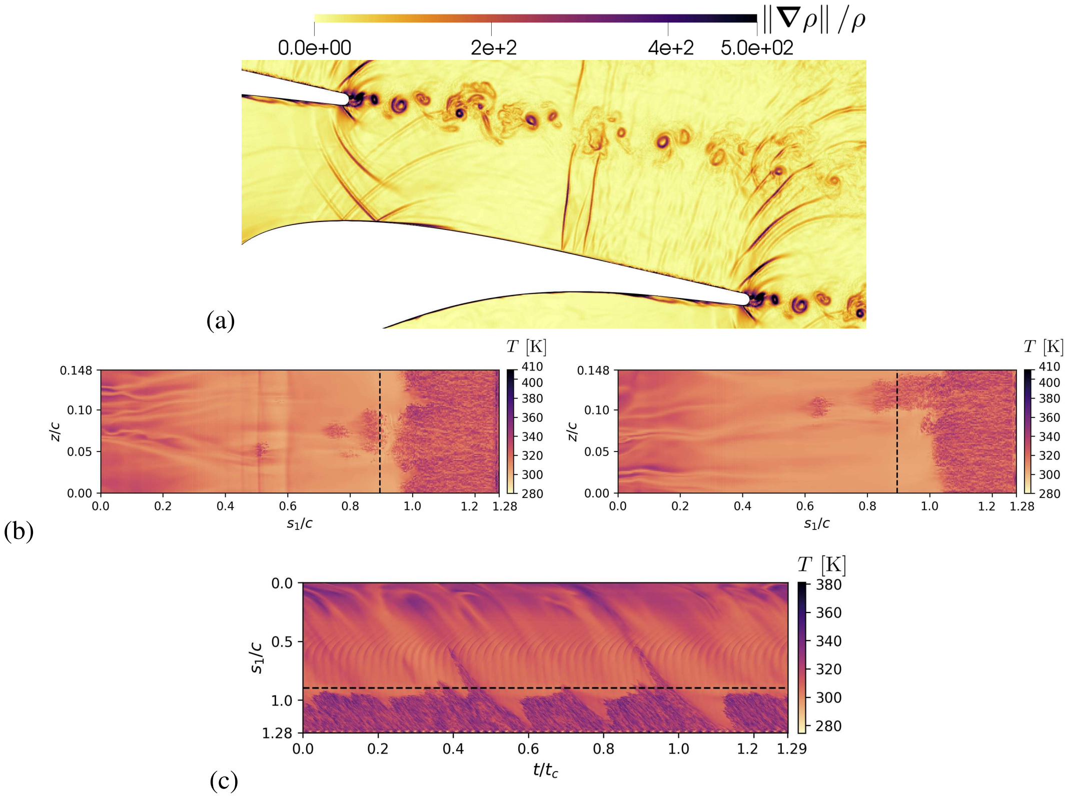


Figure 3.1: LES predictions of the LS89 cascade (experimental study by VKI): (a) instantaneous view of the flow field (norm of density gradient divided by the fluid local density value) in condition MUR235; (b) instantaneous view of local temperature along the top wall at two instants in the LES predictions (dashed lines indicate the shock position) while red indicate temperature elevation due to turbulent regimes; (c) visualisation of the mid-span temperature evolution in time.

- For wall-modeled LES, the complexity arises from the simplifications used in wall-law models. These simplifications are further emphasized in LES where numerical interactions and implementations of the laws to be inverted analytically or numerically may yield different solutions depending on the new procedure so that new developments and new implementations continue at CERFACS to be able to handle anisothermal flow states as well as the presence of pressure gradients as encountered in turbomachinery flows for example.

### 3.2.2 Heat transfer

Heat transfer in combustion chambers has multiple effects. It controls the design of the cooling system, but it also impacts the flame shape as well as its stabilisation and emission of pollutants. As they are easy to measure, wall heat fluxes are also good candidates for the validation of simulations, for example in the case of high pressure methane-oxygen combustion, studied experimentally at TU Munich in the context of liquid rocket engines [6]. The turbulent diffusion flame at 20 bars is illustrated in Fig. 3.2 with an instantaneous temperature field. By applying the coupled wall-law of AVBP, the correct wall heat flux was recovered [CFD71], indicating that the flame is correctly predicted.

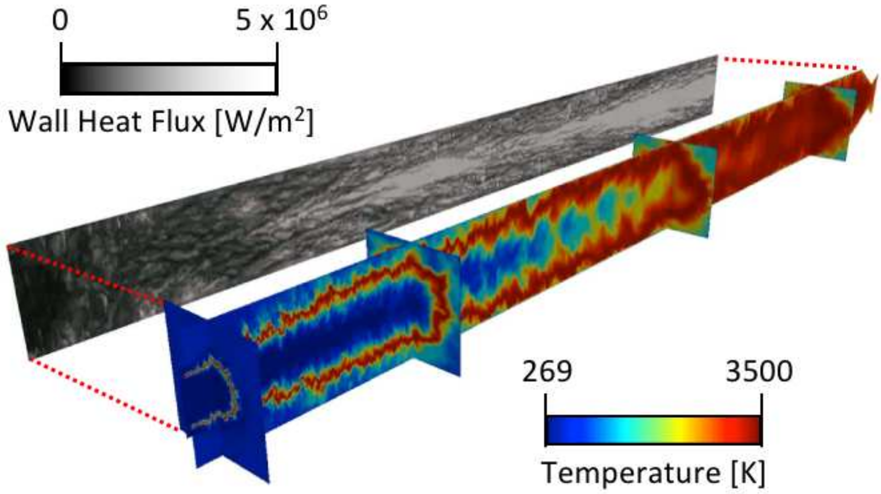


Figure 3.2: LES of the Methane-Oxygen flame of TU Munich at 20 bars [CFD71].

## 3.3 Turbulent combustion

Most turbulent combustion models in AVBP are based on the Thickened Flame concept. This approach allows the direct integration of reduced or complex chemistry. It is adapted to study fuel effects, pollutant emissions, and transient phenomena such as ignition.

### 3.3.1 ARCANE: A tool for automatic reduction of chemistry

The increasing demand for sustainable energy requires the development of innovative energy sources with a reduced footprint on Earth. In the fields of land transport and power, hydrogen, alone or mixed with carbon-based fuels such as natural gas, is a strong candidate to replace conventional fuels. There are two main objectives when using hydrogen: first, lower the carbon content of the exhaust gases and second, sustain stable combustion in very lean conditions. In contrast, for aircraft propulsion, the use of hydrogen is more complex due to storage and safety issues. One solution is to use alternative drop-in fuels containing different proportions of aromatics from fossil hydrocarbons or plant sources, alone or with hydrogen. These alternative fuels can reduce greenhouse gas emissions. Replacing existing fuels with new fuels is a revolution in the design of combustion systems but the development of combustion systems using these fuels requires mastering the physico-chemical processes involved. In particular, combustion chemistry and turbulent combustion as well as their strong interaction must be properly reproduced.
To reproduce flame structures, flow-combustion interactions in turbulent flames and pollutant emissions, Cerfacs has worked for 6 years on Analytically Reduced Chemistry (ARC), a knowledge-based reduction approach [18, 28]. ARC accurately describes combustion phenomena by retaining the most important species and reactions, and remains computationally affordable due to the introduction of Quasi Steady State (QSS) species [15]. Combined to the Dynamic Thickened Flame (DTFLES) turbulent combustion

model, ARC captures flame structure and pollutant emissions such as CO and NOx in a variety of lab-scale configurations operating with conventional fuels, from methane [11] to Jet-A1 [CFD52].
To study real multicomponent fuels such as kerosene, alternative fuels or blends of fuels, a new software called ARCANE (for Analytically Reduced Chemistry: Automatic, Nice and Efficient) has been developed with Prof. P. Pepiot (Cornell University) to address the broad need for compact and computationally efficient chemical models for reactive flow simulations. Based on a new, fully automatic and optimised multi-step reduction methodology, ARCANE provides a convenient and accessible framework for the analysis and reduction of chemical kinetics mechanisms. All chemical schemes reduced using ARCANE are described and provided online through a dedicated website (Fig. 3.3).

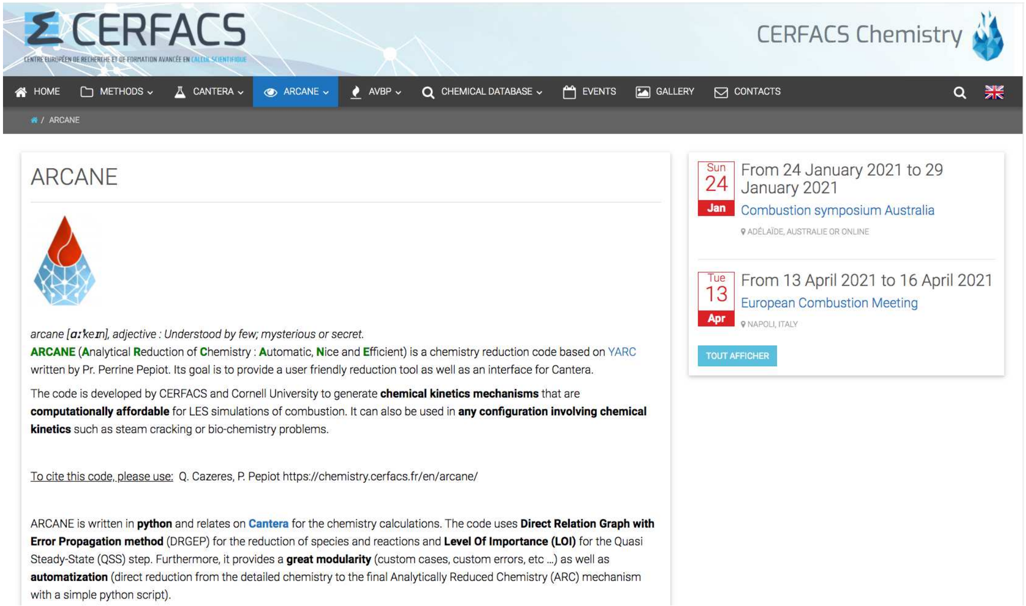


Figure 3.3: ARCANE website, https://chemistry.cerfacs.fr/en/arcane

A first step towards alternative fuels has been achieved using ARCANE. ARC for blends of hydrogen and natural gas has been derived to study the flame structure and the stabilization mechanism of a lean methane/air premixed swirled flame enriched with a non-premixed hydrogen injection [CFD63] in the MIRADAS test-rig measured at IMFT. Within the H2020 JETSCREEN project (2017-2020), ARCANE has been used to derive reduced chemical schemes for both a classical Jet-A1 modelled as a three-component mixture of n-dodecane, methyl-cyclohexane and xylene and an alternative jet fuel modelled as a three-component mixture of iso-dodecane, iso-octane and iso-hexadecane [CFD92]. The impact of alternative fuels on aircraft engine operability is now being evaluated in terms of flame structure, high-altitude ignition capability, extinction limit and combustion instabilities in lab-scales configurations measured at ONERA and DLR.

### 3.3.2 Modeling of soot emission

Soot particles emitted by combustion will soon be subject to more stringent regulations. Even though their impact has been neglected in comparison with greenhouse gases, they play an important role in global warming as well as human health: modelling soot has become an important subject of research.

The complexity of soot production modelling is fourfold. Firstly, soot particles inception is triggered by the collision of Polycyclic Aromatic Hydrocarbons (PAH) generated by the combustion process. Having an accurate description of the formation process of PAHs is thus of prior importance. Secondly, soot particles react at their surface with the gas phase (condensation of PAHs, oxidation by O2) as well as with each other (aggregation of particles). Having an accurate description of the reactions that soot particles undergo during their lifespan is also a major challenge. Then, soot population shows a large range of sizes and shapes depending on their history, which requires to solve their number density function. Finally, if soot are initially spherical, their evolution then results in the formation of large fractal aggregates which should also be modeled.

Taking advantage of both ARC which considerably improves the description of gas phase chemistry and of the parallel performances of the Lagrangian solver for droplets, an original method to simulate soot production in combustion chambers has been proposed in the PhD of L. Gallen [CFD130] in the framework of the H2020 SOPRANO project (2016-2020): ARC with accurate PAH chemistry has been coupled to a semi-deterministic Lagrangian approach for soot particles. The Lagrangian Soot Tracking (LST) method is deterministic in the sense that physical soot particles are tracked, contrary to Monte Carlo dealing with stochastic particles. However, it still includes stochastic processes to handle collisions.

This novel method based on ARC and LST has been applied to canonical one-dimensional premixed and counterflow ethylene-air laminar sooting flames, and then to the ISF5-Target Flame4 configuration representative of an aeronautical combustor. It is a turbulent gaseous confined pressurized swirled ethylene-air flame measured at DLR 3.4. Impact of PAHs and radiative transfers through the resolution of Radiative Transfer Equation has been studied. Good predictions have been obtained compared to measurements in terms of flame structure, gas temperature and soot volume fraction [CFD55], at a very affordable computational cost. The addition of real fuels such as kerosene and accounting for soot agglomerates will be worked on in the ANR ASTORIA project (2018-2022) coordinated by Cerfacs and gathering CORIA and EMAC laboratories as well as ONERA.

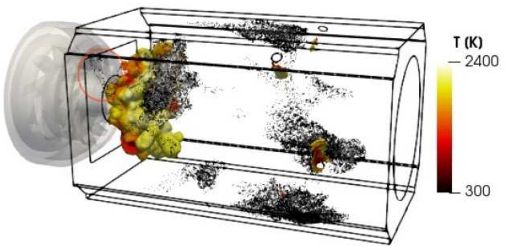

a.

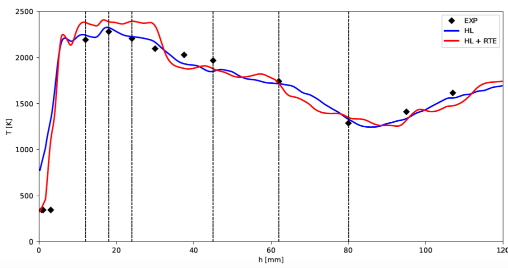

b.

Figure 3.4: ISF5-Target Flame4 configuration. a. Instantaneous view of soot particles with an isovolume of heat release rate colored by temperature. b. Comparison of experimental and numerical mean axial temperatures [CFD55].

### 3.3.3 Prediction and analysis of ignition

Guaranteeing ignition and more importantly high-altitude re-ignition is a crucial design factor of aeronautical engines. Its importance is reinforced in the context of low-emission, which often relies on lean combustion and therefore leads to even less favorable conditions. In previous works, the ability of AVBP to reproduce ignition in one or several sectors [CFD39], and even in full annular burners, both in purely gaseous or two-phase flames, has been demonstrated and validated. This has allowed to investigate further the mechanisms of ignition and to build a low-order stochastic approach to predict ignition probability maps at a low cost.

Based on the joint observation of experimental and numerical sequences in the KIAI-Spray configuration corresponding to one sector of an aeronautical engine, Collin et al. [CFD38] have been able to establish ignition and extinction scenarios following initial sparking in a two-phase flow. It has been shown that the large variety of kernel evolutions can all be interpreted as a succession of elementary events, each depending on local conditions of stoichiometry, turbulence, and temperature. Logically, ignition is favored by kernel trajectories going through regions with sufficient fuel vapor and low turbulence, and for a sufficient time. Following this analysis, all ignition sequences could be recast in series of kernel growing and shrinking processes, as illustrated in Fig. 3.5.

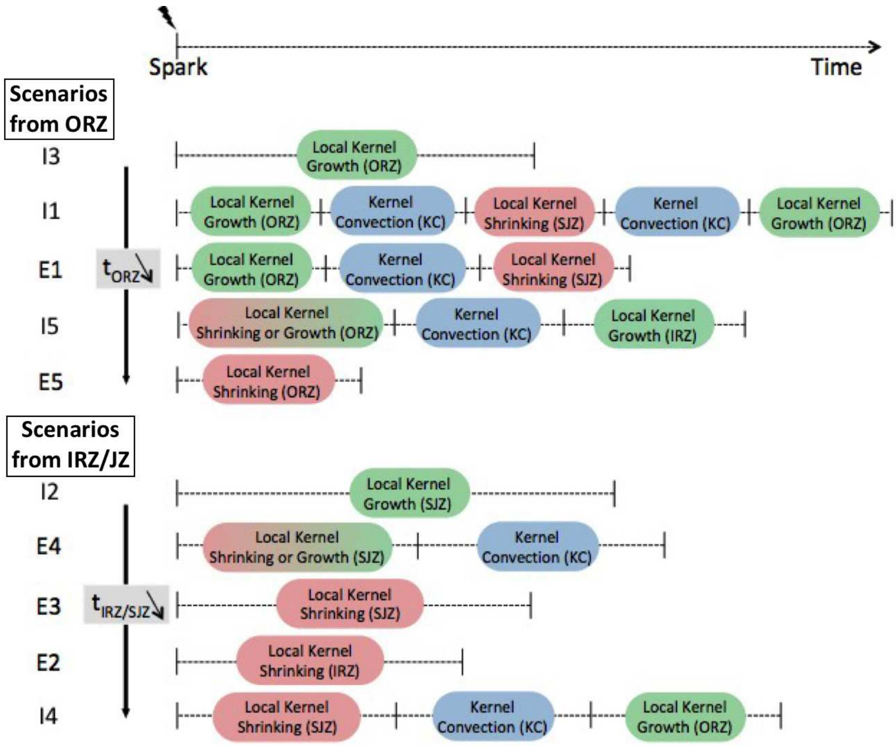


Figure 3.5: Decomposition in elementary processes of the ignition/extinction modes encountered in the KIAI-Spray configuration [CFD38].

This decomposition in elementary processes may be used to determine ignition or extinction criteria for low-order models. This has been done recently in [CFD50]. In this work the ignition probability map is predicted knowing only flow statistics in non-reacting conditions, i.e., with only one LES. Flow statistics are reconstructed along the kernel trajectory, which are then combined with local characteristics to apply ignition or extinction criteria. The model (called MIST) has been applied to a swirled burner operated in premixed, non-premixed and spray combustion modes. In all cases the experimental ignition map was recovered with good accuracy. Examples of results are shown in Fig. 3.6 for a gaseous premixed and non-premixed swirl burner [CFD50].

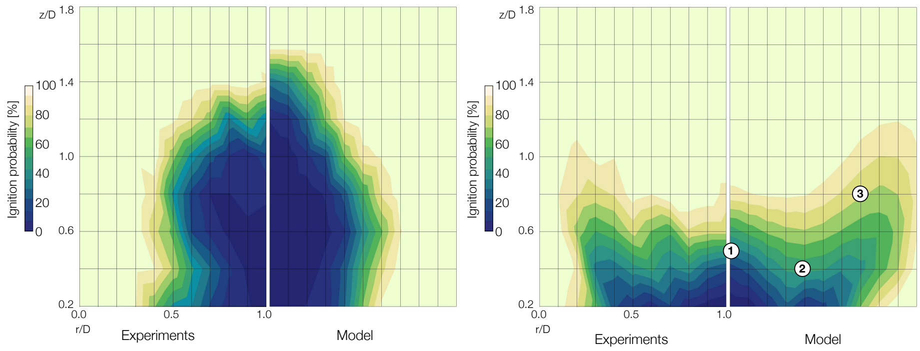


Figure 3.6: Comparison between experimental (left) and MIST (right) ignition probability maps. LEFT: premixed case. Right: non-premixed case [CFD50].

## 3.4 Spray atomization and combustion

Most industrial burners are fed with liquid fuel that is directly injected into the combustion chamber, generating a strong interaction between spray, turbulent flow and combustion. Modeling turbulent spray combustion and liquid atomization remains challenging and active research fields at Cerfacs.

### 3.4.1 Two-phase combustion and flame sensors

Turbulent spray flames are more complex and more diverse than gaseous flames. Depending on the initial droplet diameter, overall equivalence ratio, liquid loading and relative velocity between gaseous and liquid phases, spray flames exhibit very different flame structures, from fully premixed flames to highly non-premixed flames.

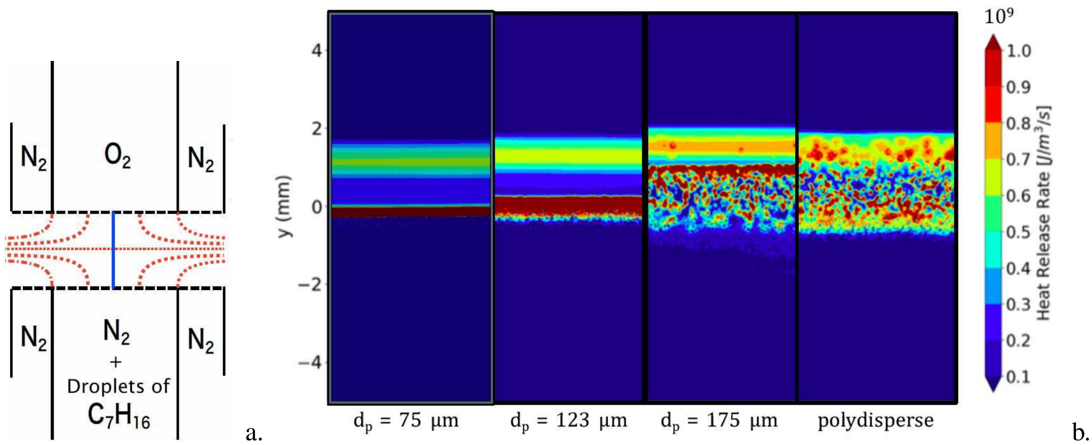


Figure 3.7: a. Sketch of the counterflow two-phase diffusion flame of [16]. b. Heat Release field for 3 monodisperse cases $d_p = 75\mu m$, $d_p = 123\mu m$, $d_p = 175\mu m$ and the polydisperse case [CFD97].

To understand these spray flame structures and model real fuel flames in complex geometries, canonical configurations need to be analysed. Two examples are described hereafter.

First, the axisymmetric configuration of counterflow two-phase diffusion n-heptane/air flame with polydisperse spray experimentally studied by [16] has been numerically investigated in an equivalent planar 2D geometry [CFD97], using a Lagrangian formalism for the liquid phase and ARC for the gas phase chemistry. A double flame structure with both diffusion and premixed flames is observed, as well as group and individual droplet burning, consistently with experiments. The comparison with monodisperse flames with varying droplet diameter reveals that the spray flame structure is similar to a gaseous one with different equivalence ratio whereas for larger droplets, the premixed mode becomes dominant and the flame power exceeds the maximum gaseous diffusion flame power (Fig. 3.7).

Second, the impact of real fuel on 1D spray flame structure has been studied, accounting for a three-component surrogate of Jet-A composed of n-dodecane, methyl-cyclohexane and xylene [CFD92]. A discrete multicomponent model for spray vapourisation has been implemented in AVBP along with an ARC. The preferential evaporation effect, unique to multicomponent fuels, causes a variation of fuel vapour composition on both sides of the flame front and this has a direct impact on the spray flame structure and propagation speed. In rich cases, multiple flame structures exist due to the staged release of vapours across the reactive zone. Spray flame speed correlations have also been extended for multicomponent fuels, to be used in turbulent efficiency models.

These two examples show the capacity of AVBP to predict multi-component spray flames. This feature is essential considering the increasing demand for sustainable energy (such as alternative fuels or fuels enriched with hydrogen).

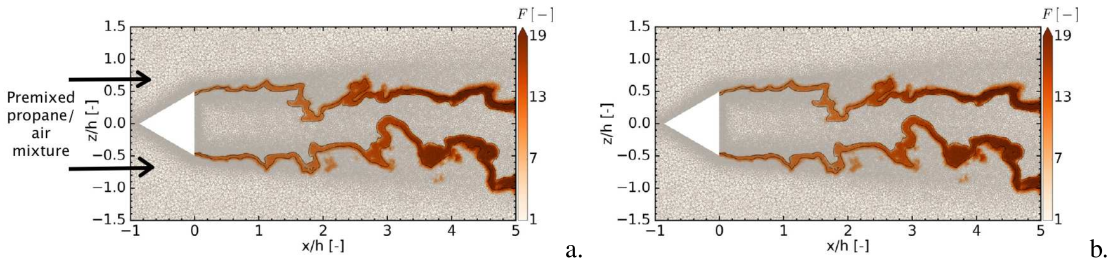


Figure 3.8: VOLVO configuration. Instantaneous thickening field with an overview of the mesh and an isoline of heat release rate for a thickened flame computed with a. the standard method, and b. the generic method [CFD88].

When performing LES of these turbulent flame structures using the DTFLES combustion model, one key aspect is the flame front detection. Within the PhD of B. Rochette [CFD138], a generic and self-adapting method for flame front detection and thickening has been developed. This approach relies solely on geometric considerations: unlike previous thickening methods, it does not need any parameterization nor preliminary calibration. The detection process is based on the analysis of the curvature of a test function, associating a bell-curve shape to the reaction rate field. Once the front is located, the front thickness is also evaluated from the test function, allowing a thickening restricted to under-resolved flame regions and a self-adapting thickening of the front. The thickening process is finally applied to the detected front, over a normal-to-the-flame distance, using a Lagrangian point-localization algorithm. The generic sensor has been evaluated and compared to the classical thickening method on several academic configurations of increasing complexity [CFD88] and in a laboratory-scale pressurised spray burner. Results show a more accurate thickening, especially in post-flame regions, as illustrated in Fig. 3.8 for the VOLVO configuration where the propane/air flame is stabilised downstream of a bluff-body flame-holder. Next step is to evaluate the generic sensor in industrial combustion chambers.

### 3.4.2 Diffuse interface methods for atomization

Two numerical approaches are investigated at CERFACS to predict atomization (PhD work of Thomas Laroche, and Julien Carmona). All methodologies rely on the concept of diffuse interface method, where an appropriate thermodynamic closure allows to handle jump conditions by smoothing the interface. The first methodology implemented in AVBP by T. Laroche relies on a 3-equations multi-components model coupled to a Peng-Robinson thermodynamic closure. Surface tension has been implemented, together as an Euler-Lagrange transition model, (Figure 3.9 (left)). Eulerian liquid clusters at ligaments extremities are detected, and transformed into Lagrangian particles when reaching a critical Weber number. Particles diameters are not prescribed, but result from the local physics. Finally, these primary droplets may experience secondary atomization, through a secondary breakup model.

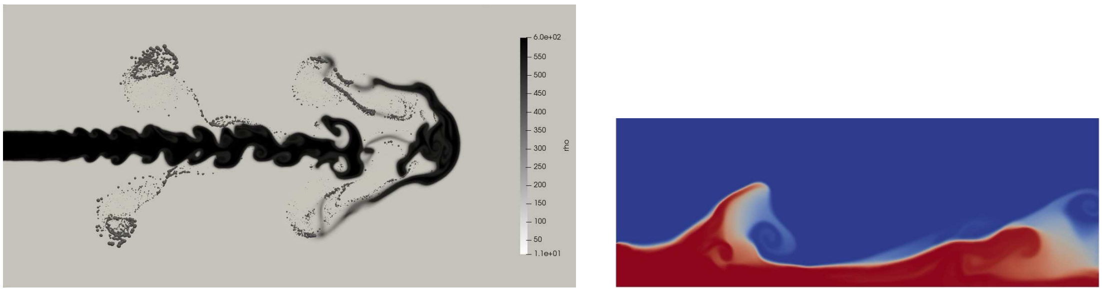

Figure 3.9: Diffuse-interface methods: Atomization of a liquid jet configuration with a 3-equations model and Euler-Lagrange transition 3.9 (left). Two-phase shear layer with a 4-equation model, using a HLLC Riemann solver 3.9 (right).

The second methodology currently implemented in AVBP through Julien Carmona's PhD relies on a 4-equations model allowing multi-components and evaporation, closed by a Noble-Abel Stiffened-Gas thermodynamic closure. Surface tension has been added and validated on academic test-cases. A HLLC Riemann solver was implemented to solve the system (described subsection 2.2.2). A two-phase shear layer with predicted with such a formalism is presented in Figure 3.9 (right).

## 3.5 Thermo-acoustic instabilities

Modern land-base gas turbines and aeroengines operating in lean conditions to reduce the production of pollutants, such as NOx, are known to be prone to thermoacoustic instabilities, an undesirable behaviour that needs to be avoided [14]. The origin of these phenomena is a feedback loop between the noise produced by the flame and the response of the flame itself to acoustic waves [14]. However, a complete understanding of all the mechanisms leading to this coupling still remains a challenge. During these two years, multiple activities have been accomplished at Cerfacs trying to understand this coupling in the PhD works of E. Lo Schiavo, F. Dupuy, C. Laurent, A. Badhe and the post-doc of D. Laera.
A crucial modeling aspect of thermoacoustics in real gas turbines is the liquid fuel injection. The importance of correctly modelling the interaction between liquid particles and the combustor has been investigated by E. Lo Schiavo and D. Laera in the *SICCA-spray* test bench developed at the EM2C laboratory (CNRS, CentraleSupelec) [21] and shown in Fig. 3.10 (left). The lagrangian formalism is adopted to model the liquid spray and a "film condition " is used to model the particle-wall interaction inside the swirler where kerosene forms a film before atomizing at the injector lips.
Figure 3.10 (right) shows the temporal evolution of pressure at the combustion chamber backplane when the film treatment is used. At the beginning of the simulation, the pressure signal features a classical exponential increase until a maximum pressure value (overshoot point) is reached [19]. The pressure oscillation then

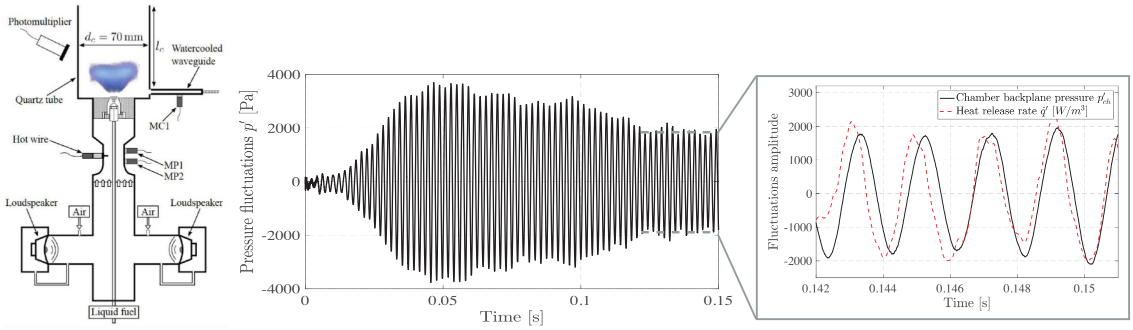


Figure 3.10: (left) SICCA-spray: experimental setup [21]. (right) LES of combustion instabilities: pressure fluctuations measured at the combustion chamber backplane with a zoom on some cycles showing how the unsteady pressure and heat release rate oscillations present the same phase satisfying the Rayleigh criterion [23].

decreases until the energy generated by the thermoacoustic coupling equals the system damping. The level of the limit cycle, $p'_{LES} \simeq 2000$ Pa, is in line with experimental measurements where a fluctuation amplitude of $p'_{exp} \simeq 1700$ Pa is recorded [21].

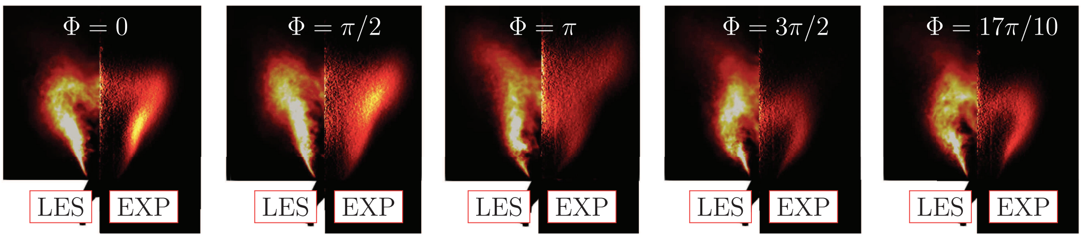


Figure 3.11: Heat release rate phase average, colormap: $\dot{q} \in [0, 250]$ MW/m$^3$, comparison with the experimental CH* chemiluminescence [21].

Fig. 3.11 compares and experimental flame shapes during the whole cycle. These results suggests the importance of liquid fuel film models to correctly reproduce the establishment of the self-sustained limit-cycle. This work has been published in [CFD95, CFD69]. A sensitivity analysis of the results on the injection parameters is the object of a work submitted to *Combustion and Flame*.
A different approach to study the thermoacosutic combustion instabilities via LES is to investigate the Flame Transfer Function (FTF), i.e., a function which links the heat release rate perturbation ($\dot{Q}$) integrated over the flame location with incoming perturbations taken at a reference point.
F. Dupuy [CFD128] computed the FTF of the NoiseDyn combustor [10] shown in Fig. 3.12 (left). This system designed at the EM2C laboratory is composed of an injection system, a swirler unit and a combustion chamber ending with a short exhaust tube. For the FTF computation, the steady flame is forced in the LES by adding to the inlet boundary condition a 30% RMS amplitude velocity modulation. Simulation results are compared to experimental data in terms of FTF gain and phase in Fig. 3.12 (right). A very good agreement is obtained for both FTF gain and phase for the eight tested frequencies. In particular, the characteristic high and low gain regions of a swirled V-shaped flame anchored on a bluff-body are well retrieved [CFD49].
Extreme regimes occur in rocket engines where thermoacoustics are a major issue: C. Laurent [CFD134] investigated the response to acoustic forcing of the Mascotte H2-O2 flame [26] sketched in Fig. 3.13 (top). This setup consists in a parallelepipedic chamber with a coaxial injector at its backplate that comprises a central round injection of liquid oxygen, surrounded by an annular injection of liquid methane. Those

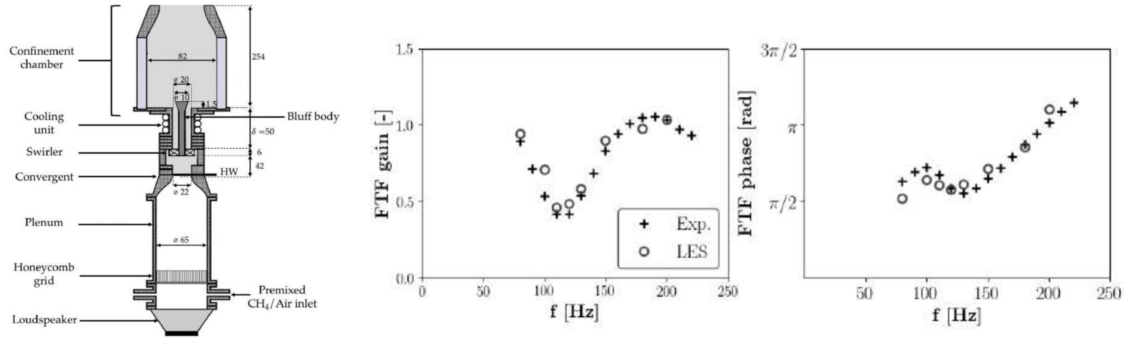


Figure 3.12: (left) Sketch of the NoiseDyn burner from EM2C laboratory [10], dimensions in mm. (right) Gain and phase of the flame transfer function of the NoiseDyn burner.

are separated by a tapered lip. For these simulations the real-gas version of the LES solver AVBP is used. Non-ideal thermodynamics are modeled thanks to the Soave-Redlich-Kwong (SRK) [27]. Reaction kinetics are based on a ARC mechanism for high-pressure $CH_4$ oxycombustion, that was reduced from the GRI3.0 mechanism, and contains 9 resolved species, 7 quasi-steady-state species, and 82 reactions. To compute

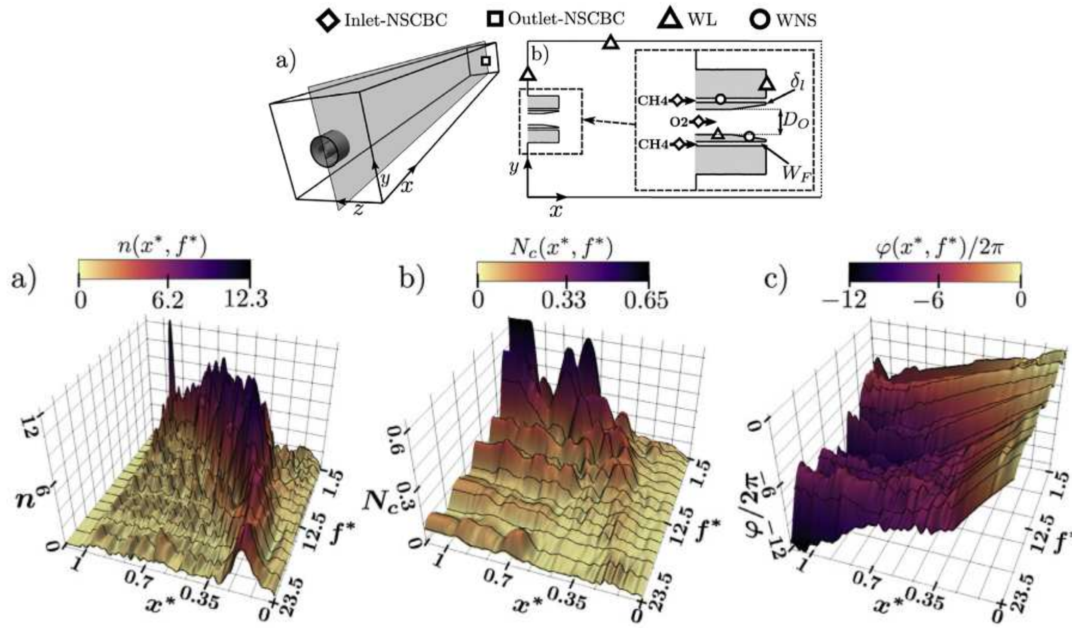


Figure 3.13: Top: (a) Three-dimensional view of the Mascotte test rig [26]; (b) Closeup view of the near injector region. Bottom: (a) Local FTF gain $n(x^*, f^*)$. (b) Cumulative FTF gain $N_c(x^*, f^*)$. (c) Local FTF phase $\varphi(x^*, f^*)$. The dark lines are points directly computed from the 16 forced frequencies [CFD67].

the FTF of this flame, acoustic harmonic forcing is imposed at the fuel inlet, for 16 forcing frequencies $f$ from 1 to 20 KHz. Differently for the previously described NoiseDy case, due to the high-frequency of thermoacoustic instabilities and the length of coaxial jet flames, the heat-release region is not assumed acoustically compact. Therefore, all quantities (including the FTF) depend on both the forcing frequency $f$ and the axial location $x$ (in the following the normalized quantities $f^* = fL_f/u^0_{CH_4}$ an $x^* = x/L_f$)

(Fig. 3.13 (bottom)). At low-frequency forcing (Fig. 3.13 (bottom-a)) the region of strongest heat-release response is long and spans over the entire second half of the flame. As the excitation frequency increases, this region shortens and shifts upstream, such that for high-frequency forcing it is localized at the injector exit. Similarly the phase (Fig. 3.13 (bottom-c)) shows a linear trend in $x^*$ at low $f^*$ which indicates a constant disturbance propagation speed. For higher $f^*$, the portion of constant propagation speed shrinks eventually reaching a plateau where it stagnates. Furthermore, the disturbance propagation speed increases with the frequency. The cumulative gain ( Fig. 3.13(bottom-b) ) shows that the second half of the flame has always the largest contribution to the overall heat-release response [CFD66, CFD67].

### 3.5.1 STORM, a novel tool to predict thermoacoustic instabilities.

A novel low-order acoustic-network modeling (LOM) tool for studying thermoacoustic combustion instabilities in complex realistic configurations based on ”state-space” framework and ”generalized modal expansions” is under development at CERFACS in the PhD work of C. Laurent [CFD65] and A. Badhe (ongoing). This new tool, named **STORM** uses modal expansions and the ’state-space’ framework that allows easy and convenient interconnections between multiple subdomains and other elements in the network such as active flames or complex boundary impedance. In the modal-expansions method introduced by F. Culick in the 60’s, the acoustic pressure field in each sub-domain of the network is expressed as a linear combination or series expansion of natural acoustic eigenmodes of that subdomain (the basis functions).

$$p(\vec{x},t) = \sum_{n=1}^{N} \dot{\Gamma}_n(t)\phi_n(\vec{x}) \tag{3.1}$$

where $N$ is the number of modes, $\phi_n(\vec{x})$ the corresponding basis functions and $\dot{\Gamma}_n(t)$ are modal amplitudes or coefficients. The natural modes are known apriori from a first computation of each element acoustics and the modal amplitudes are the unknown variables to be determined. The $\dot{\Gamma}_n(t)$ coefficient values are governed by boundary acoustic forcing exerted by the adjacent sub-domains in the network, volumetric forcing due to active flames and acoustic losses in the subdomain.

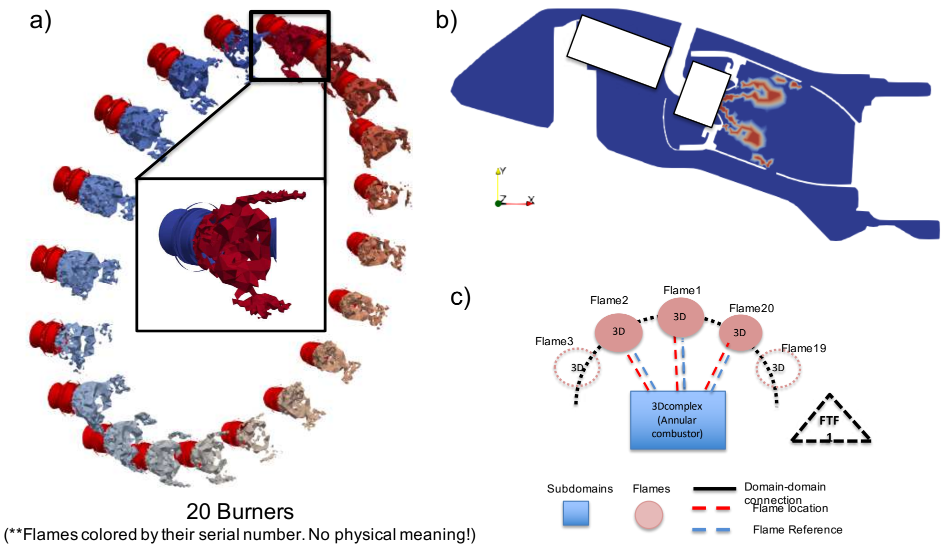


Figure 3.14: The Annular Combustor: a) 20 burners and the flame shape, b) cross-section of the combustor and c) An illustrative acoustic-network representation for STORM

Figure 3.14 shows the results of STORM for a real aeronautical engine annular combustor with twenty 3D quasi-compact flames. In this case, decomposition of the geometry into subdomains (for eg. combustor, casing, plenum etc). is not necessary: the entire geometry with all its details is represented as one subdomain in the network 3.14c) to which 20 discrete flames connect. STORM predicts all modes and their stability for this engine in less than 5 minutes, i.e., more than 2 orders of magnitude faster than the existing 3D AVSP solver.

## 3.6 Modeling and simulation of cold plasma

### 3.6.1 Simulation of plasma flows in Hall effect thrusters conditions

In an increasingly competitive satellite market, electric propulsion has recently regained attention: electric propulsion can reach higher exhaust velocities compared to chemical systems and result in lower propellant mass requirements. Hall thrusters are very competitive electric propulsion devices that are currently in use in a number of telecommunications and government spacecraft.
The physics of Hall thrusters is very intricate and non-linear because of the complex electron transport across the magnetic field and its coupling with the electric field. Even though this type of thruster is known since the 1960s, complex physical phenomena such as erosion or electron anomalous transport are not yet fully understood and directly impact the thruster performance and lifetime. Today, the design and development of Hall thrusters is still semi empirical with long and expensive qualifications in vacuum test facilities: there is no predictive numerical tool capable of simulating real thrusters and helping to design them. With the support of Safran, CERFACS develops such a numerical tool since 2014. This tool, called AVIP, is a massively parallel and unstructured 3D solver for low pressure plasmas. Its objective is to understand the plasma processes occurring in electric thrusters, to improve the efficiency of existing systems and to provide the foundation for breakthroughs in the design of new thrusters.

AVIP proposes two complementary modeling approaches:

- the Lagrangian approach (or Particle- In-Cell (PIC) approach) where different kinds of particles or macroparticles (electrons, ions and neutrals) are individually tracked. These particles can interact with each other (collisions) and with the electromagnetic field that remains defined on a Eulerian mesh.
- the Eulerian approach (or fluid approach) where the particles dynamics is described with macroscopic averaged variables. The set of equations to solve is very similar to the one solved in CFD for two-phase flows.

The development of the PIC solver of AVIP was initiated during the Post-Doc of F. Pechereau (funded by Safran, 2014-2017) and is now continued by W. Villafana (PhD thesis started in 2017, funded by Safran). The PIC approach is expensive (a very large number of particles must be tracked, typically $10^9$ - $10^{10}$) but more accurate: it is often used to perform reference simulations which can then be used to develop and test modeling options for fluid approaches. In 2019, CERFACS participated with 6 international research institutes (Stanford, Princeton, LAPLACE, LPP, etc.) in the development of a reference PIC benchmark for plasma instabilities encountered in Hall thrusters [CFD37]. CERFACS also participated in another benchmark as part of the RTRA project IMPULSE, which involved several Toulouse laboratories (LAPLACE, IMT, ONERA, CNES), with the aim of improving the models and methods used to describe the magnetized plasmas of electric thrusters.
The development of the fluid solver of AVIP started with the PhD of V. Joncquières (2016-2019, funded by Safran). This solver is based on the massively parallel architecture of AVBP but has its own specificities, necessary for the simulation of plasma flows. In particular, new numerical schemes (Riemann HLLC

(Harten-Lax-van Leer-Contact) solver) and dedicated boundary conditions had to be developed [12]. Significant effort was devoted to the resolution of the Poisson equation for the electric potential thanks to the use of the MaPHyS (Massively Parallel Hybrid Solver) library developed by the hiepacs team at INRIA. From a modeling point of view, the main advances concern the development of a 10-moment fluid model [CFD61]. This approach is much more accurate than standard drift-diffusion models classically used to model low-pressure plasma. It can reproduce plasma instabilities (Fig. 3.15), a subject of controversy in the current literature.

In order to move to realistic 3D thruster calculations, the goal is now to implement innovative calculation

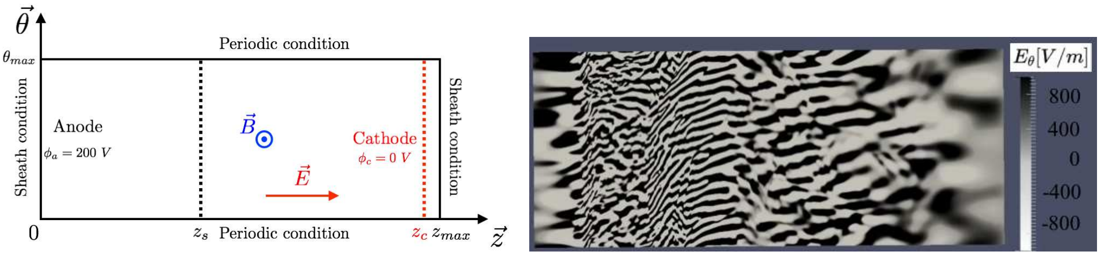


Figure 3.15: Azimuthal instability in a simplified 2D z-$\theta$ configuration of a Hall effect thruster. Left: computational domain and boundary conditions. Right: azimuthal electric field.

strategies to obtain the best ratio between calculation cost and accuracy. These strategies will be studied during the PhD of G. Bogopolsky (2020-2023, funded by Safran): use of similarity laws in order to generate self-similar (but less expensive) systems, use of hybrid methods (PIC method for one particle type, fluid methods for other species) or machine learning for the resolution of the Poisson equation.

For all of this work, AVIP benefits from the expertise of the Plasma Physics Laboratory (LPP Ecole Polytechnique), particularly within the framework of the ANR "Industrial Chair" POSEIDON (2016-2020), coordinated by Dr A. Bourdon and funded by Safran.

### 3.6.2 Ignition by NRP discharges

The reduction of pollutant emissions in aircraft engines and power plants has become a major issue for gas turbine manufacturers as a result of more stringent environmental regulations and increased environmental concern. An efficient solution to reduce pollutant formation is to maintain a relatively low temperature in the combustor primary zone, by decreasing the mixture equivalence ratio. However low flame temperatures induce slower chemical reaction rates, which can lead to flame instabilities and extinctions.

An emerging solution to enable flame stabilization in leaner regimes is to generate electrical discharges at the flame basis. Among these various types of discharges, the Nanosecond Repetitively Pulsed (NRP) discharges have shown to be particularly efficient. Despite this proven efficiency, the fundamental mechanisms of plasma-assisted combustion are not well understood. Moreover the numerical tools needed by engineers to assess the performance of NRP discharge in practical configurations and optimize their design do not exist.

The PhD work of N. Barléon (2018-2021) within the ANR projet PASTEC (2016-2021) addresses these two problems by developing a solver capable of simulating realistic turbulent combustion systems taking into account plasma-flame interactions. Starting from the AVIP plasma solver developed for the simulation of Hall thrusters, new systems of equations (drift-diffusion model), numerical schemes (Scharfetter-Gummel scheme) and functionalities have been developed to take into account the specificities of plasmas generated by NRP discharges. Detailed plasma chemistries are also needed to reproduce the effects of the discharge on combustion. These chemical schemes contain charged species as well as vibratory and electronically excited species in addition to the classical detailed mechanisms describing the combustion of fuel in air. The modeling of the plasma discharge has been first validated on canonical 2D-axisymmetric configurations such as those presented in Bagheri et al. [5] (Fig. 3.16). Then the chemistry of plasma in air was validated by comparison with experiments and detailed simulations [24] using the zero-dimensional plasma kinetics solver ZDPlasKin [17] developed by the LAPLACE laboratory. The next objective is to perform plasma-

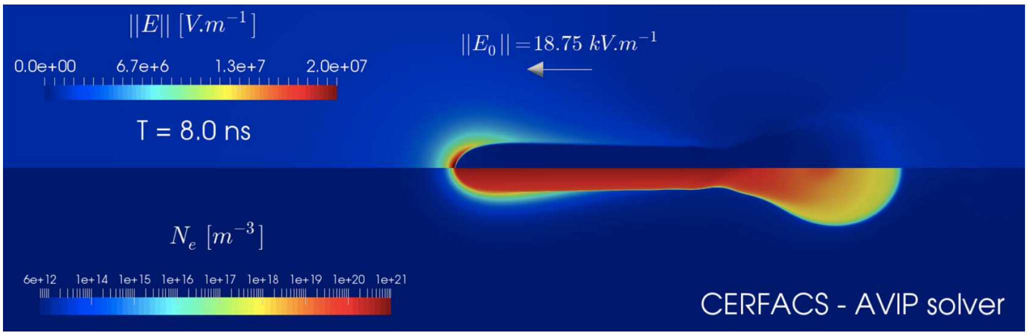


Figure 3.16: Propagation of a positive streamer in dry air between two planar electrodes, from Bagheri et al. [5]. The grounded electrode (electric potential $\Phi = 0$V) is on the left while a potential $\Phi = 18.75$kV is applied on the right. Top: electric field strength; bottom: total number of electrons.

combustion coupled simulations of the MINIPAC test rig experimentally studied at EM2C (Fig. 3.17) with and without assistance from NRP plasma discharges.

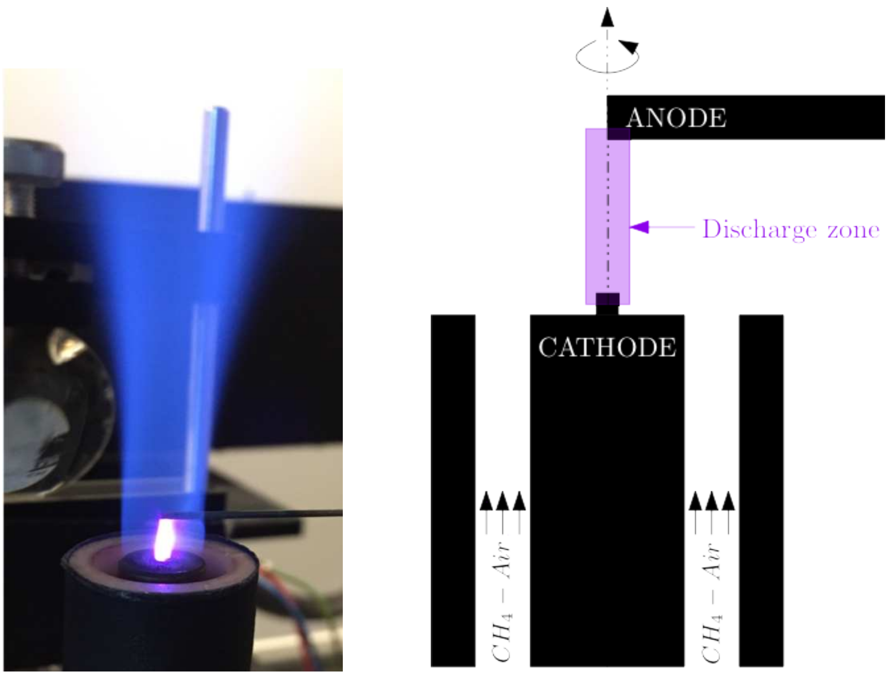


Figure 3.17: NRP discharge in the MINIPAC configuration operated at EM2C.

### 3.6.3 Flame stabilization by NRP discharges

In parallel to the work of N. Barléon in the project PASTEC, the PhD of L. Cheng, which is part of the french-german ANR project GECCO, coordinated by B. Cuenot, is focused on the use of NRP discharges to stabilize swirled flames. Three target configurations are considered, which mostly differ by the fuel state (gas or liquid) and the excitation mode (axial or azimuthal). First results have been obtained with a very simple model for the NRP discharge, describing only the thermal effect of the plasma. They are illustrated in Fig. 3.18(left) and Fig. 3.18(right), clearly showing the impact of the plasma at the flame basis: NRP discharges decrease the flame response in both amplitude and time delay. Next steps are to include a more detailed description of the discharges, based on results obtained with AVIP as described above.

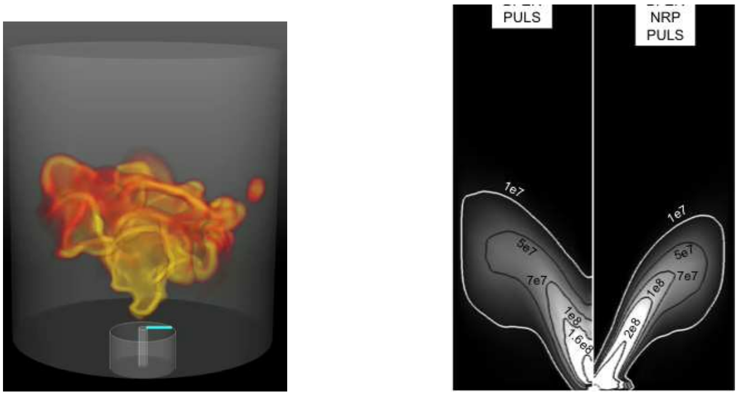


Figure 3.18: The pulsated PACCI burner with NRP discharges. Left : instantaneous view of the flame and the NRP discharge. Right: mean heat release rate without (left half) and with (right half) NRP discharge.

**References**

[5] B. Bagheri, J. Teunissen, U. Ebert, M. M. Becker, S. Chen, O. Ducasse, O. Eichwald, D. Loffhagen, A. Luque, D. Mihailova, J. M. Plewa, J. van Dijk, and M. Yousfi, (2018), Comparison of six simulation codes for positive streamers in air, *Plasma Sources Science and Technology*, **27**, 095002.

[6] M. Celano, S. Silvestri, J. Pauw, N. Perakis, F. Schily, D. Suslov, and O. J. Haidn, (2015), Heat Flux Evaluation Methods for a Single Element Heat-Sink Chamber, In *6th European Conference of Aeronautics and Space Science, Krakow, Poland.*

[7] C. Dapogny, C. Dobrzynski, and P. Frey, (2014), Three-dimensional adaptive domain remeshing, implicit domain meshing, and applications to free and moving boundary problems, *Journal of Computational Physics*, **262**, 358–378.

[8] G. Eckel, J. Grohmann, L. Cantu, N. Slavinskaya, T. Kathrotia, M. Rachner, P. Le Clercq, W. Meier, and M. Aigner, (2019), LES of a swirl-stabilized kerosene spray flame with a multi-component vaporization model and detailed chemistry, *Combustion and Flame*, **207**, 134 – 152.

[9] A. Felden, L. Esclapez, E. Riber, B. Cuenot, and H. Wang, (2018), Including real fuel chemistry in LES of turbulent spray combustion, *Combustion and Flame*, **193**, 397 – 416.

[10] M. Gatti, R. Gaudron, C. Mirat, L. Zimmer, and T. Schuller, (2019), Impact of swirl and bluff-body on the transfer function of premixed flames, *Proceedings of the Combustion Institute*, **37**, 5197 – 5204.

[11] T. Jaravel, E. Riber, B. Cuenot, and P. Pepiot, (2018), Prediction of flame structure and pollutant formation of Sandia flame D using Large Eddy Simulation with direct integration of chemical kinetics, *Combustion and Flame*, **188**, 180–198.

[12] V. Joncquieres, F. Pechereau, A. Alvarez Laguna, A. Bourdon, O. Vermorel, and B. Cuenot, (2018), A 10-moment fluid numerical solver of plasma with sheaths in a Hall Effect Thruster, In *AIAA Joint Propulsion Conference, Cincinnati, USA*, 4905.

[13] D. R. Jones, M. Schonlau, and J. William, (1998), Efficient Global Optimization of Expensive Black-Box Functions, *Journal of Global Optimization*, **13**, 455–492.

[14] T. C. Lieuwen and V. Yang, (2006), *Combustion Instabilities In Gas Turbine Engines*, American Institute of Aeronautics and Astronautics, Reston ,VA.

[15] T. Lovas, P. Amnéus, F. Mauss, and E. Mastorakos, (2002), Comparison of automatic reduction procedures for ignition chemistry, *Proceedings of the Combustion Institute*, **29**, 1387–1393.

[16] M. Mikami, S. Miyamoto, and N. Kojima, (2002), Counter flow diffusion flame with polydisperse sprays, *Proceedings of the Combustion Institute*, **29**, 593–599.

[17] S. Pancheshnyi, B. Eismann, G. Hagelaar, and L. Pitchford, (2008), *Computer code ZDPlasKin, www.zdplaskin.laplace.univ-tlse.fr*.

[18] P. Pepiot, (2008), *Automatic strategies to model transportation fuel surrogates*, PhD thesis, Stanford University.

[19] T. Poinsot and D. Veynante, (2005), *Theoretical and numerical combustion*, RT Edwards, Inc.

[20] K. Prieur, D. Durox, J. Beaunier, T. Schuller, and S. Candel, (2017), Ignition dynamics in an annular combustor for liquid spray and premixed gaseous injection, *Proceedings of the Combustion Institute*, **36**, 3717–3724.

[21] K. Prieur, D. Durox, G. Vignat, T. Schuller, and S. Candel, (2017), Experimental determinations of Flame Describing Functions of swirling spray flames., In *Colloque INCA, 2017*, Châteaufort, France.

[22] C. Pérez Arroyo, J. Dombard, F. Duchaine, L. Gicquel, and Odier, (2021), NUMERICAL INVESTIGATION OF THE INTERACTION BETWEEN GAS-TURBINE ENGINE COMPONENTS WITH DYNAMIC MODE TRACKING, In *Turbomachinery Technical Conference and Exposition*, American Society of Mechanical Engineers.

[23] L. Rayleigh, (1878), The explanation of certain acoustical phenomena, *Roy. Inst. Proc.*, **8**, 536–542.

[24] D. Rusterholtz, D. Lacoste, G. Stancu, D. Pai, and C. Laux, (2013), Ultrafast heating and oxygen dissociation in atmospheric pressure air by nanosecond repetitively pulsed discharges, *Journal of Physics D Applied Physics*, **46**, 4010–.

[25] M. Safari, M. R. H. Sheikhi, M. Janbozorgi, and H. Metghalchi, (2010), Entropy transport equation in large eddy simulation for exergy analysis of turbulent combustion systems, *Entropy*, **12**, 434–444.

[26] G. Singla, P. Scouflaire, C. Rolon, and S. Candel, (2005), Transcritical oxygen/transcritical or supercritical methane combustion, *Proceedings of the Combustion Institute*, **30 II**, 2921–2928.

[27] G. Soave, (1972), Equilibrium constants from a modified Redlich-Kwong equation of state, *Chemical Engineering Science*, **27**, 1197–1203.

[28] T. Turányi, K. Hughes, M. Pilling, and A. Tomlin, (2009), KINALC website, *http://respecth.hu/*.

[29] O. Vermorel, P. Quillatre, and T. Poinsot, (2017), LES of explosions in venting chamber: A test case for premixed turbulent combustion models, *Combustion and Flame*, **183**, 207 – 223.

[30] L.-Y. Wang, C. K. Bauer, and Ö. L. Gülder, (2019), Soot and flow field in turbulent swirl-stabilized spray flames of Jet A-1 in a model combustor, *Proceedings of the Combustion Institute*, **37**, 5437 – 5444.

[31] M. Zhu, (2015), *Large Eddy Simulation of thermal cracking in petroleum industry*, PhD thesis, Université de Toulouse - Ecole doctorale MEGeP Dynamique des Fluides.

# Applications

## 4.1 Introduction

Applications of CERFACS tools to real combustors and turbomachinery components is a primary driver of CERFACS' CFD activity and past successes. Thanks to the link with CERFACS' partners as well as to external collaborations, many applications of industrial interests have been dealt with in the 2018-2020 years. Among others, the following fields of applications were:

- Space related applications,
- Aeronautical engines,
- Turbomachinery
- Novel propulsion concepts,
- Safety,
- Large-size systems,
- Chemical processes.

## 4.2 Space propulsion

Cryogenic rocket engines are complex systems in which extremely powerful and fast phenomena occur. Their design must guarantee full operability and reliability, as any even small failure of a sub-system leads to the failure of the launcher mission. The particular operating conditions, in particular the very high chamber pressure, up to 100 bars, and the void environment during flight, make experimental testing difficult and incomplete. In addition the sector of spatial launchers has become very competitive and the question of cost (development and manufacturing) has become a major driver. In this context numerical simulation is essential, and Cerfacs has developed a specific expertise in this area. In the past 2 years, efforts have been put on the combustion chamber, the nozzle and the turbopomps.

### 4.2.1 Subcritical methane-oxygen combustion

Although still controversial, the concept of reusability to reduce spatial launcher costs is at the heart of many development programs. Another important source of cost reduction is the use of methane instead of hydrogen. Methane is interesting for its higher density, good specific impulse and lower cost for production and storage, which compensate a lower energy density. In addition methane-oxygen combustion leads to lower peak temperatures compared to hydrogen-oxygen combustion, decreasing the thermal fatigue and therefore favoring reusability.
Using methane instead of hydrogen requires to revisit the design of combustion chambers, as this impacts the flame structure and stabilization, ignition, or wall heat transfer. The PhD of Simon Blanchard, supported by CNES and ArianeGroup, is devoted to the simulation of methane-oxygen combustion in rocket engine

conditions. One major development is the introduction of finite rate chemistry to account for the non infinitely fast oxidation of methane. A reduced chemical mechanism has been developed, which contains 136 reactions and 14 species, plus 4 species in quasi-steady state (QSS). The reduced scheme allows to reproduce all flame characteristics at a reasonable computing cost (Fig. 4.1). This chemical scheme is now used in 3D LES of combustion chambers to predict wall heat fluxes.

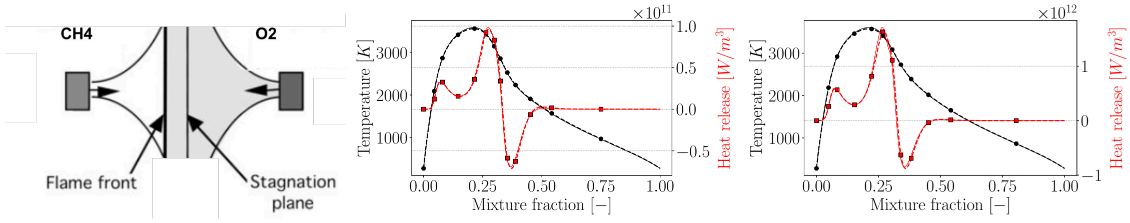


Figure 4.1: 1D profile of strained CH4/O2 diffusion flame: evolution with mixture fraction of the temperature (black) and the heat release rate (red). Thick lines: Ramec scheme. Dashed lines with markers: reduced scheme. Left: P = 49bar, strain rate = 100/s. Right: P = 59bar, strain rate = 1500/s.

### 4.2.2 Rocket Nozzles

One limiting feature that prevails from producing relevant and fast solutions is nozzle jet flow separation. This aerodynamic phenomenon occurs in the critical phases of ignition and extinction of rocket engines. It is characterized by the propagation of a non-axisymmetric separation line along the wall of the nozzle divergent which induces significant side-loads to the structure. This problem has a significant impact on the design of existing and future rocket engine nozzles.

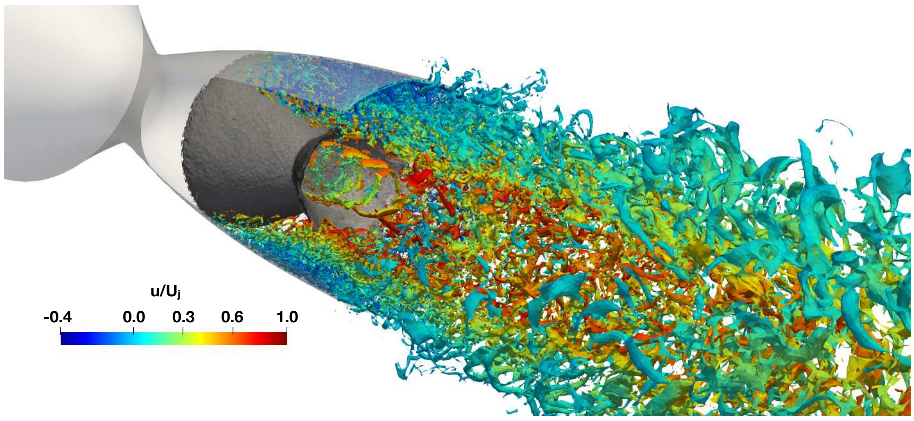


Figure 4.2: Instantaneous flow field in a Truncated Ideal Contour nozzle characterized by a Free-Shock Separation regime: iso-surface of the Q criteria $0.5(U/D)2 = 0.13$. The main shock pattern is isolated using an iso-surface of the dilatation field $\nabla u = -30D/U$ inside the nozzle [CFD42].

CERFACS uses LES in AVBP and automatic mesh refinement with ArianeGroup and CNES to understand the physical origins of side loads as well the transition between the Free Shock Separation (FSS) and the Restricted Shock Separation (RSS) regimes. In both regimes, side-loads occur due to the strong three-dimensionality and unsteadiness of the flow separation generated by the main shock pattern oscillations inside the nozzle (Fig. 4.2) [CFD42]. This work continues with a PRACE allocation project award

(2020225439) in the 21st PRACE-call, with the *STRIKE* project (Shock Transition Regime In rocKet Engine).

### 4.2.3 Turbopumps

Turbo-pumps feeding the combustion chamber are also a crucial element of liquid propulsion, investigated in the PhD M. Queguineur as a follow-up of the PhD by T. Bridel-Bertomeu both funded by CNES and ArianeGroup.

In a turbo-pump, the flow stability must be ensured in the cavities between the fixed and rotating parts, to avoid large flow variations leading to miss-tuned operating conditions in the engine and a drastic loss of performance or life-span. The primary objective of M. Queguineur's research work was to apply LES and advanced diagnostics to academic and real configurations. As a complement to these azimuthal unsteady predictions, new tools were developed to study the linear stability of these enclosed rotor-stator (RS) configurations [CFD137, CFD85, CFD84, CFD86]. It appeared that the unsteady pressure signals stem from the instability of the stator boundary layer in which coherent patterns rotate at exactly the frequencies of the pressure signals, Fig. 4.3(b).

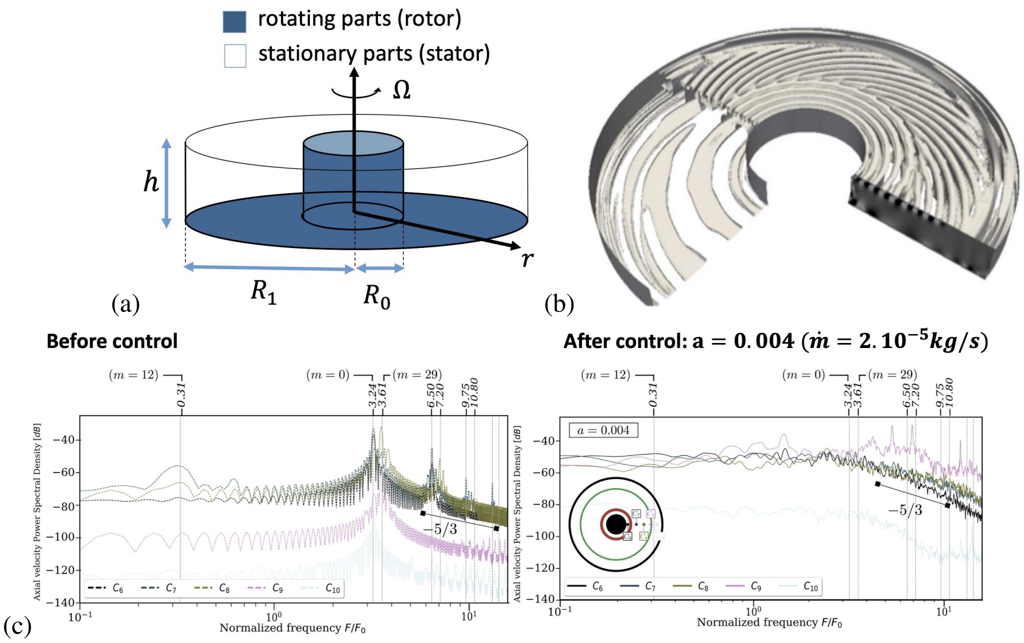


Figure 4.3: Rotor / stator cavity flow simulations: (a) geometrical view of the domain simulated by LES and (b) an axial velocity fluctuation field at a given instant of the LES. Following this LES prediction, a GLSA analysis yielded a control strategy based on the introduction of a weak aspiration / blowing on the stator: (c) presents the reported Fourier spectra obtained in the LES without (left which corresponds to views (a) & (b)) and with (right) control.

LES results were also used in conjunction with a Global Linear Stability Analysis (GLSA) to establish a predictive strategy for academic Rotor-Stator (RS) cavity flows, given the underlying mean flow field: a $2D$ axi-symmetric Linearized Navier-Stokes Equations solver applicable to simple as well as complex geometries showed to be a powerful analysis tool. The unstable modes were retrieved *a posteriori* by

GLSA and successfully controlled Fig. 4.3(c) observed in LES [CFD85]). This development was also the occasion to develop an 'on-the-fly' mode extraction and control method now available in AVBP [CFD86]. This last tool allows to conclude that for the simple RS-cavity only one out of the many observed modes needs to be control to avoid dangerous activity.

## 4.3 Aeronautical engines

Aeronautical engine applications appeared very early on in the context of the CFD team. As a continuation of previous efforts and demonstrations, recent applications focused on new issues related to the development of the next generation of aeronautical and power generation engines. These relate to engine efficiency, reliability and pollutant emissions. Those issues require to deal with multiphase turbulent reacting flow predictions as well as fully transient processes as encountered in an ignition sequence. Likewise, turbomachinery applications necessitate in-depth analyses of flow mechanisms induced by aerodynamic losses, heat transfer and mixing of hot spots. Finally, component interactions:*i.e.* combustor/turbine, compressor/combustor and full engine scale are subject of interest for which CERFACS' CFD Tean has very early on invested efforts. In that respect, year 2020 is a clear milestone for the community which has seen the generation of a LES prediction of a full engine.

### 4.3.1 Two phase flow simulations

Multiple combustor computations can be performed on the basis of the fundamental developments of Sections 3.3 and 3.4 to evaluate the multi-phase flow reacting LES solver in AVBP. Most applications use the Euler-Lagrange formalism coupled to complex chemistry and the DTFLES turbulent combustion model. Apart from confidential demonstrations with SAFRAN, two swirled turbulent spray combustors operating with real fuels and equipped with many experimental diagnostics have allowed significant progress.
First within the PhD of B. Rochette [CFD138], the HERON (High pressure facility for aero-engine combustion) test-rig measured at CORIA [32] has been studied. It is an optically accessible kerosene/air combustor to study lean combustion concepts under elevated pressure and temperature conditions. HERON is equipped with an industrial multipoint fuel injector. The various flame shapes observed experimentally varying either pressure or mean equivalence ratio make HERON a challenging configuration for simulations. LES coupled to Lagrangian approach for the fuel droplets have shown the importance of submodels used for ignition and flame sensor to correctly reproduce the flame shape.
Second in the PhD of J. Wirtz supported by the H2020 JETSCREEN project, the effect of alternative fuels burning in the Swirl-Stabilized Combustion Chamber (SSB) equipped with a prefilming airblast atomizer and measured at DLR [8] has been studied. Among the fuels experimentally tested, three fuels have been selected for simulations: the reference Jet-A1 (A1) and two alternative fuels, an Alcohol-To-Jet fuel (B1) and a high aromatic fuel (C1). As a complement to these pure fuel predcitions of the HERON burner, three-components surrogates proposed by POLIMI have been derived using the ARCANE reduction code considering the adopted multicomponent formulation for combustion and evaporation as implemented by V. Shastry [CFD92], Fig. 4.4. Comparisons with measurements are currently investigated for the three fuels. These two examples on the HERON and SSB burners show the capacity of the models implemented in AVBP to tackle real fuels, real injection systems in quasi real pressure and temperature conditions.
Another critical phase in gas turbines is ignition. To better understand spray ignition, the light-round in the two-phase annular MICCA-Spray combustion chamber of EM2C [20] has been simulated in the PhD of F. Collin [CFD126] using LES with a Lagrangian formalism for the description of the spray in order to take into account the droplet size distribution. The spray modeling approach has been first validated on a single injector configuration. An ignition sequence in the annular combustor has then been computed and compared to experimental data, Fig. 4.5. Results are in good agreement, and the individual burner

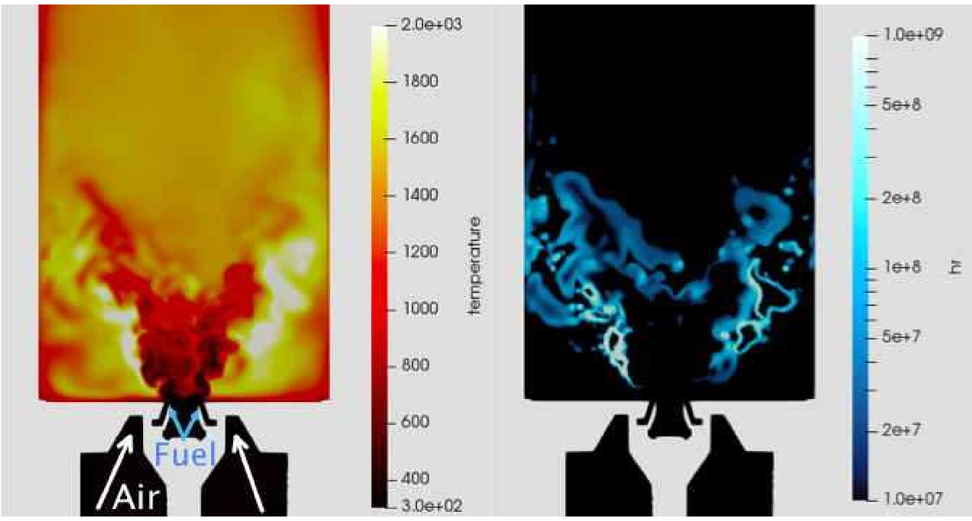


Figure 4.4: SSB configuration (DLR). Instantaneous fields of temperature (Left) and heat release (Right) for A1 fuel.

ignition timings are predicted with high accuracy. Results highlight the burnt gas expansion effect and the propagating flame dynamics during ignition. The interaction of the polydisperse spray with the igniting flame and induced flow leads to local mixture heterogeneities which alter the flame behavior. However due to important pre-evaporation, the presence of droplets does not significantly impact the overall ignition process, which exhibits the same driving mechanisms as in purely gaseous flows.

### 4.3.2 Pollutant emissions

Predictions of soot formation through simulations have been mainly limited to academic configurations burning light gaseous fuel such as ethylene. However practical combustion devices burn liquid fuels. Extending soot models to liquid fuels is a difficult task because of the complex modelling and the computational cost for the flame chemistry including soot precursors (PAHs) on one hand and the transport of fuel droplets and soot particles on the other hand. In the framework of the H2020 SOPRANO project (2016-2021), the PhD of L. Gallen [CFD130] appears as a pioneering work for soot modeling in a real-like combustor operating with real fuel which offers flame and soot measurements for validations. The test-rig is the sooting swirled turbulent spray Jet-A1/air combustor measured at UTIAS [30].

In this work, the Hybrid Chemistry (HyChem) model to model for real fuel pyrolysis is combined to ARC for oxydation of the light hydrocarbons as proposed in [9] to allow a direct integration of detailed chemistry including PAH description within AVBP. The HyChem-ARC model is coupled with a Lagrangian approach for the spray and the Lagrangian Soot Tracking model with a detailed soot chemistry described in Section 3.3.2. The comparison of the LES results with the available measurements leads to very encouraging predictions for both flow dynamics and soot predictions (Fig. 4.6) and provides valuable insights on the interaction between fuel droplets, turbulent flame, PAH and soot formation (Fig. 4.7).

This methodology is currently applied in real engines by SAFRAN-HE, SAFRAN-AE and SAFRAN-TECH engineers, as planned in the H2020 SOPRANO project.

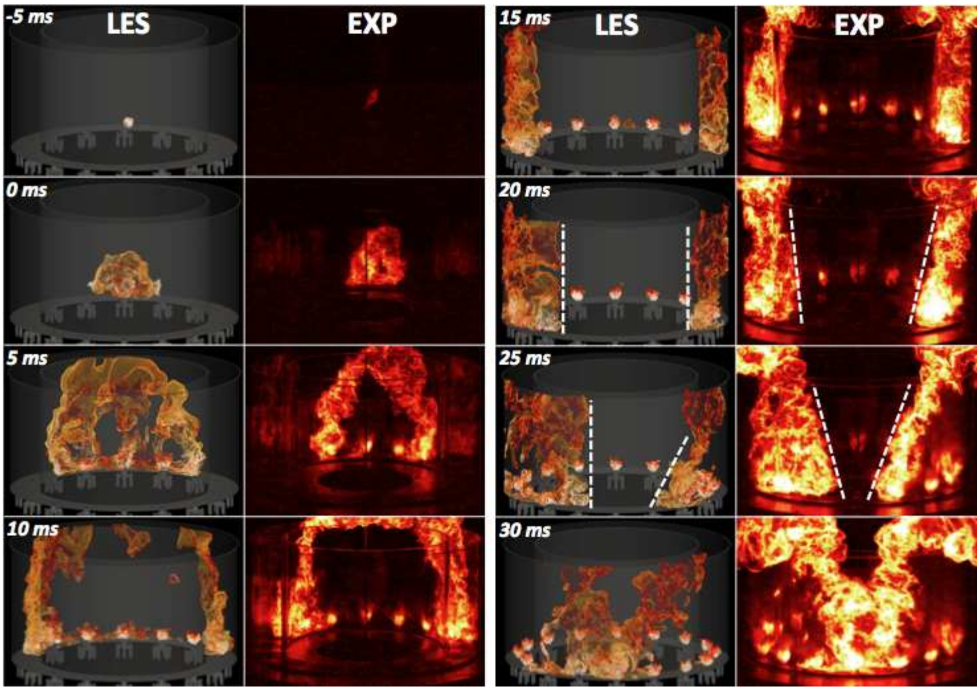


Figure 4.5: MICCA-Spray configuration. Comparison of flame evolution during the light-round between LES (left column) and measurements (right column) at different instants [CFD126].

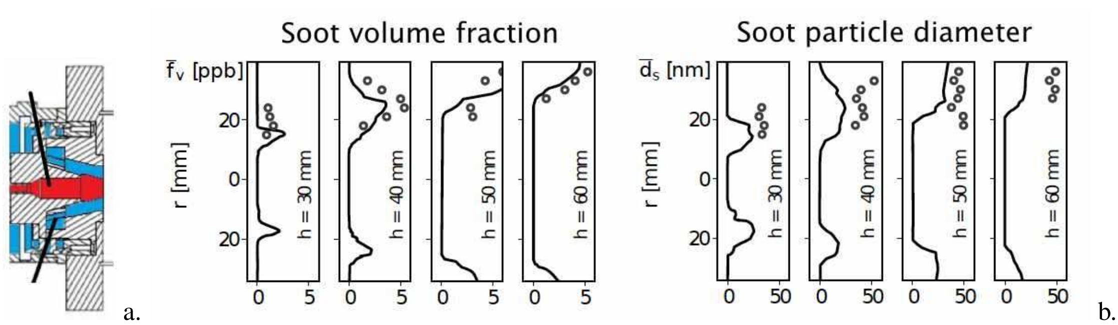


Figure 4.6: UTIAS configuration. a. Injection system. b. Comparison between measurements (symbols) and LES (solid lines) of radial profiles of soot volume fraction (Left) and soot particle diameter (Right) at several positions in the combustion chamber.

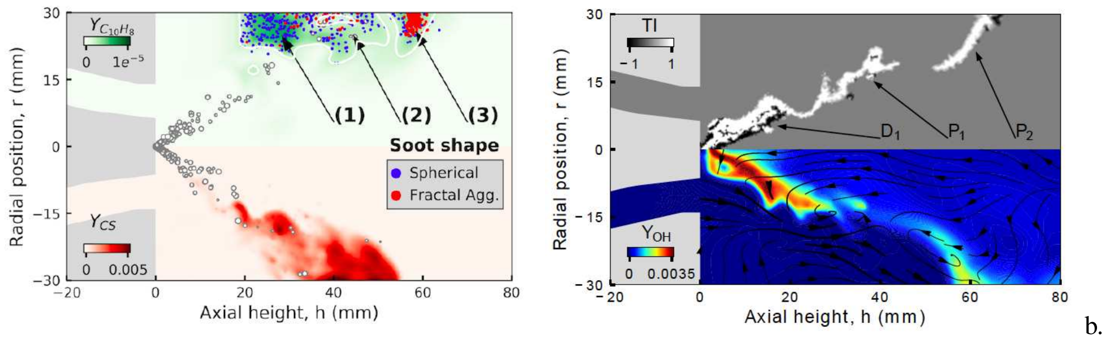


Figure 4.7: UTIAS configuration. a. Instantaneous flame structure (Top: Takeno Index, Bottom: OH mass fraction). b. Instantaneous fields of PAH (Top) and pyrolysis products (Bottom).

### 4.3.3 Turbomachinery

#### 4.3.3.1 Loss evaluation in cascade and stage cooled turbine

Losses in turbomachinery LES of cooled turbine configurations have been investigated through the PhD work of Mael Harnieh. Film cooling effectiveness was assessed in a wall resolved simulation of the highly loaded T120D turbine blade [CFD17]. This turbine blade depicts a recirculation bubble at the intrado, known to be numerically challenging to predict. The pressure load issued by the proposed wall-resolved LES provides accurate results for aerodynamics, and the adiabatic film effectiveness prediction is also found to compare well with experimental results. Losses have been then analyzed using the Second Law Analysis (SLA, [25]). Both aerodynamic and thermal losses are associated to entropy generation, and are investigated along the vane passage. Aerodynamic losses are generated in the highly sheared flow region while thermal mixing losses are produced in the mixing region between the hot and coolant flows, (Fig. 4.8). Integration of the respective loss maps shows that the film has a great impact on the overall loss generation. Such losses analyses have been also carried out on a wall-modeled configuration of the FACTOR project [CFD18], where cooling holes are meshed. LES reproduces the spatial distribution of the adiabatic film effectiveness and can be used to investigate the loss generation. This is achieved using two methodologies, first considering balance of total pressure in the vanes wakes, then using Second Law Analysis (SLA). Balance of total pressure without the contribution of thermal effects only highlights the losses generated by the wakes and secondary flows. To overcome this limitation, SLA is adopted by investigating loss maps. Thanks to this approach, mixing losses are shown to dominate in the coolant film while aerodynamic losses dominate in the coolant pipe region.
Finally, in order to alleviate the computational cost induced by the hole-meshed approach, a cooling model initially developed for combustion chamber context is applied to the Factor Nozzle Guide Vane configuration [CFD59]. The resulting hole-modeled results are compared to hole-meshed results, and confirm the capability of such a model to predict the adiabatic film effectiveness.

#### 4.3.3.2 Full engine computations and integration effet (ATOM project)

Gas turbines are traditionally designed following individual pathways for each component (e.g. compressor, combustor, turbine) by different departments in the same company. Analysis and mechanical tests are performed component by component. The components are then assembled and the resulting engine is tested experimentally. One major practical problem encountered by gas turbine manufacturers is that the individual behaviour of the components may differ from their assembled behaviour in the complete engine showing an overall poorer performance. Simulations performed using Reynolds-Average Navier-

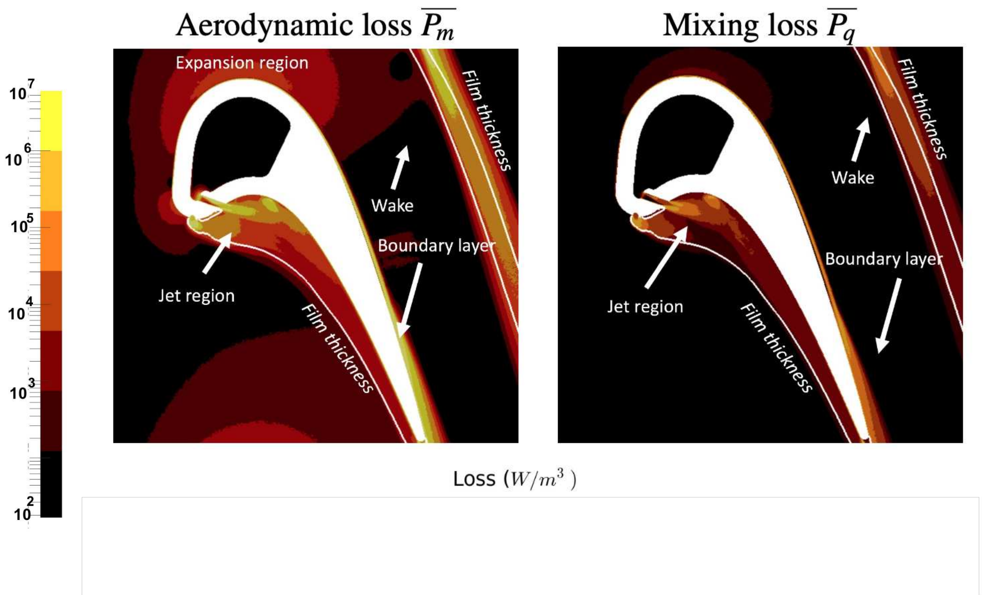


Figure 4.8: Losses generation along the T120D configuration.

Stokes (RANS) have been the main choice for industry, especially for design points of single components. Nowadays, due to the increase and accessibility to computing power, higher-fidelity methods such as URANS and LES are replacing RANS progressively. They are however mainly restricted to single components (fan, compressor, combustor, turbine, etc.). These simulations are often independent from each other: boundary conditions are usually defined either by imposing average quantities, one-dimensional profiles or steady two-dimensional contours on the inlet and outlet boundaries.

CERFACS used a PRACE allocation with 31.6 million core hours to investigate by means of a single integrated reactive LES the numerical and physical interactions of the different components of the gas-turbine demonstrator DGEN-380 (Akira Technologies), at take-off conditions. The domain illustrated in Fig. 4.9 includes the 360 azimuthal degrees of the fan, the radial compressor and the combustion chamber with over 2.1 billion mesh cells. In order to generate this mesh, new procedures have been adapted to AVBP. The integrated simulation was compared to the theoretical thermodynamic cycle giving results within 2% difference. In addition, this simulation was validated against LES of the single components with less than 1% difference. At take-off conditions, the compressor works in transonic conditions generating a shock anchored on the leading edge of the impeller. This shock propagates upstream and interacts with the boundary layer generation and modifies the wake of the fan. In the aft region of the engine, the pressure perturbations of the impeller propagate inside the combustion chamber as in [CFD25] and reach the exit of the combustion chamber. Moreover, several azimuthal acoustic modes developed in the compressor are established inside the combustion chamber at the compressor Blade Passing Frequency (BPF).

This work led to two submitted papers [CFD82, CFD83] and two proceedings [CFD25, 22]. Research of the DGEN-380 demonstrator benefited from funding or developments from projects ATOM (DGAC/SafranTech No. 2018-39), EXCELLERAT (H2020 No. 823691) and EPEEC (H2020 No. 801051). This work was granted access to the HPC resources of GENCI/TGCC (Joliot-Curie supercomputer) on the PRACE allocation project FULLEST (Project No. RA5191).

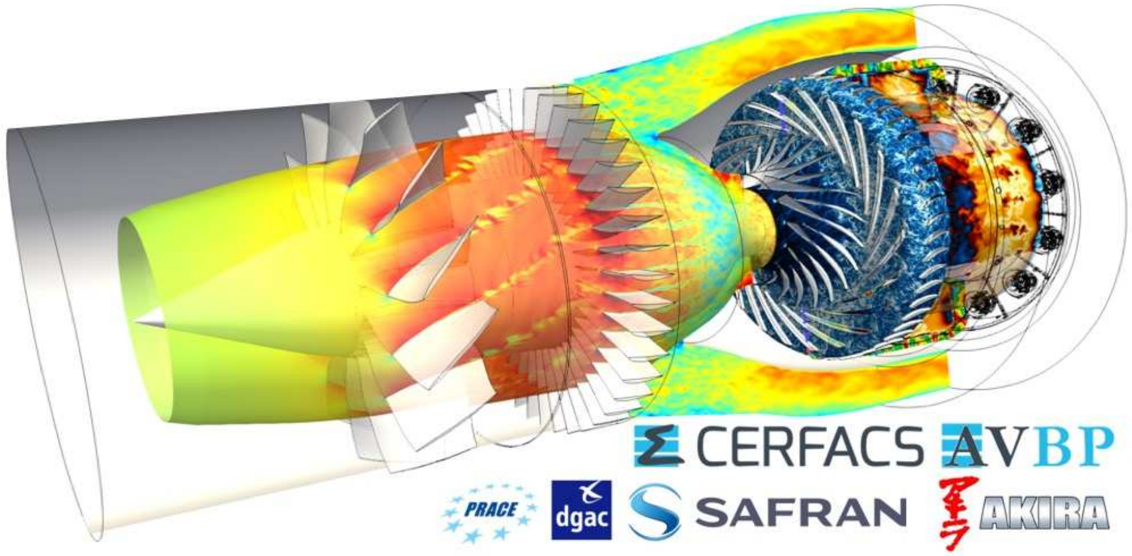


Figure 4.9: Instantaneous contours of DGEN-380 LES depicting Mach number in the forward region, density gradients in the compressor, pressure fluctuations in the casing and temperature in the combustion chamber.

### 4.3.4 Novel propulsion concepts

Ignition plays a major role in combustion science and the determination of the Minimum Ignition Energy (MIE) is a crucial element in many engines. The Phd of Paul Pouech focuses on the numerical evaluation of the influence of high-speed flows on the ignition of a premixed methane/air mixture in the context of Constant Volume Combustion systems. To analyze the dependency of MIE on the flow speed and the value of this speed beyond which ignition can not be achieved anymore for a given spark plug device the MIE is first evaluated for quiescent and constant speed flows. Following this observation, ignition by a spark placed in the recirculation zone of a backward facing step is studied to perform ignition in these high-speed turbulent flows. Various flow speeds $U_b$ are computed and for each of them Direct Numerical Simulation (DNS) is used to measure the MIE and analyze the ignition sequences (Fig. 4.10).

DNS show that a flame kernel is first created in the low-speed recirculation zone for all flow speeds. However, the subsequent flame propagation away from the recirculation zone depends on the flow speed: while low-speed cases produce a global ignition of the flow, ignition in high speed cases can lead to flame quenching when the reacting fronts try to leave the recirculation zone and enter the high speed flow region, leading to global ignition failure. DNS confirm that placing a spark behind a backward facing step allows to ignite flows at speeds which would otherwise be unreachable (Fig. 4.11).

Following common scaling arguments provided by the literature for flame stabilization over obstacles, a simple Damkohler number is built and shown to control the success of ignition. DNS also allows to investigate mechanisms controlling the success or failure of the ignition sequence and shows that heat losses to the combustor wall play a limited role on ignition while flame stretch on the flame elements leaving the recirculation zone have a major influence.

The strategy of including a step, which is commonly used in the field of supersonic combustors since a long time, is currently studied in a Constant Volume Combustor experienced at the Pprime Laboratory.

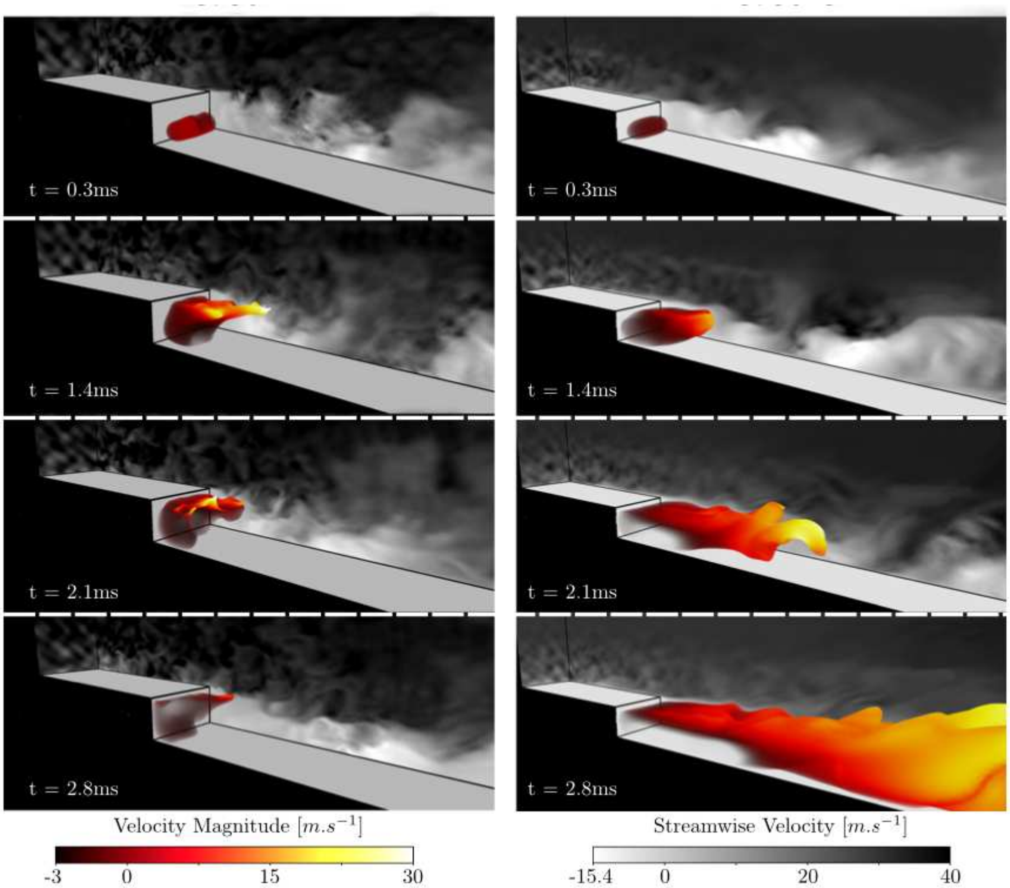


Figure 4.10: Visualisation of successful (right) and failed (left) ignition sequences at 4 different times. Isosurface of heat release coloured by velocity magnitude. The domain is colored by the streamwise velocity.

## 4.4 Large-size systems

Large-size combustion systems refer to industrial furnaces, torches and flares encountered in many industrial sectors, to produce petrochemicals, cement, glass, etc. Because of their large size, they have been out of reach of LES until recently, thanks to both the increase of computer power and the efficiency of numerical techniques.

In the framework of the European project IMPROOF (improof.cerfacs.fr), the PhD of S. Nadakkal was devoted to the study of a steam-cracking furnace [CFD22]. For the first time, the turbulent flame in a 15 meters high enclosure was computed with LES. One major difficulty was to describe in the same simulation the extremely small, but essential details of the burner, typically of a size of 0.1mm. Such scale disparities impose severe numerical restrictions if time accurate, unsteady solution is sought. The LES of the furnace, with detailed description of the burner, was made possible thanks to a set of modelling and specific techniques (Fig. 4.12):

- a reduced chemistry mechanism for methane combustion with air, with or without CO2 dilution, including NOx production,

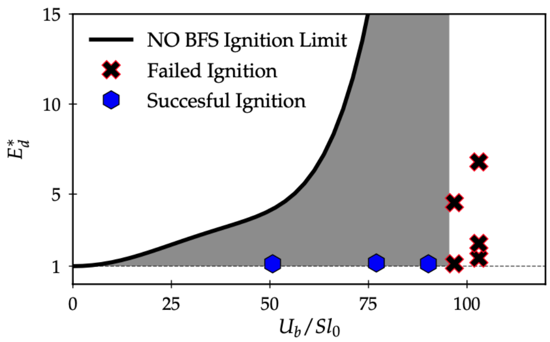


Figure 4.11: Ignition map for the backward facing step ignition sequences. The MIE is scaled by its value in a stagnant flow MIE(0) and plotted versus $U_b/s_L$. It is compared to the MIE measured in a constant speed flow. In the shaded zone, ignition is possible in the BFS configuration while it would be impossible in the free stream case.

- a multi-domain approach to allow for local time stepping with optimized parallel load balancing,
- the coupling with thermal radiation, as this heat transfer becomes dominant in large systems.

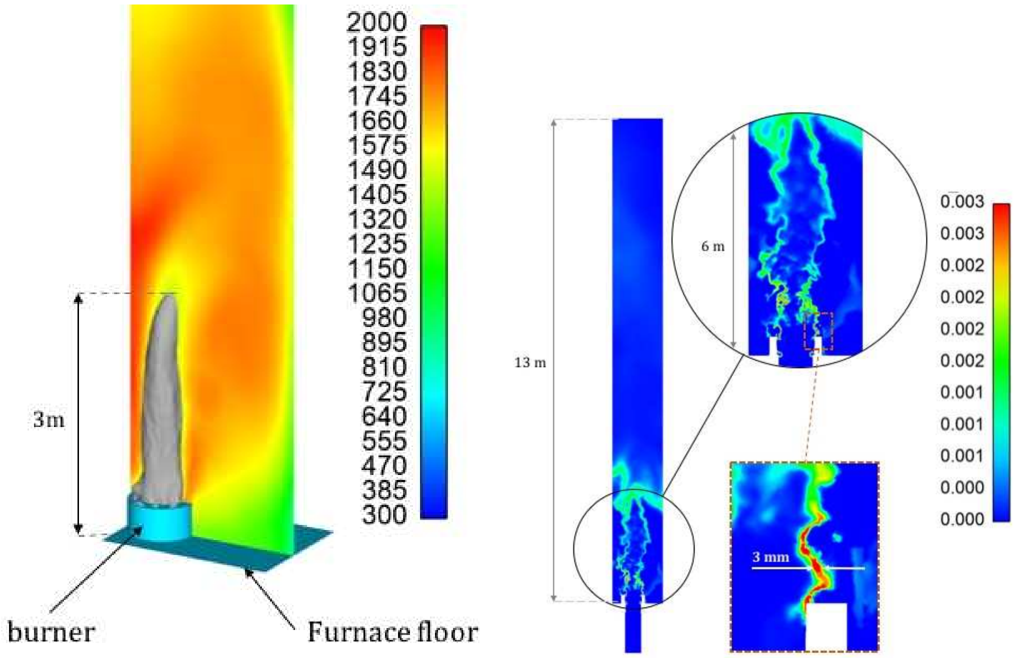


Figure 4.12: LES of a steam-cracking furnace. Left: Mean temperature isosurface showing the flame, and mean temperature field on the vertical plane passing through burner center. Right: details close to the burner of the OH mass fraction on a vertical plane passing through the center of the burner.

The numerical and modelling strategy allowed to compute the whole flame and hot gas plume, while capturing small details close to the burner. Such simulation was never performed before, and allowed to understand how the flame attaches to the burner.

## 4.5 Safety

The consequences of gas explosions can be devastating, causing numerous fatalities and the destruction of large parts of industrial facilities. In the explosion of a gas cloud, the main concern is the pressure rise, leading to the so-called overpressure peak, which controls the severity of the explosion. Predicting the overpressure generated during an explosion represents a complex problem of turbulent combustion to be solved due to the numerous physical phenomena involved: dispersion and mixing, ignition, interaction between flame and turbulence, between flame and shocks, flame acceleration and possibly transition to detonation. LES has already shown interesting predictive capacities but for relatively simple geometric configurations of small dimensions [29]. The aim of the LEFEX project (LEs For EXplosions) started in 2019 for a period of 5 years is to address the issue of scaling up explosion simulations with Total, Air Liquide and GRTgaz.
The first LEFEX topic concerns mesh aspects and is the subject of S. Sengupta's PhD. An automatic adaptive mesh refinement method using the MMG library developed by INRIA [7] was implemented in AVBP to optimize meshes. Thanks to a system of physics-based metrics, the mesh can be dynamically refined in places where physics requires it (presence of a flame front, shock, ...) and coarsened in regions where this is not necessary.
A second direction of work focuses on the modeling of premixed turbulent combustion: in realistic explosion configurations, the quality of the numerical predictions relies largely on the turbulent combustion model since an important part of the flame and its interaction with the turbulence occurs at the sub-grid scale. Several approaches are thus currently studied and developed within the framework of V. Xing's PhD, in particular a PDF approach coupled with a machine learning approach for the prediction of the sub-grid wrinkling [CFD64]. Two new PhDs will also start in 2021 as part of this LEFEX project: PhD of J.J. Hok on the modeling of chemistry-flow interactions (with a focus on $H_2$ combustion) and PhD of B. Vanbersel on the development of new physical sensors for AMR methods.

CERFACS continues to work on transition to detonation phenomena (F. Pacaud, research engineer) [CFD46, CFD60] (Fig. 4.13), as well as on the chemical inhibition of hydrogen-air explosions as part of the post-doctoral work by O. Dounia for Total [CFD45]. A new field of application also appeared in 2020: safety related to electrical storage. Technologies based on lithium-ion batteries are very attractive and popular due to their high power to weight ratio, but they can be prone to critical incidents such as thermal runaway which can cause fire or explosion. The objective of the PhD of A. Cellier (2020-2023, funded by SAFT) is to use LES to simulate and understand the complex and transient phenomena occurring during such an incident. Since thermal Runaway is also a multi-physics phenomenon involving fluid dynamics, chemistry, combustion, radiation and thermal conduction, coupling strategies will have to be developed with AVTP (heat conduction solver) and PRISSMA (radiation solver).

2020 will also see the finalization of the work of the Groupe de Travail Explosion, led by INERIS, in which CERFACS has participated since 2015. Thanks to this collaboration between industrial and research partners (Total, EDF, GRTgaz, Air Liquide, CEA, IRSN, . . . ), various CFD solvers (including AVBP) have been compared on numerous test cases to establish guidelines and recommendations for the use of CFD in the field of safety.

## 4.6 Chemical processes

Thermal steam cracking is an industrial process which transforms heavy, less valuable fractions of crude oil into lighter and commercially more important products such as olefins. A critical factor to steam cracking is heat transfer, as the chemical conversion is most efficient in narrow temperature ranges. Artificially increasing the roughness of the inner surface of the reactor or modifying the reactor geometry are passive

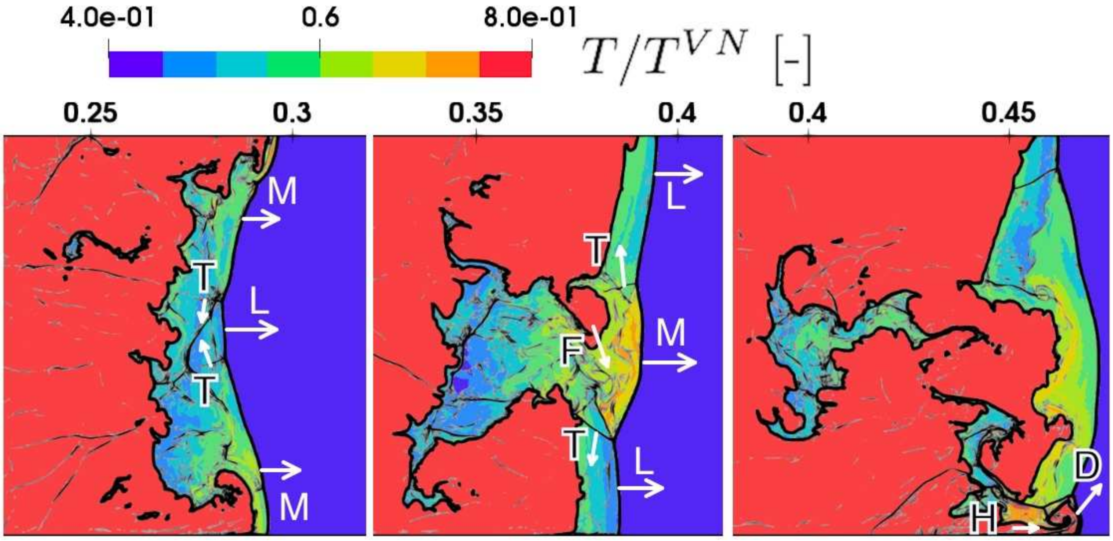


Figure 4.13: Detonation initiation in a shock tube with obstacles: temperature field with superimposed Schlieren. L: leading shock, T: transverse shock, M: Mach stem, F: flame finger, H: hotspot, D: detonation. Temperature is scaled by the von Neumann temperature $T^{VN}$ [CFD60].

and potentially efficient methods for heat transfer enhancement, which is why ribbed reactors or swirl flow tubes are now used for cracking applications. However, this method induces an increase in pressure loss and potentially coking formation, which is detrimental to the chemical selectivity of olefins. The evaluation of the overall impact of surface roughness or reactor geometry on the process is difficult due to expensive measurements, and numerical simulation appears as an attractive tool to optimize the reactor design as demonstrated in the framework of the PhD of R. Campet [CFD124] and the post doctoral work of M. Zhu within the H2020 IMPROOF project (www.improof.cerfacs.fr, 2016-2020).

Numerical simulations of steam cracking process are challenging because of the size of the reactors, the complex aerothermal flow and the cracking chemistry stiffness: a specific methodology was developed in AVBP within the PhD of M. Zhu [31] to allow accurate LES of such reacting flows within a reasonable computational time. This strategy uses a periodic configuration of one periodic pattern. The correct aerothermal flow and the thermochemistry are imposed by source terms added to the conservation equations. A detailed validation of the non-reacting aerothermal flow has been conducted in a ribbed tube configuration by comparison with detailed experiments performed at Von Karman Institute [CFD36], showing the accuracy of the methodology.

For practical applications, simulations including chemical mechanisms for both butane and propane cracking were performed inside several reactor geometries (smooth, ribbed, swirled and corrugated) provided by industrial partners. The first objective was to investigate the impact of the reactor geometry on olefin selectivity. The methodology proposed for aerothermal flows in such configurations was coupled to Analytically Reduced chemistries for cracking chemistry. Those were derived from detailed chemistries from the litterature using the ARCANE code. The second objective was to optimize the reactors geometry. To limit the number of LES, an optimization procedure based on a surrogate model constructed from Gaussian Process Regression and adaptive resampling with the Efficient Global Optimization [13] method was proposed [CFD35]. The optimization consists in the maximization of a cost function which aims at maximizing the heat transfer efficiency for similar pumping power. As an example for a ribbed reactor, only 34 simulations were necessary to find the optimal geometry varying 4 parameters, a discontinuous ribbed geometry (Fig. 4.14).

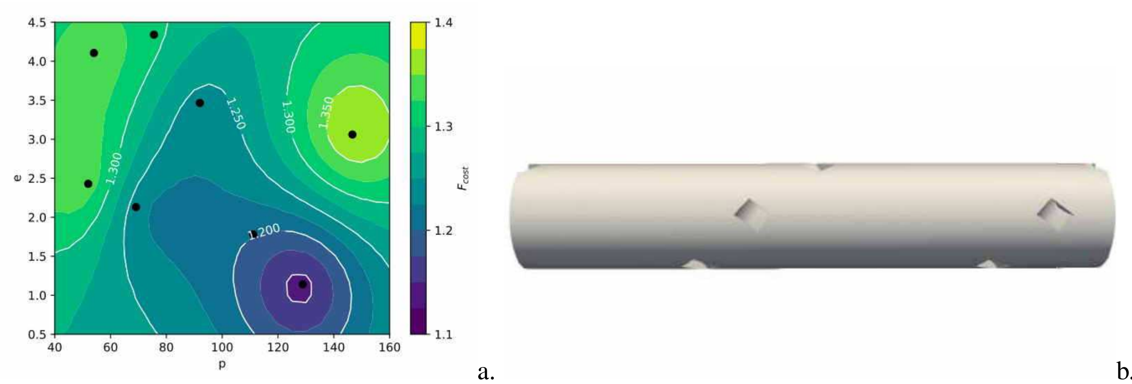


a. b.

Figure 4.14: Optimisation of petro-chemical processes. a. Example of response surface for a continous rib in a ribbed reactor constructed with the Gaussian Process Regression. b. Optimised ribbed tube geometry.

## References

[32] P. Domingo-Alvarez, P. Benard, G. Lartigue, V. Moureau, and F. Grisch, (2019), Impact of Spray Droplet Distribution on the Performances of a Kerosene Lean/Premixed Injector, *Flow, Turbulence and Combustion*.

# Publications

## 5.1 Books

[CFD1] E. Riber, B. Cuenot, and T. Poinsot, (2019), *Computer Aided Chemical Engineering*, vol. 45, Elsevier, editors:tiziano faravelli, flavio manenti, eliseo ranzi ed.

## 5.2 Conferences Proceedings

[CFD2] S. Agarwal, L. Gicquel, F. Duchaine, N. Odier, and J. Dombard, (2020), Analysis of the unsteady flow field inside a fan-shaped cooling Hole predicted by Large-Eddy Simulation, In *Proceedings of ASME Turbo Expo 2020 - September 21-25, 2020*, Virtual conference, GT2020–14201.

[CFD3] S. Agarwal, L. Gicquel, F. Duchaine, N. Odier, and J. Dombard, (2020), Effect of the in-hole vortical structures on the cylindrical-hole Film-cooling effectivenessEffect of the in-hole vortical structures on the cylindrical-hole Film-cooling effectiveness, In *Proceedings of ASME Turbo Expo 2020*, Virtual conference, GT2020–14258.

[CFD4] E. Ajuria-Illarramendi, A. Alguacial, M. Bauerheim, A. Misdariis, B. Cuenot, and E. Benazera, (2020), Towards a hybrid computational strategy based on Deep Learning for incompressible flows, In *AIAA AVIATION 2020 FORUM - VIRTUAL EVENT*, vol. AIAA 2020, Reno (Nevada, USA), p. 3058.

[CFD5] B. Cuenot, (2019), Application of Large Eddy Simulation to IC engines - Invited conference, In *International Workshop on "Clean Combustion: Principles and Applications" 2019*, Germany, Technische Universität Darmstadt.

[CFD6] B. Cuenot, (2019), Large Eddy Simulation of turbulent reacting flows : methods and applications - Invited plenary lecture, In *17th International Conference on Numerical Combustion*, Aachen (Germany, German section of the Combustion Institute.

[CFD7] J. Dombard, F. Duchaine, L. Gicquel, N. Odier, K. Leroy, S. Le-Guyader, N. Buffaz, J. Démolis, S. Richard, and T. Grosnickel, (2020), Evaluation of the capacity of rans/urans/les in predicting the performance of a high-pressure turbine: effect of load and Off design condition, In *Proceedings of ASME Turbo Expo 2020*, Virtual conference, GT2020–15447.

[CFD8] F. Duchaine, L. Segui-Troth, J. de Laborderie, N. Odier, J. Dombard, and L. Gicquel, (2019), Large-Eddy Simulations of turbomachinery flows: from wall-resolved academic configurations to wall-modeled industrial geometries, In *72nd Annual Meeting of the APS Division of Fluid Dynamics*, Seattle, Washington (USA).

[CFD9] F. Duchaine, (2019), Conjugate heat transfer methodologies for gas turbine combustion aero thermal investigation. Heat Transfer Committee Tutorial jointly with Combustion, Fuels and Emissions Committee - Invited speaker, In *ASME TurboExpo 2019*, Phoenix, USA.

[CFD10] F. Dupuy, M. Gatti, L. Gicquel, T. Schuller, F. Nicoud, and T. Poinsot, (2019), Analysis of premixed swirling flames dynamics and associated flame transfer function modeling, In *17th International Conference on Numerical Combustion*, Aachen (Germany).

[CFD11] S. Esnault, F. Duchaine, and L. Gicquel, (2019), Large-Eddy Simulations of heat transfer within a multi-perforation synthetic jets configuration, In *ASME Turbo Expo 2019: Turbine Technical Conference and Exposition*, Phoenix, Arizona, USA, GT2019–91375.

[CFD12] T. Grosnickel, F. Duchaine, L. Gicquel, and C. Koupper, (2019), Large-Eddy Simulation of the flow developing in static and rotating ribbed channels, In *ASME TurboExpo 2019*, Phoenix, AZ, USA, GT2019–90370.

[CFD13] M. Harnieh, N. Odier, J. Dombard, F. Duchaine, and L. Gicquel, (2020), Loss predictions in the high-pressure film-cooled turbin vane of the factor project by mean of wall-modeled Large Eddy Simulation, In *Proceedings of ASME Turbo Expo 2020*, Virtual conference, GT2020–14232.

[CFD14] M. Harnieh, N. Odier, J. Dombard, F. Duchaine, and L. Gicquel, (2020), Loss Predictions in the High-Pressure Film-Cooled Turbine Blade Cascade T120D by Mean of Wall-Resolved Large Eddy Simulation, In *Proceedings of ASME Turbo Expo 2020*, virtual conference, GT2020–14231.

[CFD15] C. Lapeyre, A. Misdariis, N. Cazard, V. Xing, D. Veynante, and T. Poinsot, (2019), A convolutional neural network-based efficiency function for sub-grid flame-turbulence interaction in LES, In *17th International Conference on Numerical Combustion*, Aachen (Germany).

[CFD16] E. Lo Schiavo, D. Laera, L. Gicquel, and T. Poinsot, (2019), Large Eddy Simulations of thermoacoustic instability mechanisms in swirling spray flames, In *Seventeenth International Conference on Numerical Combustion - NC19*, RWTH Aachen (Germany).

[CFD17] L. G. Mael Harnieh, Nicolas Odier, Jerome Dombard, Florent Duchaine, (2020), Loss predictions in the high-pressure film-cooled turbine blade cascade T120D by mean of wall-resolved Large Eddy Simulation, In *ASME Turbo Expo 2020: Turbomachinery Technical Conference & Exposition*, 1–11.

[CFD18] L. G. Mael Harnieh, Nicolas Odier, Jerome Dombard, Florent Duchaine, (2020), Loss preidction in the high-pressure film-cooled turbine vave of the Factor project by mean of wall-modeled Large Eddy Simulation, In *ASME Turbo Expo 2020: Turbomachinery Technical Conference & Exposition*, 1–12.

[CFD19] B. Martin, F. Duchaine, L. Gicquel, N. Odier, and J. Dombard, (2020), Wall-resolved Large-Eddy Simulation of the LES89 cascade using an explicit local time-stepping method, In *ASME TURBO EXPO 2020, Gas Turbine Technical Congress & Exposition*, London, England, GT20120–14171.

[CFD20] B. Martin, M. Thomas, J. Dombard, F. Duchaine, and L. Gicquel, (2019), Analysis of solid particle ingestion and dynamics in a turbomachine using Large-Eddy Simulation, In *Proceedings of the ASME 2019 Turbo Expo: Turbomachinery Technical Conference & Exposition Turbomachines for Clean Power and Propulsion Systems*, no. GT2019-91215, Phoenix, USA, THE AMERICAN SOCIETY OF MECHANICAL ENGINEERS (ASME), pp 1–13.

[CFD21] S. Nadakkal-Appukuttan, E. Riber, and B. Cuenot, (2019), Large Eddy Simulation of reactive flow on the fire side of a steam cracking furnace, In *17th International Conference on Numerical Combustion*, Aachen (Germany), German section of the Combustion Institute.

[CFD22] S. Nadakkal-Appukuttan, E. Riber, B. Cuenot, and T. Gilles, (2020), Large Eddy Simulation of reactive flow on the fire side of a steam cracking Furnace, In *INFUB-12*, Porto (Portugal).

[CFD23] N. Odier, T. Poinsot, F. Duchaine, L. Gicquel, and S. Moreau, (2019), Inlet and outlet characteristics boundary conditions for Large Eddy Simulations of turbomachinery, In *Proceedings of the ASME Turbo Expo 2019: Turbomachinery Technical Conference and Exposition*, vol. 2 C, Phoenix, USA, ASME, 1–11.

[CFD24] D. Papadogiannis, S. Mouriaux, J.-S. Cagnone, K. Hillewaert, F. Duchaine, and S. Hiernaux, (2019), Influence of the numerical strategy on wall-resolved LES of a compressor cascade, In *European Turbomachinery Conference ETC13*, Lausanne, Switzerland.

[CFD25] C. Pérez-Arroyo, J. Dombard, F. Duchaine, N. Odier, G. Exilard, S. Richard, N. Buffaz, and J. Démolis, (2020), Large-eddy Simulation of an integrated high-pressure compressor and combustion chamber of a typical turbine engine architecture, In *Proceedings of ASME Turbo Expo 2020 Turbomachinery Technical Conference and Exposition*, no. GT2020-16288, London, England, 10 pp.

[CFD26] A. Perrot, F. Duchaine, L. Gicquel, T. Grosnickel, N. Odier, and J. Dombard, (2020), Unsteady analysis of heat transfer coefficient distribution in a static ribbed channel for an established flow, In *Proceedings of ASME Turbo Expo 2020*, virtual conference, GT2020–14493.

[CFD27] T. Poinsot, (2019), LES of high pressure turbulent flames - Invited conference, In *Workshop on high pressure combustion.*, Universität der Bundeswehr Mûnich.

[CFD28] T. Poinsot, (2019), Performance Computing for aerospace propulsion - Invited conference, In *PASC19 (Platform for Advanced Scientific Computing conference series)*, ETH Zurich (Switzerland).

[CFD29] P. Pouech, F. Duchaine, and T. Poinsot, (2019), Ignition of a premixed methane-air flow over a turbulent backward-facing step by Direct Numerical Simulation, In *17th International Conference on Numerical Combustion*, Aachen (Germany).

[CFD30] M. Queguineur, L. Gicquel, and G. Staffelbach, (2019), Modes identification and interactions in a rotor/stator academic cavity, In *Proceedings of 13th European Conference on Turbomachinery Fluid dynamics & Thermodynamics ETC13*, Lausanne - Switzerland, EPFL, Paper ID: ETC2019–386.

[CFD31] V. Shastry, Q. Cazères, E. Riber, and B. Cuenot, (2019), Numerical study of multicomponent spray flame propagation, In *17th International Conference on Numerical Combustion*, Germany, RWTH Aachen university.

[CFD32] M. Thomas, J. Dombard, F. Duchaine, L. Gicquel, and C. Koupper, (2019), Large-Eddy Simulation of combustor and complete single-stage high-pressure turbine of the FACTOR test rig, Phoenix, AZ, USA, GT2019–91206.

## 5.3 Journal Publications

[CFD33] T. Astoul, G. Wissocq, J.-F. Boussuge, A. Sengissen, and P. Sagaut, (2020), Analysis and reduction of spurious noise generated at grid refinement interfaces with the lattice Boltzmann method, *Journal of Computational Physics*, **418**, 109645.

[CFD34] R. Biolchini, G. Daviller, C. Bailly, and G. Bodard, (2020), Temperature effects on the noise source mechanisms in a realistic subsonic dual-stream jet, *Computers and Fluids*.

[CFD35] R. Campet, P. Roy, B. Cuenot, E. Riber, and J.-C. Jouhaud, (2020), Design Optimization of an Heat Exchanger using Gaussian Process, *International Journal of Heat and Mass Transfer*, **150**, 119264.

[CFD36] R. Campet, M. Zhu, E. Riber, B. Cuenot, and M. Nemri, (2019), Large Eddy Simulation of a single-started helically ribbed tube with heat transfer, *International Journal of Heat and Mass Transfer*, **132**, 961–969.

[CFD37] T. Charoy, J. Boeuf, J. Carlsson, P. Chabert, D. Eremin, L. Garrigues, K. Hara, I. Kaganovich, T. Powis, A. Smolyakov, D. Sydorenko, A. Tavant, O. Vermorel, and W. Villafana, (2019), 2D axial-azimuthal Particle-In-Cell benchmark for low-temperature partially magnetized plasmas, *Plasma Sources Science and Technology*, **28**, paper 105010.

[CFD38] F. Collin-Bastiani, J. Marrero-Santiago, E. Riber, G. Cabot, B. Renou, and B. Cuenot, (2019), A joint experimental and numerical study of ignition in a spray burner, *Proceedings of the Combustion Institute*, **37**, 5047–5055.

[CFD39] F. Collin-Bastiani, E. Riber, and B. Cuenot, (2020), Study of inter-sector spray flame propagation, *Proceedings of the Combustion Institute*, **38**.

[CFD40] F. Collin-Bastiani, O. Vermorel, C. Lacour, B. Lecordier, and B. Cuenot, (2019), DNS of spark ignition using Analytically Reduced Chemistry including plasma kinetics, *Proceedings of the Combustion Institute*, **37**, 5057–5064.

[CFD41] S. Courtiaud, N. Lecysyn, G. Damamme, T. Poinsot, and L. Selle, (2019), Analysis of the Mixing in High Explosive Fireballs Using Small Scale Pressurized Spheres, *Shock Waves*, **29**, 339–353.

[CFD42] G. Daviller, J. Dombard, G. Staffelbach, J. Herpe, and D. Saucereau, (2020), Prediction of Flow Separation and Side-loads in Rocket Nozzle Using Large-eddy Simulation, *International Journal of Computational Fluid Dynamics*, 1–12.

[CFD43] G. Daviller, G. Oztarlik, and T. Poinsot, (2019), A generalized non-reflecting inlet boundary condition for steady and forced compressible flows with injection of vortical and acoustic waves, *Computers and Fluids*, **190**, 503–513.

[CFD44] J. de Laborderie, F. Duchaine, L. Gicquel, and S. Moreau, (2020), Wall-modeled Large-Eddy Simulations of a Multistage High-Pressure Compressor, *Flow Turbulence and Combustion*.

[CFD45] O. Dounia, O. Vermorel, T. Jaravel, and T. Poinsot, (2020), Time scale analysis of the homogeneous inhibition/suppression of premixed flames by alkali metals, *Proceedings of the Combustion Institute*, **38**.

[CFD46] O. Dounia, O. Vermorel, A. Misdariis, and T. Poinsot, (2019), Influence of kinetics on DDT simulations, *Combustion and Flame*, **200**, 1–14.

[CFD47] F. Duchaine, L. Gicquel, T. Grosnickel, and C. Koupper, (2020), Large-Eddy Simulation of the Flow Developing in Static and Rotating Ribbed Channels, *Journal of Turbomachinery*, **142**, 041003.

[CFD48] F. Dupuy, M. Gatti, C. Mirat, L. Gicquel, and F. Nicoud, (2020), Combining analytical models and LES data to determine the transfer function from swirled premixed flames, *Combustion and Flame*, **217**, 222–236.

[CFD49] D. Dupuy, L. Gicquel, N. Odier, F. Duchaine, and T. Arts, (2020), Analysis of the effect of intermittency in a high-pressure turbine blade, *Physics of Fluids*, **32**, 095101.

[CFD50] L. Esclapez, F. Collin-Bastiani, E. Riber, and B. Cuenot, (2020), A statistical model to predict ignition probability, *Combustion and Flame*, **225**, 180–195.

[CFD51] S. Esnault, F. Duchaine, L. Gicquel, and S. Moreau, (2020), Large Eddy Simulation of heat transfer within a multi-perforation synthetic jets configuration, *Journal of Turbomachinery*, **March**, 1–25 (25 pages).

[CFD52] A. Felden, P. Pepiot, L. Esclapez, E. Riber, and B. Cuenot, (2019), Including analytically reduced chemistry (ARC) in CFD applications, *Acta Astronautica*, **158**, 444–459.

[CFD53] M. Férand, T. Livebardon, S. Moreau, and M. Sanjosé, (2019), Numerical Prediction of Far-Field Combustion Noise from Aeronautical Engines, *Acoustics*, **1**, 174–198.

[CFD54] M. Fiore, N. Gourdain, J.-F. Boussuge, and E. Lippinois, (2019), Delineating loss sources within a linear cascade with upstream cavity and purge flow, *Journal of Turbomachinery*, **141**, Paper No: TURBO–18–1292.

[CFD55] L. Gallen, A. Felden, E. Riber, and B. Cuenot, (2019), Lagrangian tracking of soot particles in LES of gas turbines, *Proceedings of the Combustion Institute*, **37**, 5429–5436.

[CFD56] F.-J. Granados-Ortiz, C. Pérez-Arroyo, G. Puigt, C.-H. Lai, and C. Airiau, (2019), On the Influence of Uncertainty in Computational Simulations of a High-Speed Jet Flow from an Aircraft Exhaust, *Computers and Fluids*, **180**, 139–158.

[CFD57] S. Grimonprez, J. Wu, A. Faccinetto, S. Gosselin, E. Riber, B. Cuenot, M. Cazaunau, E. Pangui, P. Formenti, J.-F. Doussin, D. Petitprez, and P. Desgroux, (2020), Hydrophilic properties of soot particles exposed to OH radical: a possible new mechanism involved in the contrail formation, *Proceedings of the Combustion Institute*, **38**.

[CFD58] S. Guo, Y. Feng, J. Jacob, F. Renard, and P. Sagaut, (2020), An efficient lattice Boltzmann method for compressible aerodynamics on D3Q19 lattice, *Journal of Computational Physics*, **416**, 109570.

[CFD59] M. Harnieh, M. Thomas, R. Bizzari, J. Dombard, F. Duchaine, and L. Gicquel, (2020), Assessment of a coolant injection model on cooled high-pressure vanes with Large-Eddy Simulation, *Flow Turbulence and Combustion*, **104**, 643–672.

[CFD60] T. Jaravel, O. Dounia, Q. Malé, and O. Vermorel, (2020), Deflagration to detonation transition in fast flames and tracking with chemical explosive mode analysis, *Proceedings of the Combustion Institute*, **38**.

[CFD61] V. Joncquières, O. Vermorel, and B. Cuenot, (2020), A fluid formalism for low-temperature plasma flows dedicated to space propulsion in an unstructured High Performance Computing solver, *Plasma Sources Science and Technology*.

[CFD62] T. Kaiser, G. Öztarlik, L. Selle, and T. Poinsot, (2019), Impact of symmetry breaking on the FTF of a laminar premixed flame, *Proceedings of the Combustion Institute*, **37**, 1953–1960.

[CFD63] D. Laera, P. Agostinelli, L. Selle, Q. Cazères, G. Oztarlik, T. Schuller, L. Gicquel, and T. Poinsot, (2020), Stabilization mechanisms of CH4 premixed swirled flame enriched with a non-premixed hydrogen injection, *Proceedings of the Combustion Institute*, **38**.

[CFD64] C. Lapeyre, A. Misdariis, N. Cazard, D. Veynante, and T. Poinsot, (2019), Training convolutional neural networks to estimate turbulent sub-grid scale reaction rates, *Combustion and Flame*, **203**, 255–264.

[CFD65] C. Laurent, M. Bauerheim, T. Poinsot, and F. Nicoud, (2019), A novel modal expansion method for low-order modeling of thermoacoustic instabilities in complex geometries, *Combustion and Flame*, **206**, 334–348.

[CFD66] C. Laurent, L. Esclapez, D. Maestro, G. Staffelbach, B. Cuenot, L. Selle, T. Schmitt, F. Duchaine, and T. Poinsot, (2019), Flame-wall interaction effects on the flame root stabilization mechanisms of a doubly-transcritical LO2/LCH4 cryogenic flame, *Proceedings of the Combustion Institute*, **37**, 5147–5154.

[CFD67] C. Laurent, G. Staffelbach, F. Nicoud, and T. Poinsot, (2020), Heat-release dynamics in a doubly-transcritical LO2/LCH4 cryogenic coaxial jet flame subjected to fuel inflow acoustic modulation, *Proceedings of the Combustion Institute*.

[CFD68] S. Le Bras, H. Deniau, and C. Bogey, (2019), A technique of flux reconstruction at the interfaces of non-conforming grids for aeroacoustic simulations, *International Journal for Numerical Methods in Fluids*, **91**, 587–614.

[CFD69] E. Lo Schiavo, D. Laera, E. Riber, L. Gicquel, and T. Poinsot, (2020), Effects of liquid fuel/wall interaction on thermoacoustic instabilities in swirling spray flames, *Combustion and Flame*, **219**, 86–101.

[CFD70] D. Maestro, B. Cuenot, and L. Selle, (2019), Large Eddy Simulation of combustion and heat transfer in a single element GCH4/GOx rocket combustor, *Flow Turbulence and Combustion*, **103**, 699–730.

[CFD71] D. Maestro, B. Cuenot, and L. Selle, (2019), Large Eddy Simulation of combustion and heat transfer in a single element GCH4/GOx rocket combustor, *Flow Turbulence and Combustion*, **103**, 699–730.

[CFD72] Q. Malé, G. Staffelbach, O. Vermorel, A. Misdariis, F. Ravet, and T. Poinsot, (2019), Large Eddy Simulation of pre-chamber ignition in an internal combustion engine, *Flow Turbulence and Combustion*, **103**, 465–483.

[CFD73] Q. Malé, O. Vermorel, F. Ravet, and T. Poinsot, (2020), Direct numerical simulations and models for hot burnt gases jet ignition Author links open overlay panel, *Combustion and Flame*, **223**, 407–422.

[CFD74] P.-A. Masset and G. Wissocq, (2020), Linear hydrodynamics and stability of the discrete velocity Boltzmann equations, *Journal of Fluid Mechanics*, **897**, 1–54.

[CFD75] L. Muscat, G. Puigt, M. Montagnac, and P. Brenner, (2019), A coupled implicit-explicit time integration method for compressible unsteady flows, *Journal of Computational Physics*, **398**.

[CFD76] L. Muscat, G. Puigt, M. Montagnac, and P. Brenner, (2020), Spatial coupling of an explicit temporal adaptive integration scheme with an implicit time integration scheme, *International Journal for Numerical Methods in Fluids*.

[CFD77] G. Oztarlik, L. Selle, T. Poinsot, and T. Schuller, (2020), Suppression of instabilities of swirled premixed flames with minimal secondary hydrogen injection, *Combustion and Flame*, **214**, 266–276.

[CFD78] D. Paulhiac, B. Cuenot, E. Riber, L. Esclapez, and S. Richard, (2020), Analysis of the spray flame structure in a lab-scale burner using Large Eddy Simulation and Discrete Particle Simulation, *Combustion and Flame*, **212**, 25–38.

[CFD79] C. Pérez-Arroyo, G. Daviller, G. Puigt, C. Airiau, and S. Moreau, (2019), Identification of temporal and spatial signatures of broadband shock-associated noise, *Shock Waves*, **29**, 117–134.

[CFD80] C. Pérez-Arroyo, T. Léonard, M. Sanjosé, S. Moreau, and F. Duchaine, (2019), Large Eddy Simulation of a scale-model turbofan for fan noise source diagnostic, *Journal of Sound and Vibration*, **445**, 64–76.

[CFD81] P. Pouech, F. Duchaine, and T. Poinsot, (2020), Premixed flame ignition in high speed flows over a backward facing step, *Combustion and Flame*.

[CFD82] C. Pérez Arroyo, J. Dombard, F. Duchaine, L. Gicquel, B. Martin, N. Odier, and G. Staffelbach, (2020), Towards the Large-Eddy Simulation of a full engine: Integration of a 360 azimuthal degrees fan, compressor and combustion chamber.
Part I: Methodology and initialisation, *Global Power and Propulsion Society*.

[CFD83] C. Pérez Arroyo, J. Dombard, F. Duchaine, L. Gicquel, B. Martin, N. Odier, and G. Staffelbach, (2020), Towards the Large-Eddy Simulation of a full engine: Integration of a 360 azimuthal degrees fan, compressor and combustion chamber.
Part II: Comparison against stand-alone simulations, *Global Power and Propulsion Society*.

[CFD84] M. Queguineur, T. Bridel-Bertomeu, L. Gicquel, and G. Staffelbach, (2019), Large eddy simulations and global stability analyses of an annular and cylindrical rotor/stator cavity limit cycles, *Physics of Fluids*, **31**, paper 104109.

[CFD85] M. Queguineur, L. Gicquel, and G. Staffelbach, (2020), Stability and control of an annular rotor/stator cavity limit cycle, *Physics of Fluids*, **32**, 084101.

[CFD86] M. Queguineur, L. Gicquel, F. Dupuy, A. Misdariis, and G. Staffelbach, (2019), Dynamic mode tracking and control with a relaxation method, *Physics of Fluids*, **31**, 034101.

[CFD87] B. Rochette, E. Riber, and B. Cuenot, (2019), Effect of non-zero relative velocity on the flame speed of two-phase laminar flames, *Proceedings of the Combustion Institute*, **37**, 3393–3400.

[CFD88] B. Rochette, E. Riber, O. Vermorel, and B. Cuenot, (2020), A generic and self-adapting method for flame detection and thickening in the Thickened Flame model, *Combustion and Flame*, **212**, 448–458.

[CFD89] P. Roy, L. Jofre, J.-C. Jouhaud, and B. Cuenot, (2020), Versatile Sequential Sampling Algorithm using Kernel Density Estimation, *European Journal of Operational Research*, **284**, 201–211.

[CFD90] T. Schuller, T. Poinsot, and S. Candel, (2020), Dynamics and control of premixed combustion systems based on flame transfer and describing functions, *Journal of Fluid Mechanics*, **894**.

[CFD91] O. Schulz, E. Piccoli, A. Felden, G. Staffelbach, and N. Noiray, (2019), Autoignition-cascade in the windward mixing layer of a premixed jet in hot vitiated crossflow, *Combustion and Flame*, **201**, 215–233.

[CFD92] V. Shastry, Q. Cazères, B. Rochette, E. Riber, and B. Cuenot, (2020), Numerical study of multicomponent spray flame propagation, *Proceedings of the Combustion Institute*.

[CFD93] F. Tagliante, T. Poinsot, L. Pickett, P. Pepiot, L.-M. Malbec, G. Bruneaux, and C. Angelberger, (2019), A conceptual model of the flame stabilization mechanisms for a lifted Diesel-type flame based on Direct Numerical Simulation and experiments, *Combustion and Flame*, **201**, 65–77.

[CFD94] G. Vignat, E. Lo Schiavo, D. Laera, A. Renaud, L. Gicquel, D. Durox, and S. Candel, (2020), Dynamics of spray and swirling flame under acoustic oscillations : A joint experimental and LES investigation, *Proceedings of the Combustion Institute*, **37**, 5205–5213.

[CFD95] G. Vignat, E. Lo Schiavo, D. Laera, A. Renaud, L. Gicquel, D. Durox, and S. Candel, (2020), Dynamics of Spray and Swirling Flame under Acoustic Oscillations : A Joint Experimental and LES Investigation, *Proceedings of the Combustion Institute*, **37**.

[CFD96] G. Vignat, E. Lo Schiavo, D. Laera, A. Renaud, L. Gicquel, D. Durox, and S. Candel, (2020), Dynamics of Spray and Swirling Flame under Acoustic Oscillations : A Joint Experimental and LES Investigation, *Proceedings of the Combustion Institute*.

[CFD97] J. Wirtz, B. Cuenot, and E. Riber, (2020), Numerical Study of a Polydisperse Spray Counterflow Diffusion Flame, *Proceedings of the Combustion Institute*, **38**.

[CFD98] G. Wissocq, J.-F. Boussuge, and P. Sagaut, (2020), Consistent vortex initialization for the athermal lattice Boltzmann method, *Physical Review E*, **101**, 043306.

[CFD99] G. Wissocq, C. Coreixas, and J.-F. m. c. Boussuge, (2020), Linear stability and isotropy properties of athermal regularized lattice Boltzmann methods, *Phys. Rev. E*, **102**.

[CFD100] G. Wissocq, P. Sagaut, and J.-F. Boussuge, (2019), An extended spectral analysis of the lattice Boltzmann method: modal interactions and stability issues, *Journal of Computational Physics*, **380**, 311–333.

## 5.4 Technical Reports

[CFD101] M. Ahmed-Maloum, (2020), Modélisation et simulation d'une torche au kérosène pour la certification des matériaux composites aéronautiques, working note, Institut National Polytechnique de Toulouse - ENSEEIHT.

[CFD102] A. Cellier, (2020), Detection and Identification of Instability and Blow-off/Flashback Precursors in Aeronautical Engines using Deep Learning techniques, working note, Cerfacs.

[CFD103] M. Cizeron, (2020), Développement et validation d'un outil numérique pour l'étude de la dispersion de gouttelettes chargées en agents infectieux dans des environnements clos., working note, Ecole Centrale de Lyon - Cerfacs, Toulouse.

[CFD104] J. Dabas, (2019), Développement d'une condition aux limites pour la simulation numérique d'écoulements en turbomachine, working note, Ecole Normale Supérieur Paris-Saclay, Cerfacs Toulouse.

[CFD105] J. Gaucherand, (2020), Simulation of heat transfer in a combustion pre-chamber tube and 0D modeling of a burnt gas jet ignition engine, working note, École Polytechnique de l'université d'Orléans.

[CFD106] Y. Gentil, (2020), Prediction of combustion noise in aircraft engines, working note, ISAE SUPAERO TOULOUSE.

[CFD107] H. Godé, (2020), Etude de modèles réduits utilisant des techniques d'apprentissage automatique, application à la prévision instantanée de lames d'eau, working note, Institut Polytechnique des Sciences Avancées (IPSA) Toulouse - Cerfacs Toulouse.

[CFD108] T. Gresse, (2019), Simulation aux grandes échelles de l'ingestion de particules de sable par un compresseur centrifuge, working note, ENSEEIHT ET CERFACS TOULOUSE.

[CFD109] C. Guyonnet, (2020), Vers une combustion décarbonée : Impact de l'ajout d'hydrogène aux mélanges de combustibles, working note, Ecole Polytechnique , Université d'Orléans.

[CFD110] J.-J. Hok, (2020), Chemistry-flow interaction modeling for the simulation of explosions, working note, ECOLE CENTRALE DE LYON.

[CFD111] M. Jonval, (2020), Large eddy simulations of unsteady flows with high order numerical methods, working note, Université de Lille - Faculté des Sciences et Technologies: Département de Mathématiques.

[CFD112] P.-A. Masset, (2019), Linear hydrodynamics and stability of the Discrete Velocity Boltzmann Equations, working note, ISAE ET CERFACS TOULOUSE.

[CFD113] C. Mocquard, (2020), Simulation et modélisation des instabilités de combustion dans les moteurs d'avion, working note, Ecole Centrale de Lyon.

[CFD114] T. Naess, (2019), Simulation aux Grandes Echelles d'un inverseur de poussée, working note, ISAE-ENSMA ET CERFACS.

[CFD115] R. Pelé, (2020), Modélisation et Simulation aux Grandes Echelles des émissions de NOx dans un brûleur semi-industriel, working note, INSA CENTRE VAL DE LOIRE.

[CFD116] L. Plumain, (2020), Investigation des couplages paramétriques des modèles de paroi en simulations aux grandes échelles, working note, INSA Rouen.

[CFD117] L. Rogel, (2019), 3rd year internship report: A matrix-free preconditioning technique for matrix-free implicit time stepping methods, working note, INPT ENSEEIHT ET CERFACS, TOULOUSE.

[CFD118] J. Strauss, (2020), Development of Global Chemical Reaction Scheme for Methane and Oxygen in Rocket Applications to be Used in Large-Eddy Simulation, working note, Technische Universität München (Germany).

[CFD119] M. Taha, (2019), Final internship report: "Innovative design of a natural gas torch using LES", working note, Ecole Centrale de Lyon et Cerfacs Toulouse.

[CFD120] R. Theulé, (2019), Rapport de stage de spécialité - Documentation sous Jupyter Notebook en langage Python pour la Simulation aux Grandes Echelles de la combustion, working note, INSA ROUEN ET CERFACS TOULOUSE.

[CFD121] B. Thibaud, (2020), Simulation aux grandes échelles d'explosion avec adaptation de maillage dynamique, working note, INSA Toulouse - Cerfacs Toulouse.

[CFD122] J. Villard, (2020), Simulation de la production de suies avec le logiciel Cantera, working note, Université Toulouse III Paul Sabatier.

[CFD123] B. Vinot, (2020), Simulation numérique directe de la combustion turbulente, working note, ENSTA Bretagne.

## 5.5 Thesis

[CFD124] R. Campet, (2019), *Simulation and optimization of steam cracking processes*, phd thesis, Université Fédérale de Toulouse, INPT - Ecole doctorale MEGeP.

[CFD125] M. Catchirayer, (2019), *Wall-modeling in large-eddy simulations for turbomachinery flows*, phd thesis, Aix Marseille Université - Ecole Doctorale: Sciences pour l'ingénieur.

[CFD126] F. Collin-Bastiani, (2019), *Modeling and numerical simulations of two-phase ignition in gas turbines*, phd thesis, Institut National Polytechnique de Toulouse - Ecole doctorale MEGeP.

[CFD127] R. Dupuis, (2019), *Surrogate models coupled with machine learning to approximate complex physical phenomena involving aerodynamic and aerothermal simulations*, phd thesis, Université Fédérale de Toulouse, INPT - Ecole doctorale MEGeP.

[CFD128] F. Dupuy, (2020), *Reduced Order Models and Large Eddy Simulation for Combustion Instabilities in aeronautical Gas Turbines*, phd thesis, Université de Toulouse - Institut National Polytechnique de Toulouse - Ecole doctorale MEGeP.

[CFD129] M. Fiore, (2019), *Influence of inter-disc cavity flow on turbine aerodynamics*, phd thesis, Université de Toulouse - Institut Supérieur de l'Aéronautique et de l'Espace (ISAE).

[CFD130] L. Gallen, (2020), *Prediction of soot particles in gas turbine combustors using large eddy simulation*, phd thesis, INP Toulouse - Ecole doctorale : MEGeP.

[CFD131] T. Grosnickel, (2019), *Large Eddy Simulations to predict internal turbine blade cooling flows*, phd thesis, Institut National Polytechnique de Toulouse - Ecole doctorale MEGeP.

[CFD132] M. Harnieh, (2020), *Prédiction de la génération des pertes des écoulements compressibles anisothermes appliquée aux distributeurs hautes pressions avec les simulations aux grandes échelles*, phd thesis, UNIVERSITÉ DE TOULOUSE - Institut National Polytechnique de Toulouse (MEGEP).

[CFD133] V. Joncquières, (2019), *Numerical model and simulation of Hall effect thrusters*, phd thesis, Institut National Polytechnique de Toulouse - Ecole doctorale MEGeP.

[CFD134] C. Laurent, (2020), *Low-Order Modeling and High-Fidelity Simulations for the Prediction of Combustion Instabilities in Liquid-Rocket Engines and Gas Turbines*, phd thesis, Institut National Polytechnique de Toulouse - Ecole doctorale MeGEP.

[CFD135] Q. Malé, (2020), *Étude numérique de l'allumage par préchambre dans les moteurs à combustion interne*, phd thesis, Université de Toulouse III - Ecole doctoral MEGeP.

[CFD136] L. Muscat, (2019), *Couplage de schémas temporels pour la simulation des écoulements compressibles instationnaires*, phd thesis, Institut National Polytechnique de Toulouse - Ecole doctorale MEGeP.

[CFD137] M. Queguineur, (2020), *Stability and control of unsteady phenomena in rotor/stator cavities using Large Eddy Simulation*, phd thesis, Institut National Polytechnique de Toulouse - Ecole doctorale MEGeP.

[CFD138] B. Rochette, (2019), *Modeling and Simulation of two-phase flow turbulent combustion in aeronautical engines*, phd thesis, MEGEP.

[CFD139] P. Roy, (2019), *Uncertainty Quantification in High Dimensional Problem*, phd thesis, Institut National Polytechnique de Toulouse - Ecole doctorale MEGeP.

[CFD140] G. Wissocq, (2019), *Investigation of lattice Boltzmann methods for turbomachinery secondary air system simulations*, phd thesis, Université Aix-Marseille.